National Library of Canada
Bibliothèque nationale du Canada

Canadian Theses Service
Service des thèses canadiennes

Ottawa, Canada
K1A 0N4

NOTICE

The quality of this microform is heavily dependent upon the quality of the original thesis submitted for microfilming. Every effort has been made to ensure the highest quality of reproduction possible.

If pages are missing, contact the university which granted the degree.

Some pages may have indistinct print especially if the original pages were typed with a poor typewriter ribbon or if the university sent us an inferior photocopy.

Previously copyrighted materials (journal articles, published tests, etc.) are not filmed.

Reproduction in full or in part of this microform is governed by the Canadian Copyright Act, R.S.C. 1970, c C-30.

AVIS

La qualité de cette microforme dépend grandement de la qualité de la thèse soumise au microfilmage. Nous avons tout fait pour assurer une qualité supérieure de reproduction.

S'il manque des pages, veuillez communiquer avec l'université qui a conféré le grade

La qualité d'impression de certaines pages peut laisser à désirer, surtout si les pages originales ont été dactylographiées à l'aide d'un ruban usé ou si l'université nous a fait parvenir une photocopie de qualité inférieure.

Les documents qui font déjà l'objet d'un droit d'auteur (articles de revue, tests publiés, etc) ne sont pas microfilmés.

La reproduction, même partielle, de cette microforme est soumise à la Loi canadienne sur le droit d'auteur, SRC 1970, c. C-30

Canada

Ride Dynamics of Heavy Vehicles using Local Equivalent Linearization Technique

Anil Dhir

A Thesis

in

The Department

of

Mechanical Engineering

Presented in Partial Fulfillment of the Requirements
for the Degree of Master of Engineering at
Concordia University
Montréal, Québec, Canada

March 1988

© Anil Dhir, 1988

Permission has been granted to the National Library of Canada to microfilm this thesis and to lend or sell copies of the film.

The author (copyright owner) has reserved other publication rights, and neither the thesis nor extensive extracts from it may be printed or otherwise reproduced without his/her written permission.

L'autorisation a été accordée à la Bibliothèque nationale du Canada de microfilmer cette thèse et de prêter ou de vendre des exemplaires du film.

L'auteur (titulaire du droit d'auteur) se réserve les autres droits de publication; ni la thèse ni de longs extraits de celle-ci ne doivent être imprimés ou autrement reproduits sans son autorisation écrite.

ISBN 0-315-44817-2

ABSTRACT

Ride Dynamics of Heavy Vehicles using Local Equivalent Linearization Technique

Anil Dhir

The main objective of this thesis is to study the ride dynamic of articulated heavy vehicles using linear and nonlinear mathematical models subjected to randomly irregular road surface. A baseline configuration of an articulated vehicle is selected. Two- and three-dimensional mathematical models for the baseline vehicle are developed using linear suspension characteristics. A mathematical model incorporating nonlinearities arising from vehicle primary suspension elements is also developed. The power spectral density approach is utilized to determine and analyze the linear dynamic response of the baseline vehicle model traversing on road surface undulations, represented as stationary Gaussian random excitations. The input displacement amplitudes for the simulation of the nonlinear vehicle model are generated by the summation of harmonic components corresponding to discrete frequencies, that would represent the measured road displacement spectral densities.

A local equivalent linearization technique based on the energy/force balance is adopted to represent the nonlinear suspension models by their linear equivalent. The critical

lock-up behaviour of the vehicle suspension is inspected such that the nonlinear behaviour of the system can be effectively simulated by the equivalent linear system. A parametric study of nonlinear vehicle model is carried out to establish the influence of various parameters on the heavy vehicle dynamic behaviour. The ride performance of the vehicle model is assessed with reference to ISO specified criteria for ride comfort.

ACKNOWLEDGEMENTS

The author is sincerely grateful to his supervisors, Dr. S. Sankar and Dr. R.B. Bhat, for their guidance and encouragement during the preparation of this thesis.

Thanks are due to Dr. Subhash Rakheja, Mr. James Alanoly, Mr. K.G. Balasubramaniam, and other members of faculty and staff of the CONCAVE Research Centre, Department of Mechanical Engineering, Concordia University for their time and assistance during the course of this work.

The author wishes to acknowledge the support provided by FCAR fellowship and Concordia University graduate fellowship during the course of this research.

TABLE OF CONTENTS

Page

Page

LIST OF FIGURES

LIST OF FIGURES (continued)

LIST OF FIGURES (continued)

LIST OF FIGURES (continued)

LIST OF FIGURES (continued)

LIST OF FIGURES (continued)

LIST OF TABLES

NOMENCLATURE

The following is a list of frequently used symbols. Others will be defined when they are used.

a_c	cab c.g. height from the cab floor
a_o	seat c.g. height from the cab floor
a_1	fifth wheel height from the tractor c.g.
a_2	semitrailer c.g. height from the fifth wheel
a_3	cab c.g. height from the tractor c.g.
$\bar{a}(\bar{f})$	rms acceleration corresponding to center frequency
A_l	peak value of the coefficient of harmonic component
A_{rms_l}	rms value of the coefficient of harmonic component
[A]	inverse of frequency response function matrix
b_1	location of tractor c.g. from front axle
b_2	location of tractor c.g. from tractor tandem axle center
b_3	location of semitrailer c.g. from its tandem axle center
b_4	location of semitrailer c.g from fifth wheel
b_5	location of tractor c.g. from fifth wheel
b_i	intercept of the i^{th} segment
$c_{eq}(\omega, r)$	equivalent viscous damping coefficient as a function of excitation frequency and relative displacement

c_f	viscous damping coefficient due to cab front mounts
c_i	viscous damping coefficient of primary suspensions
c_r	viscous damping coefficient due to cab rear mounts
c_o	viscous damping coefficient of seat suspension
c_t	vertical viscous damping coefficient of dual-lumped tire model
c_{tl}	lateral viscous damping coefficient of dual-lumped tire model
c_A	viscous damping coefficient of articulation roll
C_n	damping coefficient due to nonlinear damping mechanism being proportional to the n^{th} power of relative velocity, $\dot{r}$.
C_{o_i}	magnitude of Coulomb friction
C_{2_i}	coefficient of quadratic damping
$[C]$, $[C_F]$	viscous damping coefficient matrices
$[C_{eq}]$, $[C_{eq_r}]$	equivalent viscous damping coefficient matrices due to Coulomb friction, and shock absorber damping.
c.g.	center of gravity
CSD	cross spectral density
d_x, d_z	driver's location from tractor c.g.
D	dissipation function
ΔE	energy loss per cycle by the nonlinear damper
f	temporal frequency - Hz
f_i	i^{th} frequency
f_l	discrete frequency of l^{th} harmonic

$\bar{f}$	center frequency of the third octave band
f_1, f_2	lower and upper frequency limits of the third octave band, respectively
Δf	frequency band
$f(r,\dot{r},t)$	nonlinear damping function
F_a^I, F_b^I, F_c^I	inertia forces at points a, b, and c (points of tractor front and rear suspensions, and semitrailer suspension attachment to their respective sprung masses), evaluated at discrete frequency, f_l
F_{d_i}	damping force
F_{k_i}	spring force
$\{f\}, \{f_r\}$	excitation force vectors
$\{F_d\}$	damping force vector
$[G(j\omega_l)]$	frequency response function matrix of the system, obtained in terms of forced damping and stiffness charateristics
$[G_m(j\omega_l)]$	modified $[G(j\omega_l)]$
$h(j\omega)$	frequency response function of the system
$[H(j\omega_l)], [H(j\omega_l)]$	frequency response function matrix of the system
$I_{op}, I_{cp}, I_{tp}, I_{sp}$	pitch mass moment of inertias for the seat, cab, tractor, and semitrailer about their center of gravities, respectively
$I_{or}, I_{cr}, I_{tr}, I_{sr}$	roll mass moment of inertias for the seat, cab, tractor, and semitrailer about their center of gravities, respectively
I_{spr}, I_{srp}	pitch-roll and roll-pitch mass moment of inertias for the semitrailer about its center of gravity, respectively

I_2, I_3	pitch mass moment of inertias for the tractor tandem axle and semitrailer axle, respectively
k_f	spring rate of cab front mounts
k_i	spring rate of primary suspensions
k_r	spring rate of cab rear mounts
k_o	spring rate of seat suspension
k_t	vertical stiffness of dual-lumped tire model
k_{tl}	lateral stiffness of dual-lumped tire model
k_{tn2}, k_{tn3}	torsional spring rate of tractor tandem axle and semitrailer axle, respectively
k_A	spring rate of articulation roll
$[K], [K_F], [K_r]$	stiffness matrices
l_2, l_3	tractor tandem axle and semitrailer axle spacing, respectively
$l_{s_1}, l_{s_2}, l_{s_3}$	tractor front and rear suspensions, and semitrailer suspension spacing, respectively
$l_{t_1}, l_{t_2}, l_{t_3}$	tractor front and rear, and semitrailer tires track width, respectively
L_{jk}	distance between axle j to axle k
L_t	tractor wheel base ($b_1 + b_2$)
L_s	semitrailer bed length between fifth wheel and its axle ($b_3 + b_4$)
m	number of response variables
m_1, m_2, m_3	unsprung masses of tractor front and rear tandem axles, and semitrailer axle, respectively
m_o, m_c, m_t, m_s	sprung masses of seat and driver, cab, tractor, and semitrailer, respectively

m_a, m_b, m_c	masses due to the static load distribution at points a, b, and c
m_A	proportion of semitrailer mass reflected on the tractor through the articulation point
m_i	slope of the i^{th} segment
M_4	total mass of the tractor $(m_t+m_1+m_2)$
M_5	total mass of the semitrailer (m_s+m_3)
M_G	gross mass of the vehicle
n	spatial frequency - c/m
N	number of vehicle axles
N_f	number of discrete frequencies
p_o	lateral distance between seat c.g. and cab c.g.
p_1	lateral distance between cab c.g. and cab front mounts
p_2	lateral distance between cab c.g. and cab rear mounts
PSD	power spectral density
{q}	vector of generalized coordinates
r_1, r_2	longitudinal distance between cab c.g., and its front and rear mounts, respectively
r_3, r_4	longitudinal distance between tractor c.g., and cab front and rear mounts, respectively
{r}	relative dispalcement vector
Re	designates real part
sgn	sign
S_M	secondary mass (m_o+m_c)
S(n)	spatial spectral density of the road roughness

$S(n_o)$	roughness coefficient
$\bar{S}(\bar{f})$	average PSD corresponding to the center frequency
$S_{rms}(f_l)$	rms input displacement spectral density corresponding to discrete frequency, f_l
$[S_l(f)]$	temporal input displacement spectral density matrix
$[S_F(f)]$	force spectral density matrix
$[S_q(f)]$	response spectral density matrix
$[S_o(f)]$	spectral density matrix of the response coordinates, other than the generalized coordinates
$[S_{\dot{q}}(f)]$	acceleration spectral density matrix of output variables
t_{jk}	time delay between j^{th} and k^{th} axles
T	kinetic energy
$[T], [T_r]$	transformation matrices
$\{u\}$	vector of displacement excitations
v	vehicle speed
V	potential energy
w_1, w_2	waviness
W_f	correction factor
$x(t)$	displacement time history
x_o, x_c, x_t, x_s	longitudinal motions coordinates of the center of gravities of the driver and seat, cab, tractor, and semitrailer, respectively
y_o, y_c, y_t, y_s	lateral motions coordinates of the center of gravities of the driver and seat, cab, tractor, and semitrailer, respectively
y_1, y_2, y_3	lateral motions coordinates of the vehicle axles

z_o, z_c, z_t, z_s	bounce motions coordinates of the center of gravities of the driver and seat, cab, tractor, and semitrailer, respectively
z_1, z_2, z_3	bounce motions coordinates of the vehicle axles
z_a, z_b, z_c	bounce motions coordinates of the suspensions attachment points, a, b, and c
z_A	bounce motion coordinate of articulation point
$\theta_c, \theta_t, \theta_s$	pitch rotation about the center of gravities of the cab, tractor, and semitariler, respectively
θ_2, θ_3	pitch rotation of the tractor tandem axle and semitrailer axle, respectively
ϕ_c, ϕ_t, ϕ_s	roll motions about the center of gravities of the cab, tractor, and semitrailer, respectively
μ_{jk}	phase angles
ϵ	limiting value - m/sec
δ	magnitude of relative displacement
ζ_i	damping ratio in the i^{th} mode
ω	excitation frequency - rad/sec
ω_{n_i}	undamped natural frequency of the i^{th} mode - rad/sec
ω_{d_i}	damped natural frequency of the i^{th} mode - rad/sec
$[\nu]$	vector of modal coordinates
$[\epsilon(t)]$	excitation force vector in terms of the modal coordinates
$[\Phi]$	modal matrix
$[\upsilon]$	diagonalized mass matrix
$[\gamma]$	diagonalized damping matrix

$[\kappa]$	diagonalized stiffness matrix
$[\eta(j\omega)]$	diagonalized frequency response function matrix
$(\dot{\ })$	denotes derivative with respect to time
$(^*)$	denotes the conjugate of a matrix or a vector
$(')$	denotes the transpose of a matrix or a vector

CHAPTER 1

INTRODUCTION, LITERATURE SURVEY AND OBJECTIVES

1.1 GENERAL

A heavy vehicle moving on a road represents a complex vibratory system. Heavy vehicles, specifically those having tractor-semitrailer configuration have a substantially different ride performance as compared to passenger cars. This is primarily due to the vast increase in mass and inertia of coupled dynamic vibrating systems. The ride vibration levels associated with articulted vehicles have been found to be 9 to 16 times greater than the passenger cars [9]. Most heavy vehicle drivers are exposed to ride vibration for approximately 10 hours a day during driving, and perhaps an additional 10 or more hours a day as passengers, if they are employed in sleeper line-dual operations. In view of such prolonged exposure and high levels of vibration, the ride comfort of heavy vehicles has drawn significant attention from various articulated vehicle dynamicists.

The study of ride quality of heavy vehicles requires an assessment of the vehicle response to various ride influencing parameters such as road roughness characteristics, vehicle speed, vehicle configuration, etc. Experimental testing of heavy vehicles on a road as well as

in laboratory are very expensive and tedious due to the difficulties encountered in isolating the effect of a particular parameter, and to determine its influence on the vehicle response. Alternatively, theoretical study of the vehicle ride behaviour becomes a practical approach, provided that the mathematical model of the vehicle can realistically represent the actual structure, and the road roughness can be accurately modelled so as to describe its random nature. Consequently, the significant parameters affecting the vehicle ride quality can be isolated and studied using a particular mathematical techniques. These analytical techniques can be used in performing design trade-off studies of vehicle system components, highlighting new concepts, and comparing alternate approaches.

The ride motion, which represents the vibartory activities of the vehicle subject to road surface irregularities, have been predicted using complex multi-degrees-of-freedom, linear as well as nonlinear mathematical models. The ride motion are obtained using either simulation technique or analytical techniques.

1.2 REVIEW OF PREVIOUS INVESTIGATIONS

A review of relevant literature is presented in the following subsections, grouped in sequence so as to develop the scope of the thesis.

1.2.1 ARTICULATED VEHICLE MODELLING

A number of articulated vehicle ride models have been developed with varying degrees of complexities depending upon the objectives of the individual investigation. Although secondary suspensions, such as suspension at cab and suspension at the seat significantly influence the ride dynamics of heavy vehicles, most investigators of articulated vehicle dynamics have considered the cab, engines and tractor chassis as one rigid body model. The semitrailer with its chassis has been also treated as a single rigid body model. Both units are allowed to translate in the fore-aft and vertical directions, and to pitch except as constrained by the fifth wheel.

Ellis [19] developed a three-degrees-of-freedom model incorporating bounce and pitch of the tractor, and semitrailer pitch motions. Noon [35] considered the cab motion on the tractor chassis, but neglected the axle bounce and fore-aft motions of the tractor and semitrailer. Walther et al. [57] have included the bounce motion of the unsprung mass of each wheel and axle assembly, but ignored the fore-aft motions of the tractor and semitrailer. They modelled the fifth wheel as a high rate spring.

A most comprehensive model with thirty eight degrees-of-freedom for a large military tractor semi-trailer was developed by Van Deusen [55]. Tractor frame was modelled as

twelve concentrated mass elements interconnected by beam to reflect the varying sectional properties. Each beam element was represented by two degrees-of-freedom incorporating bounce and pitch motions. Each of the tractor front and rear bogies was modelled having three degrees-of-freedom. The rotational motion of the bogie action is represented by a rigid beam element which has the proper inertial characteristics to represent the rotation of the entire bogie assembly on a frictionless pivot point. The unsprung mass of the wheel and axle assembly was then represented by two point masses having vertical translational freedom only. The cab was modeled as a rigid assembly having two degrees-of-freedom on a flexible cab mounts and the driver and seat assembly was modelled as a single degree-of-freedom system attached to the cab frame. The semitrailer was modelled in five degrees-of-freedom having bounce and pitch of the rigid semitrailer body with pitching motion of the walking beam assembly of its two front axles, and the bounce motions of the unsprung masses of its two rear axles.

Allan et al. [1] developed a three-dimensional mathematical model having nineteen degrees-of-freedom. The model described the longitudinal, vertical, lateral, pitching, rolling, and yawing motions of the vehicle. They also developed two in-plane models of six and three degrees-of-freedom models in order to prove that the

adequate information could be obtained from a simpler model.

1.2.2 ROAD SURFACE DESCRIPTION

Roadways traversed by vehicles are assumed to be perfectly rigid and the profiles, measured under no-load condition, represent the dynamic tire disturbances. Road surface roughness is frequently so irregular that it is more satisfactorily described as a random process [10]. Thus, concept of power spectral density is used as a measure of randomly irregular road surface roughness. Macaulay [32], and Walls et al. [56] described techniques to measure and classify road profiles, which a vehicle might traverse. These techniques require digital recording of the instantaneous heights of a road profile along its stretch and from which spectral density is obtained using frequency analyzer. But, there are practical difficulties in obtaining and handling the requisite information. Moreover, a vehicle must be designed with regard to its whole service life, not simply with regard to few road tracks. Therefore, analytical techniques which are economical both in description and analysis are sought [45].

Various analytical techniques of increasing complexity have been developed to describe stochastically the road surface undulations [16,17,27,28,46]. It has been

recognized that road surface roughness is a stationary random process with Gaussian distribution. Road surface roughness can be described conveniently by a single direct spectral density function, therefore provides a road surface description which is sufficient for multi-track vehicle response analyses [16,17].

Although random road roughness characterized by spectral density function is one of the most convenient form for simulating linear systems, the simulation of nonlinear systems requires real time displacement and velocity excitations. A number of methods have been devised for generating time histories whose spectra are replica of some given spectra [25,30,33,54]. Most conveniently, the frequency spectrum can be represented by summation of several harmonics corresponding to discrete frequencies [30,37].

1.2.3 ANALYTICAL STUDIES

Computer simulation using an analytical road vehicle model has become an important tool for evaluating the ride and handling characteristics of road vehicles. Analytical articulated vehicle ride models, primarily include rigid body representation of vehicle body, linear or nonlinear primary suspension and tire models, and highway roughness charaterization. The dynamic response analysis of such vehicles is often analyzed using linear suspension and tire

models, while the nonlinearities resulting from the dry friction in suspension elements, the characteristics of shock absorber, suspension stops, and the separation of tires from the road surface are neglected.

The linear equations of motion describing the dynamic behaviour of an articulated vehicle have been written for vehicle models ranging from a simple, three degrees of freedom model [19] to a complex thirty eight degrees-of-freedom model [55]. The linear analysis allows computation of the vehicle response in the frequency domain using transfer function which provides a clear and concise description of the system behaviour. ElMadany et al. [22] have utilized a frequency response analysis to obtain the optimum suspension of an articulated vehicle. By minimization of peak acceleration value of the cab, Walther et al. [57] compared the theoretical frequency response analysis to an experimental investigation. The experimental results showed only marginal verification of the theoretical results. Van Deusen [55] analyzed a linear model of thirty eight degrees of freedom in the frequency domain. The comparison of theoretical results with experimental data showed relatively good correlation. ElMadany [21] investigated the ride quality of a tractor-semitrailer vehicle travelling over a random road surface. Applying a stationary random input to the vehicle and using the frequency domain technique, he demonstrated the manner

in which the ride quality and ride safety are affected by suspension spring and damping characteristics, tire spring characteristics, and vehicle speed.

Since linear systems are relatively easier to analyze than nonlinear ones, preliminary performance evaluations and parametric sensitivity analyses can be efficiently carried out using the linear analytical tools. Linear approximation of nonlinear suspension elements may be considered appropriate for systems subjected to small disturbances (linear range), while the associated effects of nonlinearities are of second order. In situation where a more complete understanding of the qualitative and quantitative behaviour of the tractor-semitrailer vehicle is required, it is often necessary to include nonlinear effects.

Direct integration techniques have been employed to simulate nonlinear vehicle models of varying complexities. Nonlinear vehicle models of varying complexities have been analyzed by Potts et al. [36], Donati et al. [18], Dailey et al. [15], and Van Deusen [55] using direct integration computer simulations. Using an analogue computer, Metcalf [34] studied the ride behaviour of a three-element vehicle with nonlinear suspension. While such simulation techniques are quite adequate for evaluating the dynamic response characteristics of nonlinear vehicle models, high computing

costs and complexities in data interpretation and data reduction pose a severe limitation on feasibilty of such simulation techniques. Alternatively, the nonlinear suspension elements in the vehicle model are replaced by an equivalent suspension system with linear characteristics, such that convenient analytical tools may be employed to predict the response behaviour of nonlinear vehicle models. Equivalent linear suspension elements are selected such that the response behaviour of the equivalent linear system does not deviate significantly from the response behaviour of the nonlinear system. The equivalent linearization techniques, usually attributed to Bootan [11], Caughey [13], and Krylov et al. [29] have been extensively used for simulation of nonlinear dynamical systems. ElMadany employed an equivalent linearization technique to study the dynamic response of a nonlinear articulated vehicle subjected to random road surface undulations [23]. Nonlinear damping mechanisms have been approximated by an equivalent viscous coefficient, using force/energy balance technique by Rakheja et al. [39,41] and Bandstra [6].

Although the equivalent linearization methods have been widely accepted as efficient simulation tools for nonlinear dynamical systems, the equivalent linear system fails to include the critical effects of dry friction and clearance spring. Scanlan [48] established that the nonlinear damping mechanisms, in general, should be expressed by a local

constant applicable only in a restricted frequency band centered around a specific frequency. Specifically, nonlinearities such as Coulomb friction can not be represented correctly by a constant coefficient over an entire frequency range. Rakheja and Sankar [39] represented the nonlinear damping mechanism by an array of local viscous constants using force and energy balance techniques. The value of local viscous constant depends upon system behaviour, nature of excitation, and properties of the nonlinear element. Each of the localized linear systems, which are formulated from this technique, exhibits the response behaviour of original nonlinear system quite accurately in the vicinity of the specific frequency and amplitude of excitation.

1.3 SCOPE OF THE PRESENT INVESTIGATION

The objectives of this study are :

1) To select the most appropriate candidate vehicle configuration to carry out the ride dynamics study of an articulated vehicle.
2) To develop two-dimensional and three-dimensional mathematical models for baseline vehicle.
3) To analyze the linear dynamic response of the complex articulated vehicle system to road surface undulations which are represented as stationary Gaussian random for varying road characteristics and

vehicle speed.

4) To discuss the influence of the inclusion of seat and cab suspensions on the ride. 5) To develop a nonlinear mathematical model for baseline vehicle to study the effect of the system nonlinearities on the ride behaviour of the articulated vehicle.

6) To develop an analytical technique based on local equivalent linearization approach to predict the dynamic response of the nonlinear vehicle model to road surface irregularities.

7) To carry out a parametric study of nonlinear vehicle model to establish the influence of various parameters on the articulated vehicle dynamic behaviour.

8) To assess the ride quality of the baseline articulated vehicle with reference to the ISO specified acceptable limits of ride vibrations, such as " reduced comfort boundaries ".

This thesis has six chapters presenting the results and other relevant materials of this investigations. In chapter 1, a detailed literature survey is presented.

In chapter 2, a baseline vehicle configuration is selected and two discrete, linear, time-invariant, multi-degrees-of-freedom models for the baseline vehicle are developed. The first model is two-dimensional in the

longitudinal and vertical plane with six degrees-of-freedom. The second model having 22 degrees-of-freedom is set-up in the three-dimensional coordinate system. The major assumptions associated with the model formulation are discussed. The differential equations characterizing the dynamics of both models are developed using Lagrangian formulation.

In chapter 3, a widely accepted analytical technique to describe the random road surface undulations by power spectral densities is presented. The displacment PSD are represented by the summation of harmonic components corresponding to discrete frequencies, that would represent the measured road displacement spectral densities.

In chapter 4, the dynamic response of the baseline vehicle to the road surface irregularities is investigated using two- and three-dimensional models. The power spectral density approach is utilized to solve the stochastically described linear differential equations. The ride levels at driver-seat interface are compared to ISO specified acceptable levels of vibration to evaluate the vehicle ride quality. A comparison between the results obtained from two dimensional and three dimensional studies is carried out to show the effect of the inclusion of seat-cab dynamics in the analysis.

In chapter 5, the dynamic response of the articulated

vehicle traversing over random road surface undulations is investigated in-depth by means of nonlinear analysis. An in-plane articulated vehicle model, comprising of nonlinear damping mechanisms is developed. Various techniques for solving the stochastically described nonlinear equations of motion are briefly summarized. A technique based on local equivalent linearization approach is adapted and further developed to study the stationary response of nonlinear articulated vehicle model. The transmissibility characteristics of the linear equivalent system are obtained and compared with the transmissiblity characteristics of the nonlinear system, obtained through numerical integration technique. The accuracy of the local equivalent linearization technique is also compared with the statistical linearization technique. Finally, a parametric study of the nonlinear vehicle model is carried out to study the effect of various ride influencing factors such as vehicle suspension elements, load pattern, vehicle speed, road characteristics etc.

The conclusions and recommendations for future work are presented in chapter 6.

CHAPTER 2

SELECTION OF BASELINE HEAVY VEHICLE AND MODELLING

2.1 INTRODUCTION

A large variety of different heavy vehicles, tractor-semitrailer configurations operate on North American highways. The selection of most appropriate candidate vehicle configuration to carry out the proposed study is based on its popularity among users. The selected vehicle configuration is then referred to as the " Baseline Vehicle Configuration. "

Mathematical modelling of baseline vehicle is the first and major task in the study on ride dynamics. Modelling involves distribution of vehicle physical characteristics, and road profile excitations. Assumptions made in the modelling process could significantly influence the outcomes of analyses.

A number of heavy vehicle ride models have been developed with varying degrees of complexities depending upon the objectives of the individual investigation. Ellis [19] investigated the vehicle ride through a three degrees-of-freedom model incorporating bounce and pitch of the tractor, and semitrailer pitch motions. A mathematical model, consisting of 38 degrees-of-freedom, for a large military tractor-semitrailer was investigated by VanDeusen

[55]. Allan et al. [1] developed a three-dimensional mathematical model having nineteen degrees-of-freedom. Much of the pioneering work in the assesment of ride quality of heavy vehicles has been directed towards understanding the influence of various factors on ride, using essentially rigid body models. Through these investigations, it has been demonstrated that ride quality at driver's platform is influenced by a number of factors, namely : highway profile, tires, cargo, primary suspensions, vehicle geometry, driver location, driveline vibrations, rigid body models of the vehicle, etc.

Although secondary suspensions, such as suspension at the cab and suspension at the seat significantly influence the ride dynamics of heavy vehicles, most investigators of heavy vehicle dynamics have considered the seat, cab along with engine and tractor chassis as one rigid body. The semitrailer with its chassis has been treated similarly. Both units are allowed to translate in the fore-aft, vertical, and lateral directions, and pitch, roll, and yaw except as constrained by the fifth wheel.

In this chapter, a baseline vehicle configuration is selected and two discrete, linear, time-invariant, multi degrees-of-freedom models for the baseline vehicle are developed. The first model is two-dimensional in the longitudinal and vertical plane having longitudinal,

bounce, and pitching motions. The second model is three-dimensional having longitudinal, lateral, vertical, pitch, and roll coordinates of motion. Equations of motion for both models are developed using Lagrangian formulation. The following assumptions are made in the modelling process of both models:

1. Vehicle moves forward at a constant speed.
2. The sprung masses, tractor, and semitrailer behave as rigid bodies.
3. All suspension units and tires are modelled as linear spring and viscous dampers.
4. Both primary and secondary suspensions are constrained to translate in the vertical direction only with small motions.
5. Road is assumed to be a rigid surface with equal roughness on left and right tracks.
6. Input profile in vertical direction is considered to be applied to the vehicle through the tire contact points.

2.2 SELECTION OF BASELINE VEHICLE

The schematics of different tractor-semitrailer configurations operating across Canada and U.S.A. are presented in Figure 2.1. These variations have been determined by the local geography, the permissible sizes to protect public investments in the construction of roads,

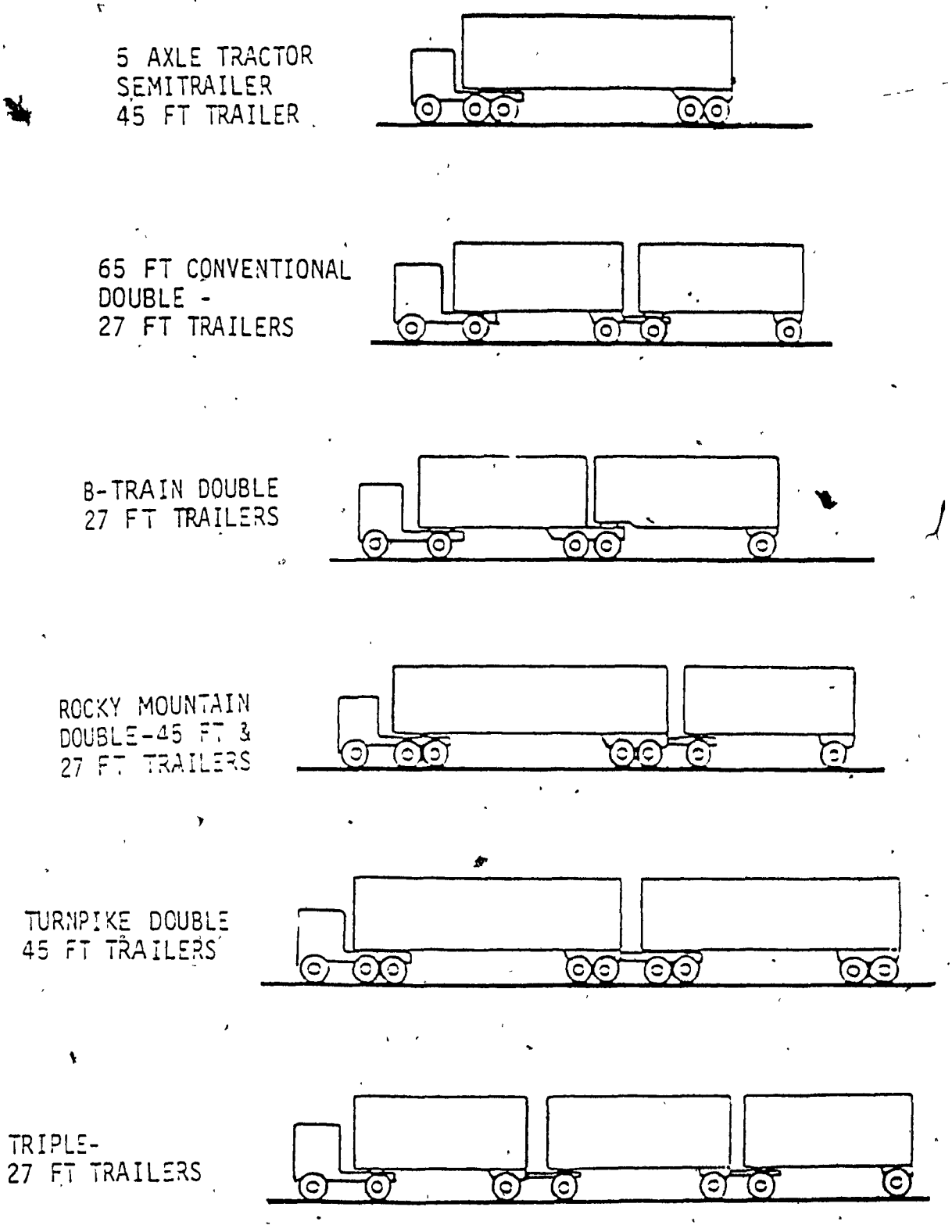

FIGURE 2.1: Configuration of commercial vehicles [9]

bridges, and tunnels. Vehicle sizes have been limited by the capacities of bridges, tunnels, and overhead signs.

The selection of baseline vehicle is based on the surveys conducted by RTAC (Road and Transport Association of Canada) [24]. Findings of the survey (Table 2.1) reports that a tractor-semitrailer type of vehicle (3-axle tractor and 2-axle semitrailer) is most commonly used on the Canadian Highways. Thus, a tractor-semitrailer type of vehicle qualifies as the most appropriate candidate vehicle to carry out the proposed study.

The set of parameters data covering the weights and dimensions of the baseline vehicle is constructed with refernce to the maximum axle loads allowed in the majority of the provinces and is presented in Figure 2.2 [24]. Further, the baseline vehicle incorporates a typical 5.5-tonnes (12,000-lb) steering axle suspension and a Hendrickson RTE-380 tandem suspension on the tractor, with Reyco 21-B suspension on trailer. The baseline vehicle is also represented with Michelin XZA 11R22.5/G tires.

2.3 DEVELOPMENT OF MATHEMATICAL MODELS FOR THE BASELINE VEHICLE

2.3.1 TWO-DIMENSIONAL (IN-PLANE) MODEL

The in-plane model of the baseline vehicle is

TABLE 2.1 [24]

% Distribution of All Combination Trucks in Each Region

Meeting Sites

Vehicle	Vancouver	Calgary	Winnipeg	Toronto	Montreal	Moncton
Tr/Semi	60	80	60	70	90	98
A-Dbls.	32	8	25	25	8	1
B-Dbls.	8	10	14	5	2	1
C-Dbls.	0	<2	<1	<1	<1	0
Triples	0	<1	<1	0	<1	0
Total	100	100	100	100	100	100

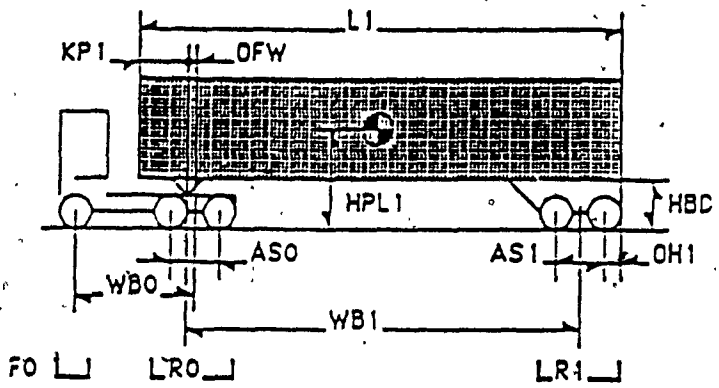

Weights:	Tonnes	(k-lbs)	Axle Loads:	Tonnes	(k-lbs)
Tractor tare	8.2	(18.0)	F0	5.5	(12.1)
Trailer Tare	6.3	(13.9)	R0	17.0	(37.5)
Payload	25.0	(55.1)	R1	17.0	(37.5)
GCW	39.5	(87.1)			

Tractor Dimensions:		meters	(inches)
WB0	Wheelbase	4.83	(190)
AS0	Tandem Spread	1.52	(60)
OFW	Fifth Wheel Offset	0.41	(15)

Trailer Dimensions:		meters	(inches)
WB1	Wheelbase	12.34	(486)
AS1	Tandem Spread	1.22	(48)
KP1	Kingpin Setback	0.91	(36)
L1	Bed/Van Length	14.63	(576)
OH1	Rear Overhang	0.76	(30)
HPL1	Payload C.G. Height	2.00	(79)
HBD	Bed Floor Height	1.37	(54)

Tires: Michelin XZA 11.00R22.5-G, full tread depth, @ 689.5 kPa (100 psi).

FIGURE 2.2: Baseline configuration of Tractor-Semitrailer [24]

illustrated in Figure 2.3. This model is seen to be two-dimensional in the longitudinal and vertical plane. The model, based on five axle baseline vehicle configuration has one axle in the front, two in the tractor rear, and two semitrailer axles. Each of all three wheel and axle assemblies is represented by a lumped unsprung mass having vertical translational freedom only. The tires are modelled as systems having vertical spring and damping characteristics.

The dynamics due to seat and cab suspensions is neglected, and therefore seat, cab, engine and tractor chassis are considered as one rigid body. Semitrailer with its chassis is also considered as one rigid body. Both units are allowed to translate in the longitudinal and vertical directions and to pitch except as constrained by the fifth wheel.

By considering the kinematic constraints imposed by the fifth wheel on the motion of the tractor and semitrailer, the model includes seven degrees of freedom. In addition, dynamic force balance in the longitudinal direction provides a relationship for tractor fore-aft motion in terms of pitch coordinates. Therefore, the total degrees of freedom for the vehicle model are expressed by the remaining six generalized coordinates. The constraint equations for this model are given in Appendix I. The

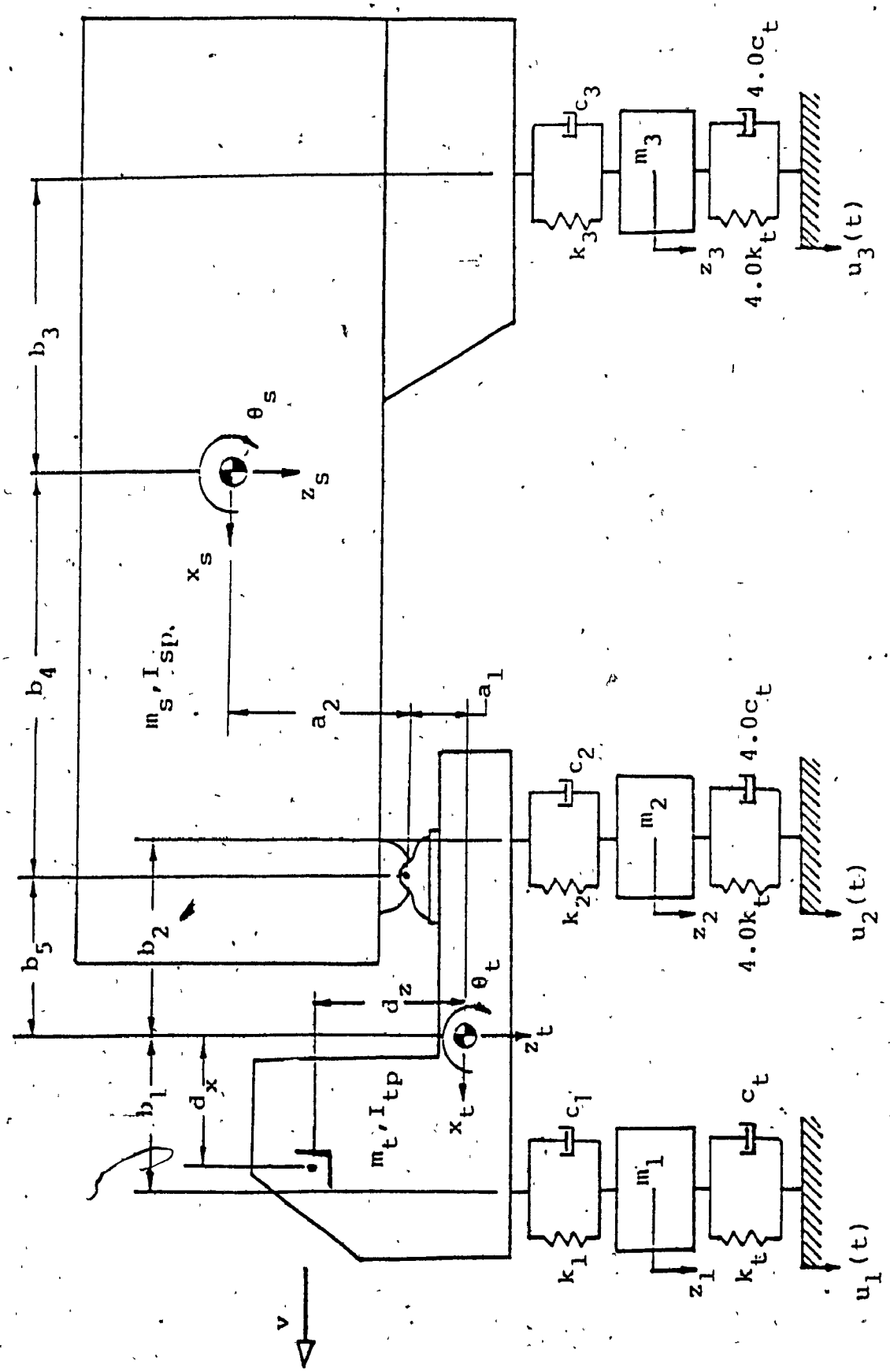

FIGURE 2.3: Schematic representation of linear, two-dimensional baseline vehicle model

generalized coordinates of the in-plane model are presented in Table 2.2.

The vehicle parameters for the in-plane model, as derived from the baseline vehicle configuration (Figure 2.2) is presented in Table 2.3.

2.3.2 THREE-DIMENSIONAL MODEL

The three-dimensional model of the baseline vehicle is illustrated in Figure 2.4. The side view is seen in the longitudinal and vertical planes, and front and rear views are illustrated in the lateral and vertical planes respectively.

The unsprung mass at tractor front wheels and axle assembly is divided into two equal masses, with one on each side of the vehicle, and are connected by a rigid link of negligible mass. This model has three degrees of freedom ; vertical translation of each mass and lateral translation of the whole assembly. The two rear wheels and axle assemblies of both tractor and semitrailer are modelled as walking beams. In each case, the combined unsprung mass of both assemblies is split into four equal masses, with two masses on each side of the vehicle, which are linked through two longitudinal rigid links and a laterally oriented 'torsional' link at the tandem center. The walking beam assembly is allowed to have lateral translational

TABLE 2.2

GENERALIZED CO-ORDINATES OF TWO-DIMENSIONAL BASELINE VEHICLE MODEL

Co-ordinate	Description of Motion at	Symbol
Bounce	Tractor	z_t
	Tractor front axle	z_1
	Tractor rear axle	z_2
	Semitrailer axle	z_3
Pitch	Tractor	θ_t
	Semitrailer	θ_s

TABLE 2.3

BASELINE VALUES FOR TWO-DIMENSIONAL VEHICLE MODEL [4,24,40]

I. General

(a) Tractor

Sprung Mass (m_t)	5350 kg
Pitch Moment of Inertia (I_{tp})	20847 kg.m^2
Front Unsprung Mass (m_1)	544 kg
Rear Unsprung Mass (m_2)	2268 kg

(b) Semitrailer

Sprung Mass (m_s)	29926 kg
Pitch Moment of Inertia (I_{sp})	573040 kg.m^2
Unsprung Mass (m_3)	1360 kg

II. Suspension Characteristics

Tractor Front :	k_1	310204 (N/m)	c_1	14980	(Ns/m)
Tractor Rear :	k_2	2626772 (N/m)	c_2	55230	(Ns/m)
Semitrailer :	k_3	2977008 (N/m)	c_3	54480	(Ns/m)

III. Dual-Lumped Tire Model Characteristics

k_t	1728416 (N/m)	c_t	500	(Ns/m)

IV. Dimensions

Fifth wheel height from Tractor c.g., (a_1)	0.20 (m)
Semitrailer c.g. height from fifth wheel, (a_2)	0.74 (m)
Tractor c.g. to front axle, (b_1)	1.50 (m)
Tractor c.g. to rear axle, (b_2)	3.33 (m)
Semitrailer c.g. to its axle, (b_3)	5.89 (m)
Semitrailer c.g. to fifth wheel, (b_4)	6.45 (m)
Tractor c.g. to fifth wheel, (b_5)	2.92 (m)

Seat location from Tractor c.g.:

d_x	1.74 (m)	d_z	0.77(m)

V. Vehicle Speed

v	90 (km/h)

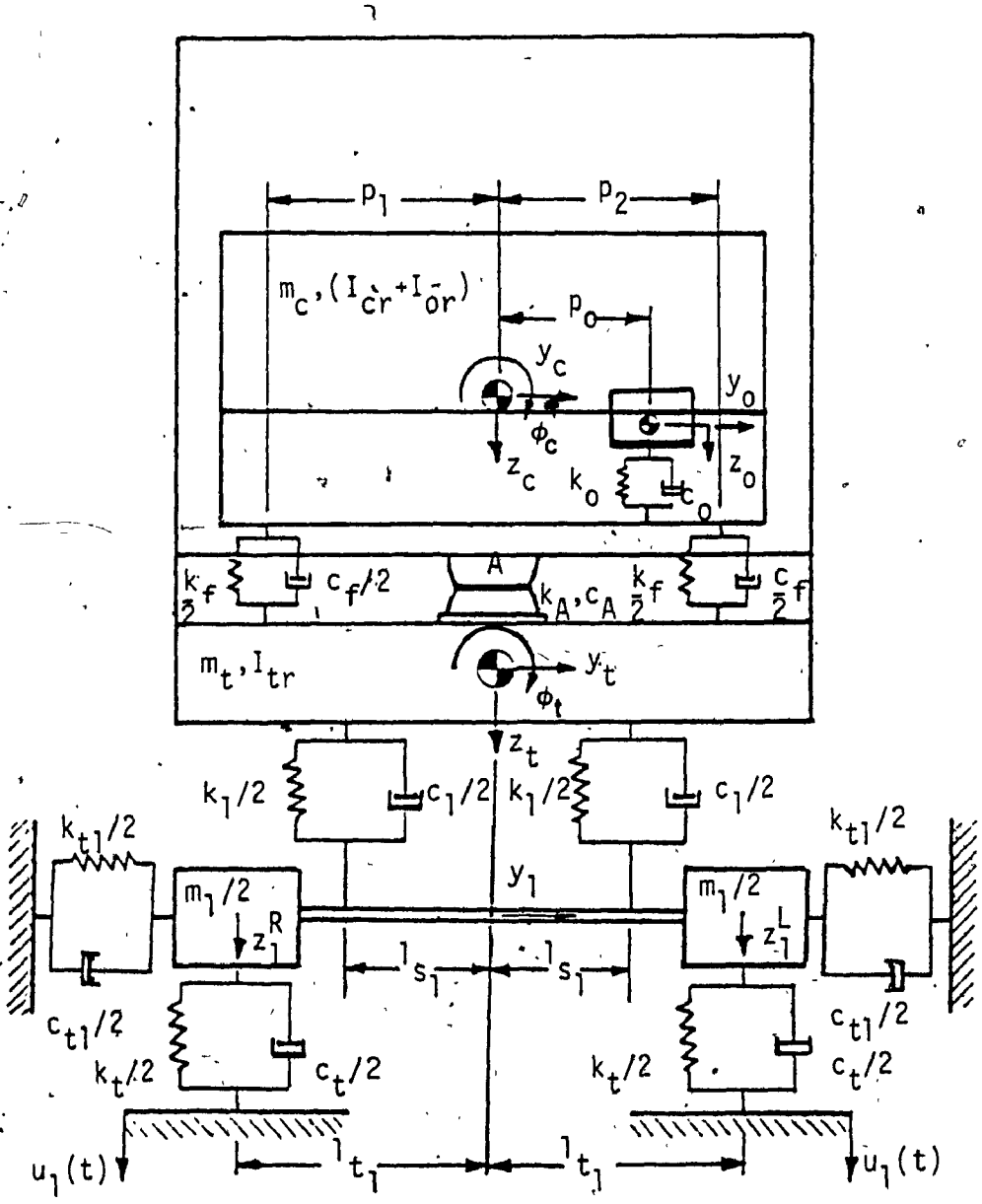

FIGURE 2.4a: Schematic representation of linear, three-dimensional baseline vehicle model - front view

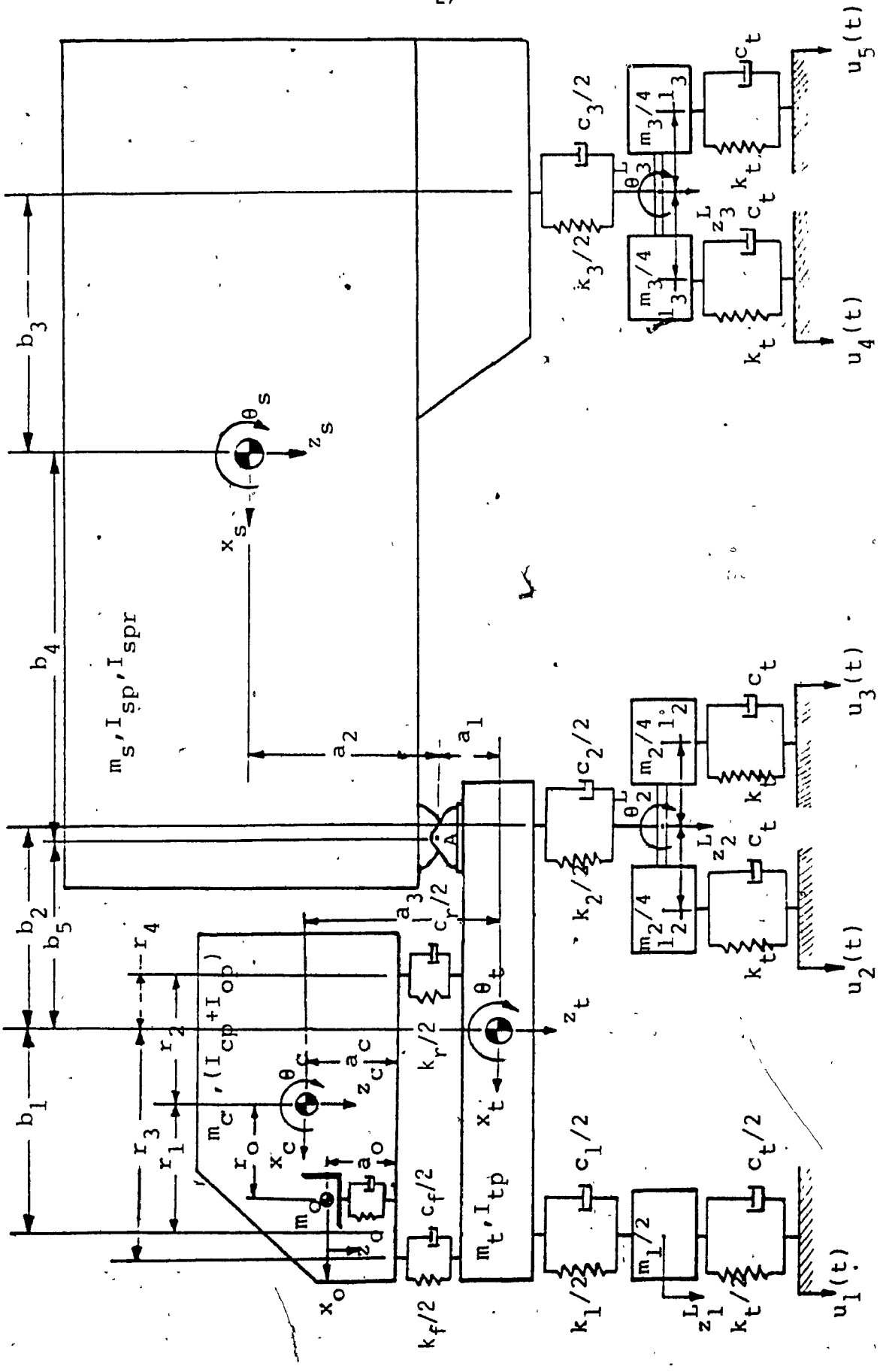

FIGURE 2.4b: Schematic representation of linear, three-dimensional baseline vehicle model - side view

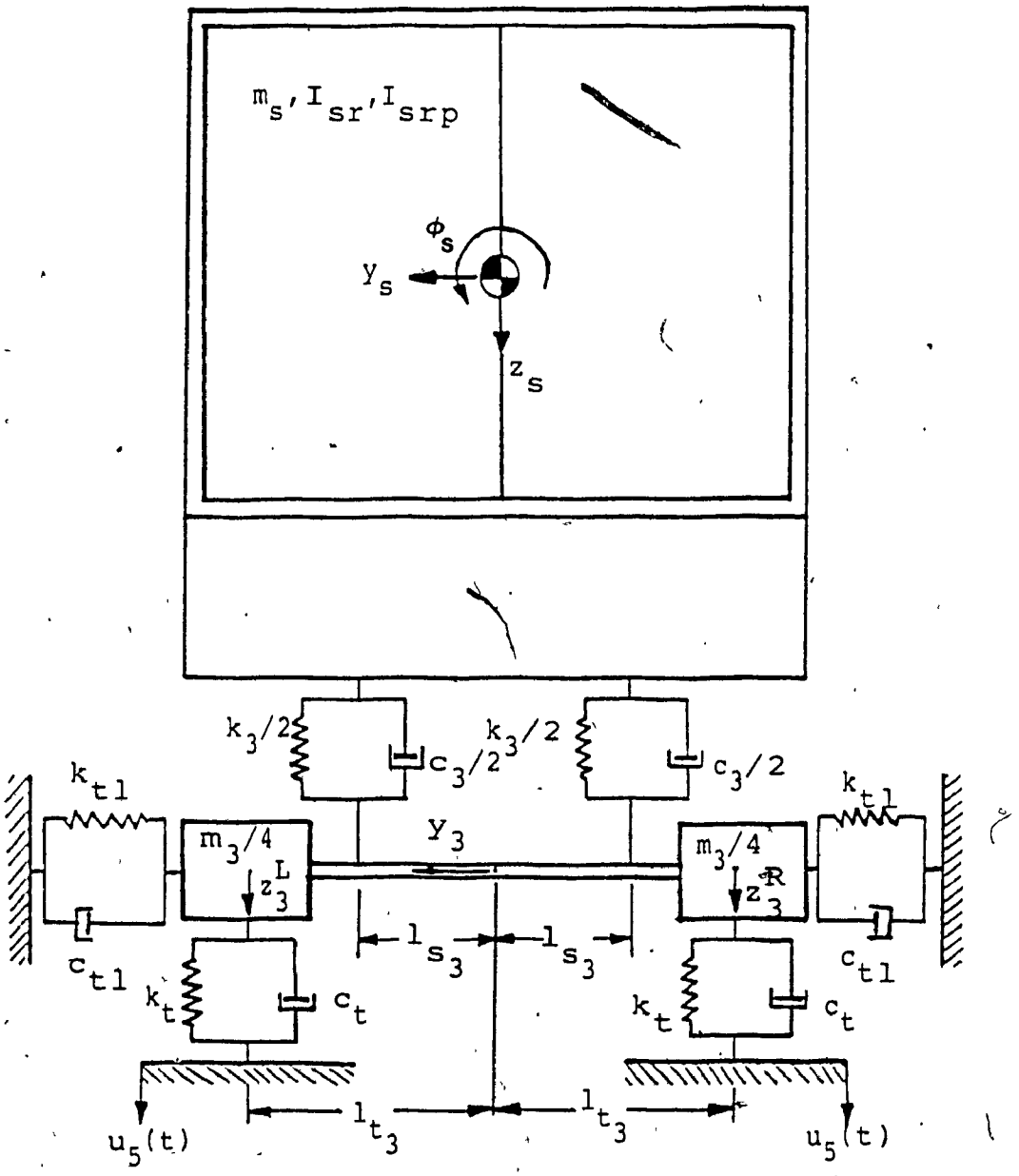

FIGURE 2.4c: Schematic representation of linear, three -dimensional baseline vehicle model - back view

freedom, and bounce and pitching motions about tandem center on each side of the vehicle. The axle assemblies are connected to the vehicle by two suspension units, with one at each end of the axle. The tires are represented to have vertical and lateral spring and damping characteristics.

The driver and seat assembly is attached to the cab frame through a flexible mount, while the cab is modelled as a rigid body mounted on flexible cab mounts at all four corners, and attached to the rigid assembly of engine and tractor chassis. The semitrailer along with its chassis is also assumed to be a rigid body. The fifth wheel connection between tractor and semitrailer units is modelled as a linear, stiff, torsional spring in the longitudinal direction, which allows a small relative roll motion between both units.

In addition to three translational degrees-of-freedom for the seat, cab, tractor and semitrailer, latter three units are also allowed to roll and pitch. Therefore, there are a total of 31 coordinates describing the motion of the vehicle as illustrated in Figure 2.4. By considering the dynamic force balance in the longitudinal direction, kinematic constraints imposed by the fifth wheel on the motion of the tractor and semitrailer, and expressing the longitudinal and lateral motions of seat and cab in terms of tractor motions, the vehicle model can be reduced to 23

degrees-of-freedom. In addition, the lateral motion of the tractor c.g. is expressed in terms of lateral translations of tractor front and rear axles. Therefore, the total degrees-of-freedom for the vehicle model are expressed by the remaining 22 generalized coordinates.

The constraint equations are given in Appendix II. The generalized coordinates and baseline values for three-dimensional vehicle model are presented in Tables 2.4 and 2.5 respectively.

2.3.3 EQUATIONS OF MOTION FOR TWO- AND THREE-DIMENSIONAL MODELS

Assuming small perturbations relative to the overall dimension, expressions for the kinetic and potential energies, and dissipation function are developed from physical and geometric characteristics of each model. The energy functions are given by the following expressions [53] :

Kinetic energy :

$$T = \frac{1}{2} \{\dot{q}\}' [M] \{\dot{q}\} \qquad (2.1)$$

Potential energy :

$$V = \frac{1}{2} \{q\}' [K] \{q\} \qquad (2.2)$$

TABLE 2.4

GENERALIZED CO-ORDINATES OF THREE-DIMENSIONAL BASELINE VEHICLE MODEL

Co-ordinate	Description of Motion at	Symbol
Bounce	Seat	z_o
	Cab	z_c
	Tractor	z_t
	Tractor front axle	z_1^{*L} , z_1^{**R}
	Tractor rear axle	z_2^L , z_2^R
	Semitrailer axle	z_3^L , z_3^R
Lateral	Tractor front axle	y_1
	Tractor rear axle	y_2
	Semitrailer axle	y_3
Pitch	Cab	θ_c
	Tractor	θ_t
	Semitrailer	θ_s
	Tractor rear axle	θ_2^{*L} θ_2^{**R}
	Semitrailer axle	θ_3^L θ_3^R
Roll	Cab	ϕ_c
	Tractor	ϕ_t
	Semitrailer	ϕ_s

(*L : Left side of the axle ; **R : Right side of the axle)

TABLE 2.5

BASELINE VALUES FOR THREE-DIMENSIONAL VEHICLE MODEL [4,24,40]

I.	General	
	(a) Driver and Seat (5/7 of the driver mass)	
	Mass (m_o)	70 kg
	Roll Moment of Inertia (I_{or})	25 kg.m^2
	Pitch Moment of Inertia (I_{op})	60 kg.m^2
	(b) Cab	
	Mass (m_c)	1360 kg
	Roll Moment of Inertia (I_{cr})	640 kg.m^2
	Pitch Moment of Inertia (I_{cp})	875 kg.m^2
	(c) Tractor	
	Sprung Mass (m_t)	3920 kg
	Roll Moment of Inertia (I_{tr})	6727 kg.m^2
	Pitch Moment of Inertia (I_{tp})	19912 kg.m^2
	Front Unsprung Mass (m_1)	544 kg
	Rear Unsprung Mass (m_2)	2268 kg
	Tandem Axle Pitch Moment of Inertia (I_2)	600 kg.m^2
	(d) Semitrailer	
	Sprung Mass (m_s)	29926 kg
	Roll Moment of Inertia (I_{sr})	91686 kg.m^2
	Pitch Moment of Inertia (I_{sp})	573040 kg.m^2
	Roll-Pitch and Pitch-Roll Moments of Inertia ($I_{srp} = I_{spr}$)	1146 kg.m^2

(Table 2.5 cont'd)

Unsprung Mass (m_3)	1360 kg
Tandem Axle Pitch Moment of Inertia (I_3)	600 kg.m^2

II. Suspensions Characteristics

(a) Primary Suspensions

Tractor Front	: k_1	310204 (N/m)	c_1	14980	(Ns/m)
Tractor Rear	: k_2	2626772 (N/m)	c_2	55230	(Ns/m)
Semitrailer	: k_3	2977008 (N/m)	c_3	54480	(Ns/m)

(b) Secondary Suspensions

Seat	: k_o	20000 (N/m)	c_o	100	(Ns/m)
Cab Front	: k_f	225000 (N/m)	c_f	200	(Ns/m)
Cab Rear	: k_r	138488 (N/m)	c_r	200	(Ns/m)

III. Dual-Lumped Tire Model Characteristics

Vertical	: k_t	1728416 (N/m)	c_t	500	(Ns/m)
Lateral	: k_{tl}	1751181 (N/m)	c_{tl}	500	(Ns/m)

IV. Tandem Axle Torsion Parameters

Tractor	: k_{tn2}	381308 (Nm/rad)
Semitrailer	: k_{tn3}	28830 (Nm/rad)

V. Articulation Roll Parameters

k_A	6473708 (Nm/rad)	c_A	148	(Nms/rad)

VI. Dimensions

(a) Longitudinal

Tractor c.g. to front axle, (b_1)	1.90 (m)
Tractor c.g. to rear tandem axle center, (b_2)	2.93 (m)
Semitrailer c.g. to its axle, (b_3)	5.89 (m)
Semitrailer c.g. to fifth wheel, (b_4)	6.45 (m)

(Table 2.5 cont'd)

Tractor c.g. to fifth wheel, (b_5)	2.52 (m)
Seat c.g. to Cab c.g., (r_o)	0.27 (m)
Cab c.g. to Cab front mounts, (r_1)	1.10 (m)
Cab c.g. to Cab rear mounts, (r_2)	1.05 (m)
Tractor c.g. to Cab front mounts, (r_3)	2.57 (m)
Tractor c.g. to Cab rear mounts, (r_4)	-0.42 (m)
Tractor axle spacing, (l_2)	0.76 (m)
Semitrailer axle spacing, (l_3)	0.61 (m)
(b) Lateral	
Seat c.g. to Cab c.g., (p_o)	0.76 (m)
Cab c.g. to cab left mounts, (p_1)	0.53 (m)
Cab c.g. to cab right mounts, (p_2)	0.57 (m)
Front suspension spacing, ($2l_{s_1}$)	0.41 (m)
Rear suspension spacing, ($2l_{s_2}$)	0.56 (m)
Semitrailer suspension spacing, ($2l_{s_3}$)	0.56 (m)
Front Tires track width, ($2l_{t_1}$)	1.02 (m)
Rear Tires track width, ($2l_{t_2}$)	0.99 (m)
Semitrailer Tires track width, ($2l_{t_3}$)	0.99 (m)
(c) Vertical	
Seat c.g. height from Cab floor, (a_o)	0.49 (m)
Cab c.g. height from Cab floor, (a_c)	0.30 (m)
Fifth wheel height from Tractor c.g., (a_1)	0.20 (m)
Semitrailer c.g. height from fifth wheel, (a_2)	0.74 (m)
Cab c.g. height from Tractor c.g., (a_3)	0.58 (m)
VII. Vehicle Speed, v	90 (km/h)

Dissipation function :

$$D = \frac{1}{2} \{\dot{q}\}' [C] \{\dot{q}\} \qquad (2.3)$$

where,

[M] is the mass matrix or equally well a combination of masses and moments of inertia.

[K] is the stiffness matrix.

[C] is the linear or viscous damping matrix.

$\{q\}$ is the set of independent generalized coordinates (Tables 2.2 and 2.4), which completely specify the configuration of the system and is measured from the equilibrium condition.

$\{\dot{q}\}$ is the time derivative of generalized coordinate vector.

Using the Lagrange's equation given by,

$$\frac{d}{dt}\left(\frac{\partial T}{\partial \dot{q}_i}\right) + \left(\frac{\partial D}{\partial \dot{q}_i}\right) + \left(\frac{\partial V}{\partial q_i}\right) = 0 \qquad (2.4)$$

a set of simultaneous, non-homogeneous, second order differential equations with constant coefficients is obtained. The differential equations of motion are presented in the following form.

$$[M] \{\ddot{q}\} + [C] \{\dot{q}\} + [K] \{q\} = [C_F] \{\dot{u}\} + [K_F] \{u\} \qquad (2.5)$$

where, $[C_F]$ and $[K_F]$ are the forced damping and stiffness matrices, respectively. $\{u\}$ and $\{\dot{u}\}$ are the column vectors

of excitation displacements and velocities, respectively.

A complete description of matrices representing equations of motion of two- and three-dimensional baseline vehicle models is presented in Appendices I and II, respectively.

2.4 SUMMARY

In this chapter, a baseline vehicle configuration is selected and two discrete, linear, time-invariant, multi-degrees-of-freedom models for the baseline vehicle are developed. The first model is two-dimensional in the longitudinal and vertical plane with six degrees-of-freedom. The second model having 22 degrees-of-freedom is set up in the three-dimensional coordinate system. The differential equations characterizing the motion of both vehicle models are developed using Lagrangian formulation. In the following chapter, road surface roughness irregularities, which will form the input forcing function to the vehicle models, are discussed.

CHAPTER 3

ROAD SURFACE DESCRIPTION

3.1 INTRODUCTION

Road surface description is an important part of ride quality evaluation of a heavy vehicle. A multi-axle vehicle traversing on a roadway is subjected to displacement inputs at all of its road-wheel contact points. Consequently, a complete description of the road surface is sought to describe adequately the displacement imposed at each wheel and all correlations between the displacements.

Roadways traversed by vehicles are assumed to be perfectly rigid and the profiles, measured under no-load condition, represent the dynamic tire disturbances. Since road surface roughness is irregular, it is more satisfactorily described as a random process [10]. Thus, concept of power spectral density is used to describe the randomly irregular road surface roughness. Various analytical techniques of increasing complexity have been developed to describe stochastically the road surface undulations [16,17,28,46].

Linear analysis of a vehicle model requires displacement power spectral densities (PSD's) and cross spectral densities (CSD's) between all inputs. Real time displacements and velocities are needed for response

simulation of a nonlinear vehicle model. In this chapter, a widely accepted analytical description for different types of roadways in the form of spectra, is given. A convenient method to generate input random time-histories, as required for the simulation of nonlinear vehicle model, is presented.

3.2 STOCHASTIC DESCRIPTION OF ROAD SURFACE ROUGHNESS

It has been shown on the basis of a very large number of road profile measurements that road roughness can be described by stationary Gaussian random functions [16,17,46]. Road random disturbances, represented by their power spectral densities, thus gives an insight into road roughness distribution corresponding to various frequency components. References [16,17,28,46] have given the spectral densities that closely approximate available experimental data and proposed that road roughness can be described by a single direct spectral density function, which provides a road surface description that is sufficient for multi-wheel vehicles. The expression for the road surface roughness is given by :

$$S(n) = \begin{cases} S(n_o).(n/n_o)^{-w_1} & ; \; n \leq n_o \\ S(n_o).(n/n_o)^{-w_2} & ; \; n > n_o \end{cases} \qquad (3.1)$$

where

$S(n)$ is the spatial spectral density of the road roughness, $(m^2/(c/m))$.

$S(n_o)$ is the roughness coefficient which yields the value of the spatial spectral density at the discontinuity frequency, n_o.

n is the spatial frequency of road roughness, (c/m)

n_o is $1/(2.\pi)$, (c/m).

w_1, w_2 are road waviness.

Assuming that the vehicle moves with a constant forward velocity, v, the corresponding temporal spectral density is given by,

$$S(f) = S(n)/v \tag{3.2}$$

where, the temporal frequency, f, and the spatial frequency, n, are related to vehicle speed, v, by

$$f = v.n \tag{3.3}$$

The temporal input displacement spectral density, S(f) for a N-axle vehicle may be written as a matrix in terms of the surface profile as follows [20] :

$$[S_i(f)] = (S(n)/v) \begin{bmatrix} 1 & e^{-i\mu_{12}} & e^{-i\mu_{13}} & \cdots & e^{-i\mu_{1N}} \\ e^{i\mu_{12}} & 1 & e^{-i\mu_{23}} & \cdots & e^{-i\mu_{2N}} \\ e^{i\mu_{13}} & e^{i\mu_{23}} & 1 & \cdots & e^{-i\mu_{3N}} \\ \vdots & \vdots & \vdots & & \vdots \\ e^{i\mu_{1N}} & e^{i\mu_{2N}} & e^{i\mu_{3N}} & \cdots & 1 \end{bmatrix} \tag{3.4}$$

The diagonal elements of $[S_i(f)]$ are the the spectral densities of the road profile given by the equation (3.2).

The off-diagonal elements are the cross spectral densities, which are computed assuming that the vehicle rear wheels follow the same profile as the front wheel, but are separated by a constant time delay,

$$t_{jk} = L_{jk} / v \tag{3.5}$$

and

$$\mu_{jk} = 2\Pi f . t_{jk} \tag{3.6}$$

$$j = 1,2,.....,N \; ; \; k = 1,2,.....,N$$

where L_{jk} is the distance between axle j to axle k.

The temporal input displacement spectral density matrices for both two- and three-dimensional vehicle models are provided in Appendices I and II, respectively. It should be noted that the cross correlation between left and right road prifiles is neglected because of the road roughness on both sides are assumed to be equal.

The road surface characteristics for two different types of roadways are given in Table 3.1. Figure 3.1 gives the road spectra in m^2 /Hz for both types of roadways.

TABLE 3.1 [21]

ROAD SURFACE CHARACTERISTICS

Route	$S(n_o)$ (m^3/c)	w_1	w_2
Motorway (Smooth)	13.0×10^{-6}	2.1	1.42
Minor Road (Rough)	28.4×10^{-6}	3.3	1.48

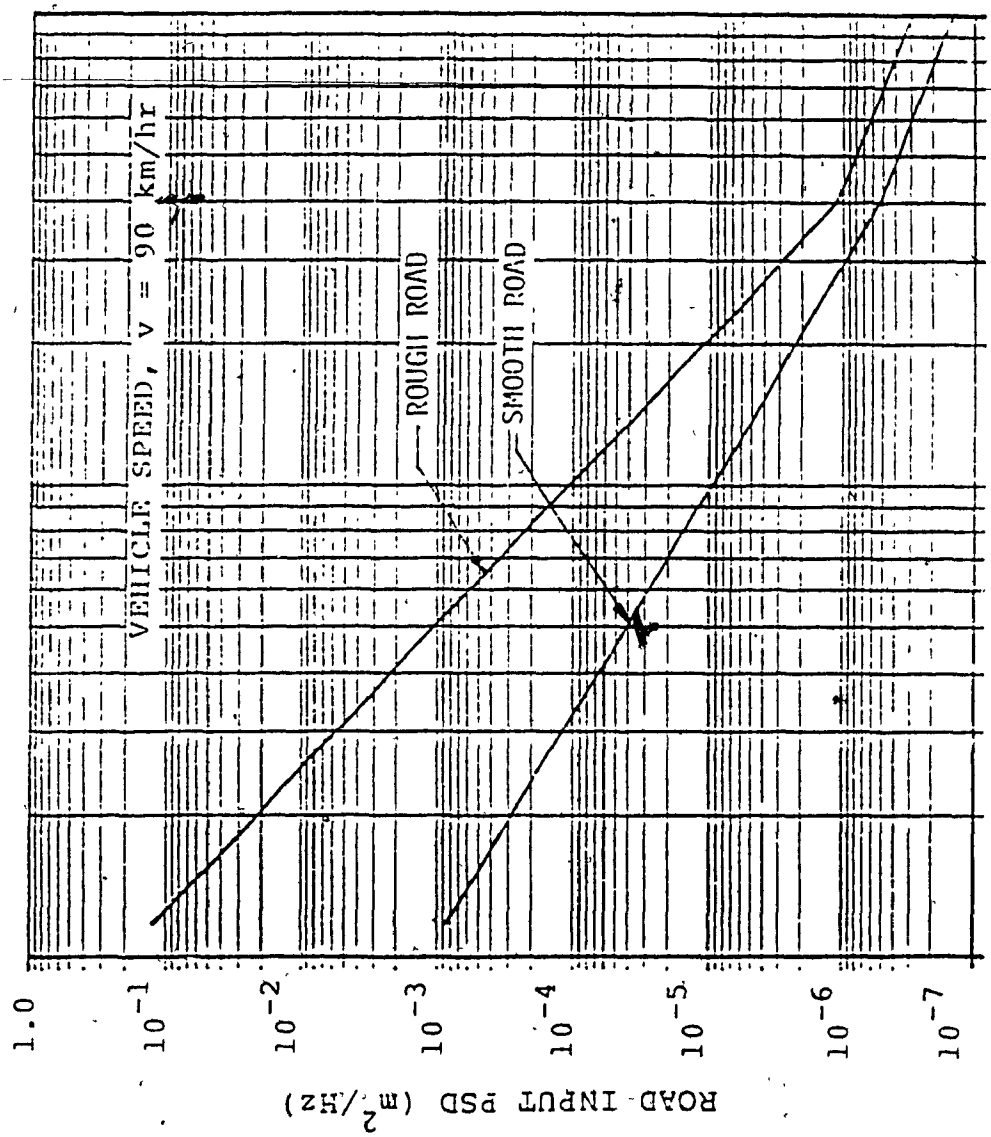

FIGURE 3.1: Road input displacement PSD - smooth and rough roads

3.3 TIME SERIES REPRESENTATION OF INPUT SPECTRAL DENSITIES

Random road disturbances characterized by PSD's are suitable for simulating linear vehicle model. Response simulation of nonlinear model requires input random time-histories. A number of methods have been developed for generating time histories whose spectra are replica of some given spectra [25,30,32,54]. The displacement time history can be represented conveniently by summing up several harmonics corresponding to discrete frequencies [30,37]. Spectral densities of this synthetically generated time-history are estimated through FFT procedure [8], which would closely follow the road roughness PSD's. The displacement time-history of the random road excitations is then expressed by,

$$x(t) = \sum_{l=1}^{N_f} (-1)^l \, A_l \sin(2\pi f_l t) \qquad (3.7)$$

where

$x(t)$ is the displacement time history, whose spectra is replica of road roughness PSD's.

N_f is the total number of discrete frequencies required to describe the frequency range of interest.

$(-1)^l$ improves the solution.

$$A_l = \sqrt{2} \cdot W_f \cdot A_{rms}(f_l) \qquad (3.8)$$

is the peak displacement amplitude determined from the frequency spectrum corresponding to frequency, f_l.

where,

W_f = correction factor

and $$A_{rms}(f_l) = \left[\int_{f_l-1}^{f_l+1} S_{rms}(f_l)\, df\right]^{1/2} \qquad (3.9)$$

= rms displacement amplitude corresponding to frequency, f_l.

where

$$S_{rms}(f_l) = (S(f_{l-1}) - S(f_{l+1}))/2 \qquad (3.10)$$

and,

$$f_l = (f_{l-1} + f_{l+1})/2 \qquad (3.11)$$

The rms value of spectral density corresponding to center frequency, f_l is obtained by trapezoidal rule, as given in Equations (3.10 & 3.11). The frequencies are specified such that successive frequencies have overlapping half-power points. The correction factor for a frequency range is arbitrarily selected in order to reduce the error between estimated and given spectra, which is usually less than or equal to unity.

Equations (3.7-3.11) provide an equivalent time history that would yield a spectra, which is replica of the power spectrum given by Equations (3.1-3.3). The validity of Equations (3.7-3.11) is examined for motorway and minor

roads, and is demonstrated in Figures 3.2 and 3.3 respectively, for $f_l \gtrsim 0.3$ Hz. Absolute peak amplitudes, A_l's variation with respect to frequency for both types of roadways, is given in Figure 3.4. The value of A_l's varies linearly in magnitude between frequencies f_{l-1} and f_{l+1}. It should be noted that amplitudes A_l's are considered from 0.3 Hz onwards for the simulation of non-linear vehicle model, because of considerable error between power spectrum generated from synthetic time-history and given power spectrum.

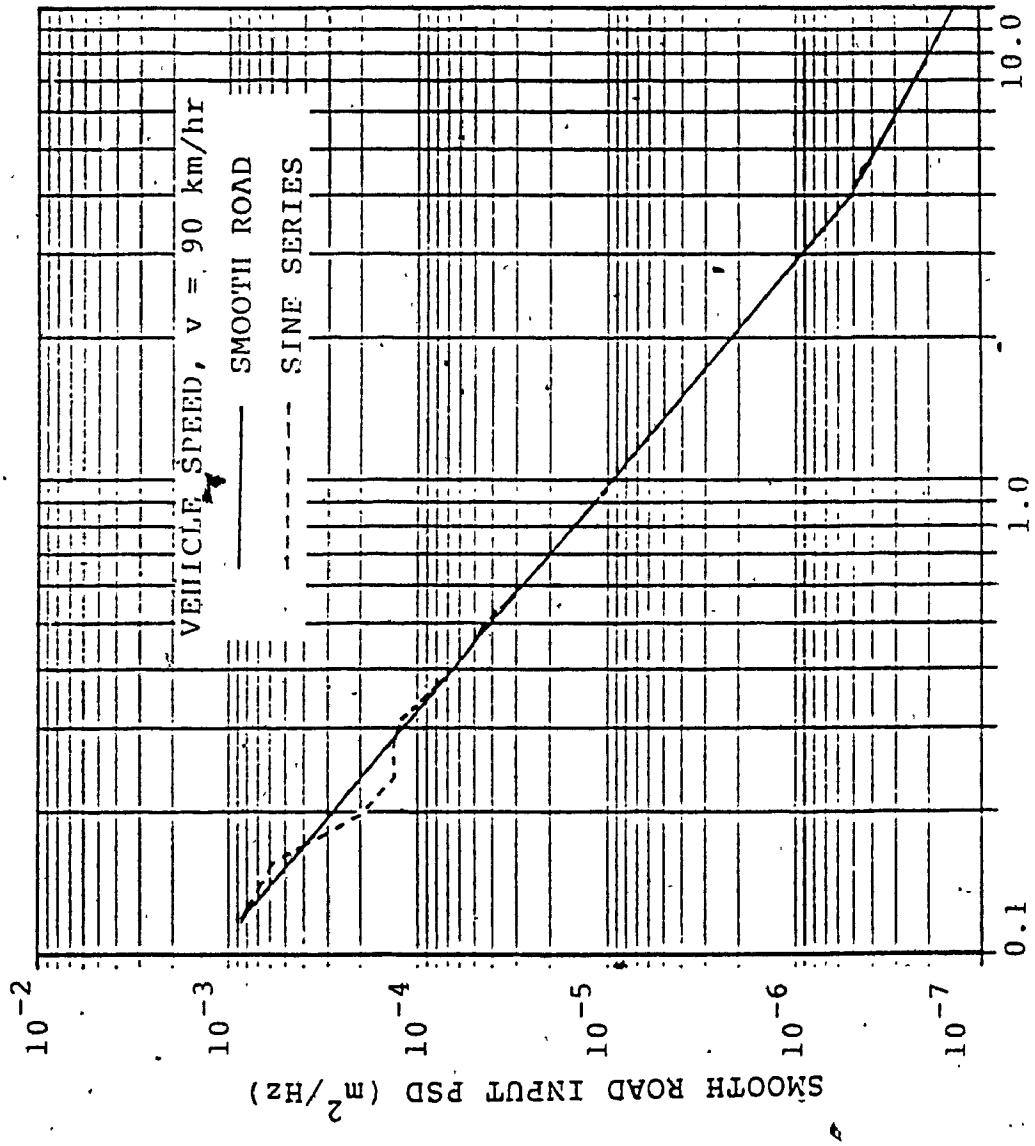

FIGURE 3.2: Road input PSD - smooth road

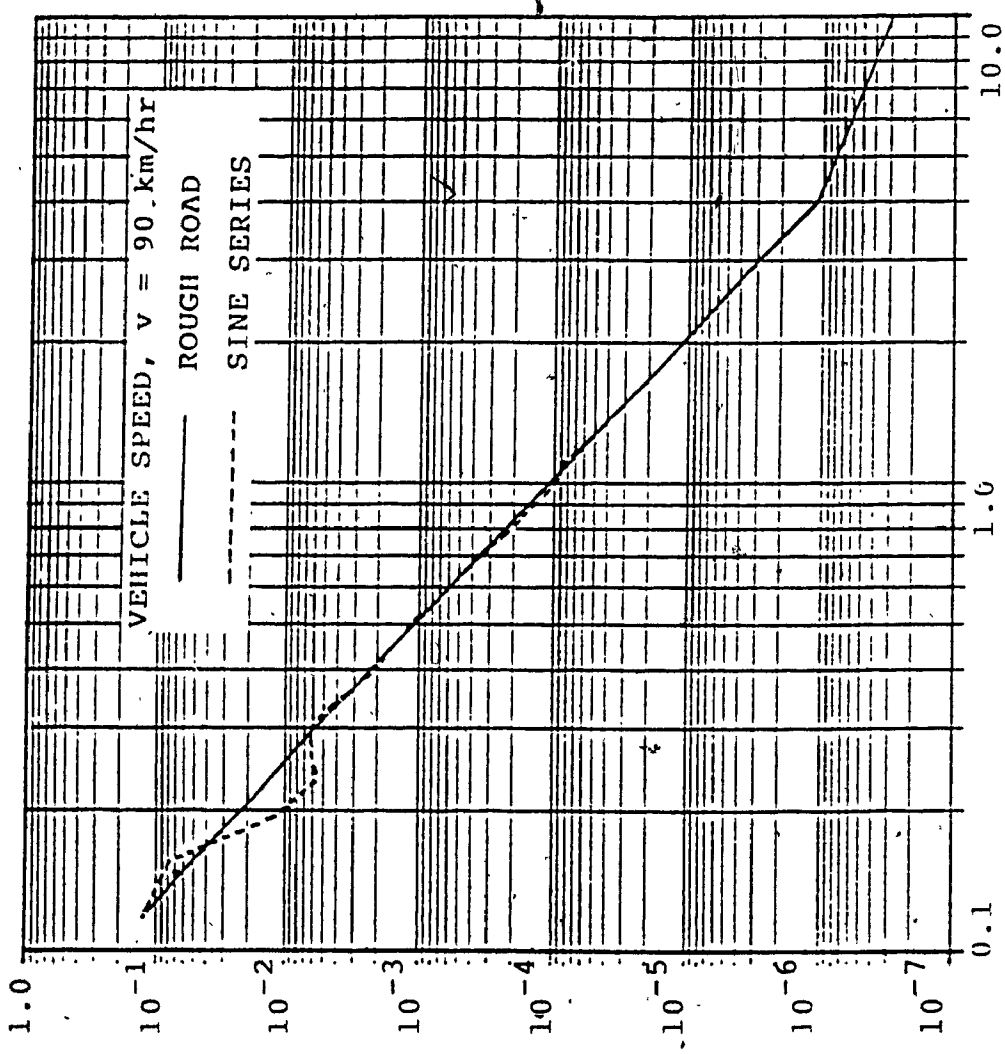

FIGURE 3.3: Road input PSD - rough road

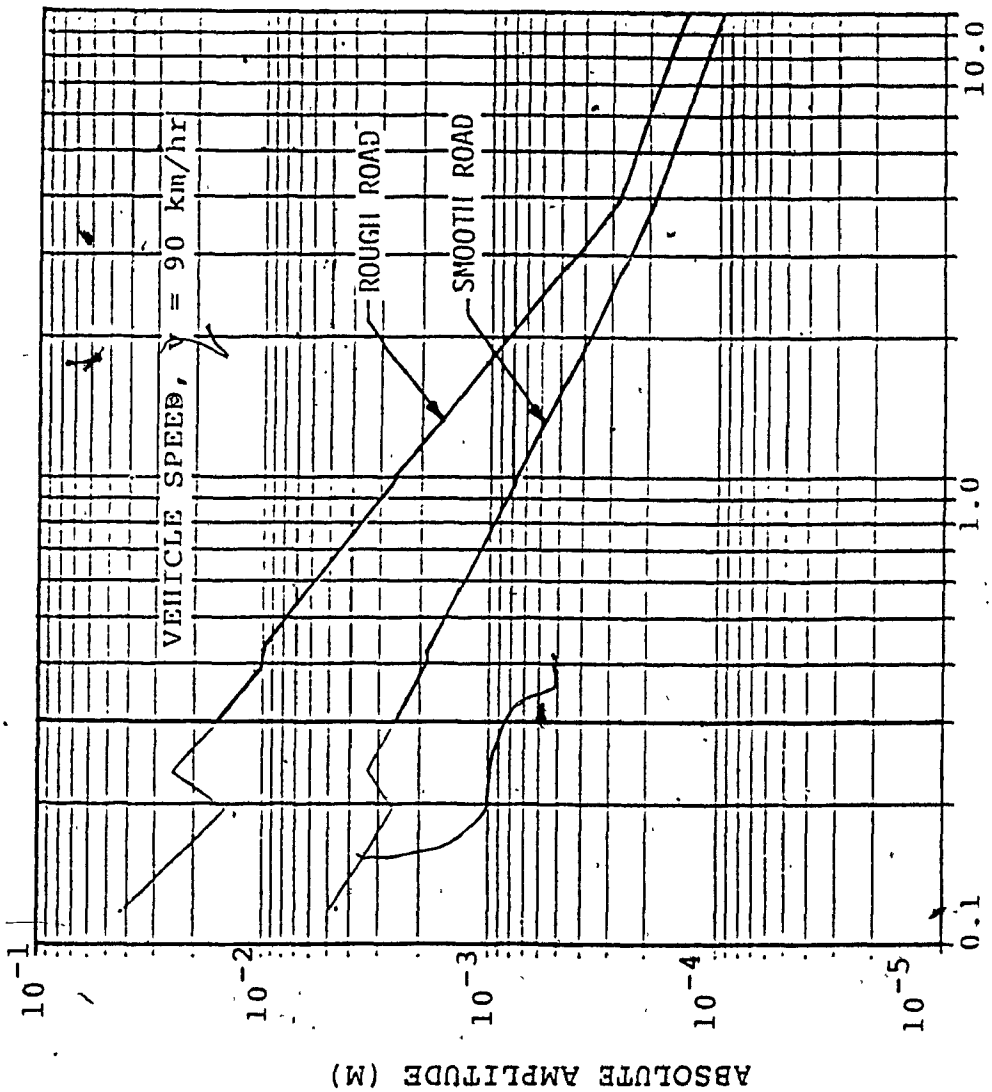

FIGURE 3.4: Absolute road input displacement amplitude - smooth and rough roads

3.4 SUMMARY

The random road roughness, characterized by displacement PSD's is presented. The displacement PSD's are represented by sine series to obtain real-time excitations as required for the simulation of nonlinear vehicle model. In the following chapter, ride response evaluation of linear model to stochastic inputs is discussed.

CHAPTER 4

RIDE RESPONSE EVALUATION OF LINEAR MODEL TO STOCHASTIC INPUTS

4.1 INTRODUCTION

The linear differential equations characterizing the dynamics of two- and three-dimensional models of baseline vehicle derived in chapter 2 will be solved in this chapter to evaluate vehicle ride performance, and to provide comparison of results from mathematical models of varying degrees of complexity. Although the linear vehicle model is used in this study, many of the fundamental effects of the vehicle-road dynamic interactions may be realistically studied, and considerable insight into the behaviour of the system may be gained.

The linear analysis allows computations of the results in the frequency domain using transfer function which provides the engineer with a clear insight into the system behaviour. This technique is particularly useful to conduct sensitivity studies of the influence of various design parameters on the vehicle dynamic response.

In the work presented here, the linear equations of motion for both models of baseline vehicle are solved in the frequency domain using power spectral density approach. The random road surface, as discussed in chapter 3, is

described by its power spectral density, presenting averaged measure of the amplitude of its frequency components. The ride vibration levels at the driver-seat interface are computed for both two- and three-dimensional models for varying road characteristics and vehicle speed. These results are assessed with respect to the ISO specified acceptable levels of vibration to evaluate the vehicle ride quality. A comparison of results obtained from two-dimensional and three-dimensional study of the mathematical models is presented.

The results of linear analysis are presented in the form of system modal parameters and acceleration power spectra. A computer animation software is developed to display the deflection modes of three-dimensional model.

4.2 RIDE QUALITY EVALUATION CRITERIA

The specification of the acceptable levels of vibration in a heavy vehicle is a dominant factor in system design. Although number of ride quality criteria have been proposed by system designers, the International Standard Organiztion (ISO) " Guide for the Evaluation of Human Exposure to Whole-Body Vibration ", ISO 2631 [2] has been widely accepted for system design feasibility studies for transport system.

The ISO has setforth rms acceleration limits for

various exposure times in the frequency range 1-80 Hz, under vertical and horizontal vibrations for a single frequency excitations. Figure 4.1 presents the 'reduced comfort ' rms acceleration limits for exposure to vertical and horizontal vibrations. It is apparent from the figure that the most sensitive frequency is 4-8 Hz for vertical motion and 1-2 Hz for horizontal motion, and human tolerance of vibration decreases with increasing exposure time.

The ISO guide which is determined under single frequency excitation condition, has been converted to a form usable for direct comparison with vibration data presented in power spectral density form in [50]. A brief discussion of the procedure followed in the conversion process is given below.

The power spectral density (PSD) is defined by the relation,

$$S(f) = \lim_{f \to 0} \frac{a^2(f)}{\Delta f} \qquad (4.1)$$

Since ISO standard assumes averaging over finite band of one-third octave width, the average PSD can be expressed as,

$$\bar{S}(\bar{f}) = \frac{\bar{a}^2(\bar{f})}{\Delta f} \qquad (4.2)$$

Where $\bar{S}(\bar{f})$ is the average PSD and $\bar{a}(\bar{f})$ is the rms

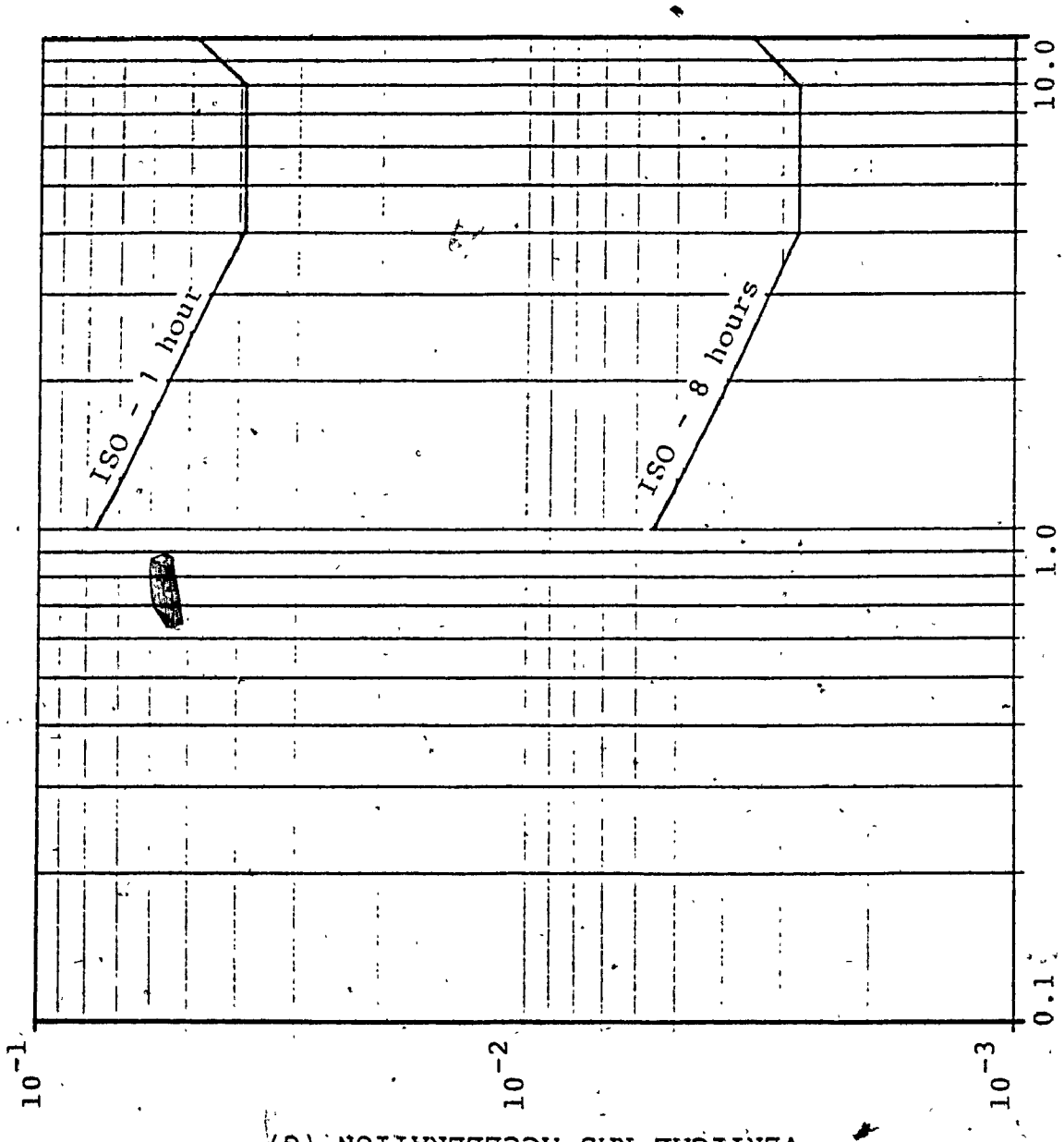

FIGURE 4.1a: Reduced comfort rms acceleration limits, for exposure to vertical vibration

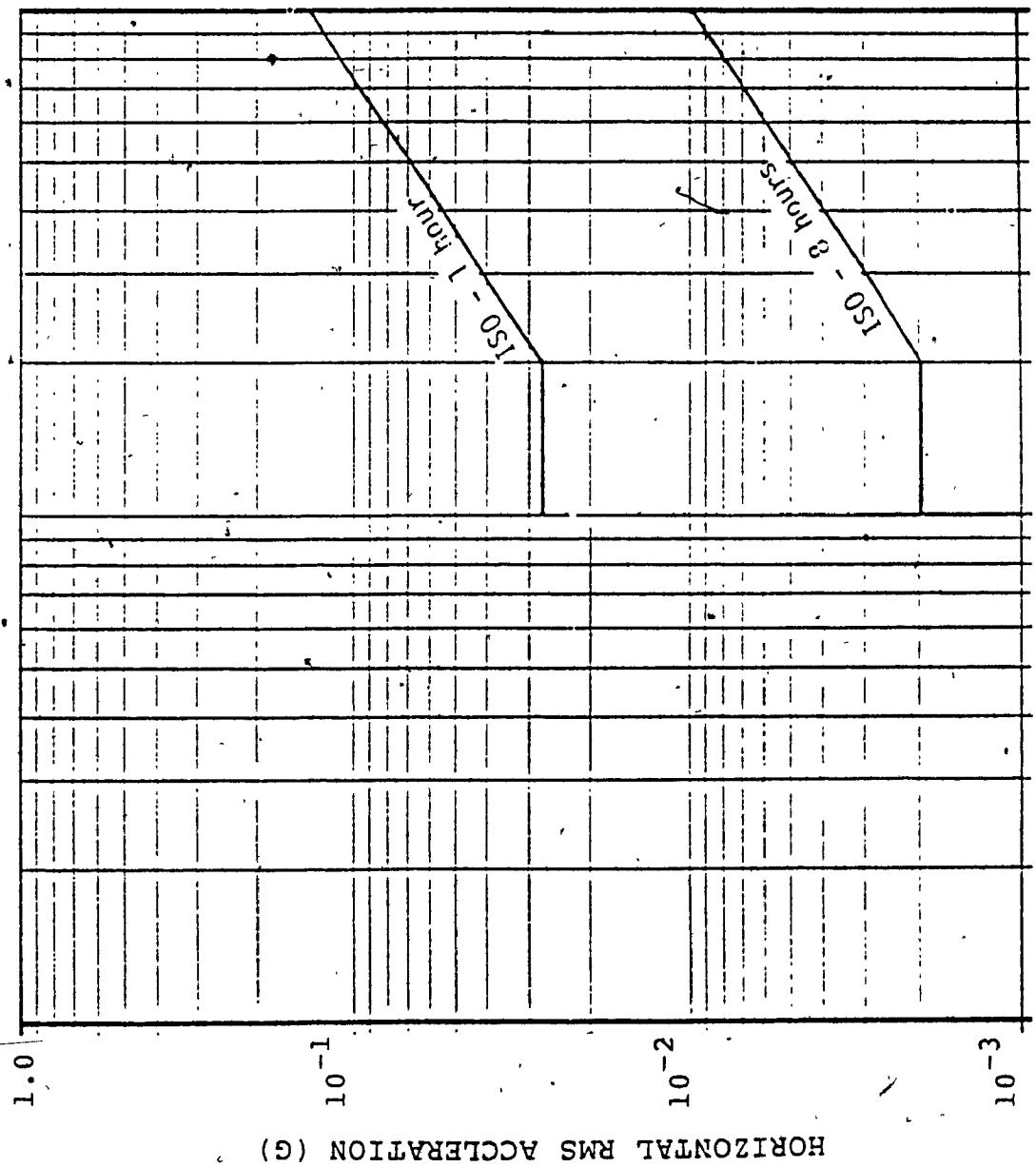

FIGURE 4.1b: Reduced comfort rms acceleration limits, for exposure to horizontal vibration

acceleration at center frequency, $\bar{f}$, of the frequency band, Δf. The relationship between the bandwidth and the center frequency for one third octave band is obtained as follows,

$$f_2 = 2^{1/3} f_1 \tag{4.3}$$

and

$$\bar{f} = \frac{f_2 + f_1}{2} \tag{4.4}$$

Where f_1, f_2 are the lower and upper frequency limits, respectively. The definition of a one-third octave band, and Equations (4.3-4.4) yields,

$$\Delta f = 0.23 \bar{f} \tag{4.5}$$

substituting (4.5) into (4.1), the average PSD is expressed as,

$$S(f) = \frac{\bar{a}^2(\bar{f})}{0.23\bar{f}} \tag{4.6}$$

The ISO boundaries $\bar{a}(\bar{f})$ are straight line segments on log-log plots of the form

$$\log \bar{a}(\bar{f}) = m_i \log \bar{f} + b_i \tag{4.7}$$

where m_i and b_i are the slope and the intercepts, respectively, for the i^{th} segment. Taking the logarithim of (4.6) and substituting (4.7) yields,

$$\log \bar{S}(\bar{f}) = (2m_i - 1) \log \bar{f} + (2b_i - \log 0.23) \tag{4.8}$$

From (4.8), it is apparent that $\bar{S}(\bar{f})$ also consists of

straight line segments plotted on log-log coordinates having slope $(2m_i - 1)$ and intercept $(2b_i - \log 0.23)$. Table 4.1 lists the slope and intercept values for various segments of ISO one hour reduced comfort boundary. The PSD equivalent limits given by equation (4.8), in vertical and horizontal modes are plotted in Figure 4.2. These are boundaries of reduced comfort for one hour and eight hour exposure time. It should be noted that rms and PSD equivalent limits for eight hour exposure time are obtained by multiplying the corresponding one hour limits by 0.071 [50].

4.3 METHOD OF SOLUTION

In the linearized analysis of a multi-degrees-of-freedom system, the use of the frequency response function along with the power spectral density representation of the input, has been the basis of frequency domain analysis. The frequency domain analysis utilizes the Fourier Transform of the time dependent variables of equations of motion.

The linear differential equations representing the dynamics of a vehicle system are given by equation (2.5),

$$[M]\{\ddot{q}\} + [C]\{\dot{q}\} + [K]\{q\} = \{f(t)\} \qquad (4.9)$$

Since $\{f(t)\}$ is the vector of stationary Gaussian random excitation forces applied to a linear system, $\{q(t)\}$ is the vector of system response variables which is also

TABLE 4.1 [50]

SLOPE AND INTERCEPTS OF ISO ONE HOUR REDUCED COMFORT BOUNDARY

Axis	Segment	rms		PSD equivalent	
		Slope m_i	Intercept b_i	Slope $(2m_i - 1)$	Intercept $(2b_i - \log 0.23)$
Vertical	1	-0.5	-0.12	-2.0	0.40
	2	0.0	-0.42	-1.0	-0.20
	3	1.0	-0.132	1.0	-2.0
Horizontal	1	0.0	-0.57	-1.0	-0.50
	2	1.0	-0.87	1.0	-1.10

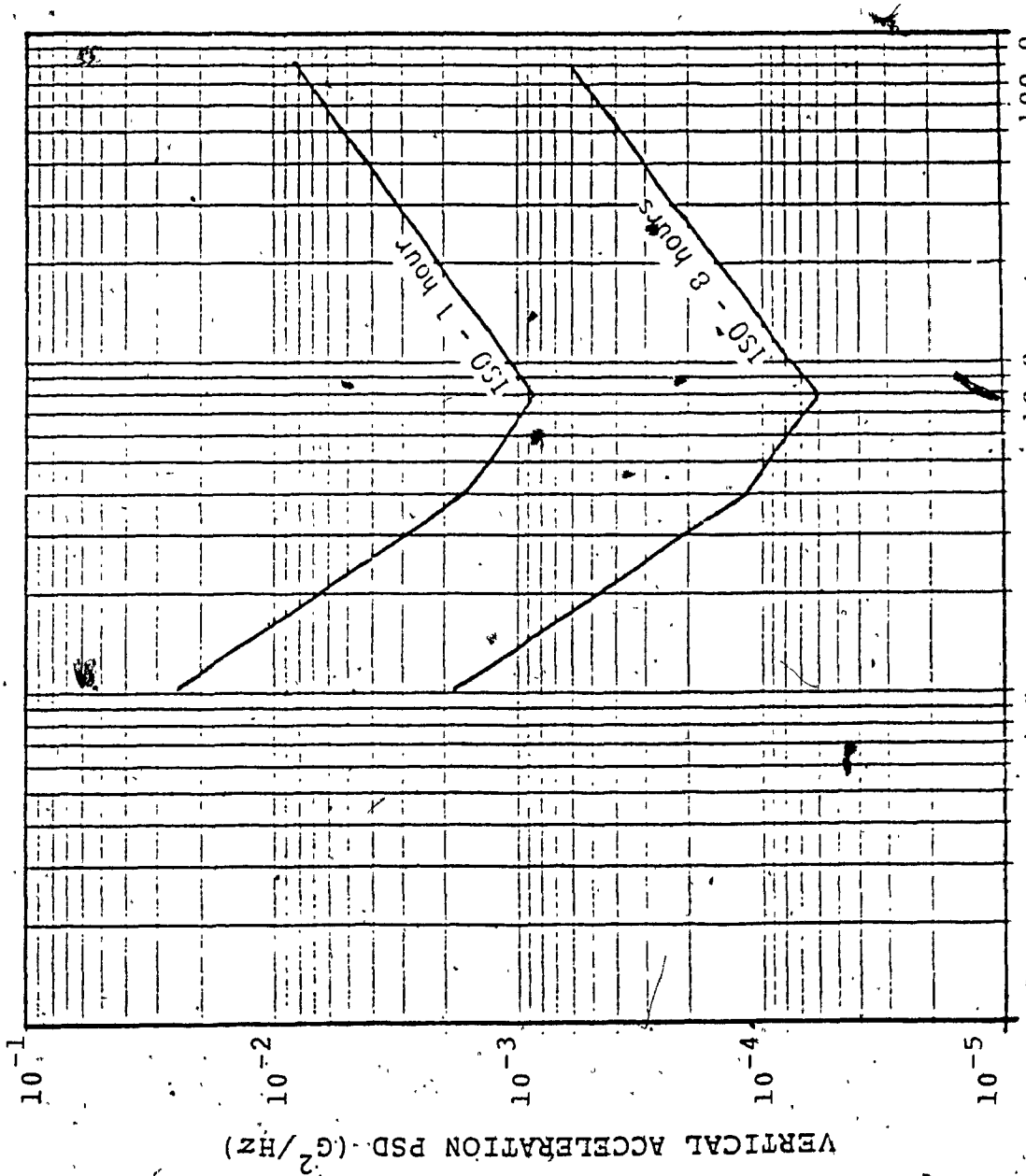

FIGURE 4.2a: Equivalent acceleration PSD reduced comfort limits, for exposure to vertical vibration

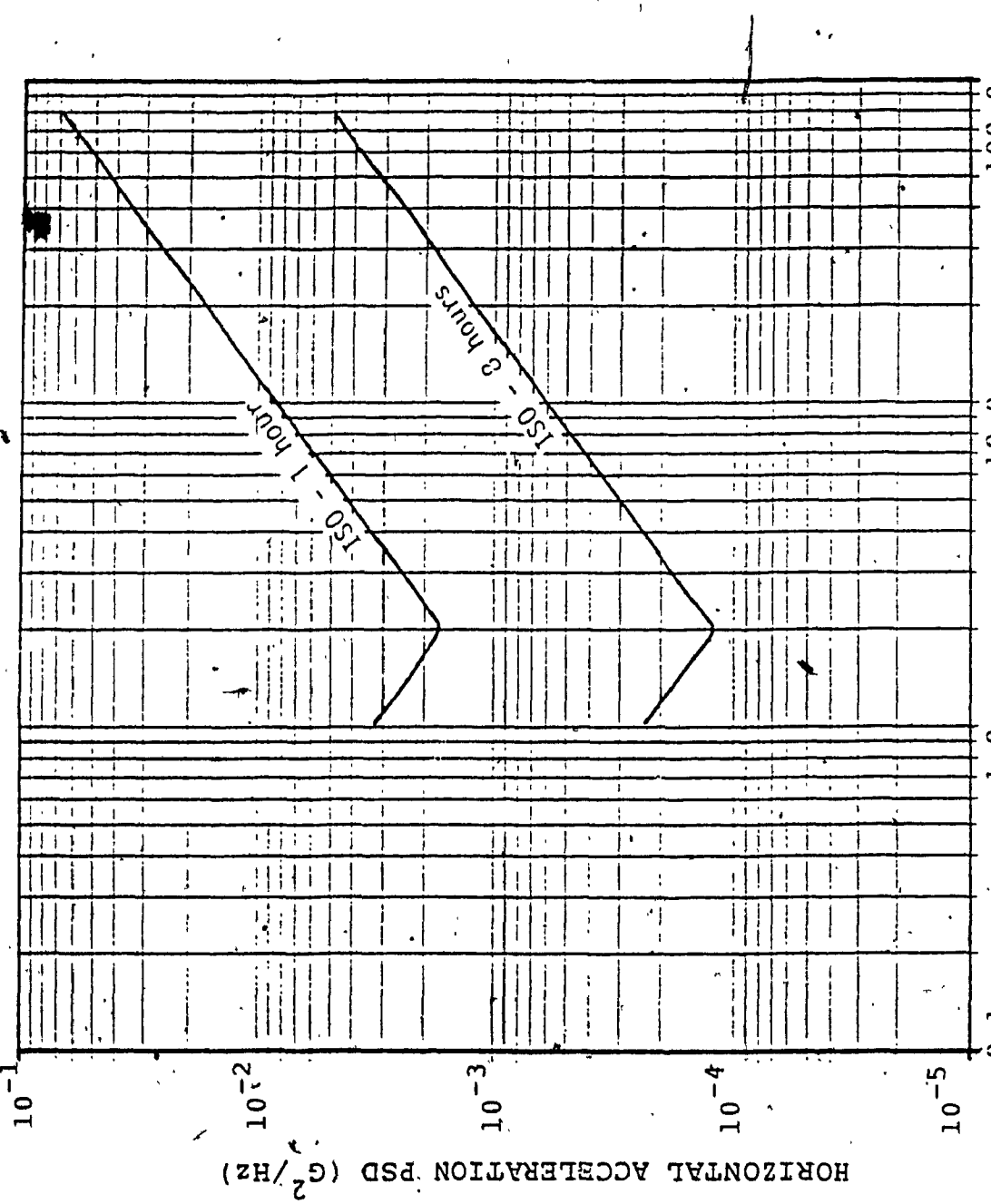

FIGURE 4.2b: Equivalent acceleration PSD reduced comfort limits, for exposure to horizontal vibration

stationary and Gaussian.

The matrix of frequency response function or the transfer function matrix, $[H(j\omega)]$ is constructed by letting the force vector to be

$$\{f\} = \{f_o\}\, e^{i\omega t} \qquad (4.10)$$

The response vector is then given by

$$\{q\} = [H(j\omega)]\,\{f\} \qquad (4.11)$$

where

$$[H(j\omega)] = [-\omega^2[M] + j\,\omega\,[C] + [K]]^{-1} \qquad (4.12)$$

For a single degree-of-freedom system subjected to a stationary Gaussian random excitation, the input and output power spectral densities are given by the following relationship [8],

$$S_q(f) = h(j\omega)\,.\,h^*(j\omega)\,.\,S_F(f) \qquad (4.13)$$

where $S_q(f)$ = PSD of the response variable

$S_F(f)$ = PSD of the excitation force

$h(j\omega)$ = Frequency response function of the system

$h^*(j\omega)$ = Complex conjugate of $h(j\omega)$

For a multi-degrees-of-freedom system with N inputs and m outputs, this is expanded to [31] :

$$S_q^m(f) = Re\left[\sum_{i=1}^{N}\sum_{k=1}^{N} h_{mi}(j\omega)\,.\,h^*_{mk}(j\omega)\,.\,S_{Fik}(f)\right] \qquad (4.14)$$

where

$S_q^m(f)$ = PSD of the m^{th} output variable

$h_{mi}(j\omega)$ = Frequency response function between i^{th} input and m^{th} output variable

$h^*_{mk}(j\omega)$ = Complex conjugate of $h_{mk}(j\omega)$

$S_{Fik}(f)$ = Spectral density of i^{th}, k^{th} input variable (Direct power spectral density for $i = k$; Cross power spectral density for $i \neq k$)

Re = Designates Real part

Equation (4.14) can be rewritten in the matrix form as [8]:

$$[S_q(f)] = [H^*(j\omega)] \cdot [S_F(f)] \cdot [H(j\omega)]' \qquad (4.15)$$

where

$[S_q(f)]$ = Spectral density matrix of the response variables

$$[S_F(f)] = [[K_F] + j\omega[C_F]]^* [S_i(f)] [[K_F] + j\omega[C_F]]' \qquad (4.16)$$

= Excitation force PSD matrix calculated in terms of the temporal input displacement PSD matrix using stiffness and damping matrices [20].

$[H(j\omega)]'$ = Transpose of $[H(j\omega)]$

The diagonal elements of $[S_q(f)]$ provides the spectral densities of the generalized displacements. The off-diagonal elements are the cross spectral densities of the generalized displacements. The power spectral densities for the corresponding accelerations can be determined in

terms of 'g^2 /Hz' from the relationship,

$$[S_{\ddot{q}}(f)] = (\omega^2/g)^2 [S_q(f)] \quad (4.17)$$

The response spectral densities at coordinates other than the generalized coordinates are obtained by using the Transformation matrix [T], given as :

$$[S_o(f)] = [T]^* [S_q(f)] [T]' \quad (4.18)$$

The Transformation matrix is obtained from the constraint equations presented in chapter 2. Since [T] is a matrix with real elements, Equation (4.18) can be rewritten as :

$$[S_o(f)] = [T] [S_q(f)] [T]' \quad (4.19)$$

AN ALTERNATE APPROACH

The calculation of the response spectral density matrix, $[S_q(f)]$ in general is carried out over all frequencies of interest and it involves matrix addition, multiplication, and inversion. In particular, during the calculation of $[S_q(f)]$, the matrix inversion is usually a time consuming operation in a computer. Further, if degrees-of-freedom or the frequencies of interest are large in number, then the computer CPU time for the evaluation of $[S_q(f)]$ also becomes large. Therefore, an alternate approach should be taken in order to avoid matrix inversion.

The method for the calculation of response spectral density for the three-dimensional model having 22 degrees-of-freedom is based on the Modal analysis approach. In this approach, the equations of motion are uncoupled by expressing them in terms of systems modal coordinates. A brief discussion of this method is given below.

The undamped natural frequencies ω_{n_i}, and the corresponding modal vector $\{\Phi_i\}$ of the system can be obtained by solving the homogeneous part of Equation (4.9) neglecting damping, given by:

$$[M]\{\ddot{q}\} + [K]\{q\} = \{0\} \qquad (4.20)$$

The Equation (4.9) can be uncoupled by expressing them in terms of modal coordinates $\{\nu\}$, given by [52]:

$$\{q\} = [\Phi]\{\nu\} \qquad (4.21)$$

where $[\Phi]$ is the modal matrix.

The equations of motion in terms of modal coordinates, $\{\nu\}$ can be rewritten as :

$$[\upsilon]\{\ddot{\nu}\} + [\gamma]\{\dot{\nu}\} + [\kappa]\{\nu\} = \{\epsilon(t)\} \qquad (4.22)$$

where

$$[\upsilon] = [\Phi]'[M][\Phi]$$

$$[\gamma] = [\Phi]'[C][\Phi]$$

$$[\kappa] = [\Phi]'[K][\Phi]$$

$$\{\epsilon(t)\} = [\Phi]'\{f(t)\}$$

Matrices $[\upsilon]$ and $[\kappa]$ are diagonal matrices due to operation by modal matrix $[\Phi]$. If $[\gamma]$ is also diagonal, then the Equation (4.22) can be written as :

$$\upsilon_i \ddot{\nu}_i + 2\zeta_i \upsilon_i \omega_{n_i} \dot{\nu}_i + \kappa_i \nu_i = \epsilon_i \qquad (4.23)$$

$$i = 1,2,.....,m$$

where m is the total number of degrees of freedom considered for the vehicle and ζ_i is the damping ratio in the i^{th} mode.

In general, however, the resulting damping matrix, $[\gamma]$ is not diagonal. It can be diagonalized by operating on it by the modal matrix $[\Phi]$, if, (a) the damping is proportional to stiffnesss or mass or both, or, (b) the damping in the system is very low and the off-diagonal terms can be neglected. For a vehicle, (a) and (b) are not true, since the damping in the suspension is much larger than at other locations. Therefore, the damping ratio can not be obtained from the diagonal element of the undiagonalized damping matrix.

The damping ratio for the i^{th} mode can be obtained as,

$$\zeta = \sqrt{\left(1 - (\omega_{d_i}/\omega_{n_i})^2\right)} \qquad (4.24)$$

where, ω_{d_i}, the damped natural frequency of the i^{th} mode, can be obtained by the complex eigenvalue analysis of the system. This is accomplished by converting the m-number of

second order differential equations into 2m-number of equations as follows [49] :

$$[M]\{\dot{\xi}\} + [K]\{\xi\} = \{0\} \tag{4.25}$$

where

$$\underset{(2mx2m)}{[M]} = \begin{bmatrix} [0] & [M] \\ [M] & [C] \end{bmatrix} \qquad \underset{(2mx2m)}{[K]} = \begin{bmatrix} -[M] & [0] \\ [0] & [K] \end{bmatrix}$$

$$\underset{(2mx1)}{\{\xi(t)\}} = \begin{Bmatrix} \dot{\bar{q}}(t) \\ \hline \bar{q}(t) \end{Bmatrix} \qquad \underset{(2mx1)}{\{\dot{\xi}(t)\}} = \begin{Bmatrix} \ddot{\bar{q}}(t) \\ \hline \dot{\bar{q}}(t) \end{Bmatrix}$$

Equation (4.25) provides m complex conjugate pairs of eigenvalues and corresponding eigenvectors. The imaginary part defines the damped natural frequency while the real part defines an associated decay rate related to the ammount of modal damping.

The frequency response function for the i^{th} mode can then be obtained from the Fourier representation of the Equation (4.23) as :

$$\eta_i(j\omega) = \frac{1}{\kappa_i - \upsilon_i\omega^2 + j2\zeta_i\omega_{n_i}\omega\upsilon_i} \tag{4.26}$$

The transfer function matrix, $[H(j\omega)]$ as given by Equation (4.12), can be alternatively obtained as :

$$[H(j\omega)] = [\Phi]\,[\eta(j\omega)]\,[\Phi]' \tag{4.26}$$

where $[\eta(j\omega)]$ is a diagonal matrix with its diagonal

elements being the frequency response function, $\eta_i(j\omega)$ for all m modes.

The response spectral density matrix, $[S_q(f)]$ can therefore, be obtained from Equation (4.15)

4.4 RESULTS AND DISCUSSION

4.4.1 TWO-DIMENSIONAL MODEL

4.4.1.1 MODAL PARAMETERS

The modal parameters of a system are important to both designers and development engineers of vehicle in that they indicate the relative stability, damping ratios, and damped and undamped natural frequencies and associated deflection modes of the system.

The modal parameters are calculated using normal and complex eigenvalue analysis as discussed in the previous section. Table 4.2 lists the undamped and damped natural frequencies, damping ratios, and associated deflection modes for two-dimensional model of the baseline vehicle.

4.4.1.2 INFLUENCE OF ROAD CHARACTERISTICS

The ride quality of a vehicle is strongly influenced by the type of road it traverses. Figure 4.3 and 4.4 show the bounce and fore-aft acceleration spectra at the driver-seat interface for both smooth and rough roads, and compared to

TABLE 4.2

MODAL PARAMETERS FOR THE TWO-DIMENSIONAL BASELINE VEHICLE MODEL

No.	Undamped Natural Frequency (Hz)	Damped Natural Frequency (Hz)	Damping Ratio	Dominant Deflection Mode
1	1.355	1.354	0.045	Tractor Bounce
2	1.892	1.890	0.046	Tractor Pitch
3	2.574	2.561	0.100	Vehicle Pitch
4	9.761	9.347	0.288	Front Axle Hop
5	10.425	10.072	0.258	Tractor Rear Axle Hop
6	13.652	13.091	0.283	Semitrailer Axle Hop

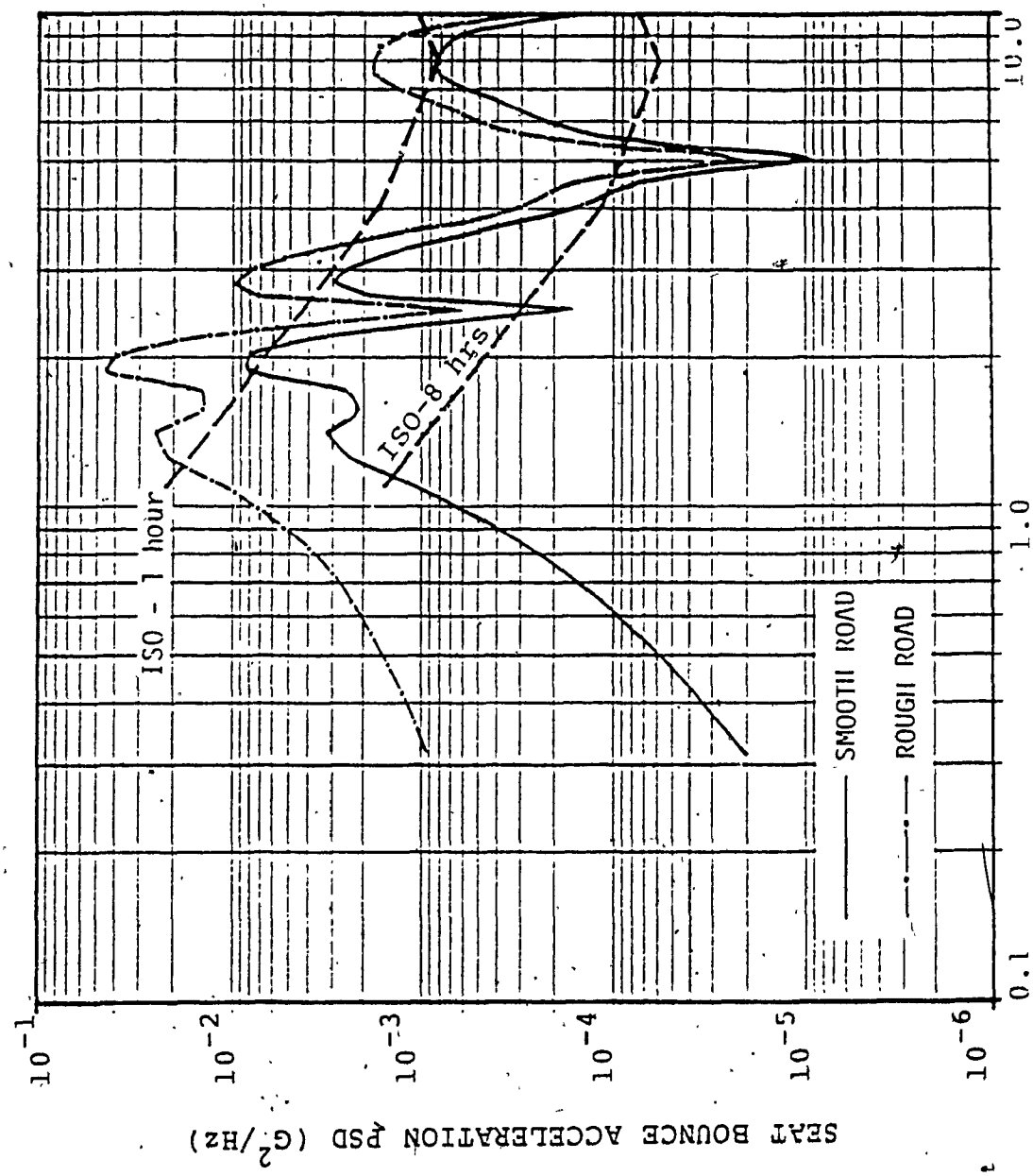

Figure 4.3: Influence of road profile on seat bounce acceleration spectra - linear, two-dimensional baseline vehicle model

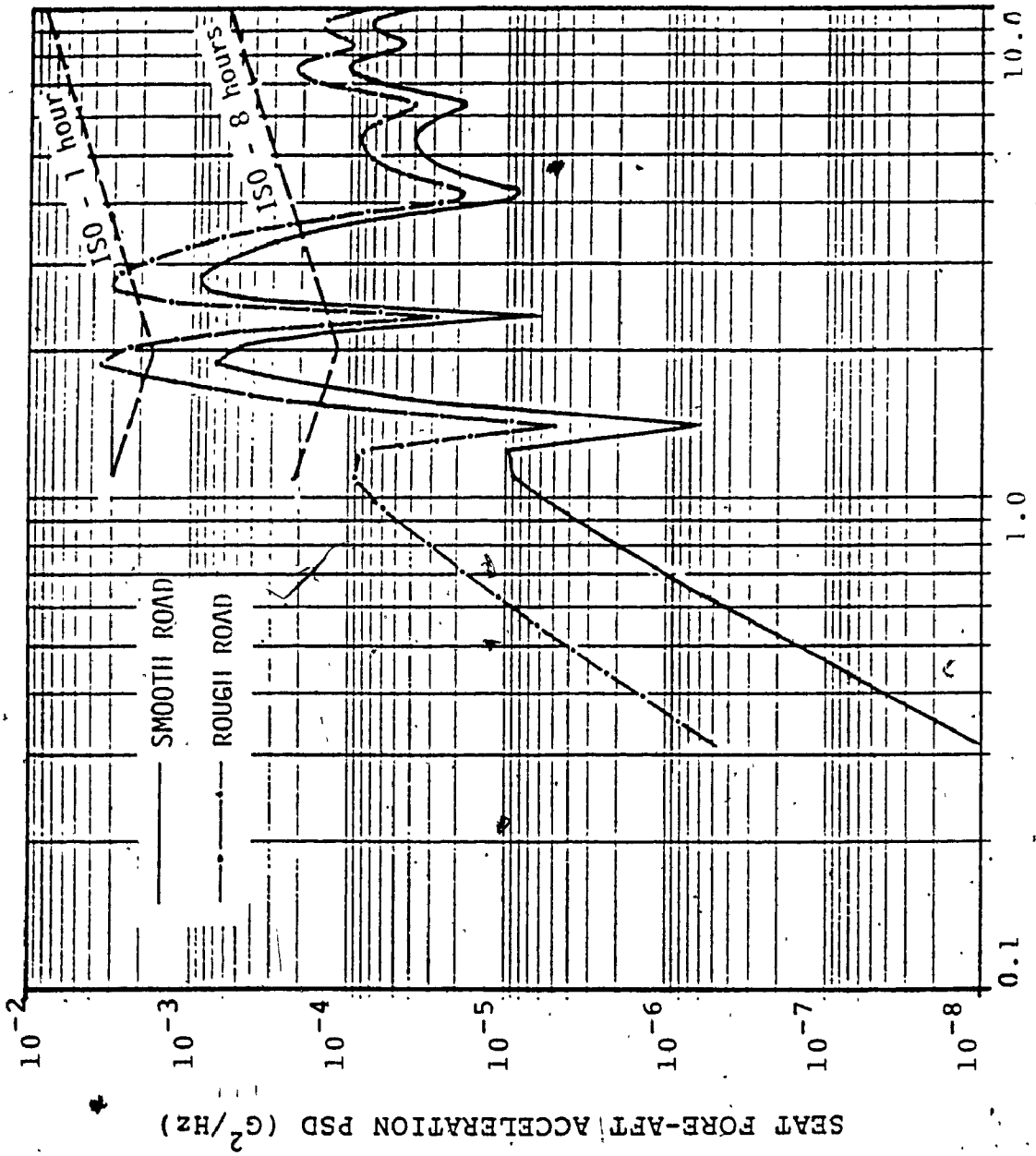

FIGURE 4.4: Influence of road profile on seat fore-aft acceleration spectra - linear, two-dimensional baseline vehicle model

ISO one hour and eight hours reduced comfort boundaries. The general shape of the response spectra for both types of roads is consistent. However, in the low frequency range, the rate of increase of accleration spectra for smooth highway is much higher than that for the rough road. There is an increase in the whole frequency range content of both fore-aft as well as bounce vibration due to rough profile. The bounce acceleration PSD for a rough road is about five times higher around the maximum peak value. As seen in these figures, the acceleration spectra for the smooth and rough roads exceed the 8 hour ISO guide by a considerable margin. Thus, the ride vibration levels for the baseline vehicle are excessive in the bounce as well as in the fore-aft motions.

The seat bounce acceleration spectra (Fig. 4.3) shows two dominant peaks around 1.4 Hz and 1.9 Hz corresponding primarily to tractor bounce and pitch modes respectively, while remainder of peaks relate to higher modes. This occurs because the seat vertical motion is a function of tractor bounce and pitching motions. The reason for the absence, or shift of some of the expected peaks corresponding to system natural frequencies is due to the spatially distributed road inputs to the vehicle, and the effects of coupling in a multi-degrees-of-freedom system where one vibration is likely to influence others.

Figure 4.4 shows two dominant peaks between 1.8 and 2.8 Hz, which correspond to vehicle pitching modes. This occurs because the seat fore-aft motion is a funcion of the combined tractor and semitrailer pitching motion.

Figures 4.5 and 4.6 show the root mean square acceleration amplitudes of seat bounce and fore-aft random motions respectively, for smooth and rough highways. Although these plots provide almost identical conclusions as the PSD plots, they yield an average value of acceleration in terms of g's experienced at the driver-seat interface.

4.4.1.3 INFLUENCE OF VEHICLE SPEED

The bounce and fore-aft ride vibration levels at the driver seat are obtained for different vehicle speeds and presented in Figures 4.7 and 4.8, respectively. Figure 4.7 presents the influence of the vehicle speed on the seat bounce acceleration spectra. A decrease in the speed to 70 km/hr increases the bounce ride levels around the low frequency, but the dominant peaks encpuntered at higher speeds are suppressed below the ISO one hour limit. The fore-aft ride quality (Fig. 4.8) also improves by a considerable ammount by decreasing the speed to 70 km/hr. Although the dominant peaks of bounce as well as fore-aft acceleration spectra are suppressed by reducing the speed to 70 km/hr, there is a considerable increase in vibration

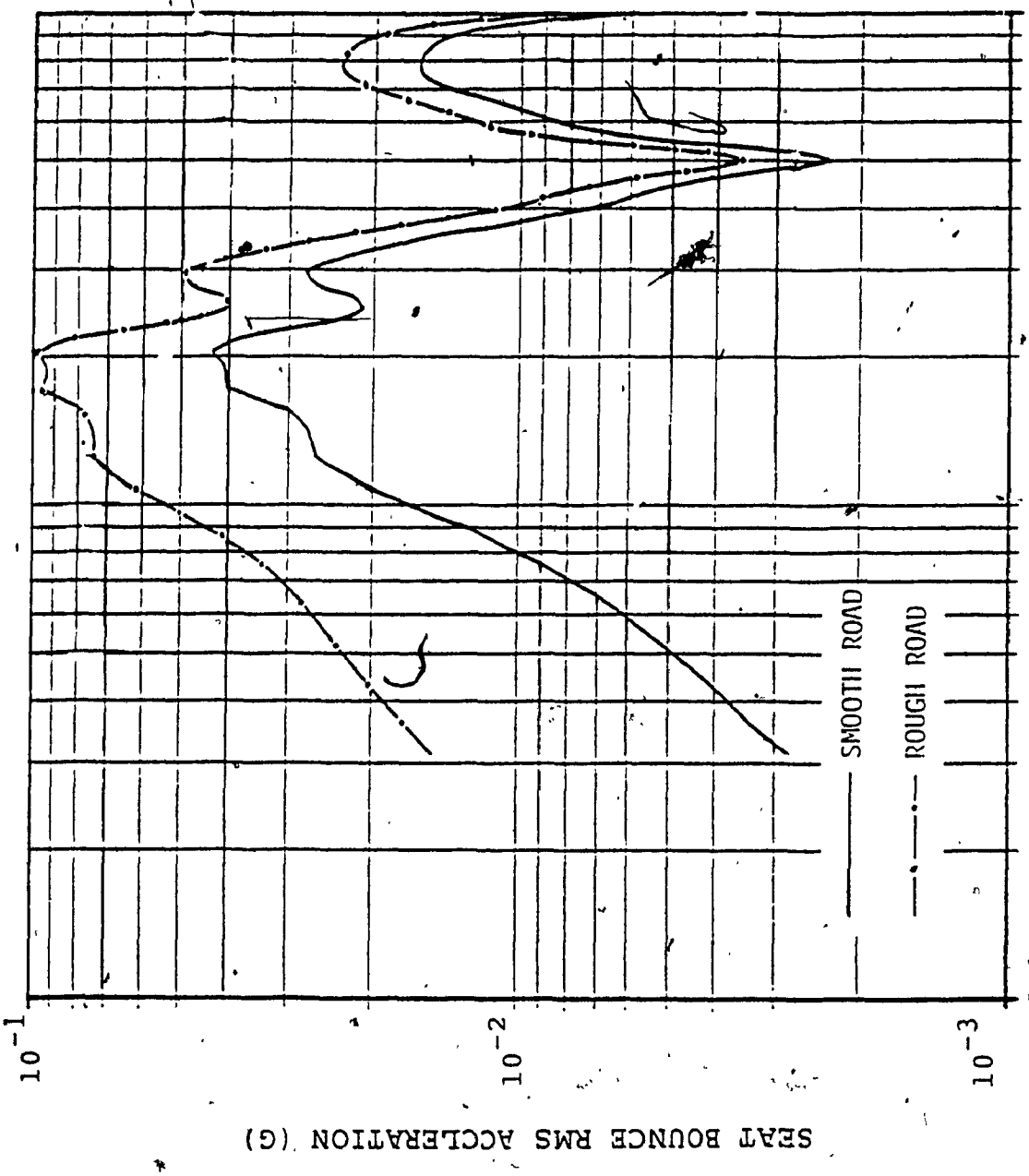

FIGURE 4.5: Influence of road profile on seat bounce rms acceleration response - linear, two-dimensional baseline vehicle model

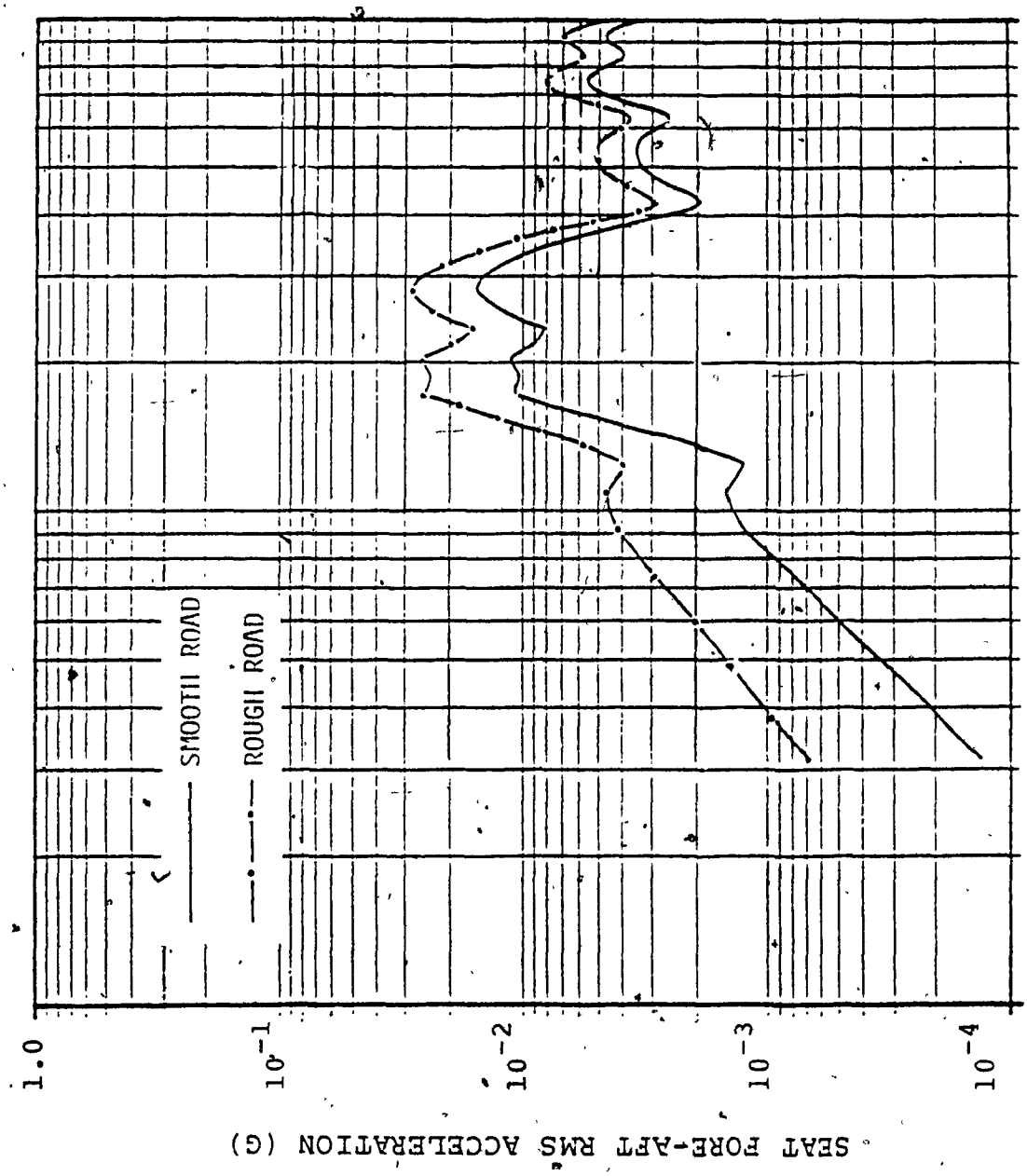

FIGURE 4.6: Influence of road profile on seat fore-aft rms acceleration response - linear, two-dimensional baseline vehicle model

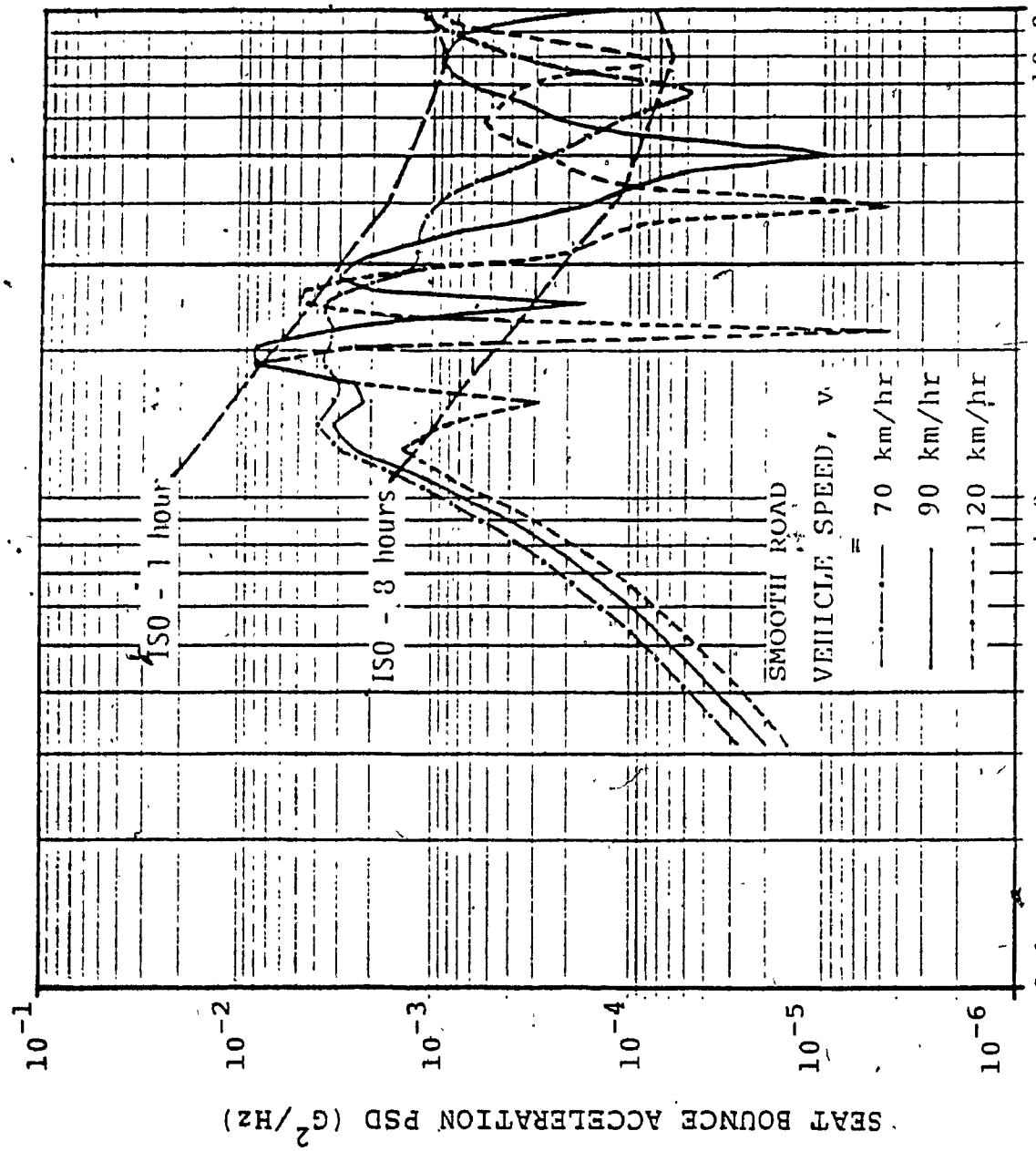

FIGURE 4.7: Influence of vehicle speed on seat bounce acceleration spectra - linear, two-dimensional baseline vehicle model

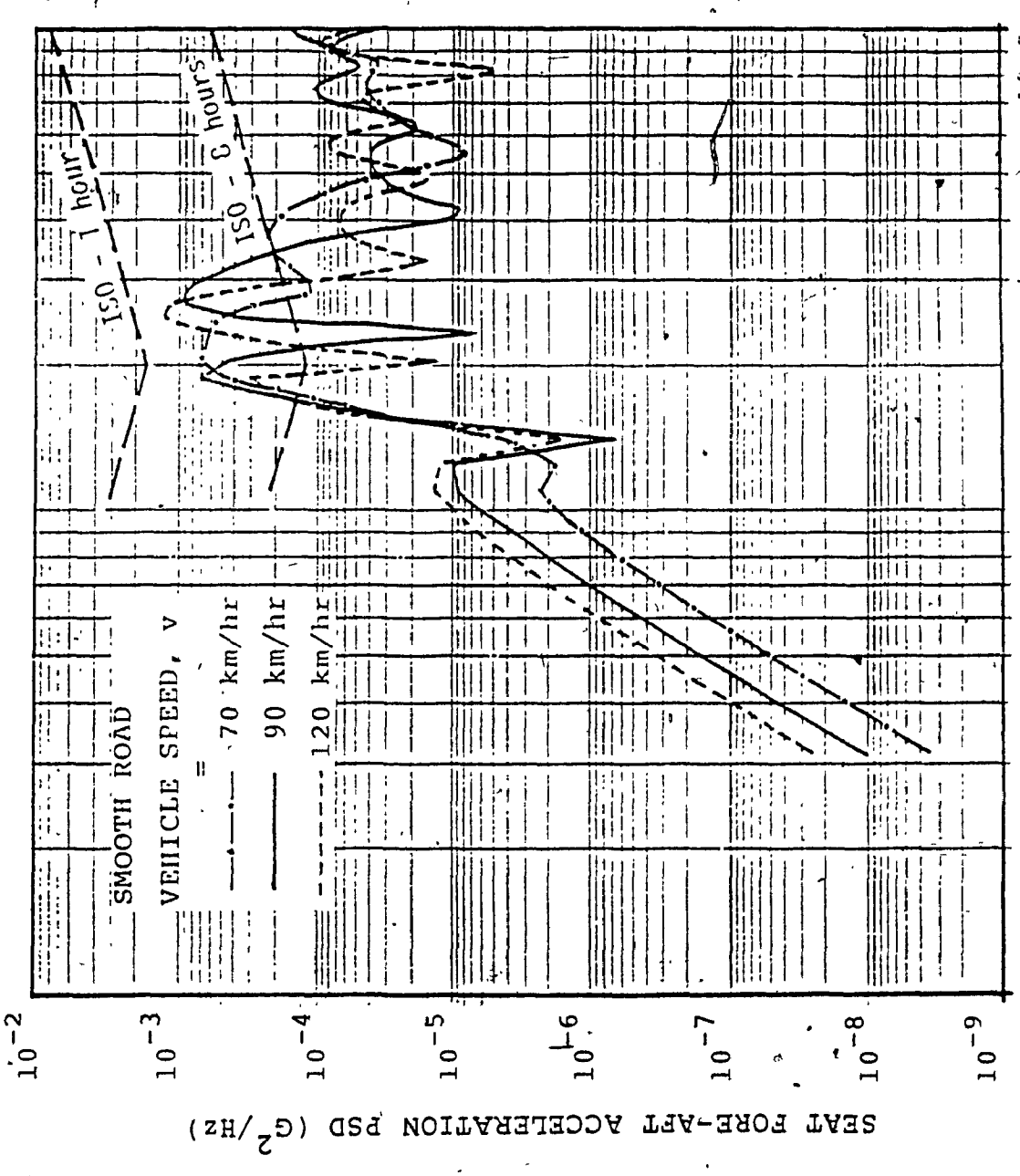

FIGURE 4.8: Influence of vehicle speed on seat fore-aft acceleration spectra - linear, two-dimensional baseline vehicle model

levels in the frequency range, 3-5 Hz.

4.4.2 THREE-DIMENSIONAL MODEL

4.4.2.1 MODAL PARAMETERS

The undamped and damped natural frequencies, damping ratios, and associated dominant deflection modes for three dimensional model are listed in Table 4.3. Due to the higher degree of complexity, this model possesses many natural modes due to its individual components and their interaction as a whole.

The animation of natural modes is the best way to visualize the relative deflection of various components of the vehicle at its various natural frequencies. An animation program is written in FORTRAN which is used in conjunction with NORPAK graphic system to animate the natural modes of three-dimensional model [3,51]. As seen in Figure 4.9, side view of the vehicle model is displayed on the lower half of the screen, while front and back views appear on the upper half of the screen. The side view displays all the deflections in bounce and pitching modes, while the front and back views display the vehicle lateral and rolling modes of motion. The mode shape at first or fundamental natural frequency is shown Figure 4.10. As it could be seen from the front and back views, the lateral and roll motions are dominant, while bounce and pitch

TABLE 4.3

MODAL PARAMETERS FOR THREE DIMENSIONAL BASELINE VEHICLE MODEL

No.	Undamped Natural Frequency (Hz)	Damped Natural Frequency (Hz)	Damping Ratio	Dominant Deflection Mode
1	0.5413	0.5413	0.0055	Tractor Rear Axle Lateral; Tractor Roll
2	0.9873	0.9872	0.0154	Seat Bounce; Cab Pitch
3	1.8008	1.7939	0.0876	Seat Bounce; Semitrailer Axle Lateral & Pitch
4	1.8897	1.8895	0.0156	Seat Bounce; Tractor Roll
5	1.9229	1.9213	0.0414	Seat Bounce; Tractor Roll
6	2.4332	2.3810	0.2105	Seat Bounce; Cab Pitch
7	2.6607	2.6158	0.1828	Seat Bounce; Semitrailer Axle Lateral & Pitch
8	2.9223	2.9197	0.0424	Tractor and Seat Bounce
9	3.7363	3.7358	0.0160	Tractor and Seat Bounce
10	5.3147	5.3005	0.0734	Tractor Rear Axle; Tractor Roll
11	7.2773	7.2769	0.0107	Tractor Front Axle Roll

(Table 4.3 cont'd)

No.	Undamped Natural Frequency (Hz)	Damped Natural Frequency (Hz)	Damping Ratio	Dominant Deflection Mode
12	8.5549	8.5546	0.0088	Semitrailer Pitch;Tractor Front Axle Roll
13	8.8621	8.8618	0.0071	Tractor Front Axle Lateral; Cab Bounce
14	9.1006	9.0881	0.0526	Cab Pitch;Tractor Bounce
15	9.3309	9.2725	0.1117	Cab Roll ; Tractor Pitch
16	9.4007	9.3869	0.0542	Semitrailer Axle Pitch & Roll
17	9.5402	9.4003	0.1706	Semitrailer Axle Pitch & Roll
18	9.7558	9.5388	0.2097	Tractor Bounce;Cab Pitch
19	10.4032	10.0847	0.2456	Cab Roll;Tractor Pitch
20	13.9892	13.9881	0.0125	Semitrailer Axle Lateral
21	14.5236	14.4708	0.0852	Tractor Rear Axle Pitch & Roll
22	15.8168	15.3180	0.2491	Tractor & Semitrailer Roll;Tractor Rear Axle Pitch & Roll

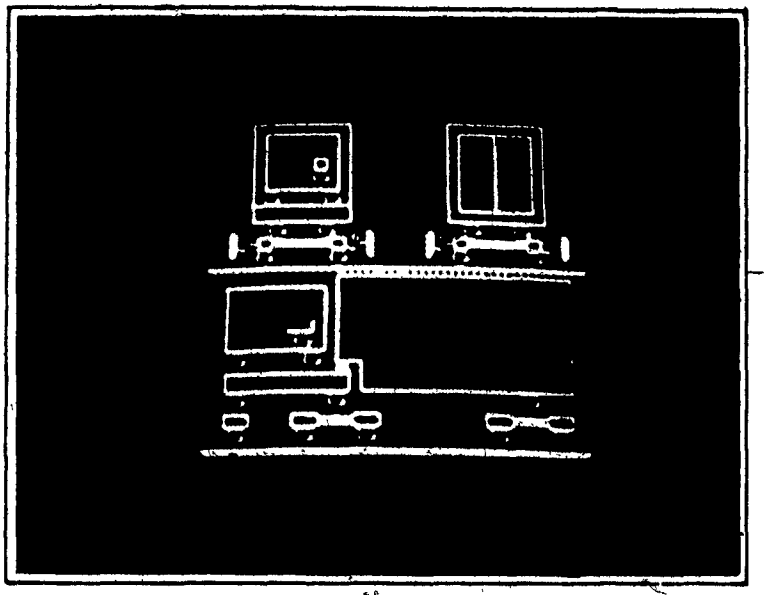

FIGURE 4.9: Display of vehicle stationary views

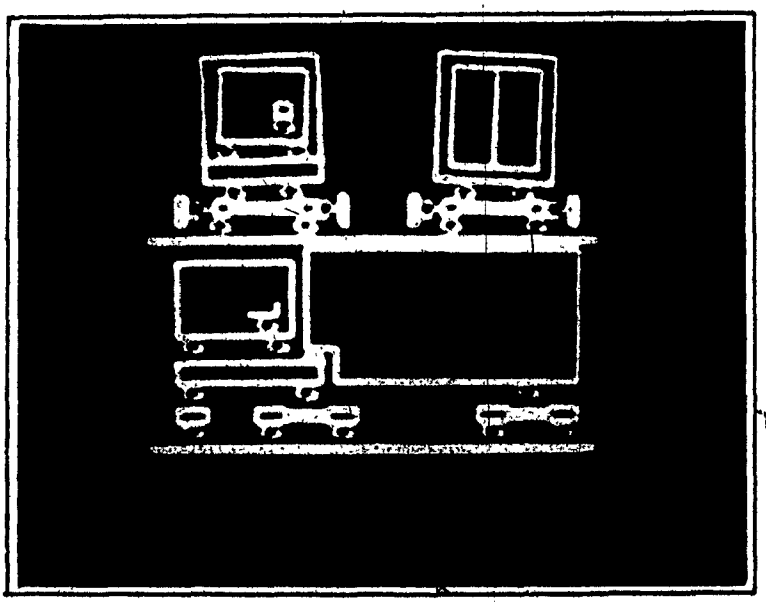

FIGURE 4.10: Display of vehicle position for Fundamental mode shape

motions as seen in side view are not significant. Similarly, all other mode shapes can be displayed one by one in any order as required.

4.4.2.2 INFLUENCE OF ROAD CHARACTERISTICS

The bounce, fore-aft, and lateral acceleration PSD's of seat for smooth and rough roads, which are obtained from three-dimensional study of the baseline vehicle model, are presented in Figures 4.11, 4.12, and 4.13 respectively. There is a considerable increase in ride vibration level in the entire frquency range for rough road. In comparison to the results obtained from two dimensional model, bounce and fore-aft spectra shows more number of peaks simply due to the inclusion of more degrees of freedom.

The seat bounce accleration PSD's obtained from two-dimensional and three-dimensional study show a maximum peak at 1.8 Hz, but the peak value in the latter case is about 17 times higher. The bounce ride levels, as shown in Figure 4.11 are in the range of field measured vibrations levels [40]. Consequently, the inclusion of seat-cab suspensions in the vehicle model yields more reliable results, but the general characteristics, such as fundamental frequencies, can be conveniently obtained using a simplified model.

The fore-aft accleration spectra, as shown in Figure

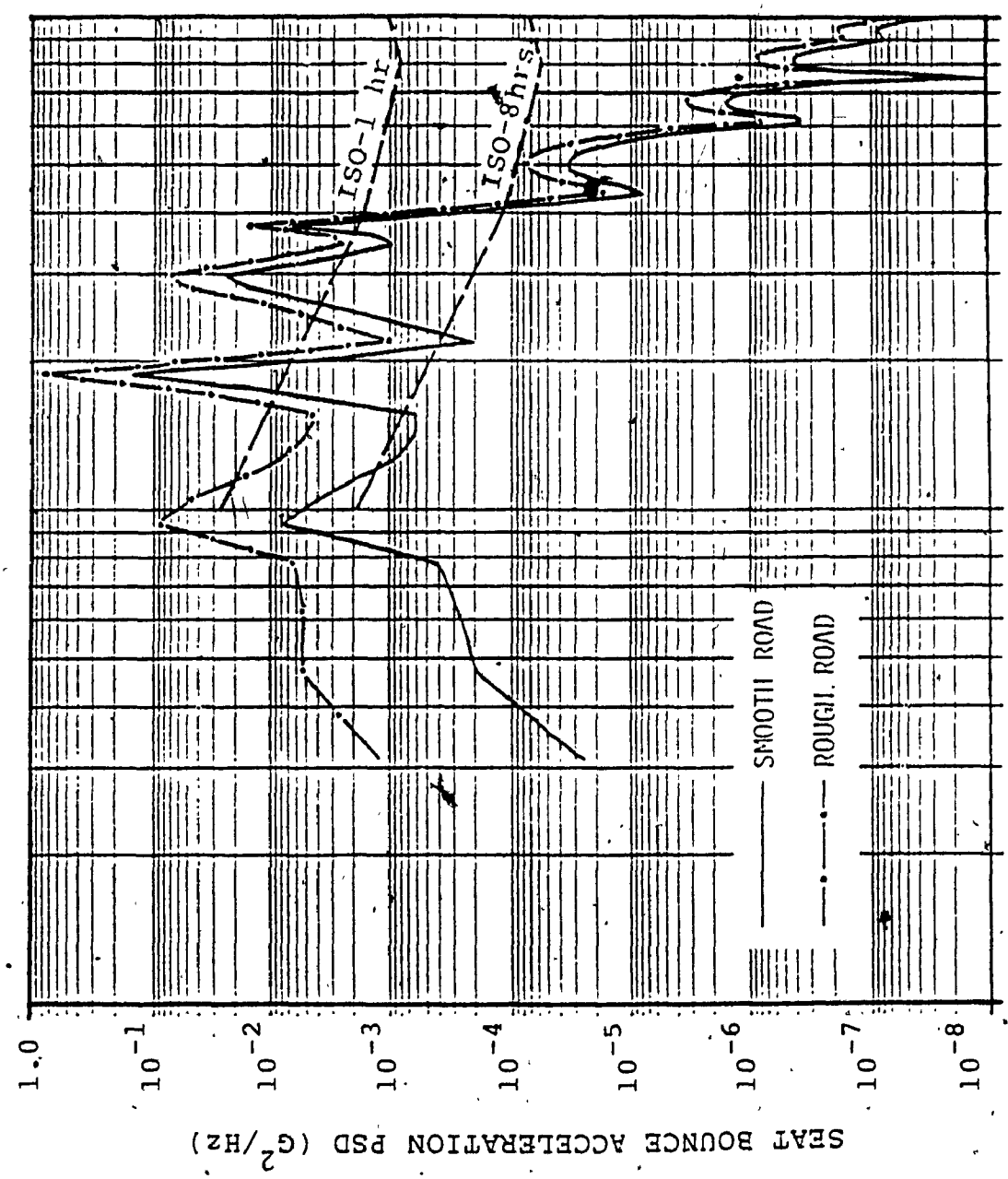

FIGURE 4.11: Influence of road profile on seat bounce acceleration spectra - linear, three-dimensional baseline vehicle model

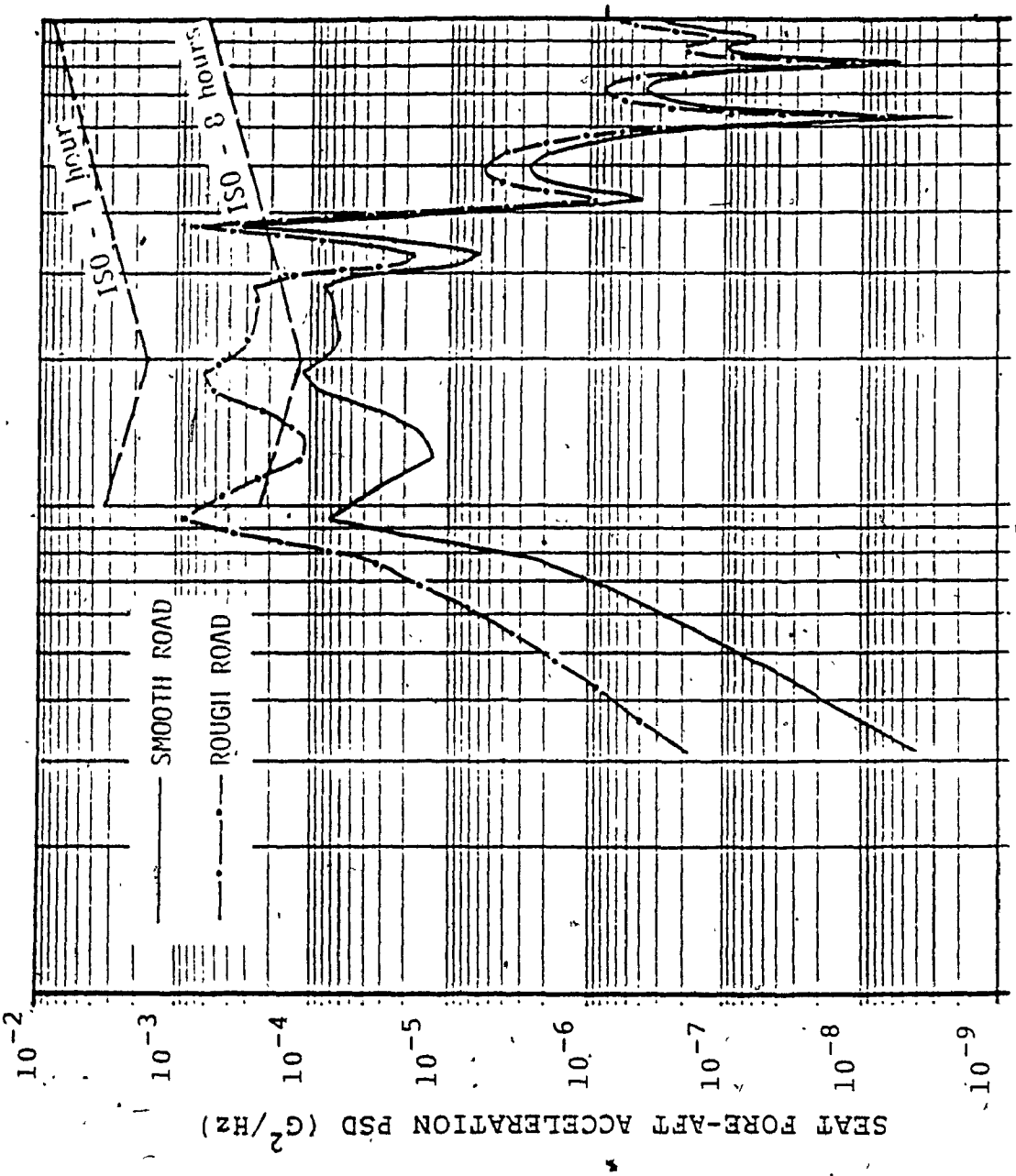

FIGURE 4.12: Influence of road profile on seat fore-aft acceleration spectra - linear, three-dimensional baseline vehicle model

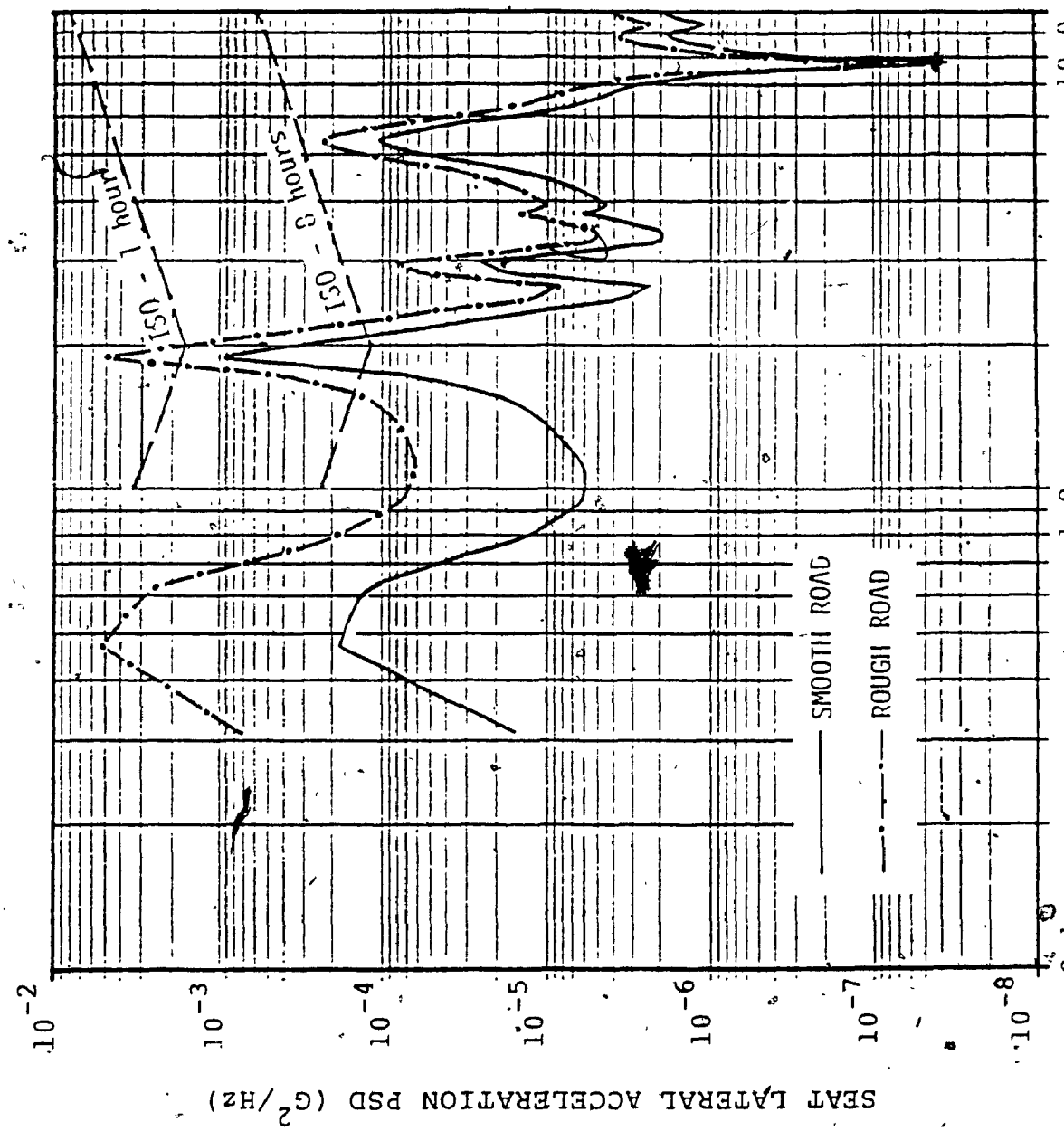

FIGURE 4.13: Influence of road profile on seat lateral acceleration spectra - linear, three-dimensional baseline vehicle model

4.12 indicates a significant improvement in the ride vibration levels in comparison to the fore-aft ride levels obtained from the two-dimensional study. Specifically for smooth road, the ride levels are below 1 hr ISO guide.

The lateral accleration spectra at the seat-driver interface is obtained and shown in Figure 4.13. The ride levels in the lateral direction are acceptable beyond 2.25 Hz, according to ISO specified levels.

4.4.2.3 INFLUENCE OF VEHICLE SPEED

The influence of various vehicle speeds on the bounce, fore-aft, and lateral ride vibration levels is demonstrated in Figures 4.14, 4.15, and 4.16, respectively. The bounce ride levels in low frequency range are increased by reducing the speed to 70 km/hr, but the dominant peaks encountered at higher speeds are suppressed below ISO 1 hr guide. The fore-aft ride quality at 70 km/hr is excellent according to ISO specified comfort levels. Figure 4.16 presents the lateral accleration spectra at various speeds. A decrease in the speed to 70 km/hr increases the lateral ride levels in low frequency range, but the lateral ride comfort is acceptable beyond 2.25 Hz.

In comparison to the bounce and fore-aft ride levels computed for various speeds, without considering the seat-cab suspensions (two-dimensional model), the magnitude of

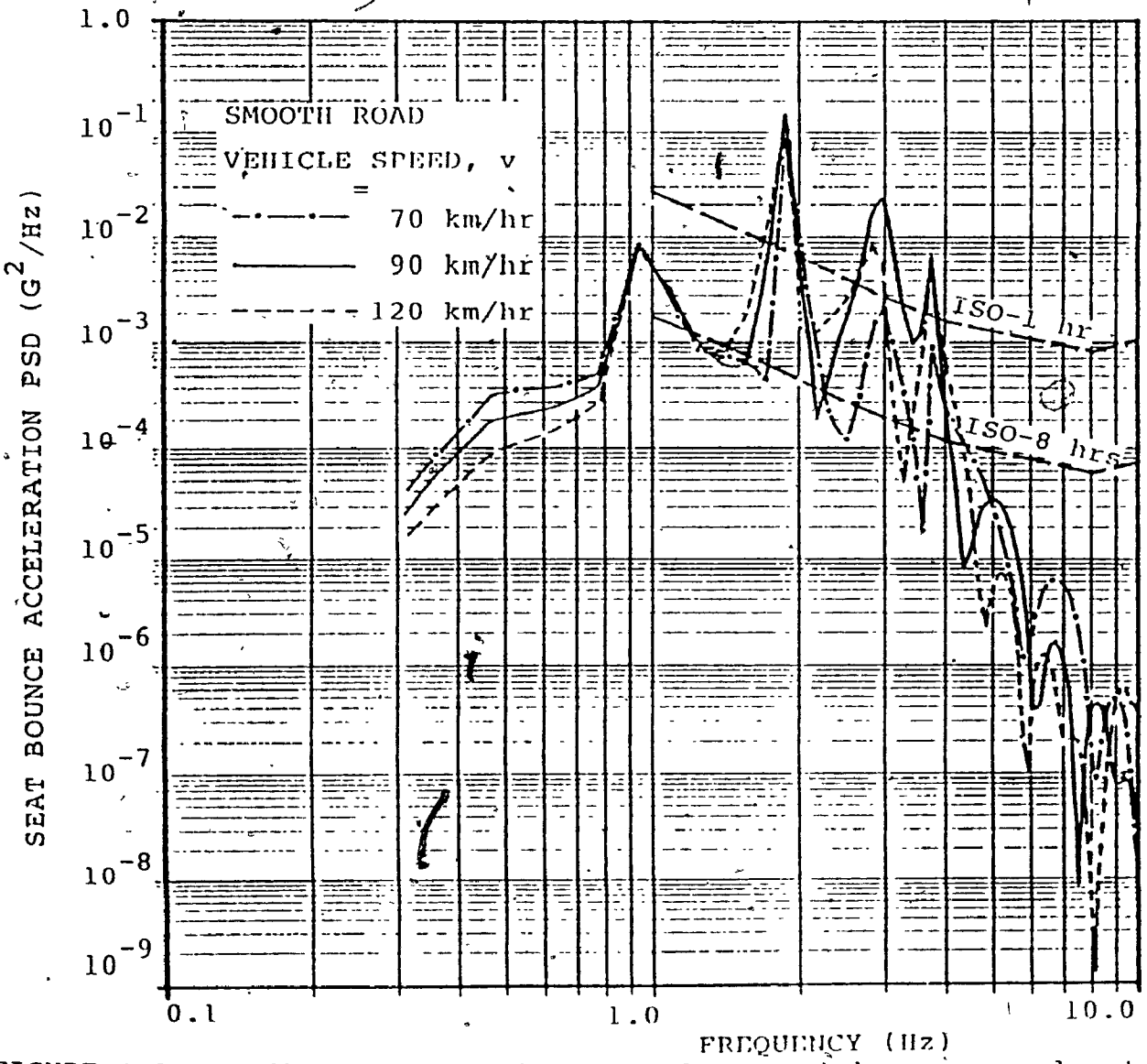

FIGURE 4.14: Influence of vehicle speed on seat bounce acceleration spectra - linear, three-dimensional baseline vehicle model

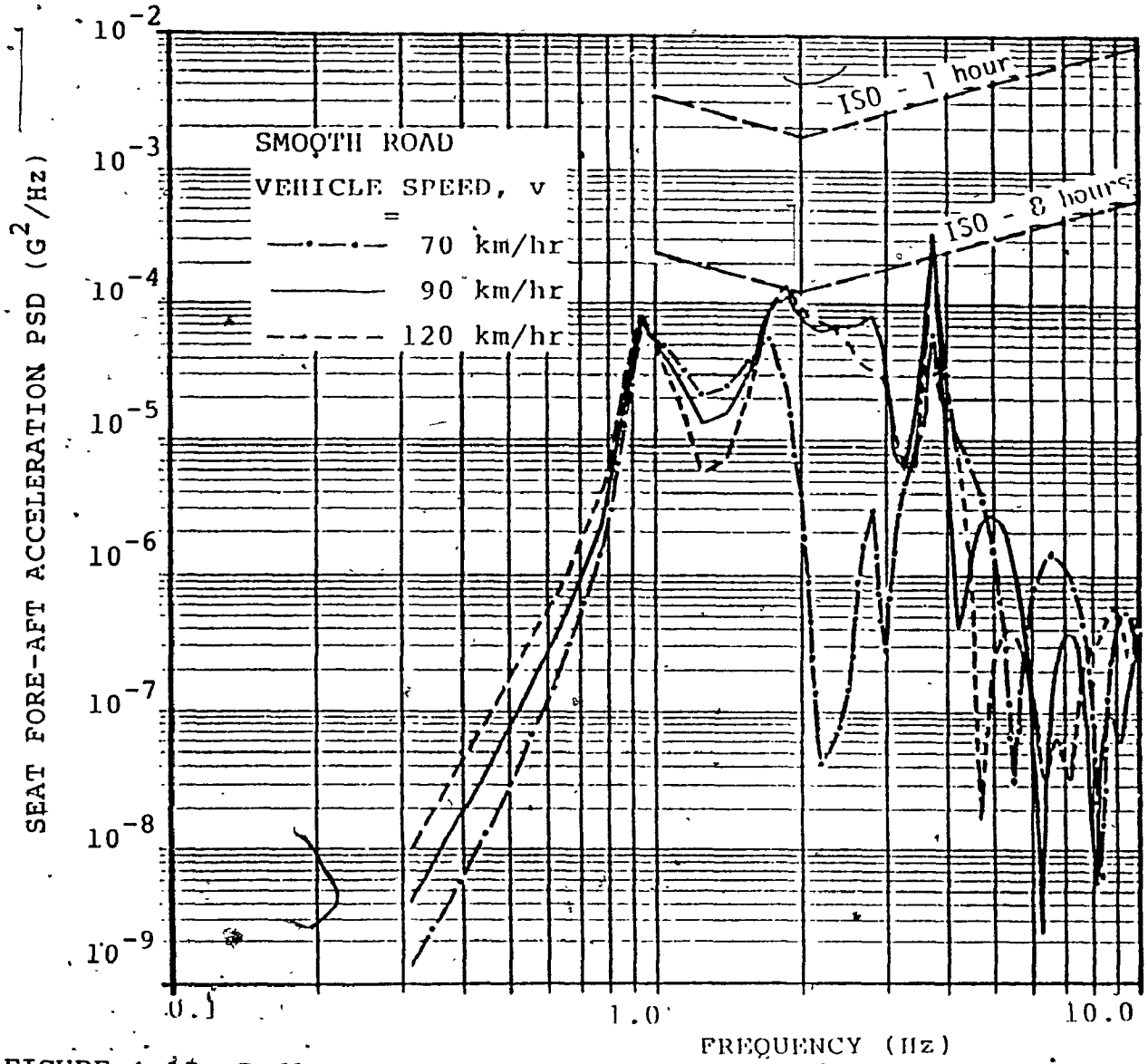

FIGURE 4.15: Influence of vehicle speed on seat fore-aft acceleration spectra - linear, three-dimensional baseline vehicle model

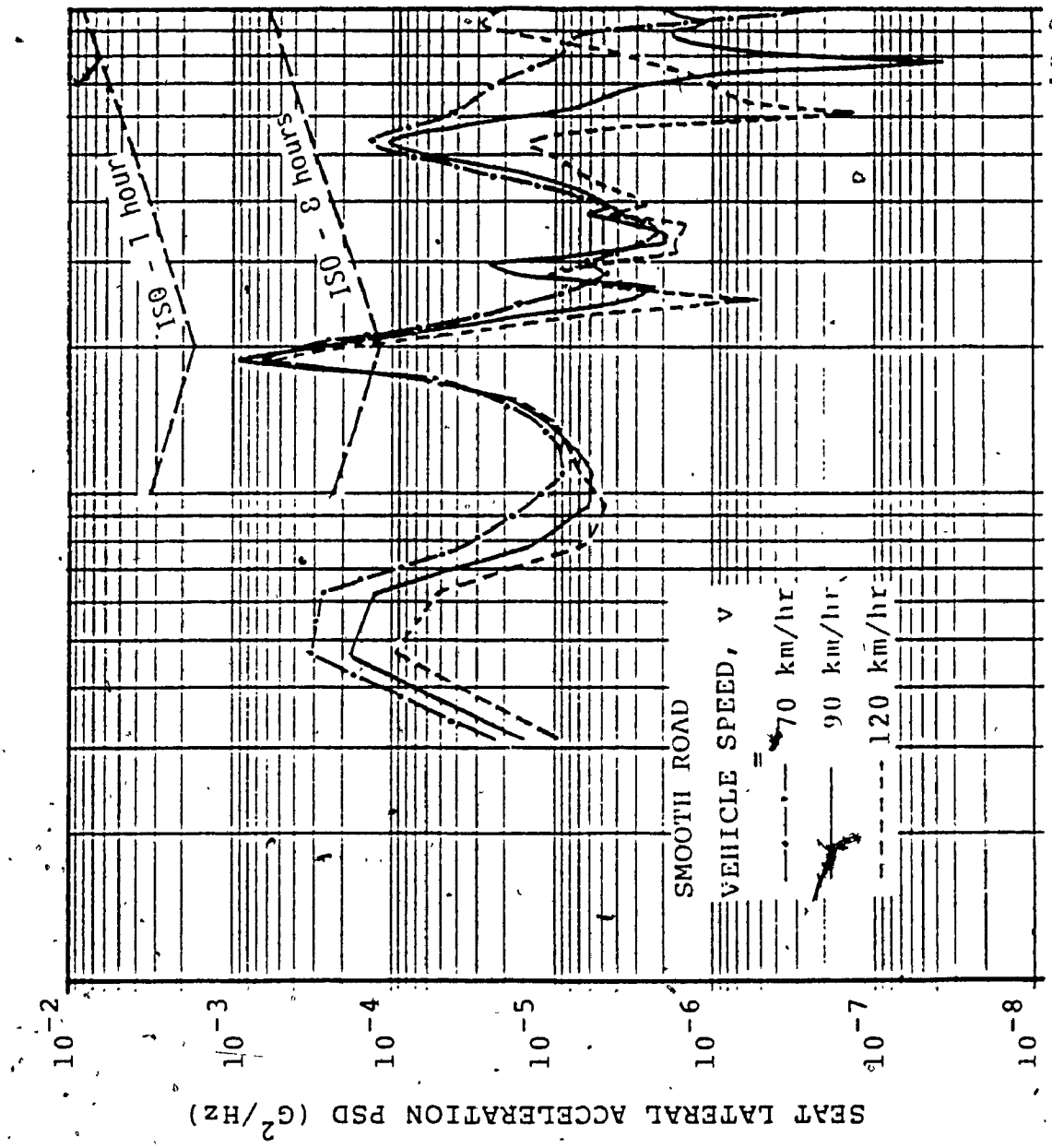

FIGURE 4.16: Influence of vehicle speed on seat lateral acceleration spectra - linear, three-dimensional baseline vehicle model

bounce ride levels is much higher, but the fore and aft ride levels are improved significantly with the inclusion of seat-cab suspensions (three-dimensional model).

4.5 SUMMARY

The dynamic response of the articulated vehicle to the road undulations, which are represented as stationary Gaussian random excitations is investigated using two-dimensional and three-dimensional models. The power spectral density approach is utilized to evaluate the effects of road characteristics and vehicle speed. These results are assessed with respect to the ISO specified acceptable levels of vibration to evaluate the vehicle ride quality. A comparison between the ride levels obtained from two-dimensional and three-dimensional studies is carried out to indicate the influence of the inclusion of the seat-cab dynamics in the analysis. In the next chapter, ride response evaluation of nonlinear model to random excitations is carried out.

CHAPTER 5

RIDE RESPONSE EVALUATION OF NONLINEAR MODEL TO STOCHASTIC INPUTS

5.1 INTRODUCTION

In the previous chapter, the dynamic response of the baseline vehicle was analyzed using two-dimensional and three-dimensional models having linear suspension systems. Since linear systems are relatively easier to analyze than the nonlinear ones, preliminary performance evaluations and parametric sensitivity analyses are effectively carried out using linear analytical tools even for higher degrees-of-freedom systems. Linear approximation of the nonlinear suspension elements may be considered appropriate for systems subjected to small disturbances (linear range), while the associated effects of nonlinearities are of second order. Vehicle suspensions, in general, do not operate in their linear range and exhibit nonlinearities associated with the hysteretic nature of the leaf and rubber type suspensions, suspension stops, and wheel hop. Such vehicle suspensions, thus cannot be accurately analyzed using linear analytical tools.

Direct integration techniques can be employed to simulate the nonlinear equations of motion. However, the simulation of nonlinear vehicle model to random terrain inputs, using numerical integration techniques, is

extremely demanding on computer and human resources. Alternatively, the nonlinear suspension elements in the vehicle model are replaced by an equivalent suspension system with linear stiffness and damping characteristics, such that the convenient analytical tools for the linear systems may be employed to predict the response behaviour of nonlinear vehicle models. Such processes are referred to as equivalent linearization techniques.

In this chapter, a brief summary of the available analytical techniques to study the stochastically excited nonlinear systems are discussed. A technique based on local equivalent linearization process is adapted and further developed to give a technique applicable to study the ride dynamics of a heavy articulated vehicle, comprising of nonlinear suspension damping mechanisms. It is the object of this chapter to gain an insight into the relative importance of these nonlinearities on the ride quality of a heavy vehicle, and to obtain a better understanding of various ride influencing factors such as vehicle suspension elements, load pattern, vehicle speed, and road characteristics.

5.2 NONLINEAR VEHICLE MODEL

The bounce and pitching motions of tractor and semitrailer have significant contribution to the driver discomfort and thus, the mathematical model of actual

vehicle should have all these dominant motions without introducing unnecessary complications or irrelevant degrees-of-freedom. The mathematical model of the baseline vehicle adapted for this study is similar to the simplified two-dimensional model described in chapter 2. This model is set-up in the bounce and pitch plane as shown in Figure 5.1. The nonlinear characteristics of this model are discussed in the following paragraphs.

Although a number of nonlinearities such as, dry or Coulomb friction due to interleaf friction of multi-leaf spring, bump stop, and wheel hop can be expected to influence the ride dynamics of the vehicle to an appreciable degree, the Coulomb friction has a large influence on the ride comfort and ride safety of the vehicle [23]. Consequently, there is a need to evaluate the effect of dry friction on the ride dynamics of the vehicle.

The general form of the relationship between the suspension spring force and deflection is shown in Figures 5.2 and 5.3 for a four spring suspension of a tractor and semitrailer, respectively. These curves are obtained by gradually loading and unloading the suspension and measuring the deflection. The hysteresis loop is due to the effect of Coulomb friction in the suspension and the enclosed area represents the energy dissipated/cycle. For the vehicle model under study, the Coulomb friction present

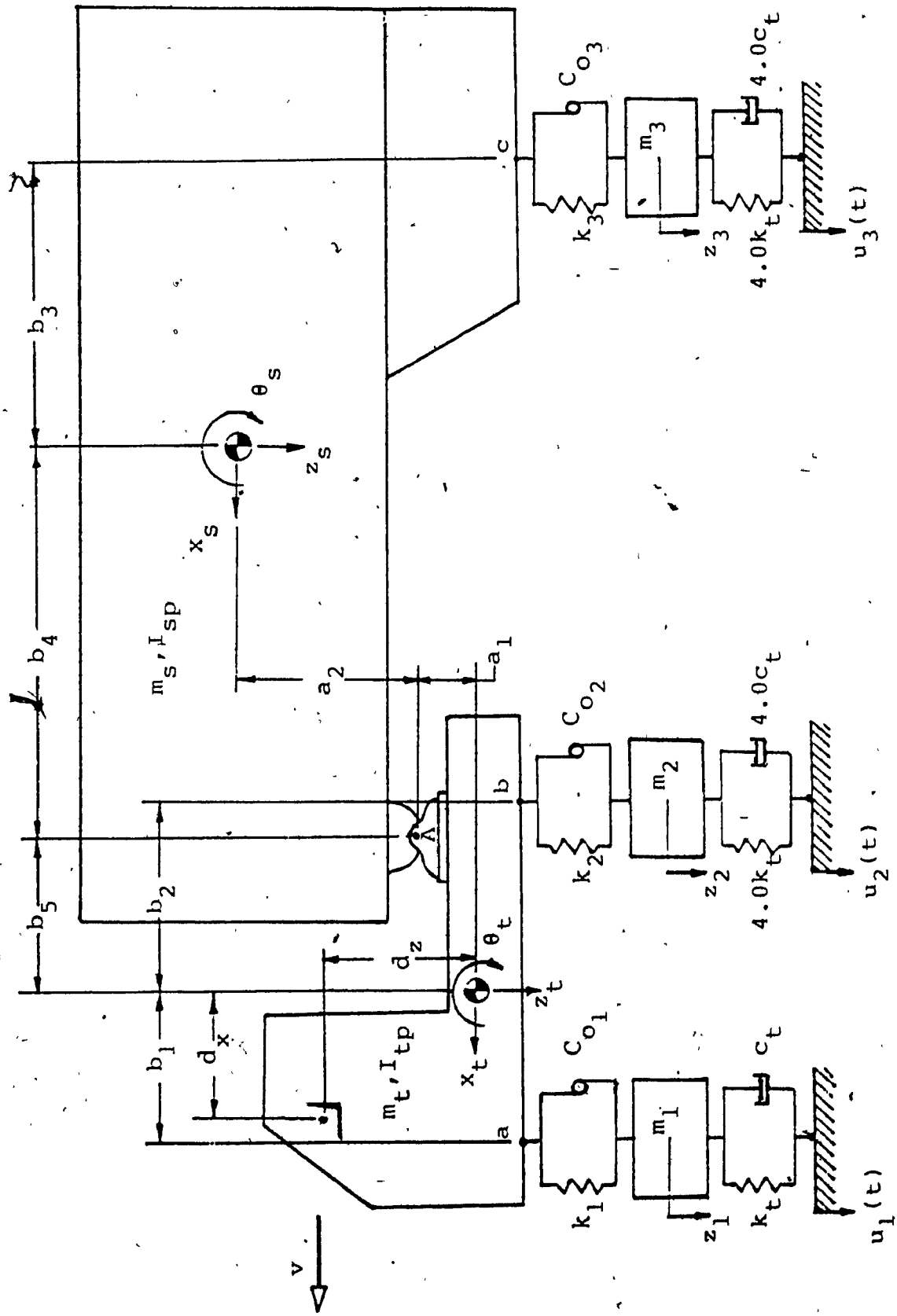

FIGURE 5.1: Schematic representation of nonlinear, two-dimensional baseline vehicle model

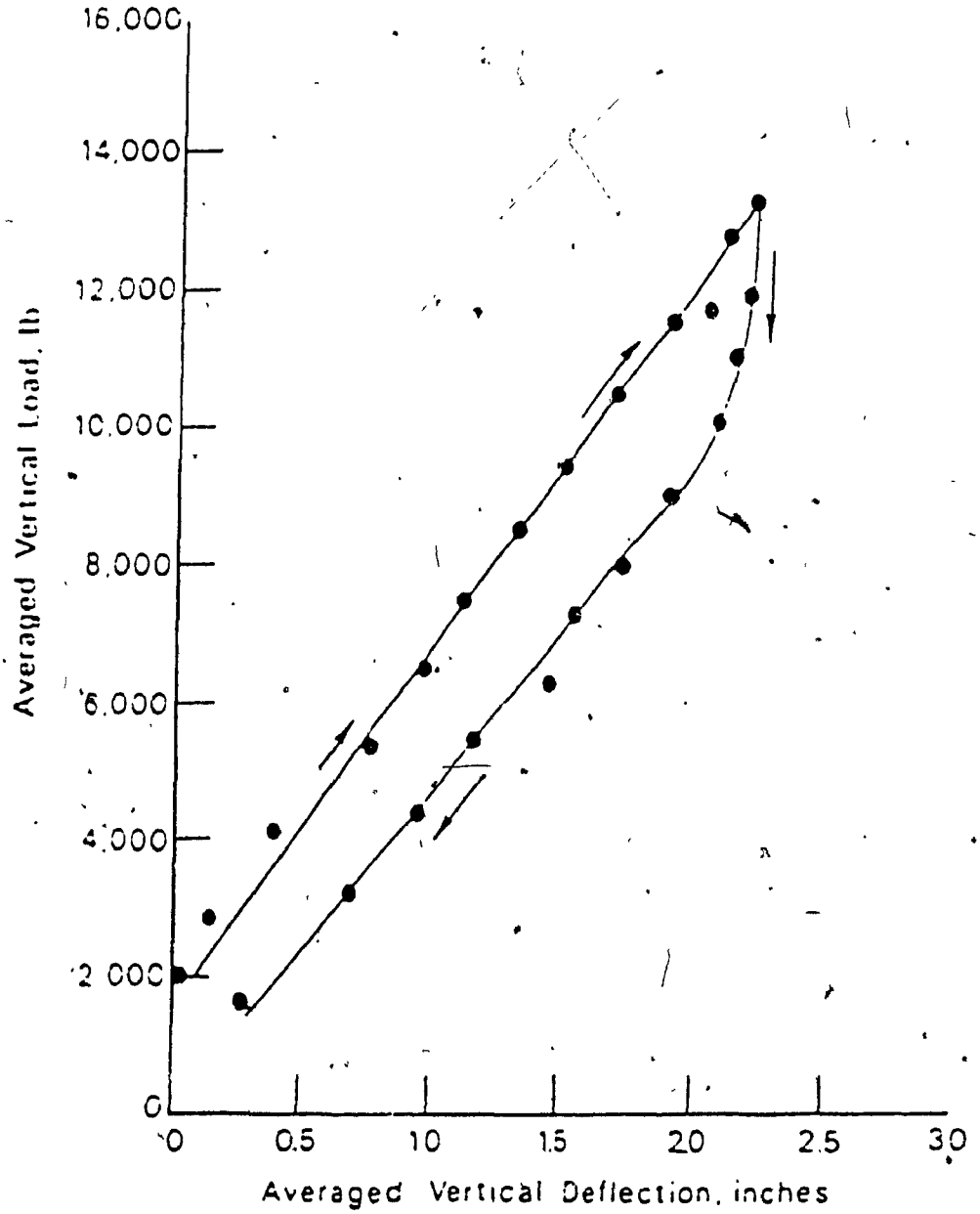

FIGURE 5.2: Averaged vertical deflection characteristics of four spring suspension of tractor [58]

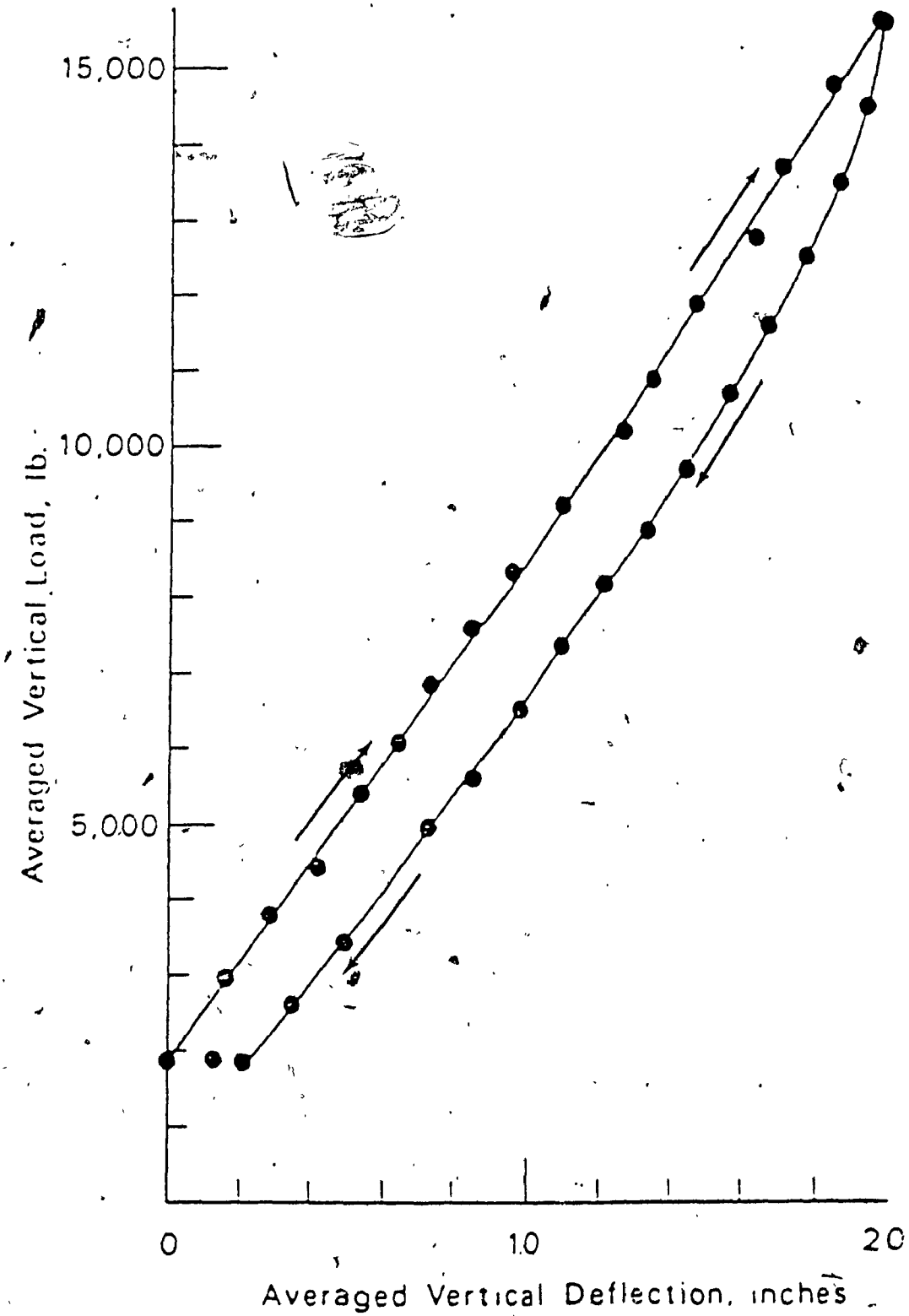

FIGURE 5.3: Averaged vertical deflection characteristics of four spring suspension of trailer [58]

in all three suspension units is modelled as a linear spring and friction damper acting in parallel. This configuration of the suspension unit is referred as a directly coupled friction damping system [47]. It is shown in Figure 5.4 along with its force-deflection characteristics. The values of linear spring constants k_i for all three suspension units are listed in Table 2.3 along with baseline values of other parameters. The magnitude of friction forces C_{o_i} depends on the frictional surfaces, their material and quality. The friction force is as much as 7-20% of the static load on the front axles, and 15-30% of the static load on the rear axles for the semi-elliptical multi-leaf springs [20]. In classical dynamics, the magnitude of the kinetic value of Coulomb friction is considered to be about 75% of the corresponding static friction value [7]. The magnitude of Coulomb friction considered within each suspension unit of the baseline vehicle is obtained in terms of static friction value. A list of Coulomb frictional forces for all three suspension units is presented in Table 5.1.

The nonlinear equations of motion for the nonlinear vehicle model are developed using Lagrangian formulation. The equation of motion characterizing tractor bounce (z_t), tractor pitch (θ_t), semitrailer pitch (θ_s) and wheel hop, (z_1, z_2, z_3) are written as follows :

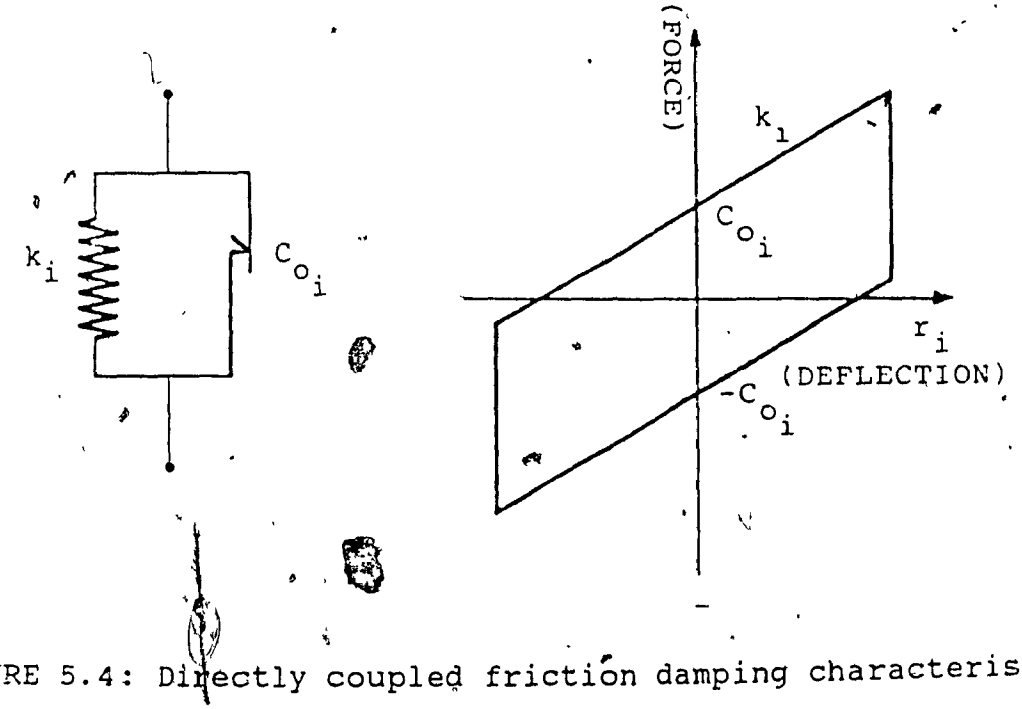

FIGURE 5.4: Directly coupled friction damping characteristics

TABLE 5.1 [24]

STATIC FRICTION VALUES

i	SUSPENSION	STATIC FRICTION, $C^s_{o_i}$ (N)
1	TRACTOR FRONT AXLE	4225.0
2	TRACTOR REAR AXLE	6230.0
3	SEMITRAILER AXLE	8675.0

Tractor Bounce :

$$(m_t + m_s)\ddot{z}_t + (b_5 m_s)\ddot{\theta}_t + (b_4 m_s)\ddot{\theta}_s + \sum_{i=1}^{3}(F_{k_i} + F_{d_i}) = 0 \qquad (5.1)$$

Tractor Pitch :

$$(b_5 m_s)\ddot{z}_t + (I_{tp} + b_5^2 m_s + M_m a_1^2)\ddot{\theta}_t + (b_4 b_5 m_s - a_1 a_2 M_m)\ddot{\theta}_s - b_1(F_{d_1} + F_{k_1}) + b_2(F_{d_2} + F_{k_2}) + b_5(F_{d_3} + F_{k_3}) = 0 \qquad (5.2)$$

Semitrailer Pitch :

$$(b_4 m_s)\ddot{z}_t + (b_4 b_5 m_s - a_1 a_2 M_m)\ddot{\theta}_t + (b_4^2 m_s + a_2^2 M_m + I_{sp})\ddot{\theta}_s + (b_3 + b_4)(F_{d_3} + F_{k_3}) = 0 \qquad (5.3)$$

Wheel Hop :

$$m_i \ddot{z}_i + (c_{t_i}\dot{r}_j - F_{d_i}) + (k_{t_i} r_j - F_{k_i}) = 0 \qquad (5.4)$$

for $i = 1,2,3$ and $j = i+3$

where m_t , m_s , I_{tp} , and I_{sp} represent the sprung mass of tractor, semitrailer, pitch mass moment of inertia of tractor and semitrailer, respectively. m_i is unsprung mass of axle i, and

$$M_m = \frac{m_t M_5^2 + m_s M_4^2}{(M_4 + M_5)^2}$$

where $M_4 = m_t + m_1 + m_2$

$M_5 = m_s + m_3$

c_{t_i} and k_{t_i} are the linear damping and stiffness characteristics of i^{th} tire unit. r and $\dot{r}$ represent relative displacement and relative velocity, respectively, across vehicle suspensions and tires. F_{d_i} and F_{k_i} are the damping and spring force, respectively, of the i^{th} suspension unit, given by :

$$F_{d_i} = C_{o_i} \, sgn(\dot{r}_i) \qquad (5.5a)$$

$$F_{k_i} = k_i r_i \qquad (5.5b)$$

where C_{o_i} and k_i are the magnitude of Coulomb friction and the linear spring constant, respectively, due to i^{th} suspension unit. The sign function $sgn(\dot{r}_i)$ accounts for phase between the damping force, F_{d_i}, and the relative velocity, $\dot{r}_i$ and has the value of 1.0 for $\dot{r}_i > 0$ and -1.0 for $\dot{r}_i < 0$. Therefore, the Coulomb damping force has a step discontinuity as shown in Figure 5.5. Since differential equations should be continuous in nature for the simulation purposes, this discontinuity can be approximated to yield a continous function by employing a limiting value, ϵ, as shown by the dotted line. The limiting value, ϵ, should be as small as possible to represent the true characteristic of Coulomb friction.

The vector {r} defining the relative displacement across suspensions and tires, is expressed as :

$$\{r\} = [T_r]\{q\} - \{u\} \qquad (5.6)$$

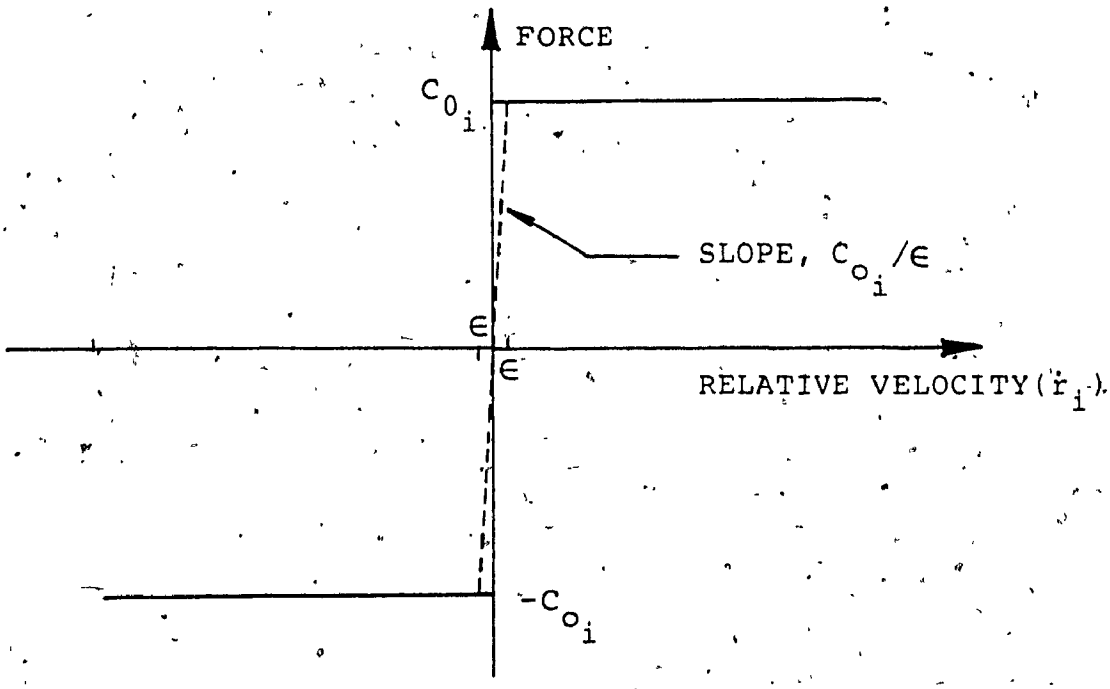

FIGURE 5.5: Coulomb force characteristics

where $[T_r]$ is 6x6 transformation matrix, given by :

$$[T_r] = \begin{bmatrix} 1 & -b_1 & 0 & -1 & 0 & 0 \\ 1 & b_2 & 0 & 0 & -1 & 0 \\ 1 & b_5 & b_3 + b_4 & 0 & 0 & -1 \\ 0 & 0 & 0 & 1 & 0 & 0 \\ 0 & 0 & 0 & 0 & 1 & 0 \\ 0 & 0 & 0 & 0 & 0 & 1 \end{bmatrix} \quad (5.7)$$

$\{q\}$ and $\{u\}$ are vectors of generalized response and excitation coordinates :

$$\{q\} = \{z_t, \theta_t, \theta_s, z_1, z_2, z_3\}' \quad (5.8a)$$

$$\{u\} = \{0, 0, 0, u_1(t), u_2(t), u_3(t)\}' \quad (5.8b)$$

The nonlinear equations of motion can be then expressed in the matrix form in terms of relative displacement response coordinates as :

$$[M_r]\{\ddot{r}\} + \{F_d\} + [K_r]\{r\} = -[M_r]\{\ddot{u}\} \quad (5.9)$$

where $[M_r]$ is the mass matrix in terms of relative coordinates, given by :

$$[M_r] = [M][T_r]^{-1} \quad (5.10)$$

$[M]$ is the mass matrix in terms of generalized coordinates, and is given by equation (I.8) in Appendix I.

$\{F_d\}$ is the vector of damping forces, given by :

$$[F_d] = \begin{Bmatrix} C_{o_1}\,\mathrm{sgn}(\dot{r}_1) + C_{o_2}\,\mathrm{sgn}(\dot{r}_2) + C_{o_3}\,\mathrm{sgn}(\dot{r}_3) \\ -b_1 C_{o_1}\,\mathrm{sgn}(\dot{r}_1) + b_2 C_{o_2}\,\mathrm{sgn}(\dot{r}_2) + b_5 C_{o_3}\,\mathrm{sgn}(\dot{r}_3) \\ (b_3 + b_4)\, C_{o_3}\,\mathrm{sgn}(\dot{r}_3) \\ c_{t_1}\dot{r}_1 - C_{o_1}\,\mathrm{sgn}(\dot{r}_1) \\ c_{t_2}\dot{r}_2 - C_{o_2}\,\mathrm{sgn}(\dot{r}_2) \\ c_{t_3}\dot{r}_3 - C_{o_3}\,\mathrm{sgn}(\dot{r}_3) \end{Bmatrix} \qquad (5.11)$$

$[K_r]$ is the matrix of spring constants in terms of relative displacement coordinates, given by :

$$[K_r] = \begin{bmatrix} k_1 & k_2 & k_3 & 0 & 0 & 0 \\ -b_1 k_1 & b_2 k_2 & b_5 k_3 & 0 & 0 & 0 \\ 0 & 0 & (b_3 + b_4) k_3 & 0 & 0 & 0 \\ -k_1 & 0 & 0 & k_{t_1} & 0 & 0 \\ 0 & -k_2 & 0 & 0 & k_{t_2} & 0 \\ 0 & 0 & -k_3 & 0 & 0 & k_{t_3} \end{bmatrix} \qquad (5.12)$$

5.3 ANALYTICAL TECHNIQUES TO EVALUATE STATIONARY RESPONSE OF NONLINEAR SYSTEMS

A number of analytical techniques have been developed to study nonlinear, multi-degrees-of-freedom systems subjected to random excitations. These techniques include Fokker-Planck equation approach, the perturbation approach, and the equivalent linearization approach. A brief summary of these techniques is discussed as follows :

a) Fokker-Planck Equation Approach

The Fokker-Planck equation approach [5,12,43,44] provides an exact method for studying the stationary response of a nonlinear system. The transitional probability density of the response is governed by the Fokker-Planck equation only if the excitation is a Gaussian white noise. The response statistics can be completely defined by this transitional probability density. The stationary form of the Fokker-Planck equation is applicable under three severe restrictions [26] : damping forces being proportional to the velocity, Gaussian white noise excitations, and the spectral density matrix of excitation being proportional to the damping matrix of the system. These conditions are seldom satisfied by the physical systems. The hysteretic systems such as vehicle suspension with Coulomb friction thus cannot be handled by this approach.

b) Perturbation Approach

This approach can be effectively used if the dynamical systems have sufficiently small nonlinearities, and the level of excitation is sufficiently low. In this approach, the solution is represented as an expansion in powers of some small parameters, which specifies the size of nonlinearity. The assumed power series solution is substituted into the original equations of motion and the

coefficients of like powers of the nonlinearity parameter are then equated [14,42]. This leads to a set of linear differential equations for the terms in the solution expansion. A first order approximation is obtained by solving two sets of linear differential equations. The first set of differential equations is obtained by setting all nonlinearities to zero, and the second set of differential equations is formualted with the excitation as a function of the solution of first set. The practicality of this approach is severely limited by the lengthy calculations, which becomes progressively tedious as the order of expansion parameter increases. Major difficulties arises in the application of this approach to study the nonlinear vehicle model because of the absence of linear viscous damping and high dry friction value in the primary suspensions.

c) **Equivalent Linearization Techniques**

Among the analytical methods mentioned above to study nonlinear random vibration problems, equivalent linearization technique is the one that has been extensively applied [42]. It gives good results for even highly nonlinear systems, whereas other methods are only useful for slightly nonlinear system. In most cases, the only restriction placed on the system is that the excitations are assumed to be stationary and Gaussian.

The equivalent linearization techniques, usually attributed to Bootan [11], Caughey [13], who generalized the deterministic linearization methods of Krylov and Bogoliubov [29] to stochastic cases, is based on the concept of replacing the nonlinear system by a related linear system in such a way that difference between the two systems is minimized. Since, in the random vibration analysis, the system variables are represented as statistical quantities, minimization criterion selected is mean square of the response error between the two systems. Therefore, this linearization process is referred as statistical linearization.

It has been established that although the statistical linearization technique can be applied to a broad class of problems and is not limited by restrictions encountered in other approximation approaches, it cannot include the often critical effects of nonlinearities such as Coulomb friction, and clearance spring [37]. Nonlinear damping mechanisms are approximated by an equivalent viscous damping coefficient over the entire input frequency range using statistical linearization [20]. Scanlan [48] established that the nonlinear damping mechanisms, in general should be expressed by a local constant applicable only in a restricted frequency band centered around a specific frequency. Specifically, nonlinearities such as Coulomb friction are not correctly represented by a

constant damping coefficient over an entire frequency range of interest. For a nonlinear damping phenomenon, in general, one needs an array of average " locally constant " linear damping coefficients. These locally constant values must be appropriately changed for different frequency ranges and amplitudes of excitation [38].

In the following section, an iterative algorithm based on ' local equivalent linearization technique [39] ' is presented. This algorithm establishes a set of equivalent viscous damping coefficients as a function of local values of frequency, amplitude of excitation, and type of nonlinearity.

5.4 LOCAL EQUIVALENT LINEARIZATION TECHNIQUE

The local equivalent linearization technique is based on equating the energy dissipated or average force transmitted per cycle due to nonlinear damping to that of an equivalent viscous damper [6,39]. The nonlinear damping phenomena are expressed by an array of 'local constants', whose value depend upon excitation frequency, excitation amplitude, general properties of the damping element and upon the dynamics of the multi-degrees-of-freedom system. Thus, the nonlinear system is replaced by several localized linear systems corresponding to every discrete frequency and amplitude of excitation. The linear system, thus formulated, will characterize the behaviour of nonlinear

system accurately in the vicinity of the specific frequency and amplitude of excitation [39].

In this section, the local viscous damping coefficients due to velocity dependent nonlinear damping are obtained using energy and force balance techniques. An iterative algorithm which expresses the nonlinear damping by an array of local constants is presented.

5.4.1 ENERGY AND FORCE BALANCE

The nonlinear damping mechanisms are expressed in two general forms: velocity dependent and displacement dependent. The nonlinear damping force, in general, can be expressed as either being proportional to n^{th} power of relative velocity across the damper or as proportional to the p^{th} power of relative displacement across damper [39]. The force due to nonlinear damping inherent in vehicle suspension can be expressed as being proportional to the n power of relative velocity, $\dot{r}$ across damper :

$$F_d = f(r,\dot{r}) = C_n |\dot{r}|^n \, sgn(\dot{r}) \qquad (5.13)$$

where the damping coefficients C_n and exponent n may have any positive value, and the sign function $sgn(\dot{r})$ ensures that the damping force is in phase with the relative velocity. Application of such generalized formulations are illustrated as follows :

Coulomb damping (n=0) $$F_d = C_o \, \mathrm{sgn}(\dot{r}) \qquad (5.14)$$

Viscous damping (n=1) $$F_d = C_1 \dot{r} \qquad (5.15)$$

Orifice damping (n=2) $$F_d = C_2 |\dot{r}| \, \dot{r} \qquad (5.16)$$

where C_o is the magnitude of Coulomb force, and C_1 and C_2 are coefficients of viscous and quadratic damping respectively. Higher values of exponent n may be selected to represent nonlinear damping characteristics applicable for a given physical damper.

For a single degree of freedom system subjected to harmonically forced vibration, the general solution is given by :

$$r = \delta \sin(\omega t) \qquad (5.17)$$

where δ is the magnitude of relative displacement and ω is the excitation frequency. The energy loss per cycle by the nonlinear damper is computed as :

$$\Delta E = \oint C_n \, |\dot{r}|^n \, \mathrm{sgn}(\dot{r}) \, \dot{r} \, dt \qquad (5.18)$$

Combining equations (5.17) and (5.18) yields the following:

$$\Delta E = \begin{cases} 4 \, C_o \delta & ; \; n = 0 \\ 4 \, \Phi \prod_{i=1}^{j} \left[\dfrac{n - 2i + 2}{n - 2i + 3} \right] C_n \omega^n \delta^{n+1} & ; \; n > 0 \end{cases} \qquad (5.19)$$

where

$$\Phi = \begin{cases} 1 \\ \pi/2 \end{cases} \quad \text{and} \quad j = \begin{cases} n/2 & ; \; n = 2,4,6,\ldots \\ (n+1)/2 & ; \; n = 1,3,5,\ldots \end{cases} \tag{5.20}$$

The local equivalent viscous damping coefficients $c_{eq}(\omega, \delta)$ corresponding to excitation frequency, ω , and response amplitude is evaluated by equating the energy loss of nonlinear damper to that of a viscous damper. The local equivalent viscous coefficient is then evaluated as :

$$c_{eq}(\omega, \delta) = \begin{cases} \dfrac{4\,C}{\pi \omega \delta} & ; \; n = 0 \\ (2/\lambda) \displaystyle\prod_{i=1}^{j} \left[\frac{n + 2 - 2i}{n + 3 - 2i}\right] C_n \omega^{n-1} \delta^{n-1} & ; \; n > 0 \end{cases} \tag{5.21}$$

where

$$\lambda = \begin{cases} \pi/2 & ; \; n = 2,4,6,\ldots\ldots \\ 1 & ; \; n = 1,3,5,\ldots\ldots \end{cases} \tag{5.22}$$

Alternatively, the local equivalent viscous damping coefficient can be computed by equating the average transmitted force of the nonlinear damper to that of a viscous damper :

$$c_{eq}(\omega, \delta) = \begin{cases} \dfrac{\sqrt{2}\, C_o}{\omega \delta} & ; \; n = 0 \\ C_n \, (\omega\delta/2)^{n-1} & ; \; n > 0 \end{cases} \tag{5.23}$$

The nonlinear damping force corresponding to excitation frequency can then be expressed as :

$$F_d(\omega) = f(r,\dot{r}) = c_{eq}(\omega,\delta)\dot{r} \qquad (5.21)$$

Such a linear model with a constant damping coefficient has its most appropriate application in small frequency band centered around either the predominant frequency or the selected excitation frequency [39].

5.4.2 ALGORITHM

The local equivalent algorithm developped by Rakheja and Sankar [39] is used to establish the local equivalent viscous coefficients for the nonlinear damping. The algorithm primarily assumes initial values of c_{eq} for nonlinear damping mechanism corresponding to an excitation frequency, ω. Thus the equation of motion is linearized for the selected frequency. Linear analytical tools are employed to compute relative displacement, δ , for a given excitation. The equivalent viscous coefficients are then computed using Equation (5.21-5.22) or (5.23), and the error between the assumed and computed values is evaluated. If the error exceeds certain specified bounds, the process is repeated with the computed values of damping constant and is continued until convergence is achieved. The algorithm is then repeated to obtain the local viscous coefficients in the entire frequency range.

5.5 APPLICATION OF LOCAL EQUIVALENT LINEARIZATION TECHNIQUE TO NONLINEAR ARTICULATED VEHICLE MODEL

In this section, the local equivalent linearization approach is adapted and further developed to obtain the stationary response of the nonlinear articulated vehicle model subject to stochastic inputs. The input spectrum, as discussed in chapter 3, is discretized and treated in a deterministic manner. The effectiveness of the algorithm is demonstrated by comparing the response predicted by the iterative algorithm to the exact solution obtained through direct integration of nonlinear differential equations. A comparison between the local equivalent approach and the statistical linearization technique is also presented.

5.5.1 RIDE RESPONSE EVALUATION OF NONLINEAR VEHICLE MODEL

The nonlinear equations of motion expressed in Equation (5.9) are solved in the frequency domain by representing the nonlinear damping forces in terms of an array of local viscous damping coefficients. The nonlinear equations are thus expressed by an array of local linear equations of motion, where each local linear equation is best applicable in a narrow frequency band. The local linear equations of motion are expressed as :

$$[M_r]\{\ddot{r}\} + [Ceq_r(\omega,r)]\{\dot{r}\} + [K_r]\{r\} = -[M_r]\{\ddot{u}\} \qquad (5.25)$$

where $[Ceq_r(\omega,r)]$ is the matrix of equivalent viscous damping coefficients corresponding to excitation frequency, ω, and response vector $\{r\}$. The equivalent viscous damping coefficients are obtained by equating the energy dissipated or force transmitted per cycle by nonlinear damping to that of a viscous damper, at each excitation frequency. However, in order to evaluate the energy dissipated by nonlinear damping, the relative displacement response vector of the system is required. The relative displacement response of the articulated vehicle model subjected to harmonic excitations with adequate phase information at tire-road interface is described as :

$$\{r\} = [H_r(j\omega)]\{f_r\} \qquad (5.26)$$

where

$$\{f_r\} = \omega^2 [M_r]\{u\} \qquad (5.27)$$

$[M_r]$ is the mass matrix given by Equation (5.10), and $\{u\}$ is the vector containing amplitudes of harmonic excitation obtained from Equation (5.8b) as :

$$\{u\} = [0,\ 0,\ 0,\ A,\ A\,e^{-j\mu_{12}},\ A\,e^{-j\mu_{13}}]'\,e^{j\omega t} \qquad (5.28)$$

where A is peak value of input displacement amplitude, and μ_{ik} describes the phase between wheel i and wheel k, and is given by equation (3.6) as :

$$\mu_{ik} = \omega . L_{ik} / v \qquad (5.29)$$

$$i = 1 \ ; \ k = 2,3$$

$[H_r(j\omega)]$ is the transfer function matrix given by :

$$[H_r(j\omega)] = [[K_r] - \omega^2[M_r] + j\omega[Ceq_r(\omega, r)]]^{-1} \quad (5.30)$$

where $[K_r]$ is the stiffness matrix given by Equation (5.12) and the equivalent viscous damping matrix $[Ceq_r(\omega, r)]$ for in-plane, nonlinear articulated vehicle model is given as :

$$[Ceq_r(\omega, r)] = \begin{bmatrix} c_{eq_1} & c_{eq_2} & c_{eq_3} & 0 & 0 & 0 \\ -b_1 c_{eq_1} & b_2 c_{eq_2} & b_5 c_{eq_3} & 0 & 0 & 0 \\ 0 & 0 & (b_3+b_4)c_{eq_3} & 0 & 0 & 0 \\ -c_{eq_1} & 0 & 0 & c_{t_1} & 0 & 0 \\ 0 & -c_{eq_2} & 0 & 0 & c_{t_2} & 0 \\ 0 & 0 & c_{eq_3} & 0 & 0 & c_{t_3} \end{bmatrix} \quad (5.31)$$

where the equivalent damping coefficients for all three suspension units may be obtained either from energy dissipation expression of Equations (5.21) and (5.22) or from Equation (5.23) i.e;

Energy balance : $$c_{eq_i} = \frac{4}{\pi} \frac{C_{o_i}}{\omega \delta_i} \quad (5.32a)$$

Force balance : $$c_{eq_i} = \sqrt{2} \frac{C_{o_i}}{\omega \delta_i} \quad (5.32b)$$

$$i = 1, 2, 3$$

It should be noted from Equations (5.32a) and (5.32b) that for very small value of relative velocity, the local equivalent viscous coefficient tends to be infinite as shown in Figure 5.6, which represents the general behaviour

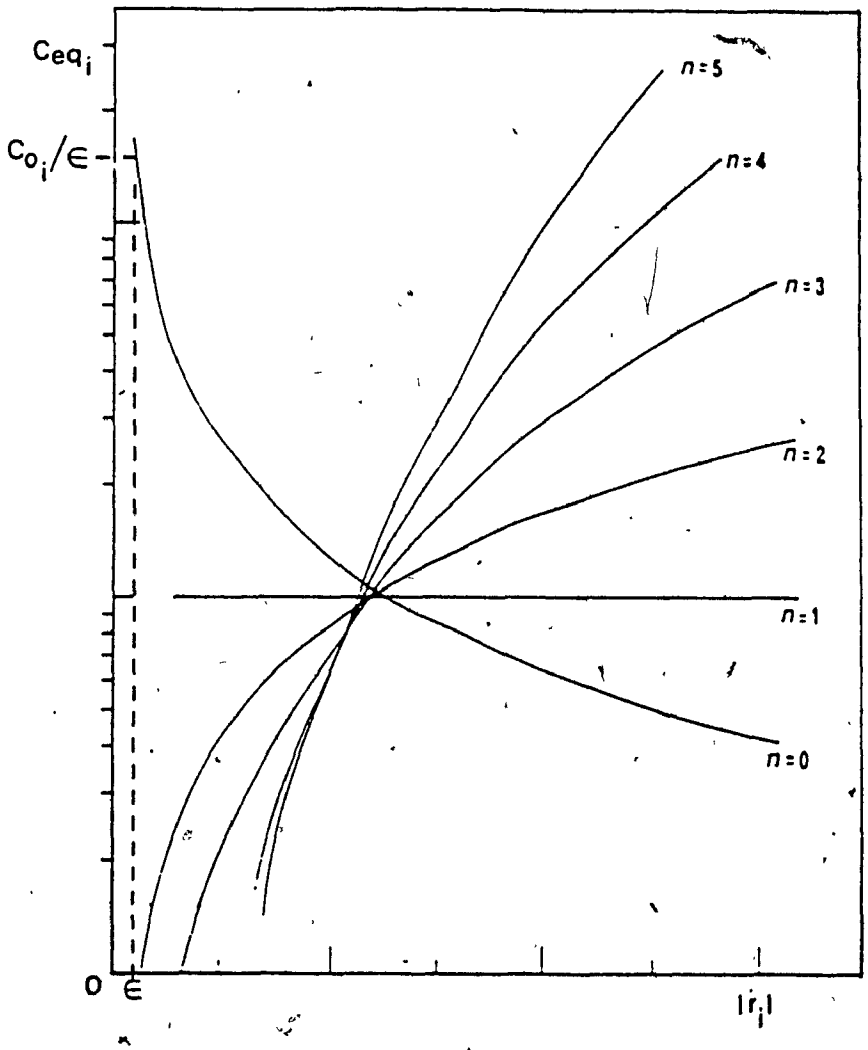

FIGURE 5.6: Local equivalent coefficients due to nonlinear velocity dependent damping [39]

of local equivalent coefficients due to nonlinear velocity dependent damping with various exponent values. This occurs due to discontinuous nature of Coulomb friction. Thus, for very small value of relative velocity ($\dot{r}_i < \epsilon$), the local equivalent viscous coefficient can be taken as the slope value (Figure 5.5), which remains constant as shown by the dotted line in Figure 5.6 for relative velocity less than or equal to selected limiting value, ϵ. The limiting value, selected to limit c_{eq_i} at low relative velocity will have significant effect on the vehicle response, as it would be seen later in this chapter. It should also be noted that the force balance approach gives slightly higher value of equivalent viscous damping coefficients than those obtained via energy balance approach. The equivalent viscous damping coefficient due to velocity squared damping can also be included in the above expressions, if one wishes to add a shock absorber in the vehicle suspension.

The localized linear system described by Equation (5.25), can be only solved in frequency domain if the values of c_{eq_i} ($i = 1,2,3$), and $\{r\}$ are available, Thus an iterative algorithm, as discussed previously, is developed to establish the value of local damping constants and relative displacement vector. The relative displacement vector $\{r\}$ is computed during every iteration, which involves matrix inversion to obtain transfer function matrix. Since matrix inversion is a time consuming

operation in a computer, it should be either avoided or the size of the matrix should be reduced. The matrix partitioning approach is employed to reduce the matrix size for inversion purpose.

The upper half of the vector {r} contains relative displacements across all suspension units, which are needed to evaluate the local damping constants. The lower half contains relative displacements across all the tire units. Therefore, the relative displacement vector {r} can be partitioned as follows :

$$\{r\} = \left\{\begin{array}{c} \bar{r}_1 \\ \hline \bar{r}_2 \end{array}\right\} \qquad (5.33)$$

where, $\{r_1\}$ is the vector of relative displacements across all three suspension units comprising of nonlinear damping mechanisms, and $\{r_2\}$ contains relative displacements across all the linear wheel models.

Rewriting Equation (5.26) as follows :

$$[A]\{r\} = \{f_r\} \qquad (5.34)$$

where,

$$[A] = [H_r(j\omega)]^{-1} \qquad (5.35)$$

Since the elements of matrix [A] are evaluated from the corresponding elements of system mass, damping, and stiffness matrices, the matrix [A] can be written in its expanded form with partitioning as :

$$[A] = \left[\begin{array}{ccc:ccc} a_{11} & a_{12} & a_{13} & a_{14} & a_{15} & a_{16} \\ a_{21} & a_{22} & a_{23} & a_{24} & a_{25} & a_{26} \\ a_{31} & a_{32} & a_{33} & a_{34} & a_{35} & a_{36} \\ \hdashline a_{41} & 0 & 0 & a_{44} & 0 & 0 \\ 0 & a_{52} & 0 & 0 & a_{55} & 0 \\ 0 & 0 & a_{63} & 0 & 0 & a_{66} \end{array}\right] \qquad (5.36)$$

Therefore, Equation (5.34) can be rewritten as ;

$$\left[\begin{array}{c:c} [A_{11}] & [A_{12}] \\ \hdashline [A_{21}] & [A_{22}] \end{array}\right] \left\{\begin{array}{c} \bar{r}_1 \\ \hdashline \bar{r}_2 \end{array}\right\} = \left\{\begin{array}{c} \bar{f}_{r_1} \\ \hdashline \bar{f}_{r_2} \end{array}\right\} \qquad (5.37)$$

or

$$[A_{11}]\{r_1\} + [A_{12}]\{r_2\} = \{f_{r_1}\} \qquad (5.38a)$$

$$[A_{21}]\{r_1\} + [A_{22}]\{r_2\} = \{f_{r_2}\} \qquad (5.38b)$$

From Equation (5.38b),

$$\{r_2\} = [A_{22}]^{-1} (\{f_{r_2}\} - [A_{21}]\{r_1\}) \qquad (5.39)$$

Substituting (5.39) into (5.38a) yields,

$$\{r_1\} = [[A_{11}]-[A_{12}][A_{22}]^{-1}[A_{21}]]^{-1} \{\{f_{r_1}\} - [A_{12}][A_{22}]^{-1}\{f_{r_2}\}\} \qquad (5.40)$$

where

$$[A_{22}]^{-1} = \begin{bmatrix} 1/a_{44} & 0 & 0 \\ 0 & 1/a_{55} & 0 \\ 0 & 0 & 1/a_{66} \end{bmatrix} \qquad (5.41)$$

For a given excitation frequency, ω and excitation vector $\{u\}$, the sub-matrices $[A_{12}]$, $[A_{22}]$, and vector $\{f_r\}$

remain constant, while sub-matrices $[A_{11}]$ and $[A_{21}]$ are updated with new values of equivalent viscous damping for each suspension unit during every iteration. Therefore, Equation (5.40) can be rewritten as :

$$\{r_1\} = [[A_{11}] - [Q][A_{21}]]^{-1} \{p\} \qquad (5.42)$$

where

$$[Q] = [A_{12}][A_{22}]^{-1} \quad ; \quad \{p\} = \{\{f_{r_1}\} - [Q]\{f_{r_2}\}\}$$

Since the size of the matrix to be inverted during each iteration has been reduced to one half, the iterative process becomes twice as much faster. The relative displacements across tires, $\{r_2\}$ can be computed using Equation (5.39), once the convergence is achieved. The generalized displacement vector, $\{q\}$ can then be obtained using Equation (5.6), given by:

$$\{q\} = [T_r]^{-1} \{\{r\} + \{u\}\} \qquad (5.43)$$

The local equivalent linearization technique can be conveniently extended to stochastically described excitations (stationary random excitations measured from the smooth and rough highways). Since the linearization technique establishes the local equivalent damping parameter as a function of localized excitation and response variables, the stochastically described highway profiles can be discretized to yield local amplitudes of excitation corresponding to each discrete frequency. A

suitable technique for generating local excitation amplitudes was discussed in chapter 3. Such that the input excitation vector can be rewritten in the following manner:

$$\{u_l\} = \{0,\ 0,\ 0,\ A_l,\ A_l e^{-j\mu'_{12}},\ A_l e^{-j\mu'_{13}}\}\ e^{j\omega_l t} \qquad (5.44)$$

$$l = 1,2,3,\ldots\ldots,N_f$$

where N_f is the number of harmonics considered to represent the road profile, and f_l is the frequency of the l^{th} harmonic.

The local excitation amplitude is used to determine the values of local damping constants as discussed above. The local frequency response function matrix $[H(j\omega_l)]$ is then evaluated as :

$$[H(j\omega_l)] = [[K] - \omega_l^2[M] + j\omega_l[Ceq]]^{-1} \qquad (5.45)$$

where mass and stiffness matrices for in-plane vehicle model are given in Appendix I, and the local equivalent damping matrix is established in the same manner as the viscous damping matrix given in Appendix I. The response power spectral densities $[S_q(f_l)]$ are then evaluated from Equations (4.16) or alternatively :

$$[S_q(f_l)] = [G(j\omega_l)]^* [S_i(f_l)]\ [G(j\omega_l)]' \qquad (5.46)$$

where

$$[G(j\omega_l)] = [H(j\omega_l)]\ [[K_F] + j\omega_l [C_F]] \qquad (5.47)$$

5.5.2 RESPONSE EVALUATION DURING SUSPENSION LOCK-UP

Due to the presence of high Coulomb friction, the primary suspensions become very stiff and cause the vehicle to vibrate on the tires, since there is no deflection of the springs until the inertia forces produce sufficient force to overcome the breakaway friction. Consequently, the critical lock-up behaviour due to Coulomb friction must be inspected such that the nonlinear behaviour of the system can be effectively simulated by the equivalent linear system.

For a single-degree-of-freedom base excited system the, lock-up condition for Coulomb damping is expressed as [39]:

$$m \left|\ddot{x}(\omega_1)\right| < C_o \qquad (5.48)$$

where, $\left|\ddot{x}(\omega_1)\right|$ is the absolute acceleration response of the system, and C_o is magnitude of Coulomb friction. Above condition implies that the lock-up is experienced , when the inertia force is less than the magnitude of Coulomb friction. Hence the mass acceleration becomes equal to the acceleration of base excitation and the relative displacement across the suspension is zero [39].

For the baseline vehicle (Figure 5.1), the lock-up conditions for tractor front and rear suspensions, and semitrailer suspension must be inspected at every discrete frequency. This is accomplished by evaluating the inertia

forces at points a, b, and c (points of suspension attachment to the sprung masses) :

$$F_a^I = m_a \left|\ddot{z}_1(\omega_1)\right| \tag{5.49a}$$

$$F_b^I = m_b \left|\ddot{z}_2(\omega_1)\right| \tag{5.49b}$$

$$F_c^I = m_c \left|\ddot{z}_3(\omega_1)\right| \tag{5.49c}$$

where m_a , m_b and m_c are calculated from the static load distribution at points a, b, and c , given by :

$$m_a = \frac{m_t b_2 + m_a(b_2 - b_5)}{L_t} \tag{5.50a}$$

$$m_b = m_t + m_A - m_a \tag{5.50b}$$

$$m_c = \frac{m_s \cdot b_4}{L_s} \tag{5.50c}$$

and

$$m_A = m_s - m_c \tag{5.50d}$$

where L_t , and L_s are the tractor and semitrailer wheel bases, respectively. m_A represents the proportion of the semitrailer mass reflected on the tractor through the articulation point, A. $\left|\ddot{z}_1(\omega_1)\right|$, $\left|\ddot{z}_2(\omega_1)\right|$ and $\left|\ddot{z}_3(\omega_1)\right|$ are the absolute acclerations of unsprung masses obtained at each discrete frequency, from Equation (5.43). It should be noted that the inertia contribution due to the coupling effects of vehicle pitching are neglected.

The magnitudes of inertia forces are then compared to

corresponding Coulomb friction value considered within each suspension unit in order to establish the lock-up. If one or more suspension is locked, the vehicle bounce and pitch response would be changed. These changes could be conveniently reflected through appropriate changes in the frequency response function matrix $[G(j\omega_l)]$.

The generalized response vector of the baseline vehicle at discrete frequency, ω_l, and corresponding excitation vector, $\{u_l\}$, as given by Equation (5.43), can be alternatively obtained as :

$$\{q_l\} = [G(j\omega_l)]\{u_l\} \tag{5.51}$$

Let z_a, z_b and z_c be the bounce coordinates of points a, b and c, given by kinematic relations as :

$$z_a = z_t - b_1\theta_t \tag{5.52a}$$

$$z_b = z_t + b_2\theta_t \tag{5.52b}$$

$$z_c = z_t + b_5\theta_t + (b_3+b_4)\theta_s \tag{5.52c}$$

Substituting Equation (5.52) in Equation (5.51) and rearranging gives :

$$\begin{Bmatrix} z'_a \\ z'_b \\ z'_c \end{Bmatrix} = \begin{bmatrix} (g_{14}-b_1g_{24}) & (g_{15}-b_1g_{25}) & (g_{16}-b_1g_{26}) \\ (g_{14}+b_2g_{24}) & (g_{15}+b_2g_{25}) & (g_{16}+b_2g_{26}) \\ (g_{14}+b_5g_{24} & (g_{15}\ b_5g_{25} & (g_{16}+b_5g_{26} \\ (b_3+b_4)g_{34}) & +(b_3+b_4)g_{35}) & +(b_3+b_4)g_{36} \end{bmatrix} \begin{Bmatrix} u'_1 \\ u'_2 \\ u'_3 \end{Bmatrix} \tag{5.53}$$

When all the suspension units lock-up :

$$F_a' < C_{o_1} \tag{5.54a}$$

$$F_b' < C_{o_2} \tag{5.54b}$$

$$F_c' < C_{o_3} \tag{5.54c}$$

and the relative displacement vector, $\{r_1\}$ is zero i.e;

$$z_a' = z_1' \tag{5.55a}$$

$$z_b' = z_2' \tag{5.55b}$$

$$z_c' = z_3' \tag{5.55c}$$

Therefore, Equation (5.53) can be rewritten as :

$$\begin{Bmatrix} z_a' \\ z_b' \\ z_c' \end{Bmatrix} = \begin{bmatrix} g_{44} & g_{45} & g_{46} \\ g_{54} & g_{55} & g_{56} \\ g_{64} & g_{65} & g_{66} \end{bmatrix} \begin{Bmatrix} u_1' \\ u_2' \\ u_3' \end{Bmatrix} \tag{5.56}$$

Alternatively, the tractor pitch and bounce, and semitrailer pitch can be expressed in terms of z_a' , z_b' and z_c' as follows :

$$z_t' = \frac{b_2 z_a' + b_1 z_b'}{(b_1 + b_2)} \tag{5.57a}$$

$$\theta_t' = \frac{z_b' - z_a'}{(b_1 + b_2)} \tag{5.57b}$$

$$\theta_s' = \frac{z_c' - z_A'}{(b_3 + b_4)} \tag{5.57c}$$

where z_A' represents the vertical displacement of the

$$
\left[G_m(j\omega_t)\right] = \left[\begin{array}{c|ccc}
 & (b_2 g_{44} + b_1 g_{54})/L_t & (b_2 g_{45} + b_1 g_{55})/L_t & (b_2 g_{46} + b_1 g_{56})/L_t \\
\text{- 0 -} & (g_{54} - g_{44})/L_t & (g_{55} - g_{45})/L_t & (g_{56} - g_{46})/L_t \\
\text{(3x3)} & (L_t g_{64} - L_2 g_{44} - L_1 g_{54})/L_t L_s & (L_t g_{65} - L_2 g_{45} - L_1 g_{55})/L_t L_s & (L_t g_{66} - L_2 g_{46} - L_1 g_{56})/L_t L_s \\
\hline
 & g_{44} & g_{45} & g_{46} \\
\text{- 0 -} & g_{54} & g_{55} & g_{56} \\
\text{(3x3)} & g_{64} & g_{65} & g_{66}
\end{array}\right]_{(6\times 6)}
$$

where

$$L_1 = b_1 + b_5$$

$$L_2 = b_2 + b_5$$

Similarly, the frequency response function matrix can be modified to reflect changes in the vehicle response during one or more suspensions lock-up.

5.5.3 VERIFICATION OF RESULTS

The transmissibility characteristics obtained for the local linear equivalent system are compared to the steady state transmissibility response of the original nonlinear baseline vehicle computed through numerical integration techniques. The local equivalent damping coefficients are computed through energy balance as well as force balance approach. The absolute transmissibility response of the articulated vehicle model is determined for harmonic excitations with phase information at the tire-road interface as given by Equation (5.28). The peak value of input displacement amplitude is taken as 0.025 m. The nonlinearities include Coulomb and orifice damping at the tractor front axle (C_{o_1} = 2.5 KN, C_{2_1} = 10 KNs^2/m^2), tractor rear axle (C_{o_2} = 5 KN, C_{2_2} = 10 KNs^2/m^2), and at semitrailer axle (C_{o_3} = 5 Kn, C_{2_3} = 0).

The value of local damping constant calculated based on force balance approach yields slightly higher value than the one obtained in the energy balance approach. The average number of iterations taken to establish a local value of equivalent viscous coefficient using force balance are higher than those taken in energy balance approach.

Therefore, energy balance method is employed to obtain local equivalent viscous coefficients. Figures 5.7 and 5.8 present the bounce $|(z_t/A)|$ and pitch $|(\theta_t . L_t/A)|$ response of the tractor, respectively. The bounce response predicted by the iterative algorithm is compared to exact solution, established by direct integration as shown in Figure 5.7. The comparison reveals that the local equivalent linearization algorithm can duplicate the response behaviour of nonlinear system quite precisely, except for small errors around resonant peaks. Effectiveness of the iterative technique is further demonstrated by comparing the tractor pitch response ratios obtained from these two methods, as shown in Figure 5.8.

5.5.4 COMPARISON OF LOCAL EQUIVALENT LINEARIZATION APPROACH WITH STATISTICAL LINEARIZATION TECHNIQUE

Statistical linearization have been widely used to study the stationary response of nonlinear mechanical systems. ElMadany [23] has used this technique to study the influence of nonlinearities such as dry friction in primary suspension on the dynamic response of articulated vehicle. Figures 5.9 and 5.10 show the vertical and fore-aft accleration spectra at the driver's position, where in addition to viscous damping in each suspension, Coulomb friction force was considered to be a percent of corresponding axle static load, P_j

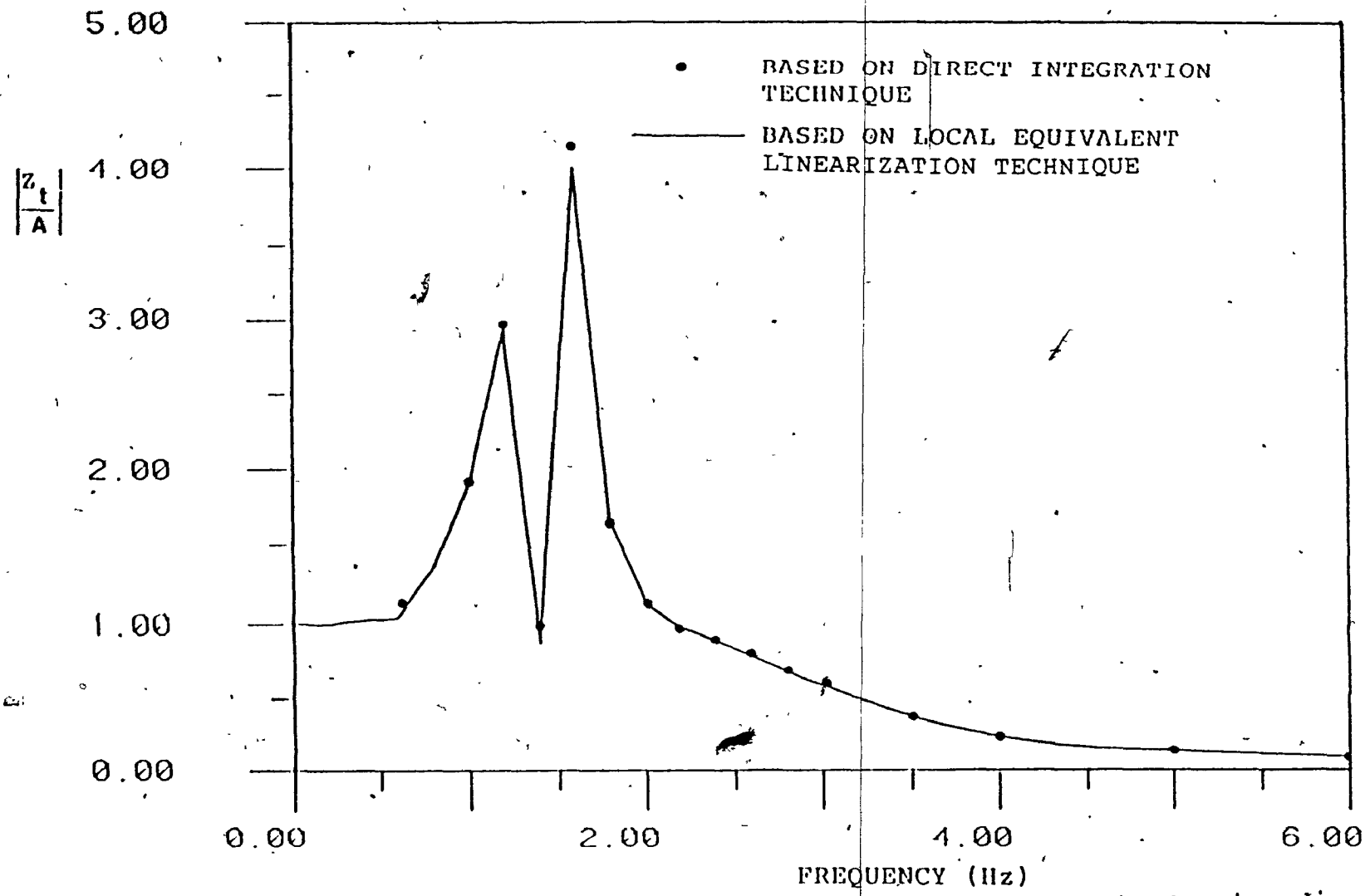

FIGURE 5.7: Comparison of tractor bounce response obtained using direct integration and local equivalent linearization technique [41]

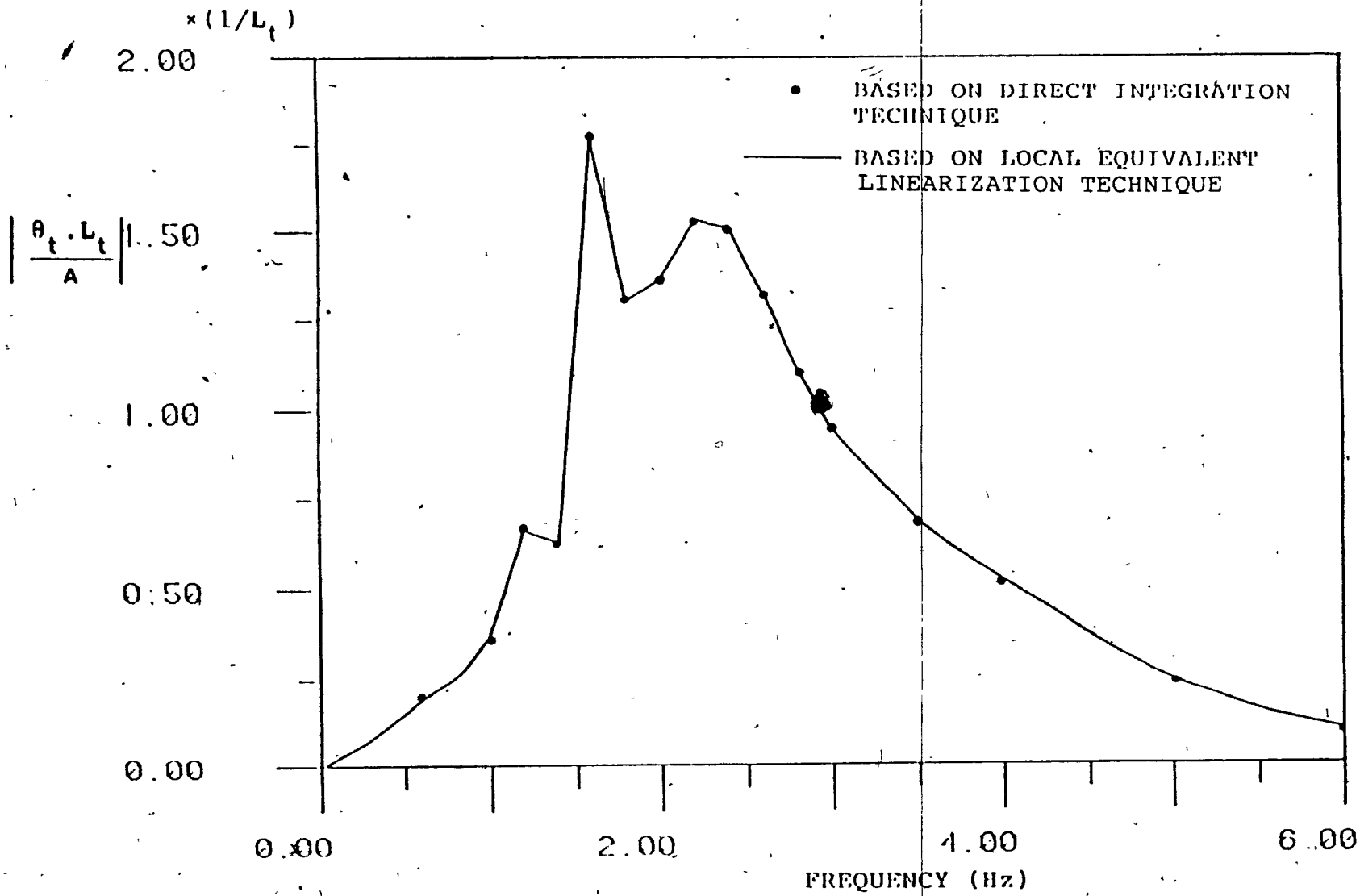

FIGURE 5.8: Comparison of tractor pitch response obtained using direct integration and local equivalent linearization technique [41]

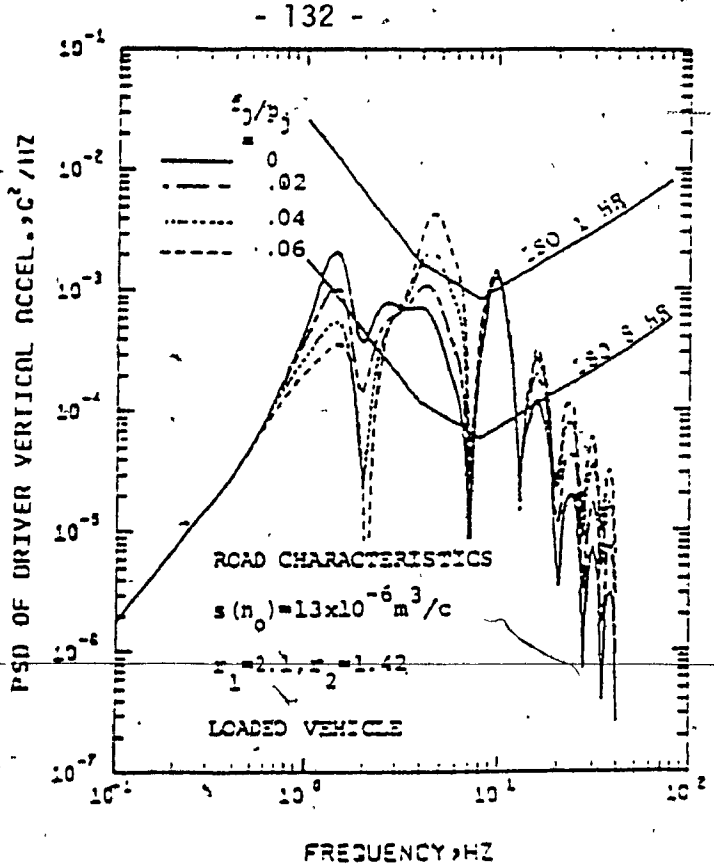

FIGURE 5.9: Influence of Coulomb friction forces on seat bounce acceleration spectra [23]

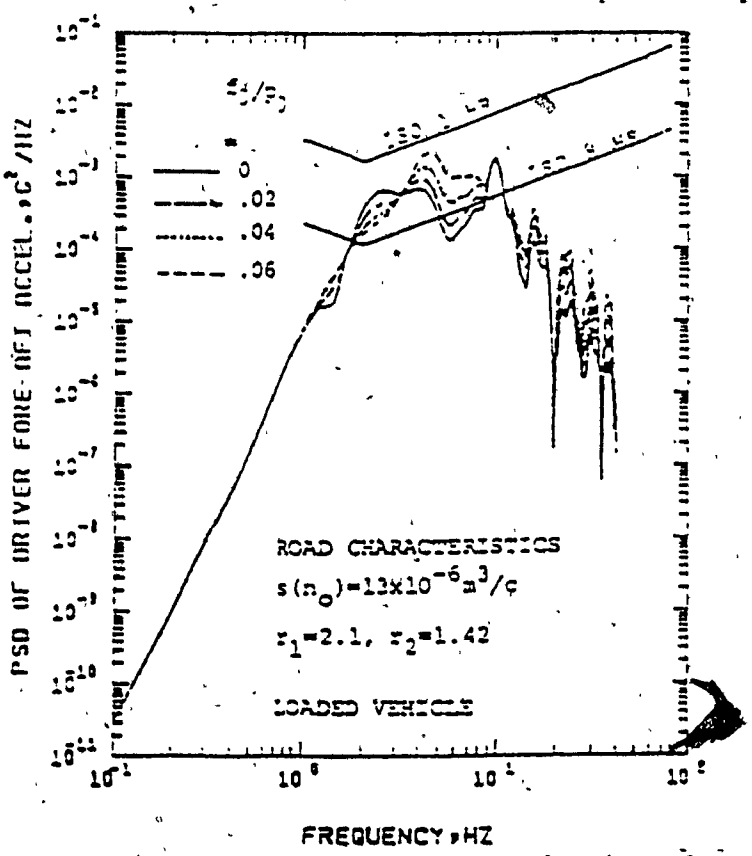

FIGURE 5.10: Influence of Coulomb friction forces on seat fore-aft acceleration spectra [23]

Vertical and fore-aft acceleration spectra at driver's position of the baseline vehicle with identical parameters as in Elmadany's model are generated using local equivalent approach. These results, as shown in Figures 5.11 and 5.12, are plotted for a limiting value of $\epsilon = 0.1$ m/sec (to approximate the step discontinuity of Coulomb friction, as shown in Figure 5.5), and no lock-up condition. The comparison between Figures 5.9 and 5.11, and 5.10 and 5.12 shows an excellent aggrement. A high limiting value tends to represent the Coulomb friction characteristic by a linear curve over the entire frequency range of input. Thus, equivalent damping coefficient evaluated from the slope value (Figure 5.6) during iterative process is constant over the entire frequency range. These results are regenerated with the same bound value and lock-up condition, and plotted, as shown in Figures 5.13 and 5.14. There is continuous lock-up of vehicle suspensions for 4% dry friction, while lock-up breaks around 6 Hz for 2% dry friction. As it is obvious from the data exhibited in Figures 5.13 and 5.14, there is considerable decrease in the bounce and as well as fore-aft spectra at frequencies corresponding to tractor bounce and vehicle pitching modes, but accompanied by a significant increase in high frequency range. This occurs because of high value of dry friction considered within each suspension, which stiffen the suspension. Therefore, tires act as main suspension medium,

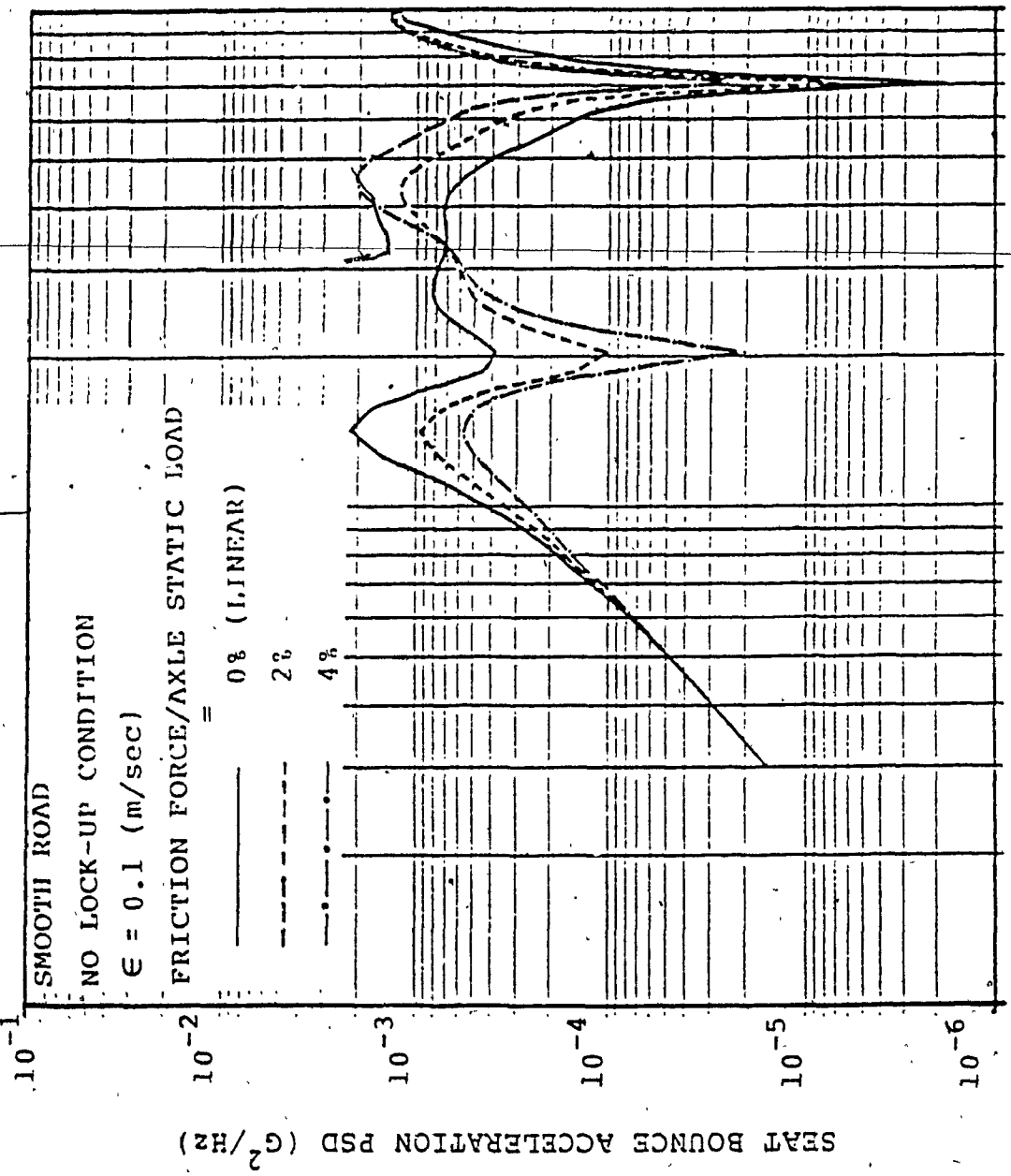

FIGURE 5.11: Influence of Coulomb friction forces on seat bounce acceleration spectra - ElMadany's parameters

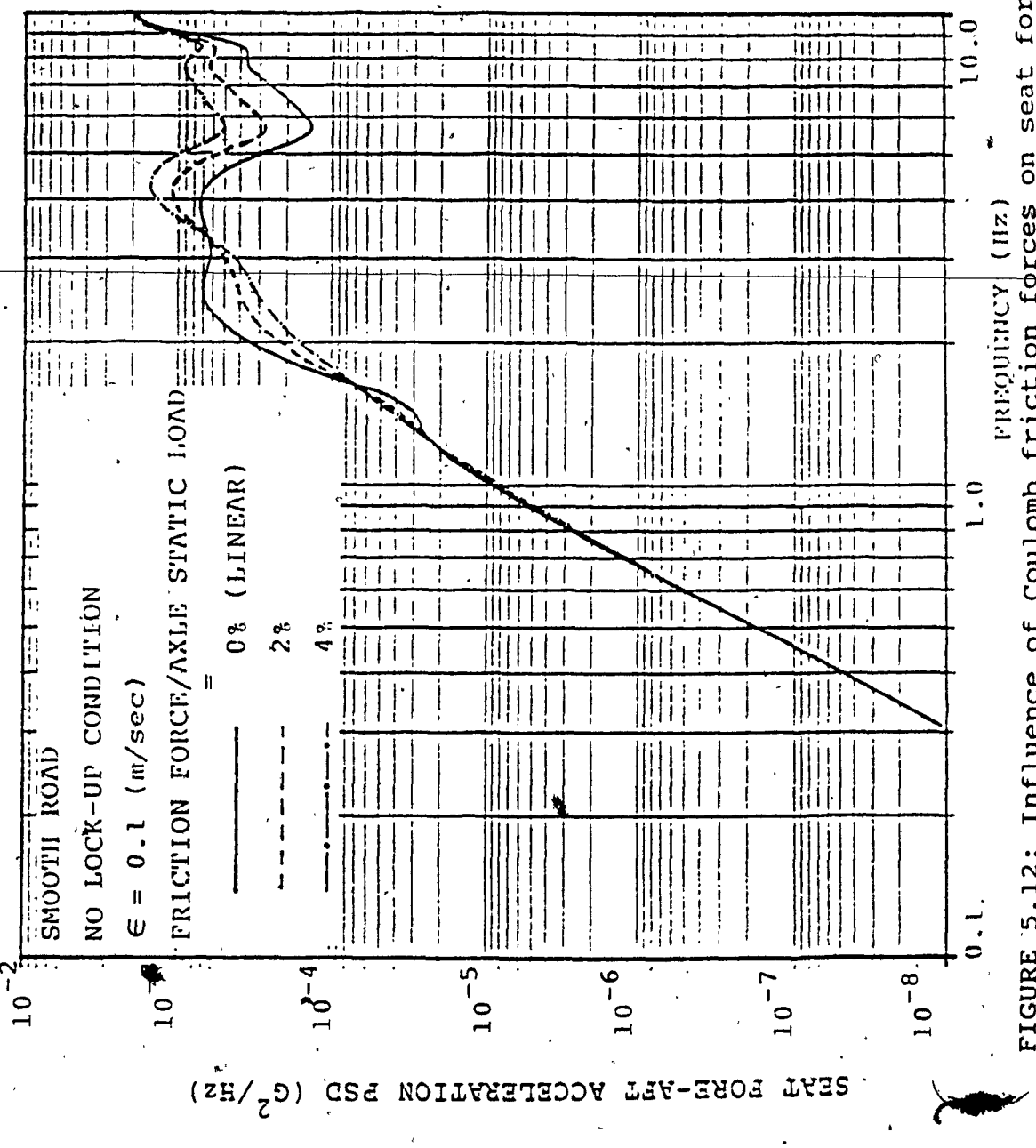

FIGURE 5.12: Influence of Coulomb friction forces on seat fore-aft acceleration spectra - ElMadany's parameters

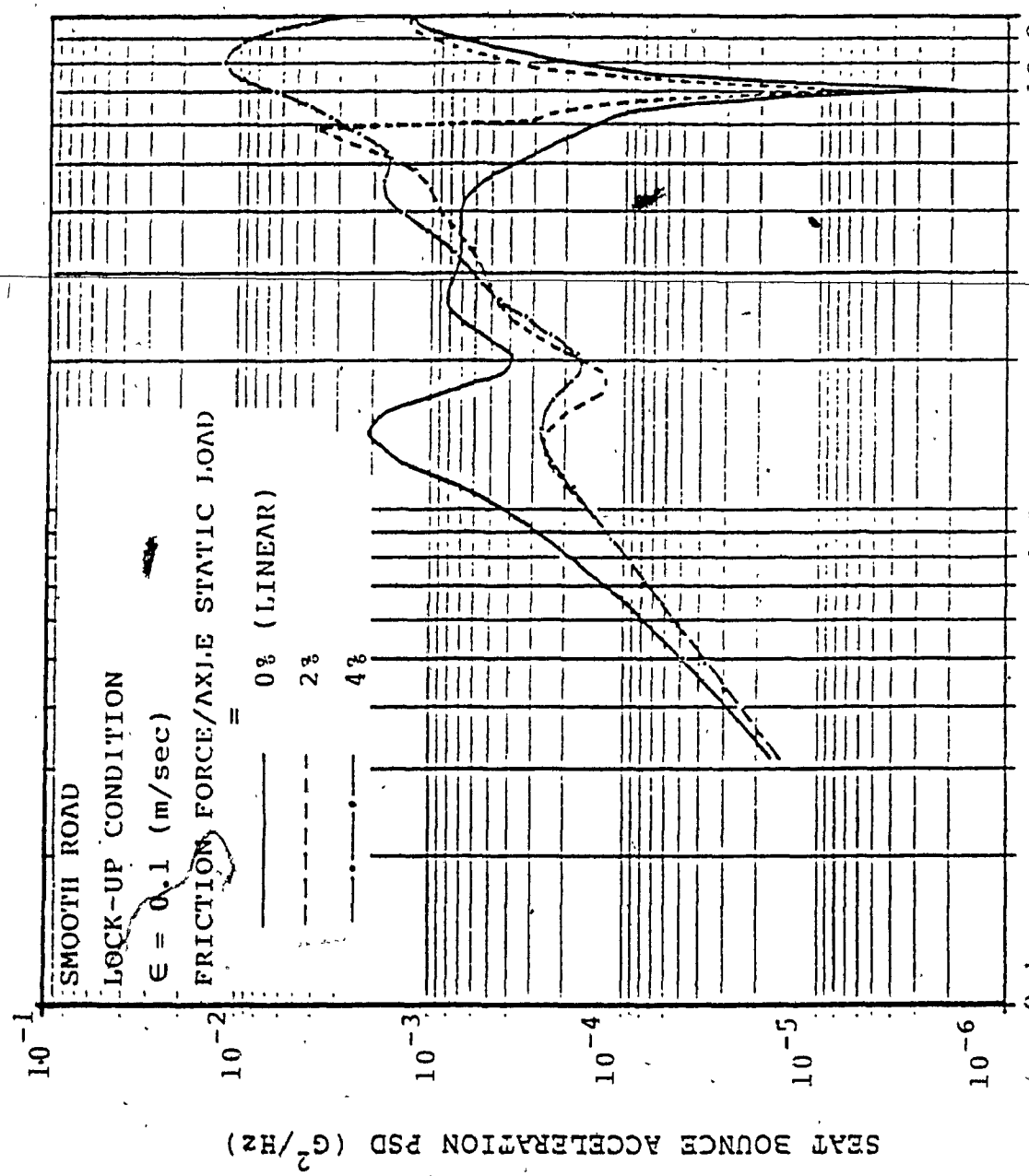

FIGURE 5.13: Influence of Coulomb friction forces on seat bounce acceleration spectra - ElMadany's parameters

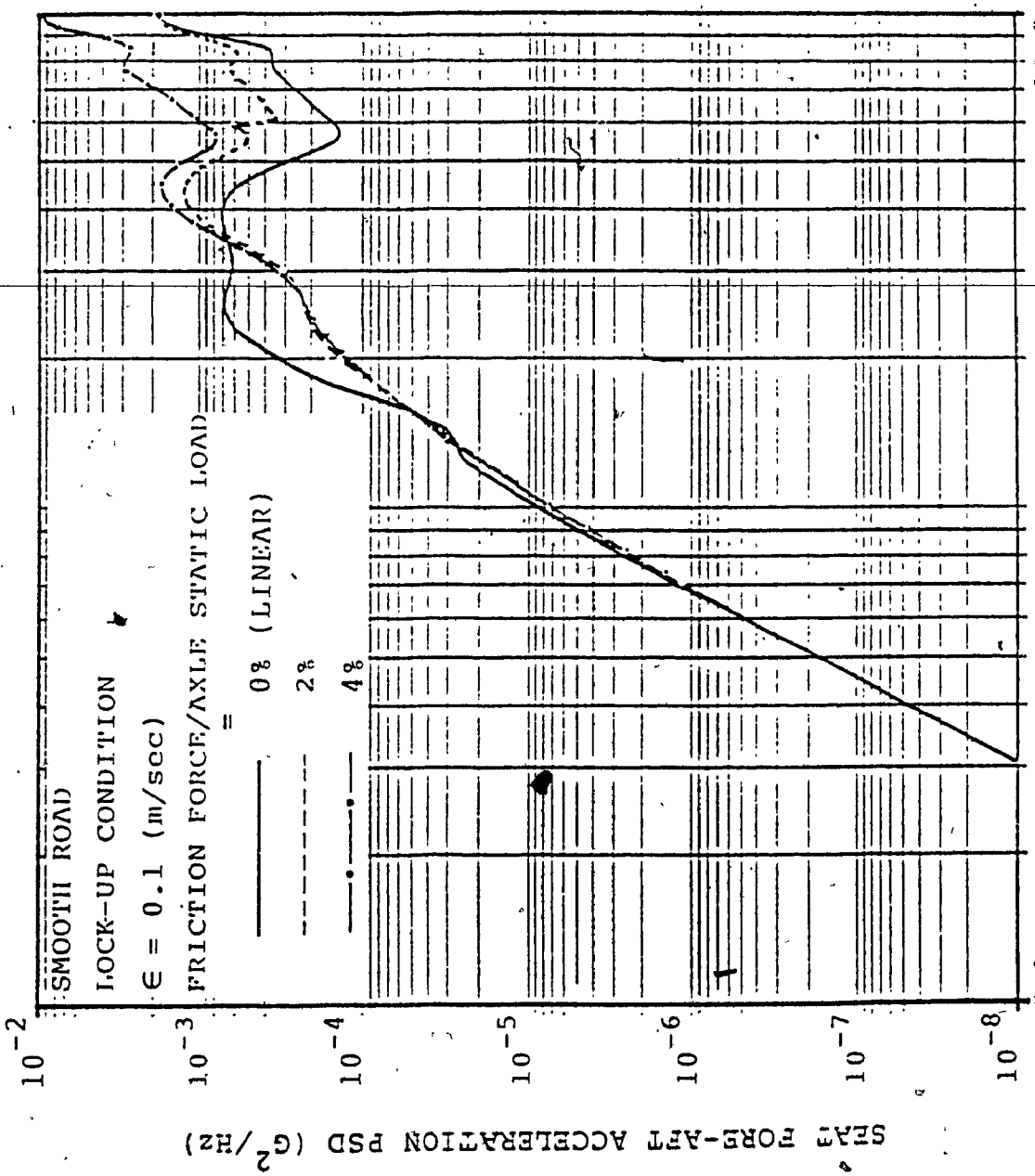

FIGURE 5.14: Influence of Coulomb friction forces on seat fore-aft acceleration spectra - ElMadany's parameters

which causes resonances at frequencies in the vicinity of wheel hop resonant frequencies. Therefore on the basis of the comparison between results obtained from local equivalent approach with lock-up (Figures 5.11 - 5.14), and the results computed using statistical linearization (Figures 5.9 and 5.10), it can be concluded that in latter technique : a) the nonlinear damping mechanism is approximated by an equivalent viscous coeffiecient over the entire input frequency range, and b) the lock- up due to the critical effects of Coulomb friction is not simulated in the response.

The limiting value selected to approximate the step discontinuity of Coulomb friction has significant influence on the vehicle response. A high value of ϵ does not represent the true characteristic of the Coulomb friction and gives a constant value of equivalent viscous coefficient, as discussed in the previous paragraph. The influence of lowering the limiting value to 0.01 m/sec, is demonstrated in Figures (5.15-5.16) and (5.17-5.18) for no lock-up and lock-up conditions, respectively. Comparison of results from no lock-up and lock-up conditions for relatively low limiting value of ϵ = 0.01 m/sec, shows very little difference. The effect of further decrease in limiting value on the ride response is demonstrated in Figures 5.19 to 5.22. On the basis of the data exhibited in Figures 5.19 and 5.20 (ϵ = 0.001 m/sec), and 5.21 and 5.22

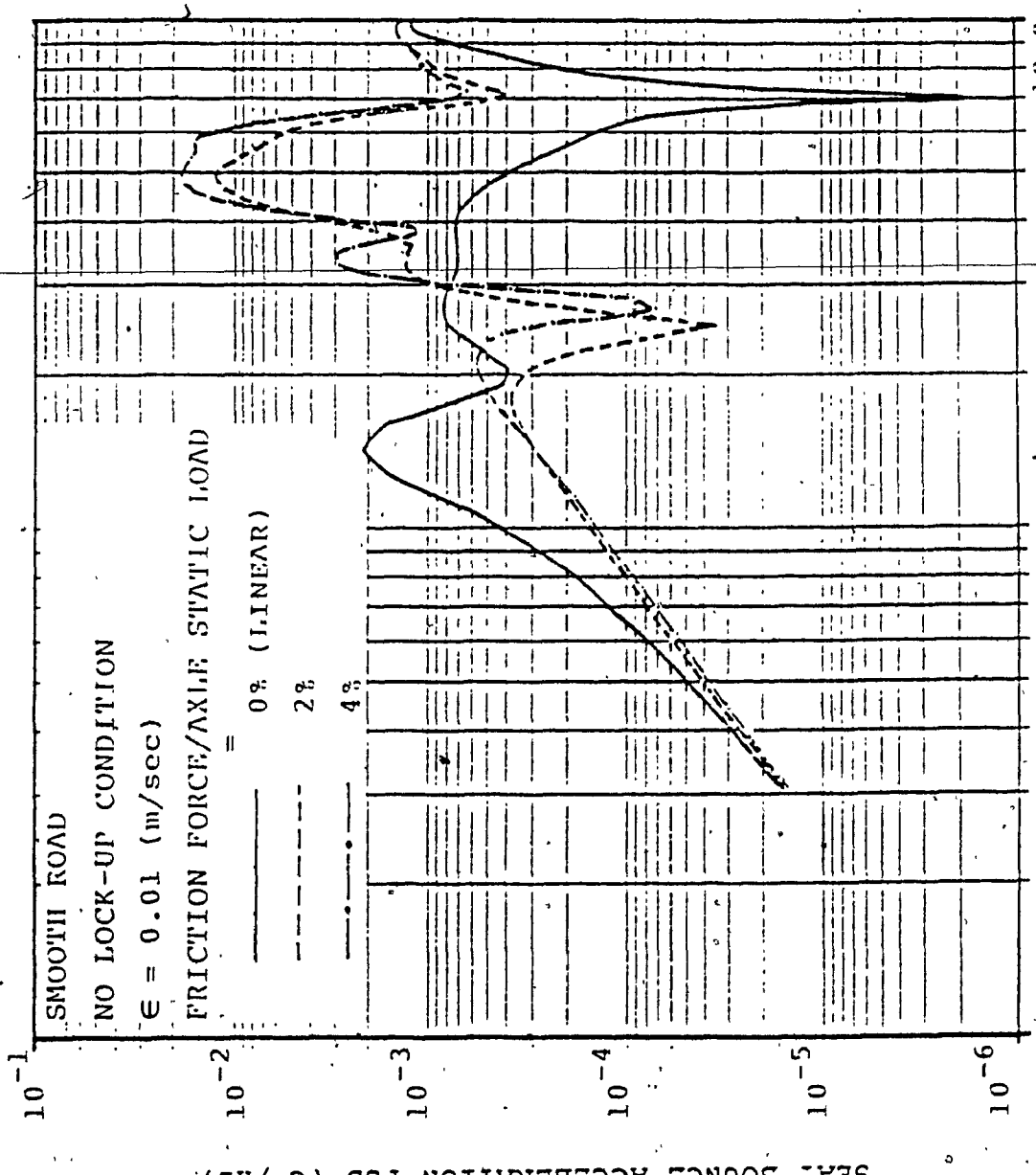

FIGURE 5.15: Influence of Coulomb friction forces on seat bounce acceleration spectra - ElMadany's parameters

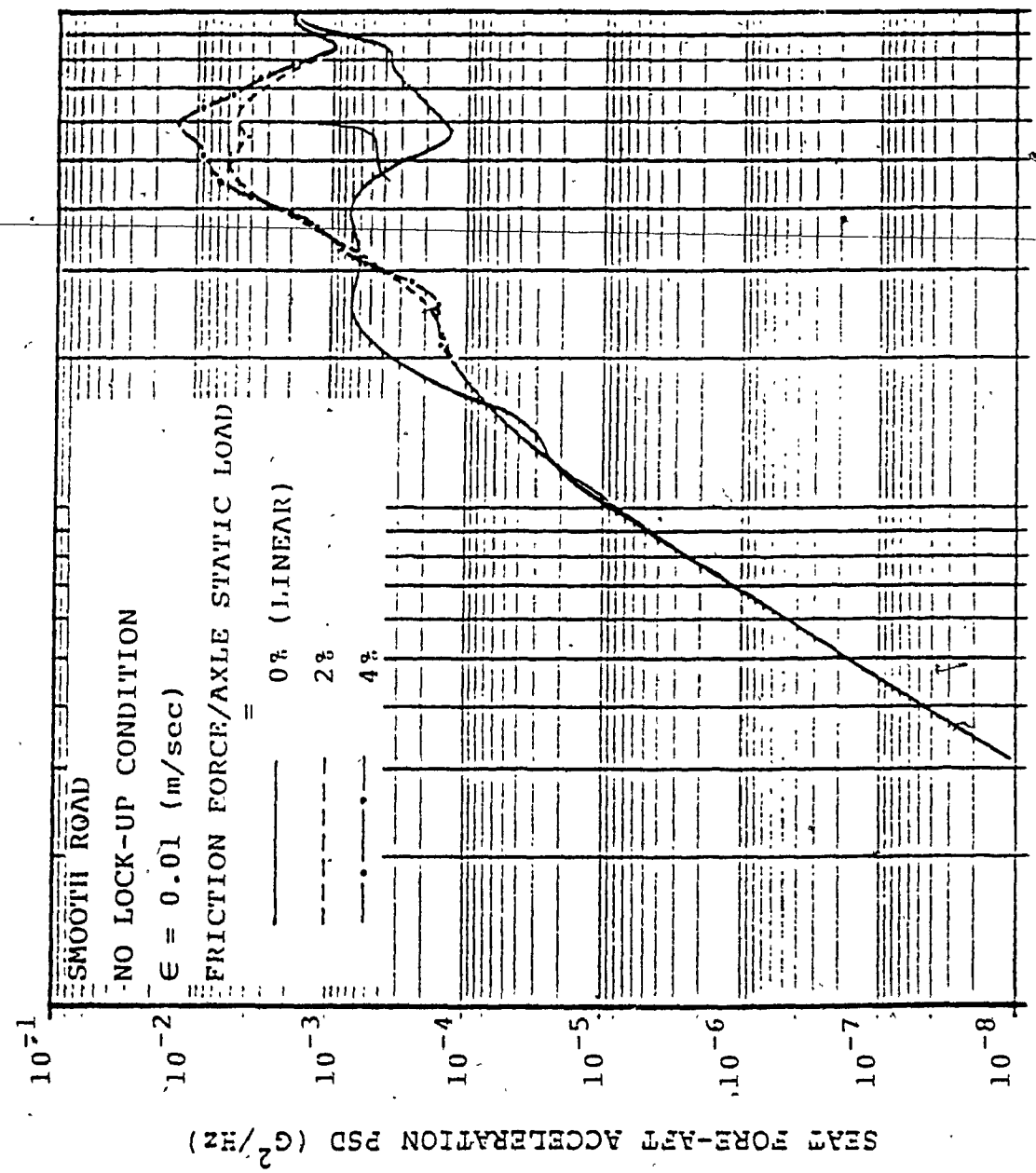

FIGURE 5.16: Influence of Coulomb frcition forces on seat fore-aft acceleration spectra - ElMadany's parameters

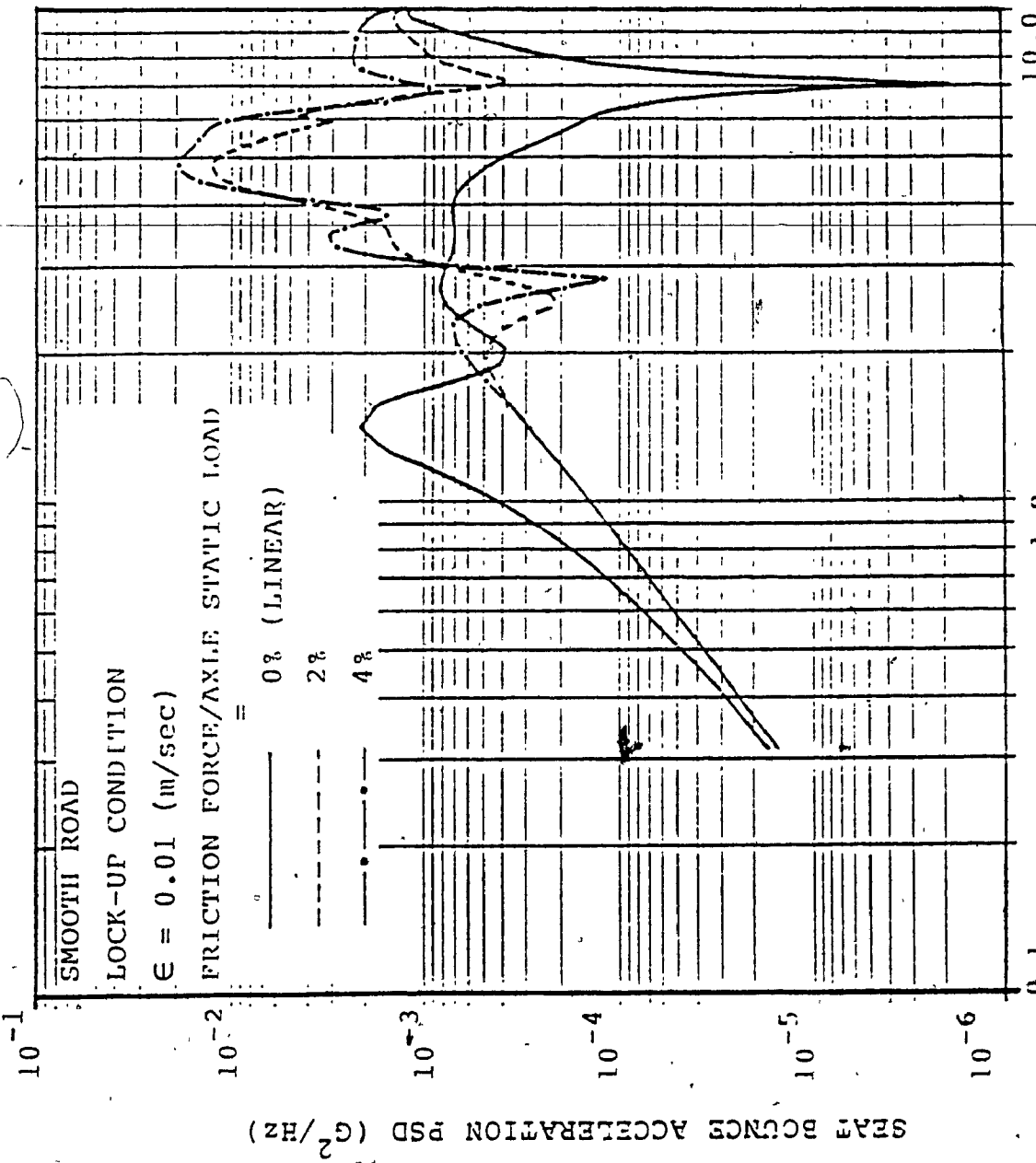

FIGURE 5.17: Influence of Coulomb friction forces on seat bounce acceleration spectra - ElMadany's parameters

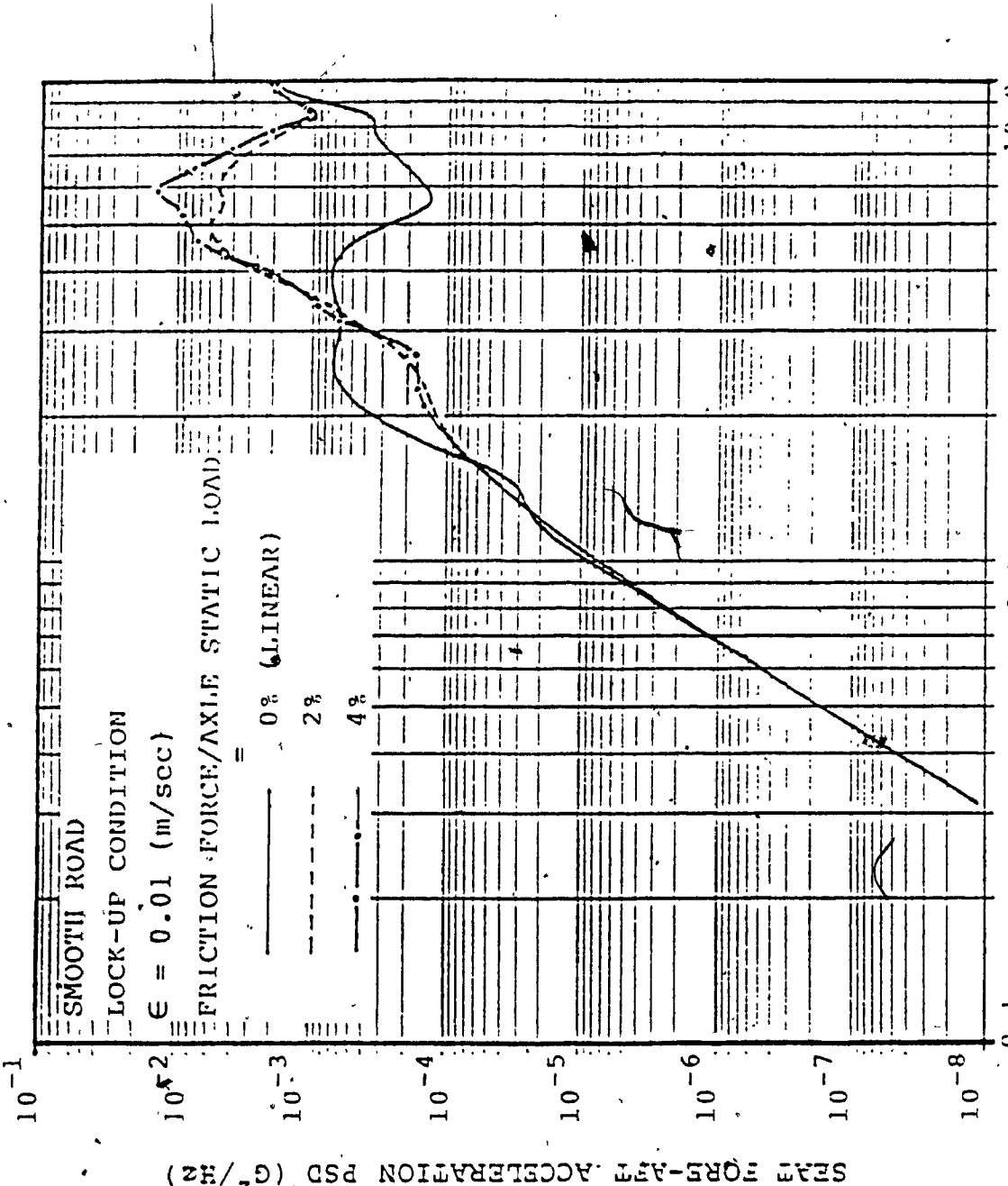

FIGURE 5.18: Influence of Coulomb friction forces on seat fore-aft acceleration spectra - ElMadany's parameters

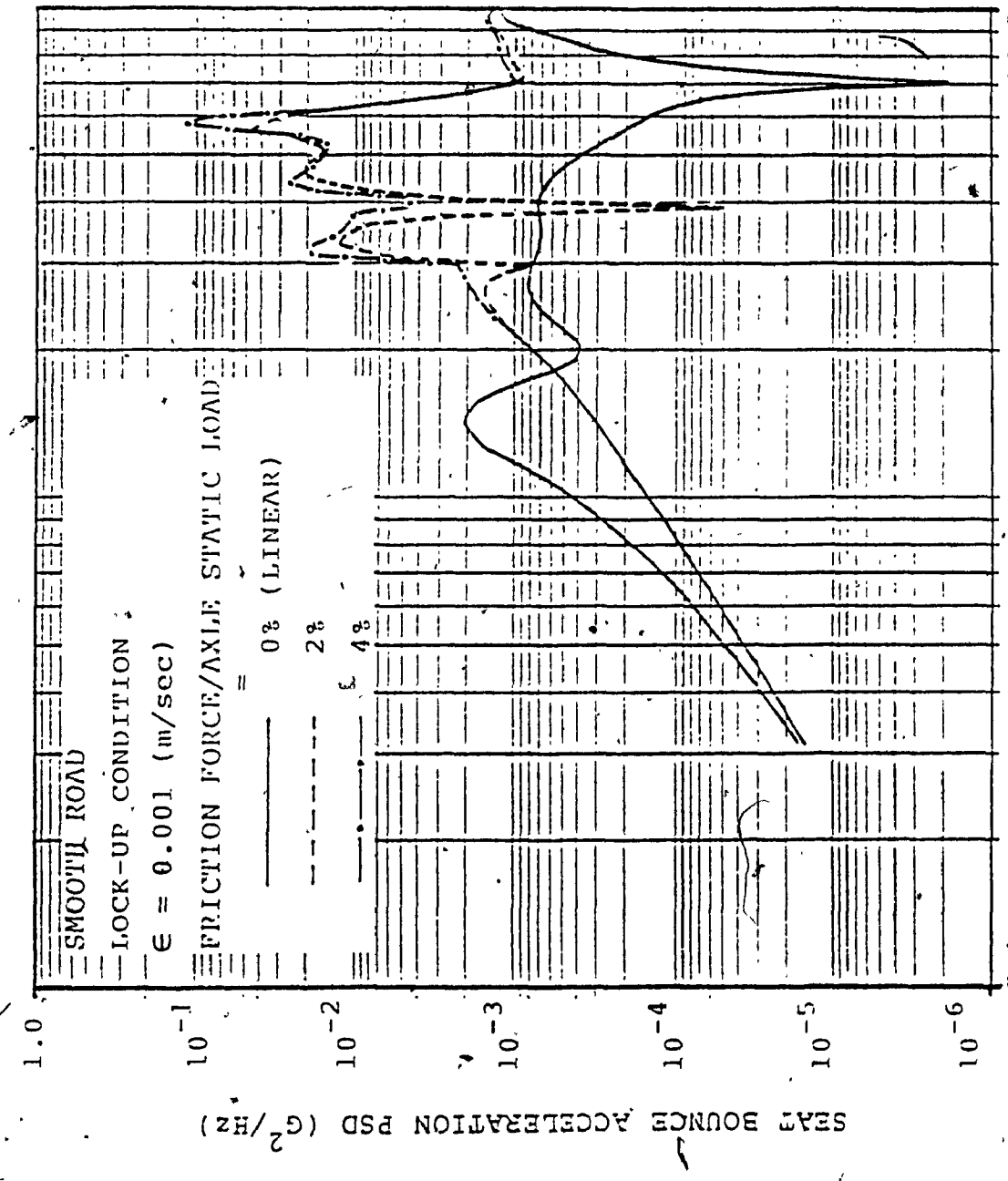

FIGURE 5.19: Influence of Coulomb friction forces on seat bounce acceleration spectra - ElMadany's parameters

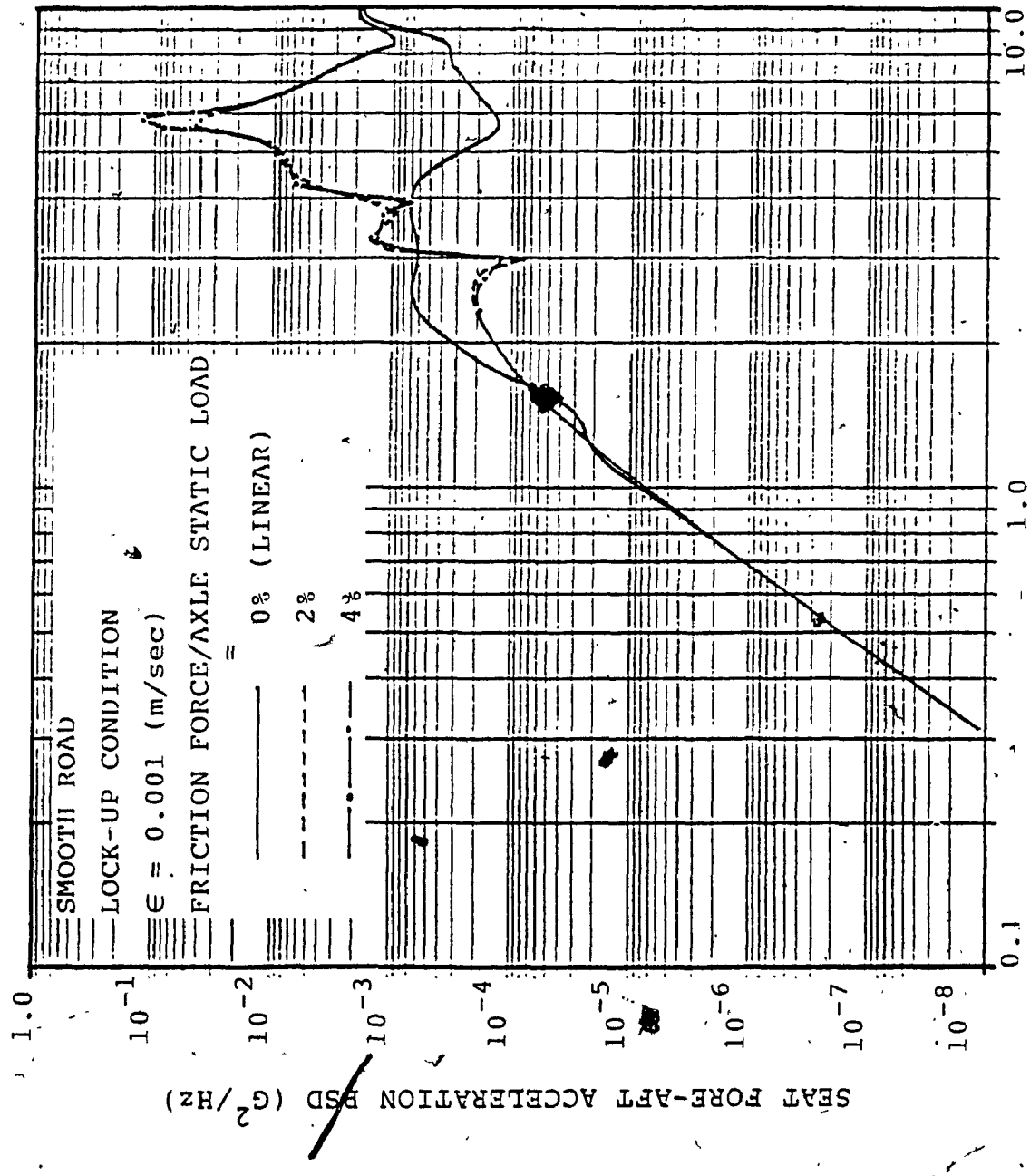

FIGURE 5.20: Influence of Coulomb friction forces on seat fore-aft acceleration spectra - ElMadany's parameters

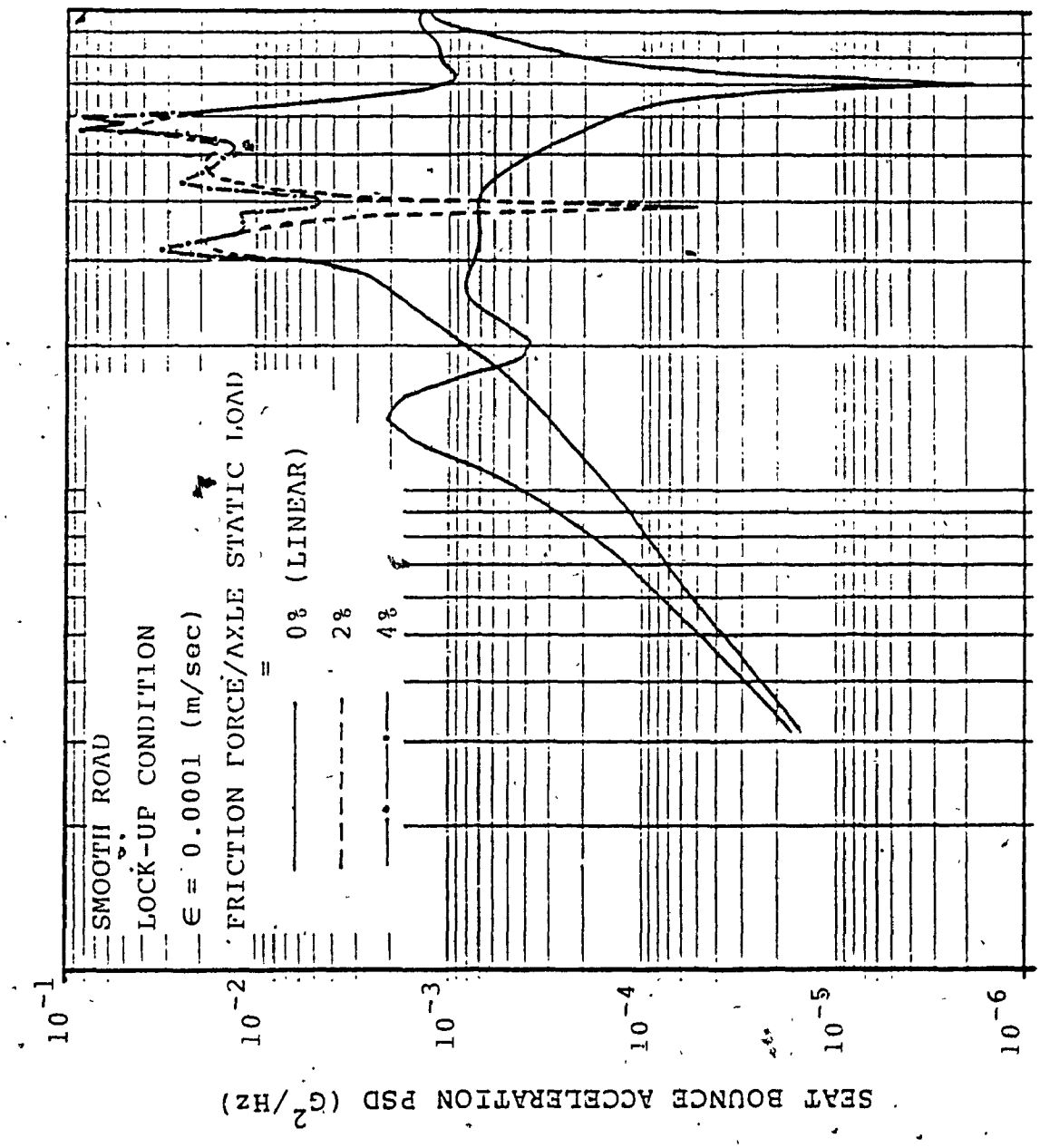

FIGURE 5.21: Influence of Coulomb friction forces on seat bounce acceleration spectra - ElMadany's parameters

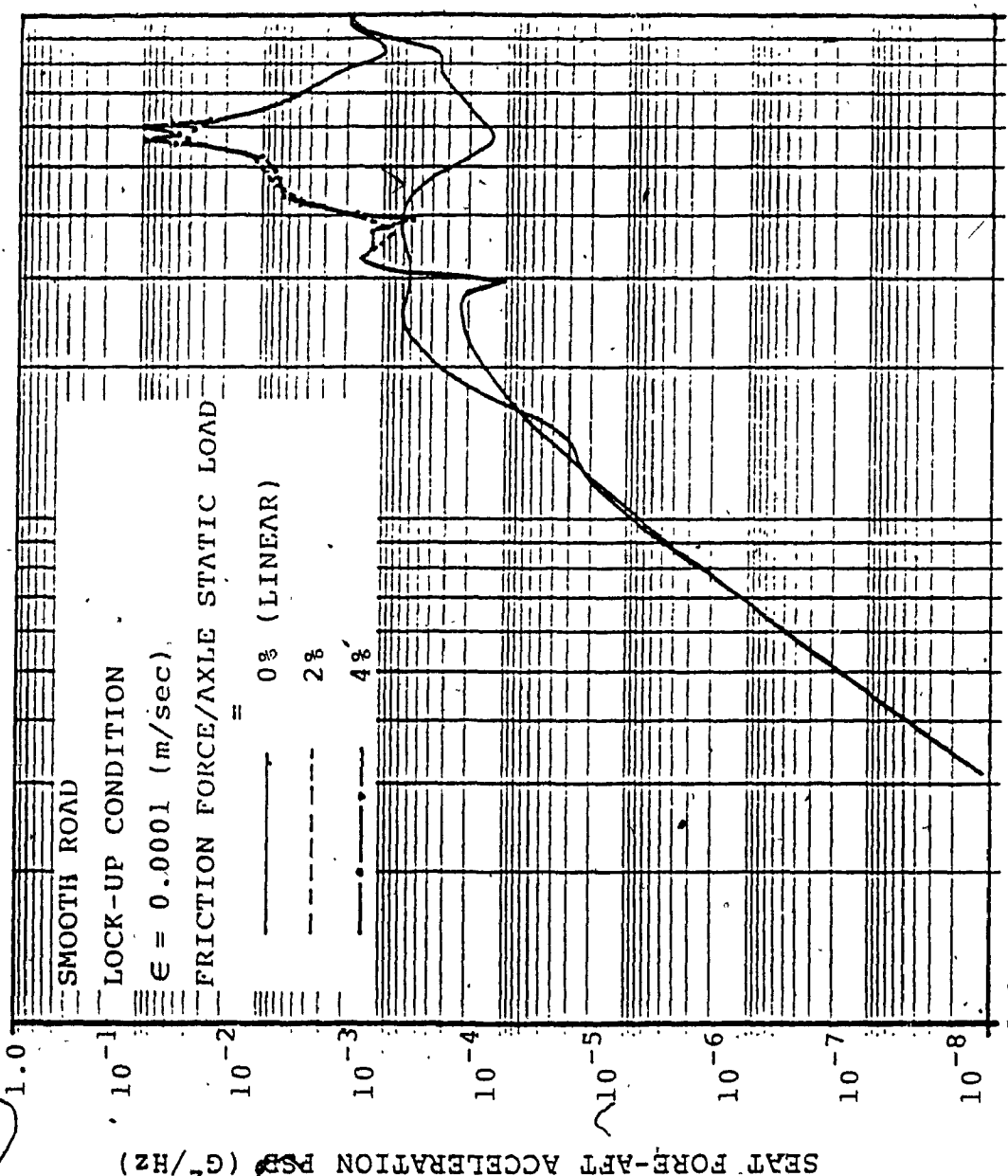

FIGURE 5.22: Influence of Coulomb friction forces on seat fore-aft acceleration spectra - ElMadany's parameters

(ϵ = 0.0001 m/sec), it can be concluded that for a very small limiting value, thus a relatively more realistic representation of Coulomb friction, a very high value of equivalent viscous damping coefficient is obtained (as shown in Figure 5.6 for n=0). As a result, the suspension becomes very stiff and more energy is transmitted to the sprung masses. Consequently, the response with lock-up condition is same as the response without lock-up condition.

This study has demonstrated that the critical effect of dry friction on the vehicle response can be simulated satisfactorily through a reasonably low limiting value, ϵ , along with the inclusion of lock-up condition in the analysis. A limiting value of 0.01 m/sec will be considered to perform parametric study in the following section.

5.6 PARAMETRIC STUDY OF BASELINE VEHICLE MODEL

5.6.1 GENERAL

The ride vibration levels at driver-seat interface are influenced by a number of factors, such as road profiles, primary suspension, loading pattern, vehicle geometry, vehicle speed etc.. A better understanding of these factors is achieved through a parametric study of the ride model. In order to investigate the parameter sensitivity, a performance index may be chosen either as the peak value

of the steady state response or the response spectra over the frequency range of interest. The response PSD over a frequency range provides a better basis for comparing the ride quality with respect to ISO guide.

In this section, a detailed parametric study is presented utilizing the response power spectral densities at the driver position in the frequency range upto 10 Hz obtained from the solution of nonlinear model of baseline vehicle. The study involves finding the effect of variation of each parameter independently when subject to road input acceleration PSD's.

5.6.2 PARAMETRIC STUDY OF THE NONLINEAR RIDE MODEL

The parametric study results indicate a trend on the effect of various parameters on the response and provides a basis for selecting the vehicle parameters that yield optimal ride at the driver-seat interface. The influence of various vehicle parameters is presented in the following sub-sections.

5.6.2.1 INFLUENCE OF COULOMB FRICTION

The frictional forces generated in the multi-leaf springs have a large influence on the ride dynamics of the vehicle. The vertical and fore-aft acceleration spectra at the driver's position for baseline vehicle are presented in Figures 5.23 and 5.24, respectively. The vehicle is

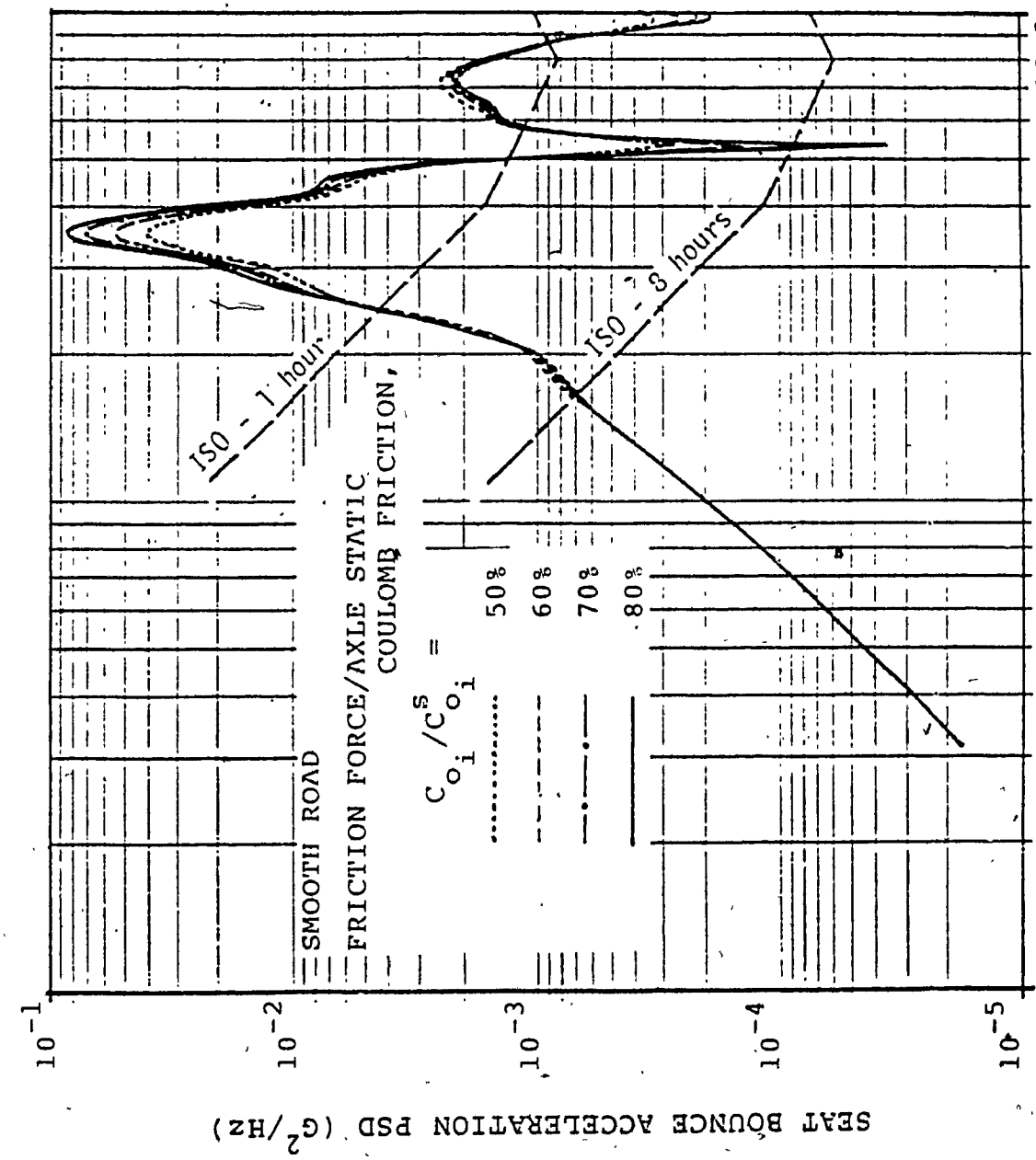

FIGURE 5.23: Influence of Coulomb friction forces on seat bounce acceleration spectra - nonlinear, two-dimensional model

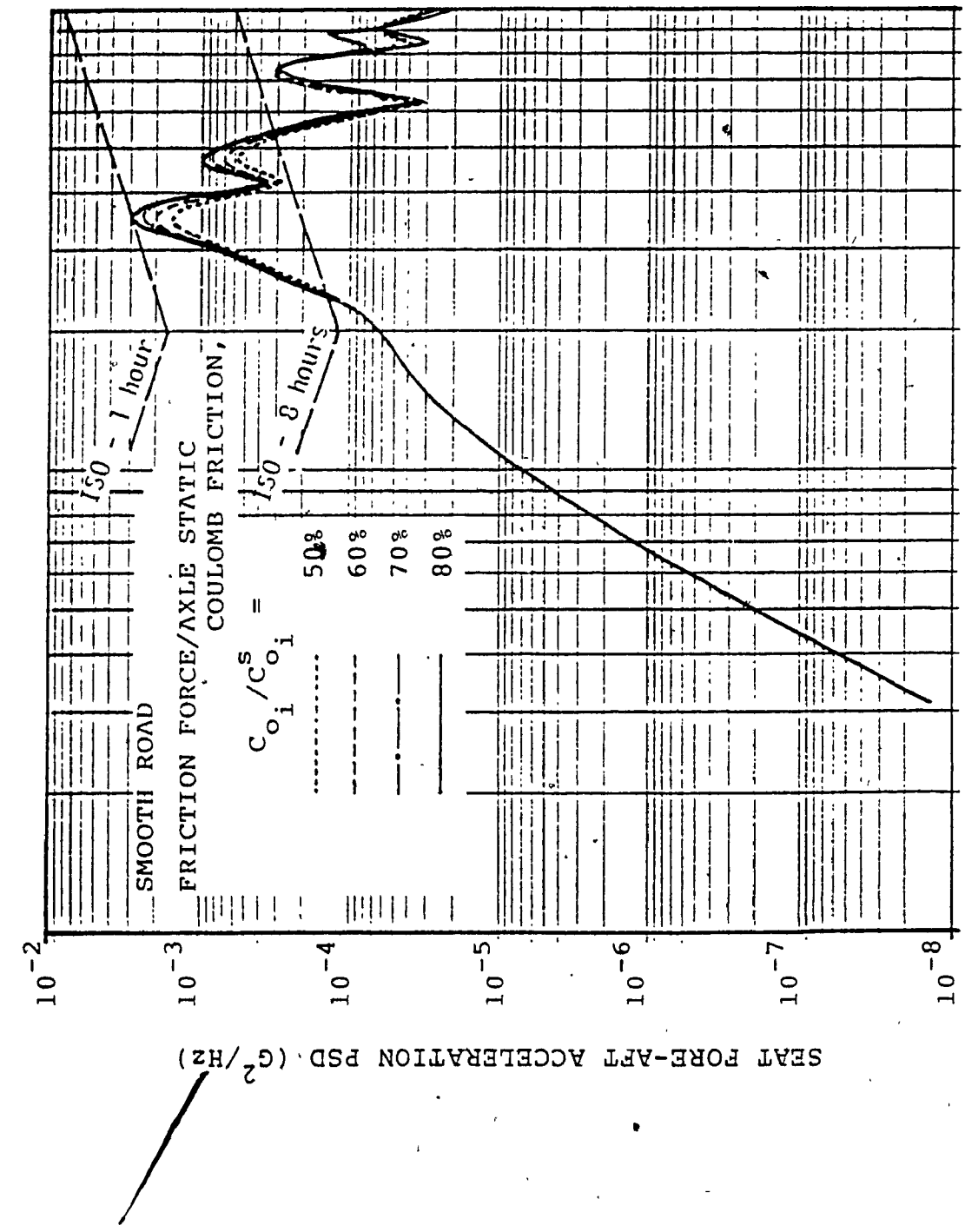

FIGURE 5.24: Influence of Coulomb friction forces on seat fore-aft acceleration spectra - nonlinear, two-dimensional model

considered to be travelling at 90 km/hr on a smooth highway. The Coulomb frictional force in each suspension is considered to be a percent of the corresponding static friction value (Table 5.1). These curves are plotted for different percentage values : 50%, 60%, 70%, and 80%.

The results indicate that the inclusion of Coulomb friction has a significant effect on vehicle ride quality. For the seat bounce accleration, increasing the Coulomb friction force diminishes the peak response in the low frequency region corresponding primarily to tractor bounce and pitch, as observed in the linear analysis. However, the response increases in the high frequency region by increasing the Coulomb friction force. Specifically, the vibration level in the frequency range 3-5 Hz becomes poorer and exceeds the ISO 1 hour reduced comfort boundary. These frequencies are in the range where the human body is more sensitive, and hence, it is deleterious to the ride motion. It may also be seen from the Figures that increasing the friction will stiffen the suspension and more energy will be transmitted to the sprung masses.

Figure 5.24 shows the effect of Coulomb friction damping on the fore-aft acceleration spectra at the driver position. Increasing the frictional forces will suppress first two resonance peaks primarily corresponding to vehicle pitching modes, as was shown in the linear

analysis. However, the frictional forces have a worsening effect and impair the fore-aft acceleration spectra at the medium and higher frequencies.

On the basis of the data exhibited in Figures 5.23 and 5.24, it may be concluded that due to the presence of high Coulomb friction in the suspension, the ride dynamics of an articulated vehicle is largely determined by the fact that the tires are main suspension medium. This results in inadequate damped vibrations with resonance at frequencies less tolerable by human beings i.e; frequencies to which human is particularly sensitive. Consequently, the magnitude of Coulomb friction considered within all suspensions should be lowered such that a satisfactory compromise is made between resonant vibration control and high frequency vibration isolation.

5.6.2.2 INFLUENCE OF VEHICLE SUSPENSION SYSTEM

Vehicle suspension system for the baseline vehicle, as discussed previously, is modelled as a directly coupled frictional damping system. In practice, multi-leaf construction is used for the vehicle suspension system. The stiffness and Coulomb friction associated the vehicle suspension system can be varied by selecting the appropriate number of leaves. For the sake of parametric variation, a linear relationship between stiffness and Coulomb friction is assumed. Excursion in each of the

vehicle suspension system parameters are then obtained, one by one, while all of the remaining system variables are held constant at the baseline values. The motion of the vehicle are obtained, while it is operating on a smooth highway.

Variation in the stiffness characteristics of the front axle suspension can alter the ride vibration levels at the seat location considerably. A soft front axle suspension suppresses the first resonant peaks of bounce, but there is considerable increase in vibration levels in high frequency range as shown in Figure 5.25. Stiffer suspension at front axle deteriorates the ride quality, specifically, the fore-aft accleration spectra exceeds the 1-hr ISO specified level (Figure 5.26).

Influence of tractor rear suspension characteristics on the ride vibration levels at the driver's position is investigated for vehicle equipped with Hendrickson Rte. 380, Hendrickson Rte. 440 and Mack Camel Back SS38C. There is insignificant influence of the selected suspension on the bounce (Figure 5.27) as well as fore-aft acceleration spectra at driver's position because of high value of Coulomb friction.

Figures 5.28 and 5.29 show the influence of variations in the stiffness characteristics of semitrailer axle suspension on the seat bounce and fore-aft ride vibration

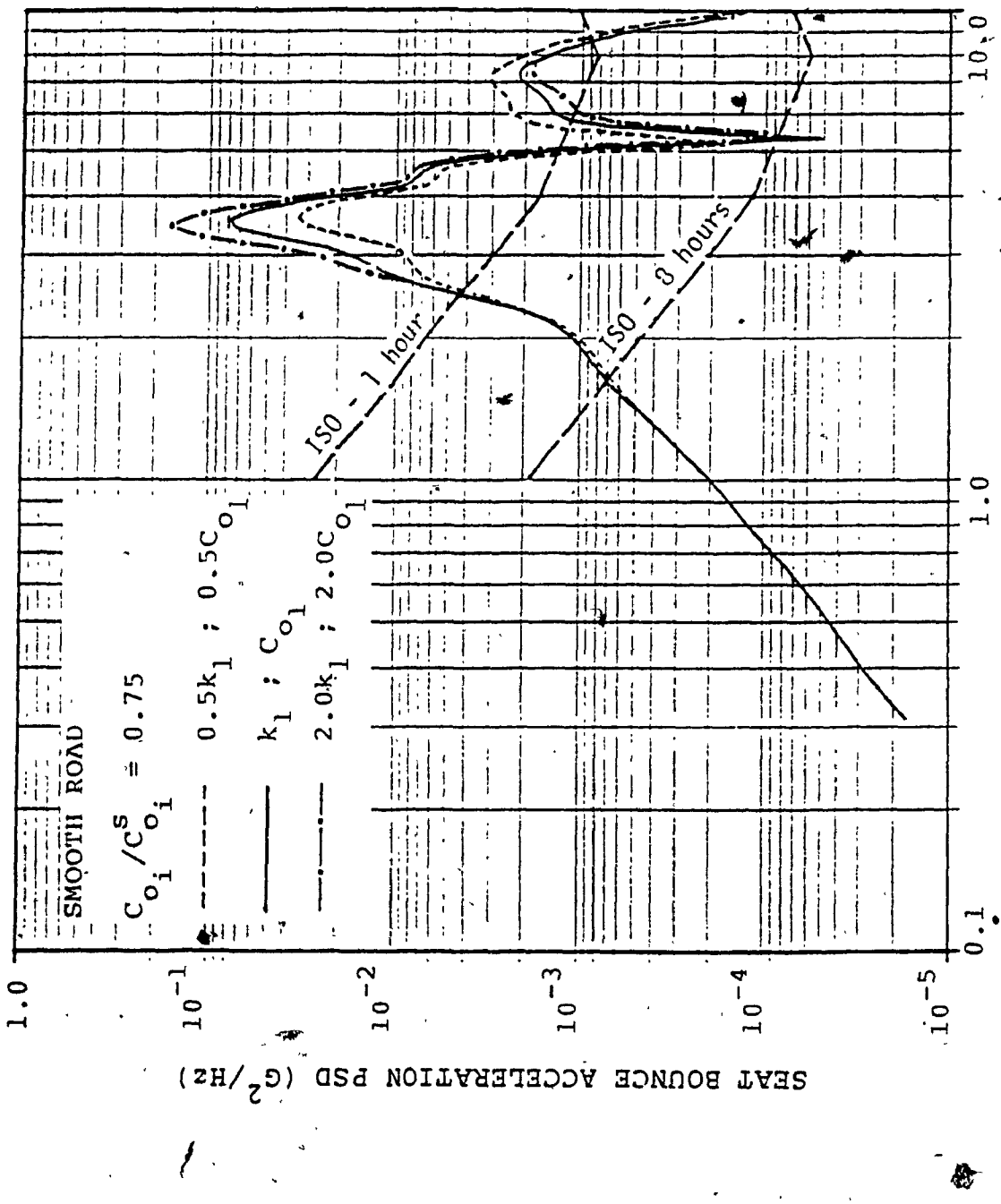

FIGURE 5.25: Influence of tractor front suspension on seat bounce acceleration spectra - nonlinear, two-dimensional model

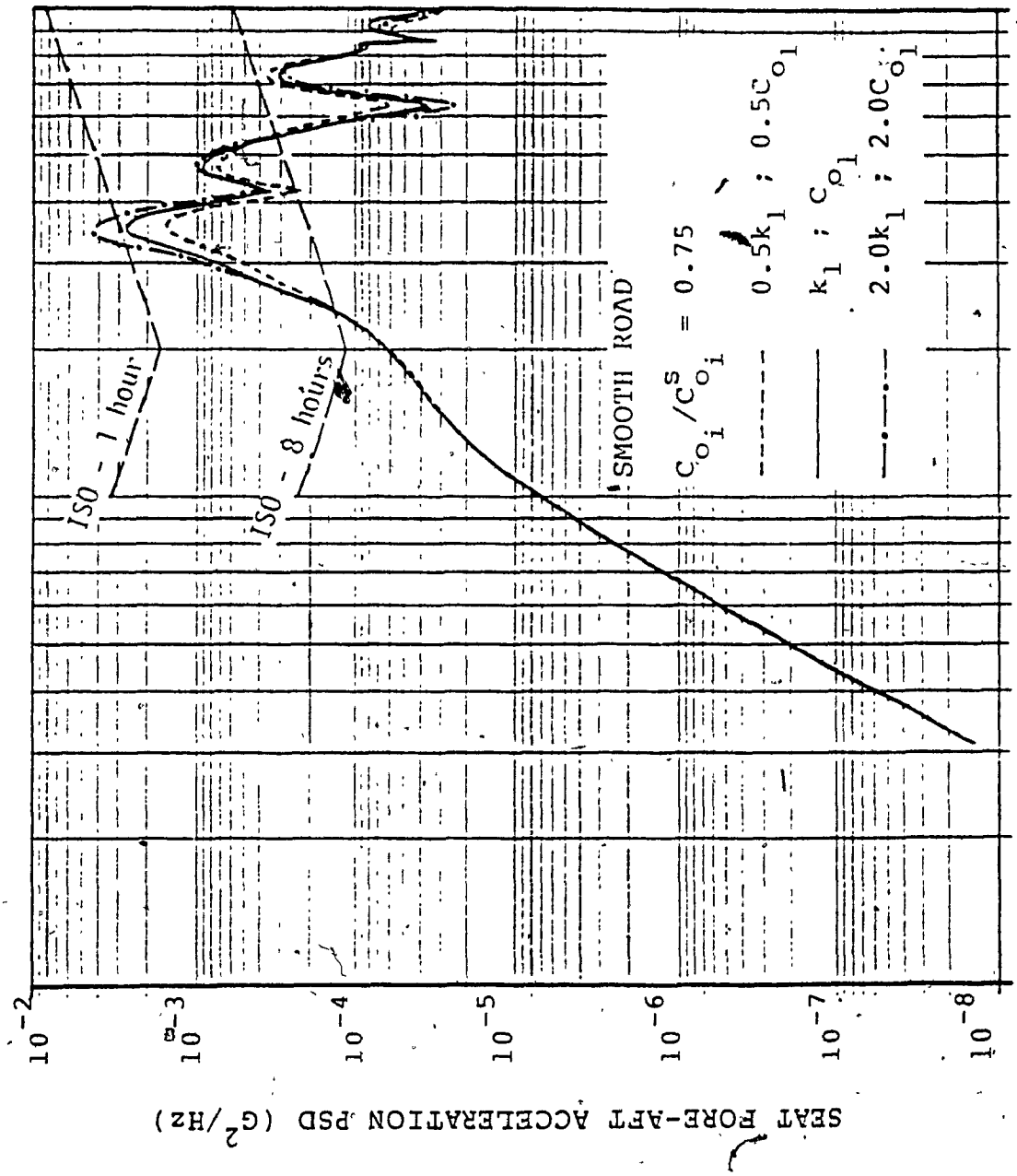

FIGURE 5.26: Influence of tractor front suspension on seat fore-aft acceleration spectra - nonlinear, two-dimensional model

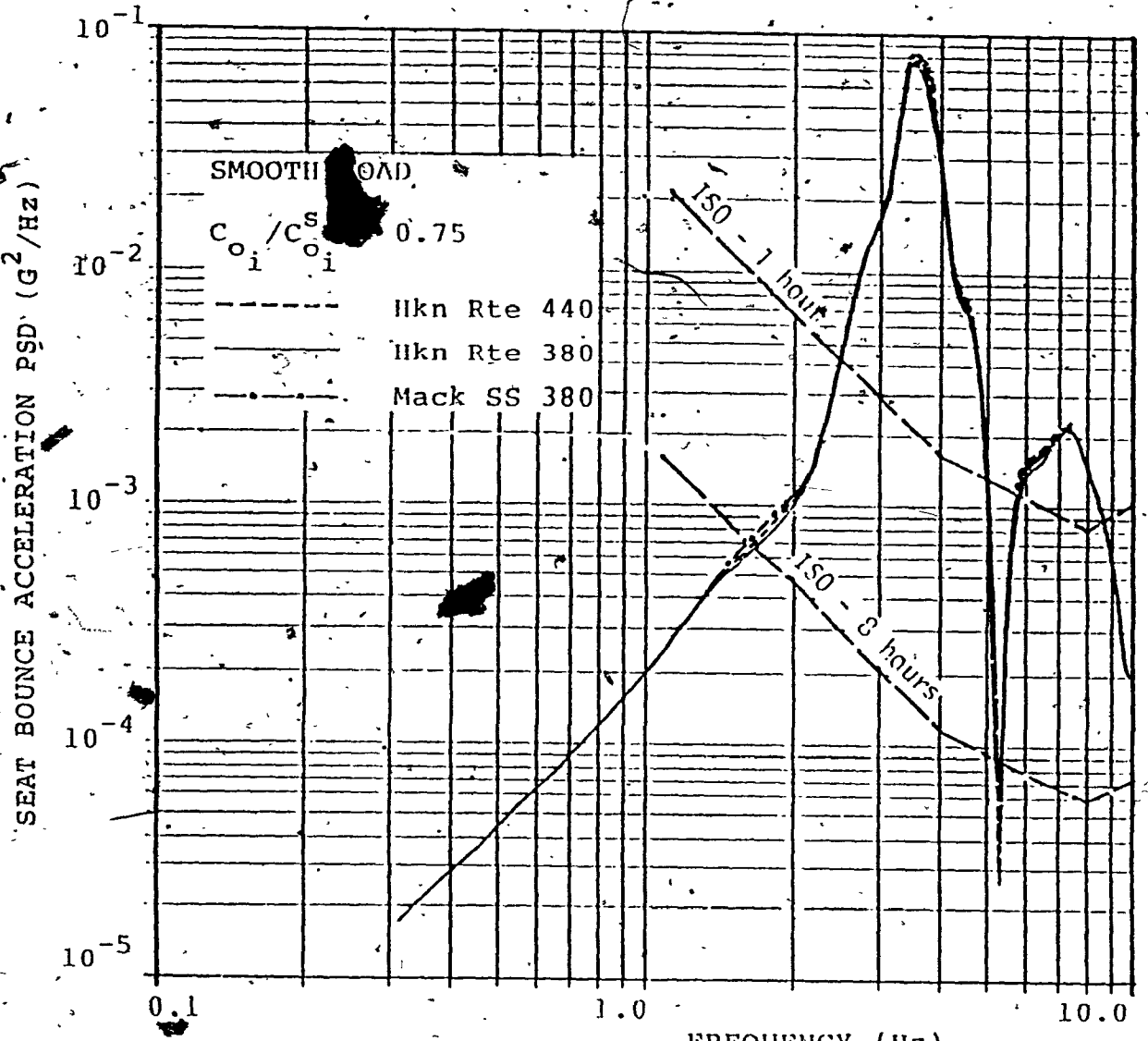

FIGURE 5.27: Influence of tractor rear suspension on seat bounce acceleration spectra - nonlinear, two-dimensional model

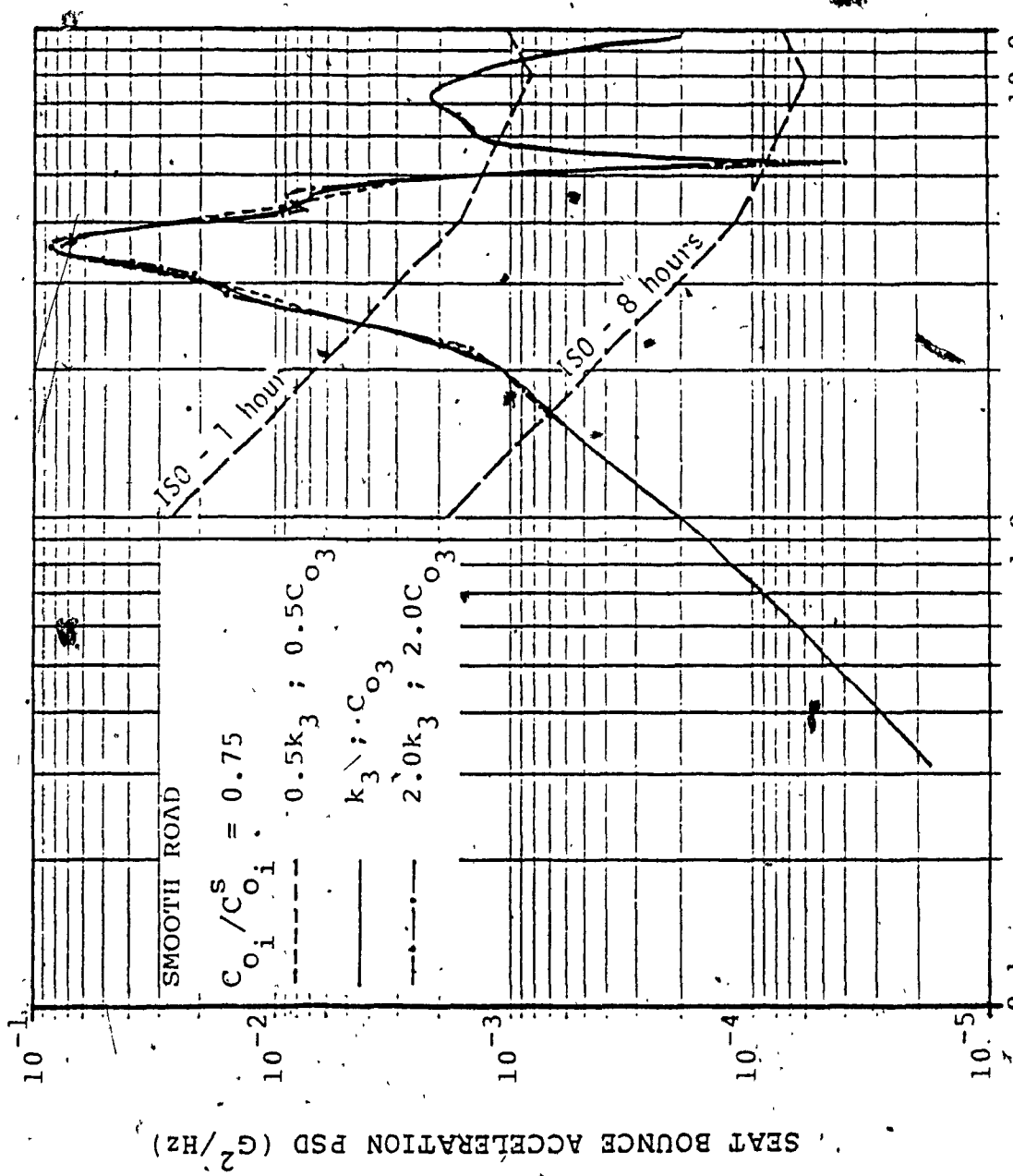

FIGURE 5.28: Influence of semitrailer suspension on seat bounce acceleration spectra - nonlinear, two-dimensional model

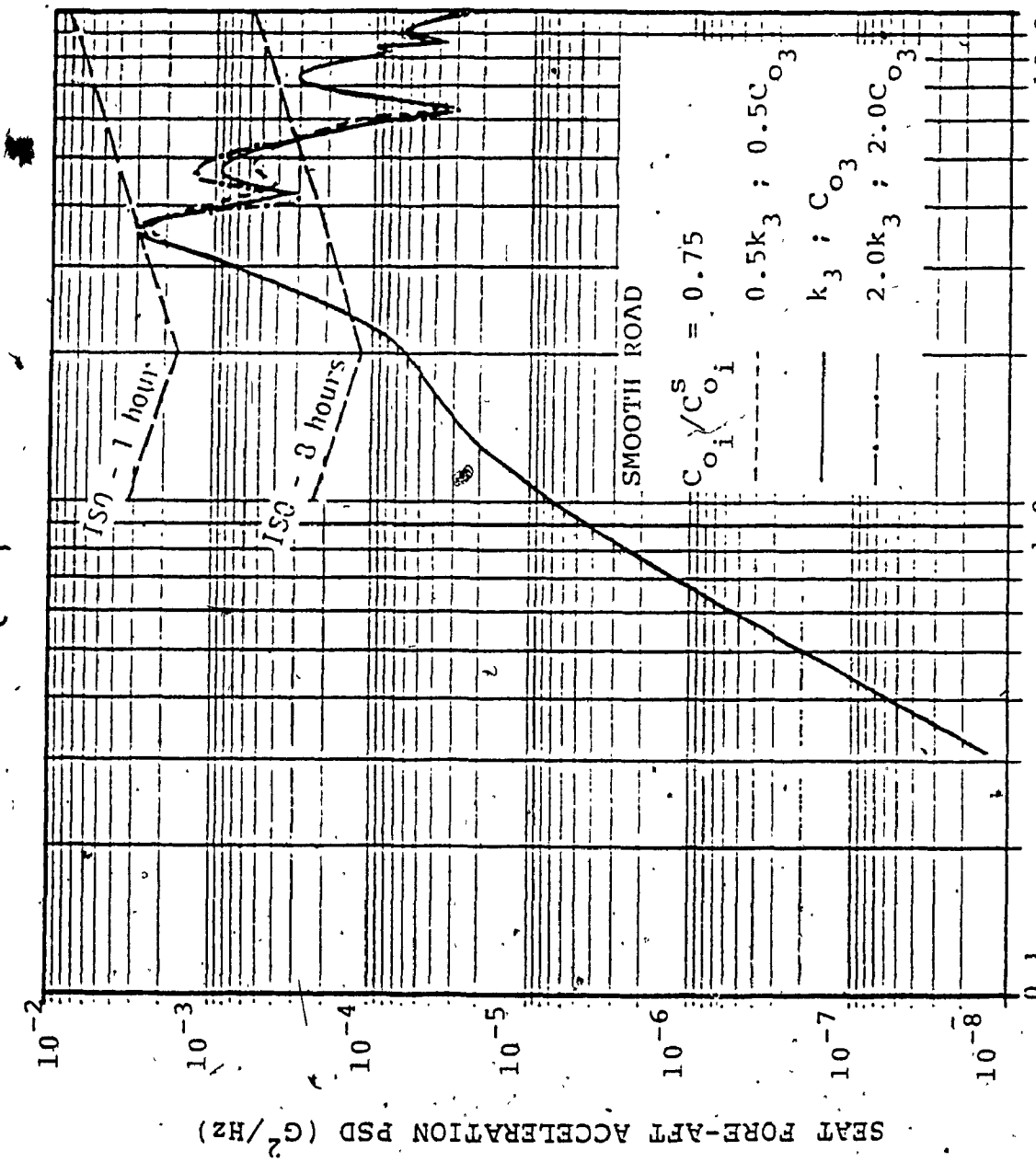

FIGURE 5.29: Influence of semitrailer suspension on seat fore-aft acceleration spectra - nonlinear, two-dimensional model

levels, respectively. These results show that a softer suspension yield comfortable ride.

5.6.2.3 INFLUENCE OF ROAD CHARACTERISTICS

Figures 5.30 and 5.31 show the bounce and fore-aft acceleration spectra at the driver's position for both smooth and rough highways, while Figures 5.32 and 5.33 yield the root mean square acceleration amplitudes in bounce and longitudinal directions, respectively. By comparing the response for smooth and rough highways, it is obvious that there is a definite increase in the seat bounce as well as fore-aft vibration levels for the complete frequency range of interest. The rate of increase of amplitude spectra for smooth highway is much higher than that for the rough road in the low frequency range. The seat bounce acceleration PSD for rough highway is about 2.5 times higher around the maximum peak value.

5.6.2.4 INFLUENCE OF VEHICLE SPEED

The bounce and fore-aft acceleration spectra at driver location are presented in Figures 5.34 and 5.35, respectively, for different vehicle speeds. The fore-aft ride quality is considerably deteriorated when the vehicle speed is increased to 120 km/hr as shown in Figure 5.35. A reduction in speed to 70 km/hr improves the seat bounce and fore-aft ride quality considerably , while the ride levels

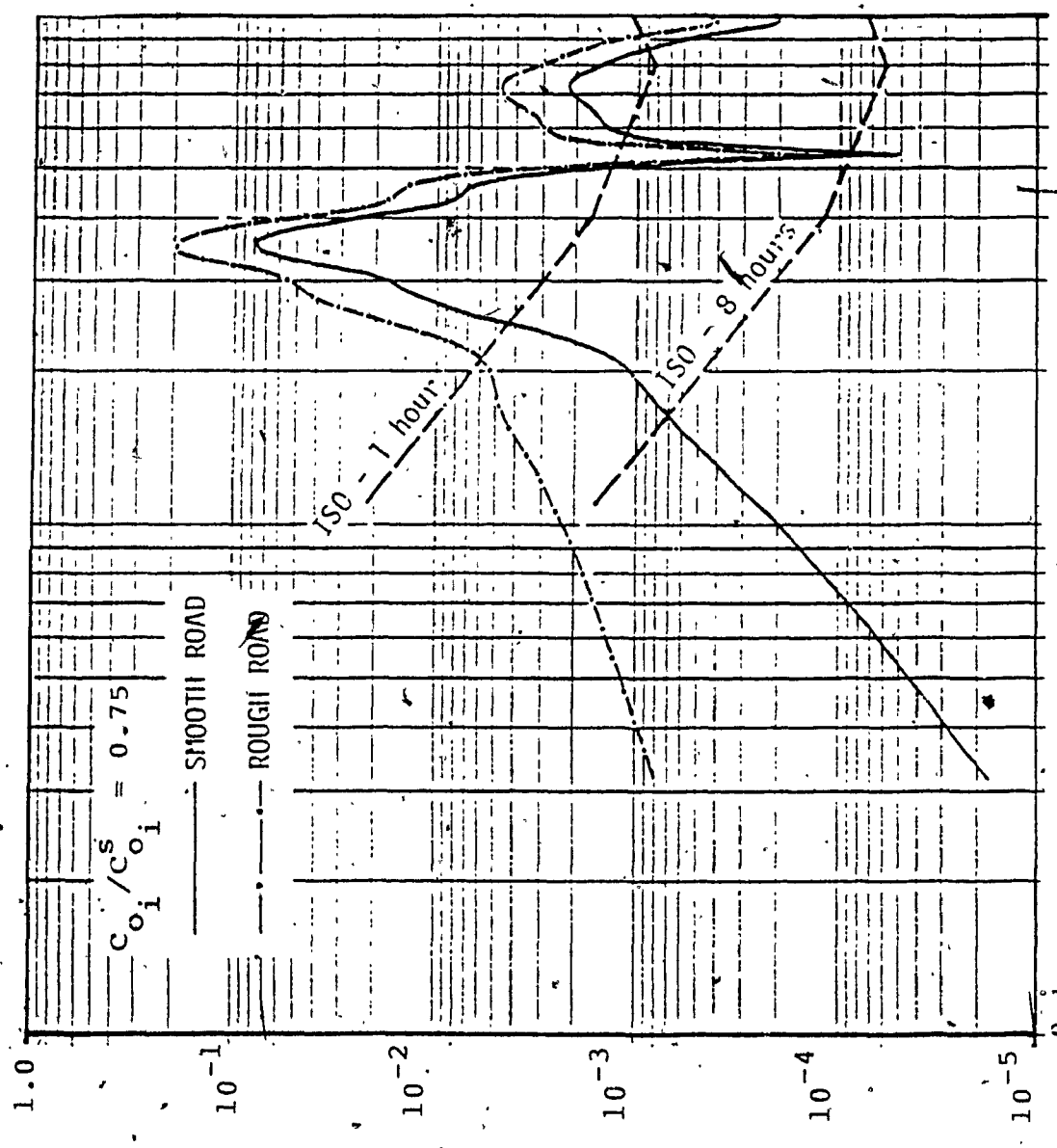

FIGURE 5.30: Influence of road profile on seat bounce acceleration spectra - nonlinear, two-dimensional model

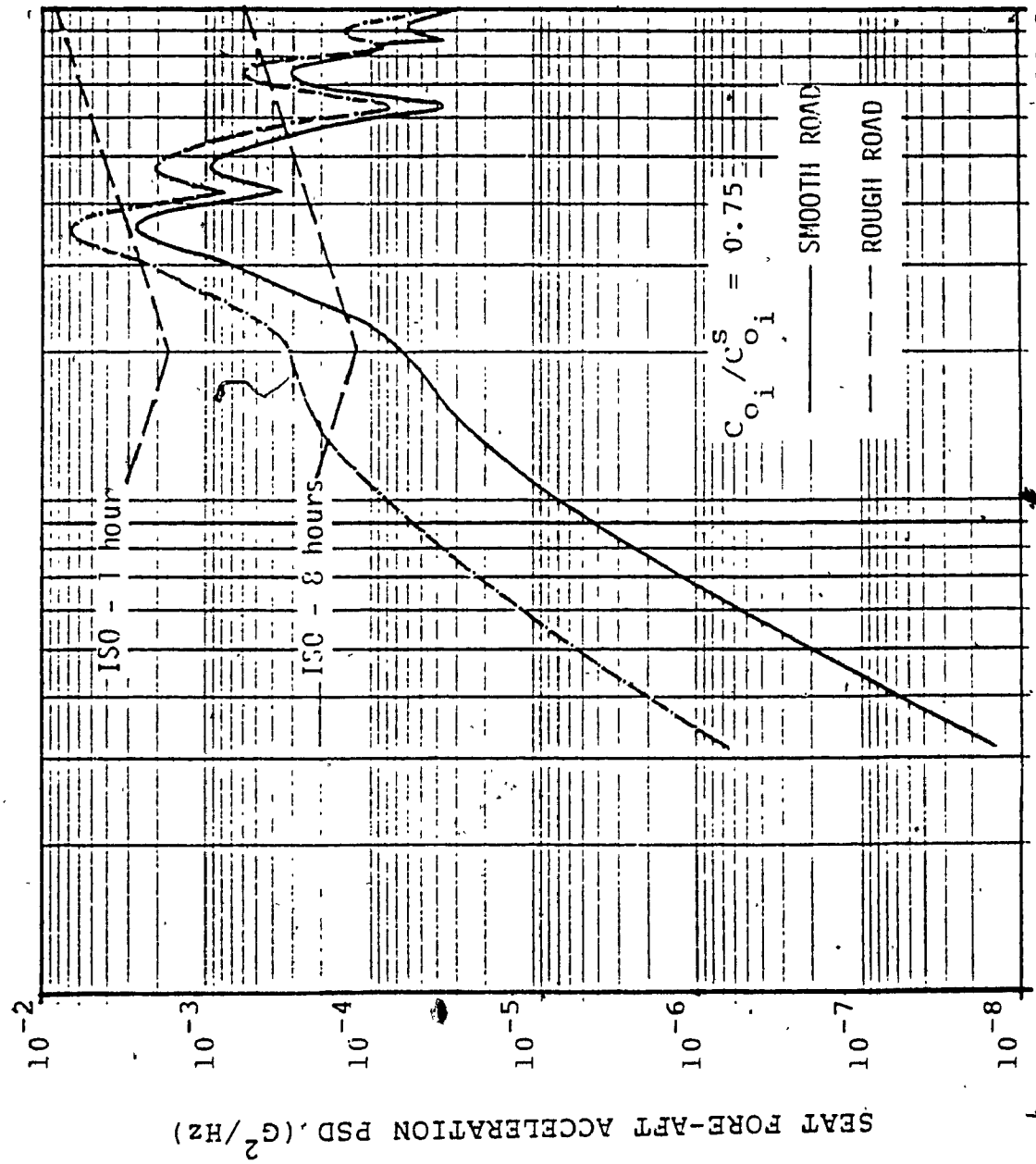

FIGURE 5.31: Influence of road profile on seat fore-aft acceleration spectra - nonlinear, two-dimensional model

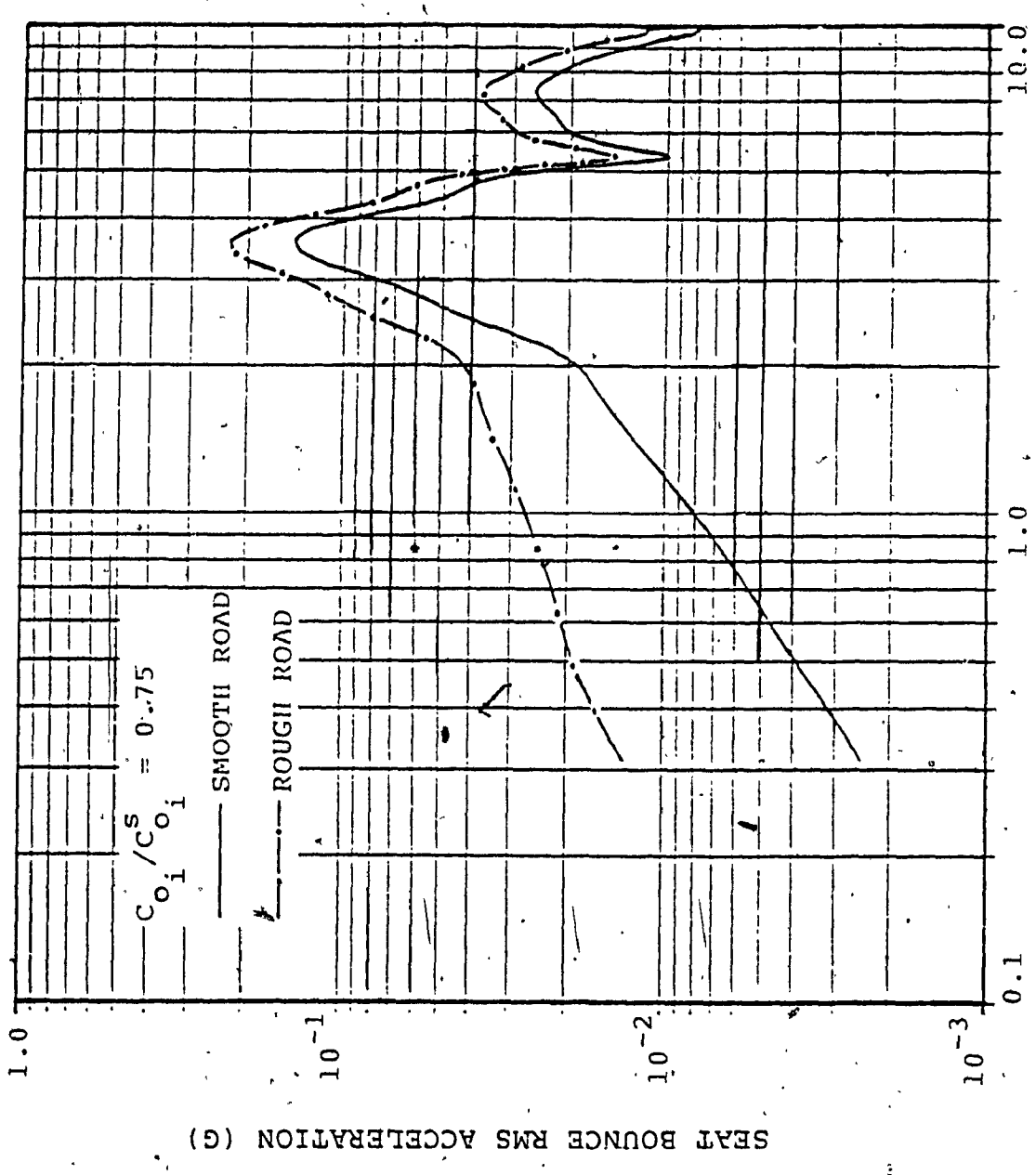

FIGURE 5.32: Influence of road profile on seat bounce rms acceleration response - nonlinear, two-dimensional model

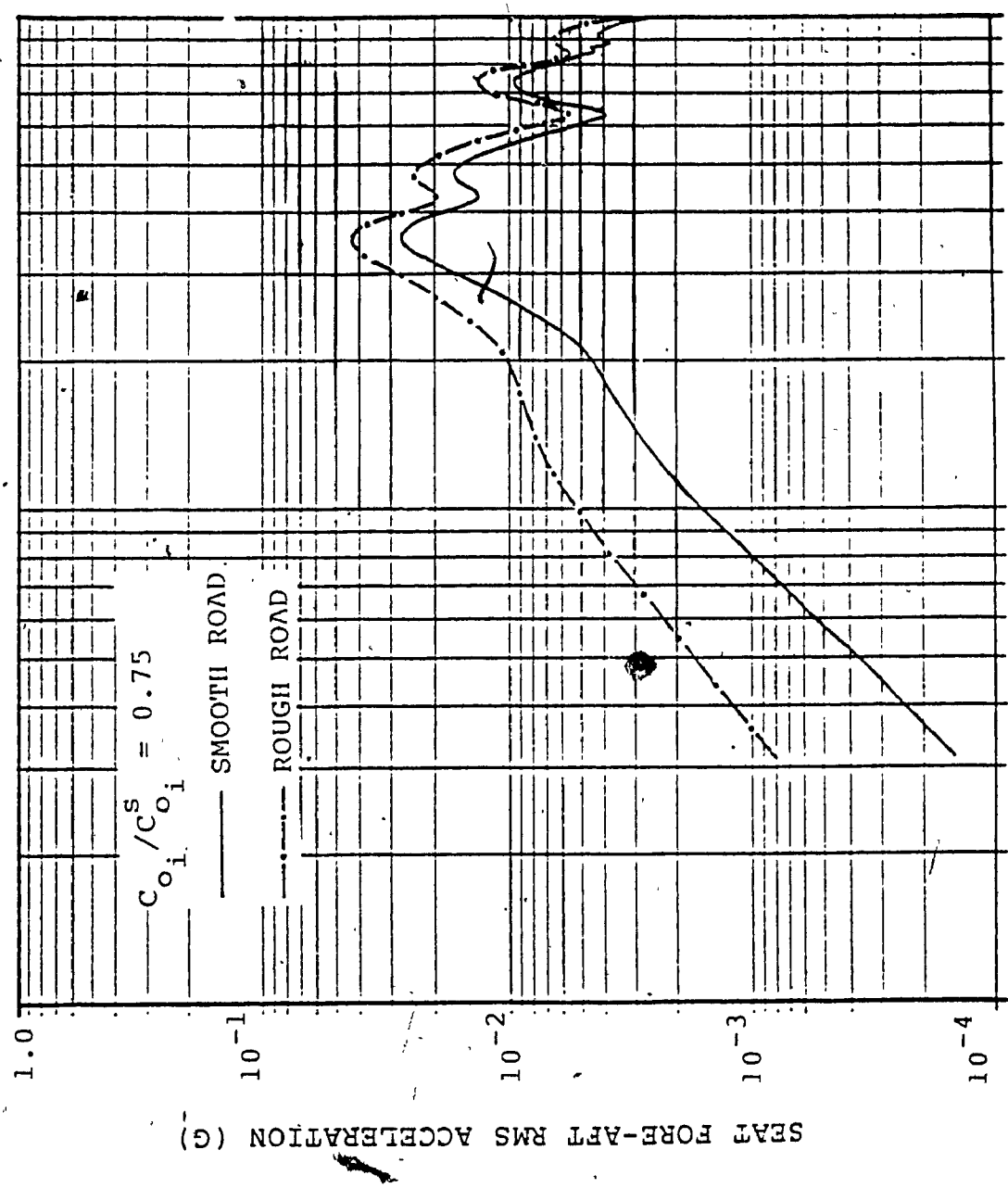

FIGURE 5.33: Influence of road profile on seat fore-aft rms acceleration response - nonlinear, two-dimensional model

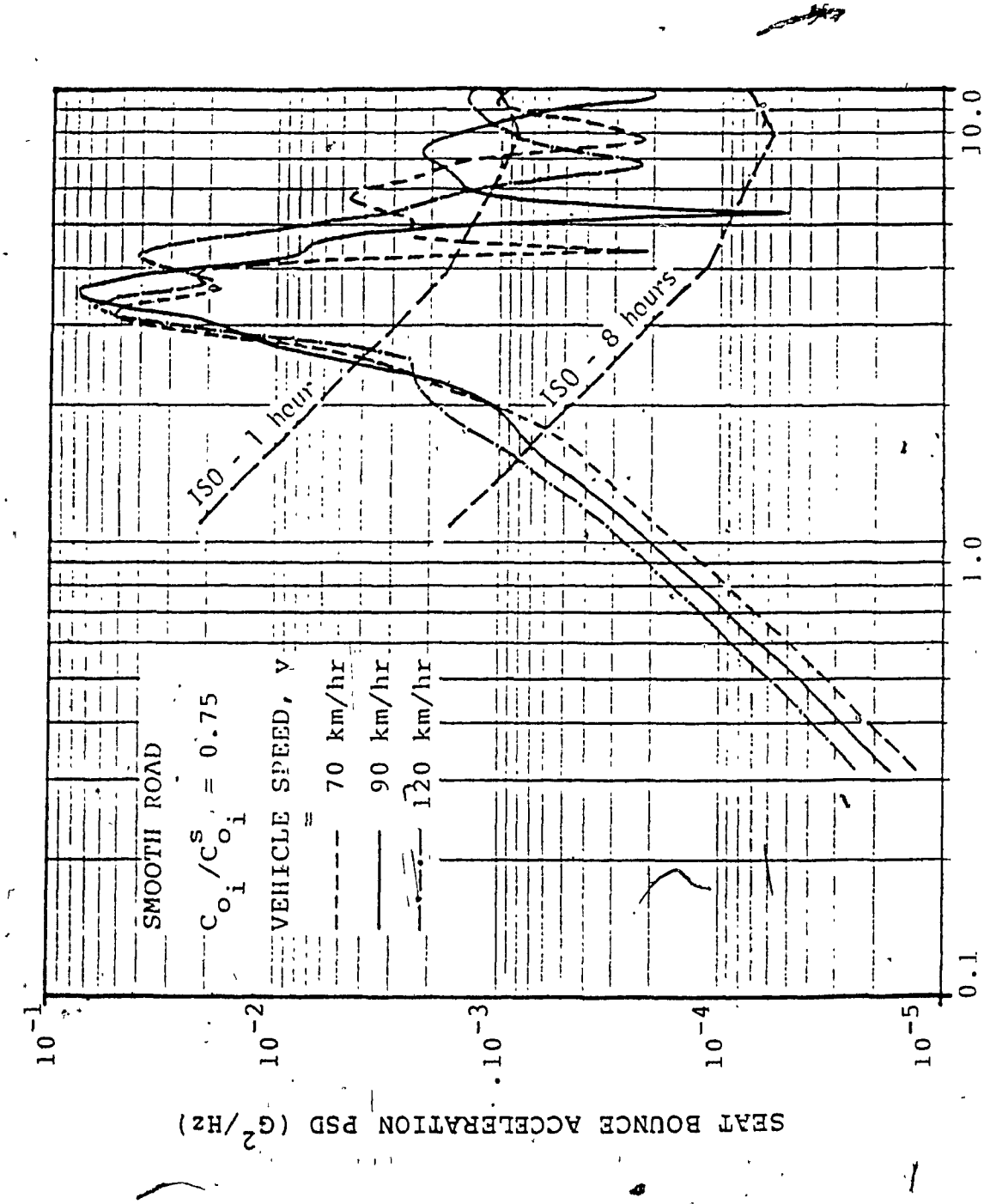

FIGURE 5.34: Influence of vehicle speed on seat bounce acceleration spectra - nonlinear, two-dimensional model

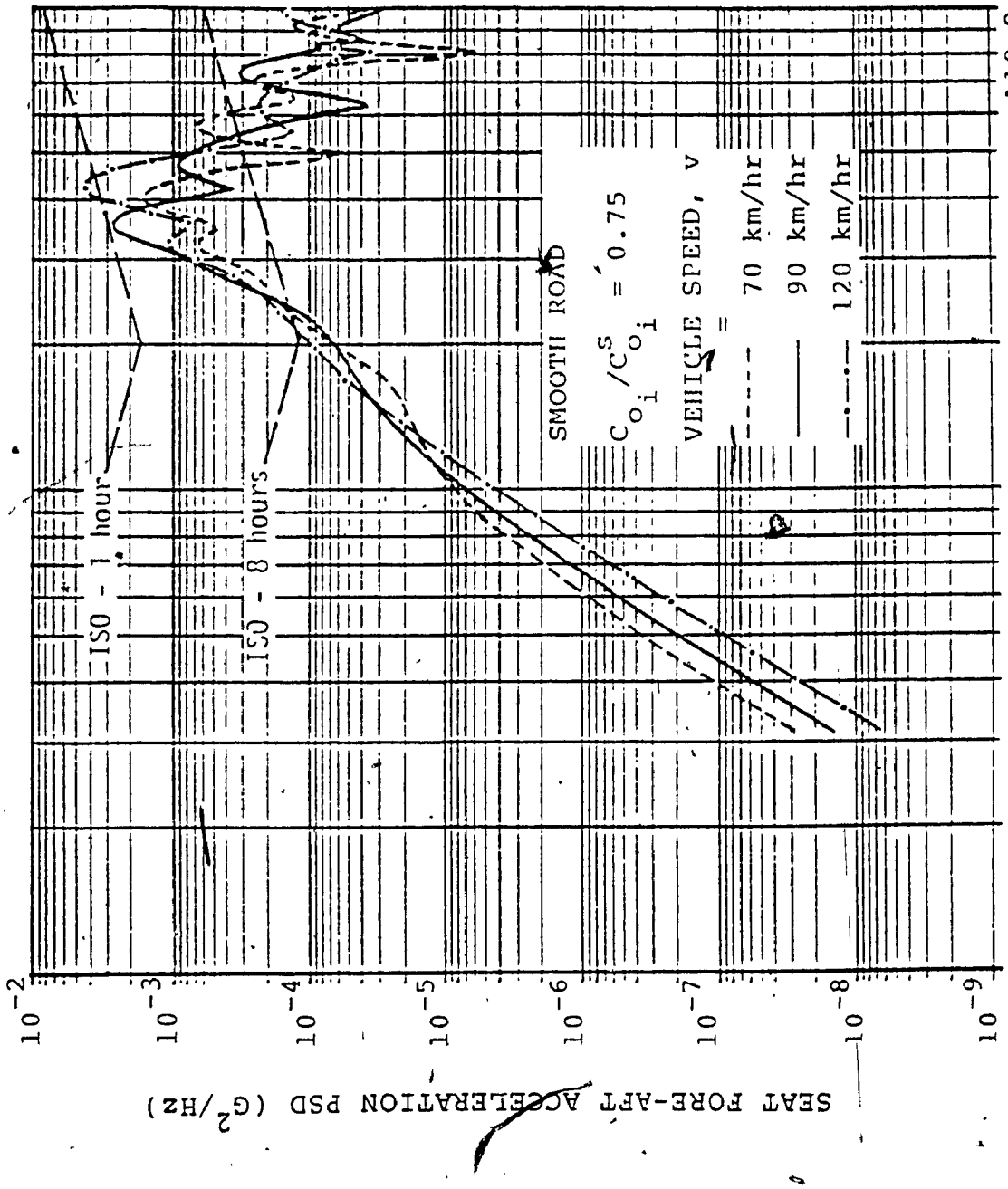

FIGURE 5.35: Influence of vehicle speed on seat fore-aft acceleration spectra - nonlinear, two-dimensional model

increase at medium frequency range.

5.6.2.5 INFLUENCE OF FIFTH-WHEEL LOCATION

The variations in the location of fifth-wheel with respect to tractor c.g. changes the front axle load, which affect the vehicle ride quality considerably. The front axle load is increased when fifth wheel location is moved closer to tractor c.g. The adverse effect of increased front axle load on the seat bounce ride vibrations is demonstrated in Figure 5.36. Fifth-wheel located at the tandem center yields the best bounce ride at the driver's position. The fore-aft levels at the driver's location also increase considerably, as the front axle load is increased as shown in Figure 5.37.

5.6.2.6 INFLUENCE OF KINGPIN SETBACK

The kingpin setback determines the location of cargo c.g. from the fifth wheel. A higher value of kingpin setback moves cargo c.g. closer to fifth wheel location, which in turn increases the fifth wheel load. A variation in the value of kingpin setback is achieved by changing the distance between the cargo c.g. and fifth-wheel. Figures 5.38 and 5.39 demonstrate the influence of the variation in kingpin setback on seat bounce and fore-aft ride vibration levels, respectively. As it can be seen from the plots that for lower value of kingpin setback, the seat bounce

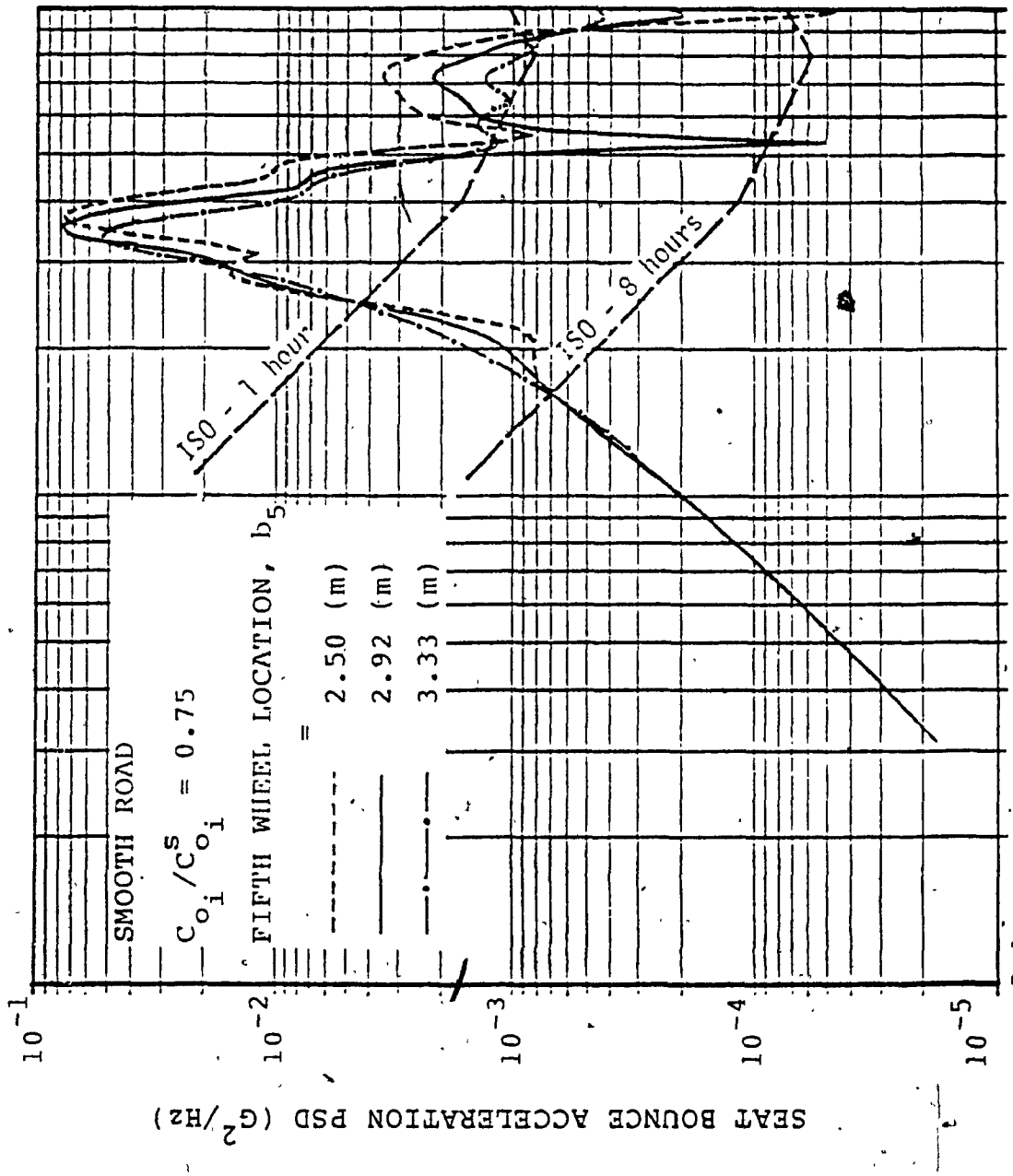

FIGURE 5.36: Influence of fifth-wheel location on seat bounce acceleration spectra - nonlinear, two-dimensional model

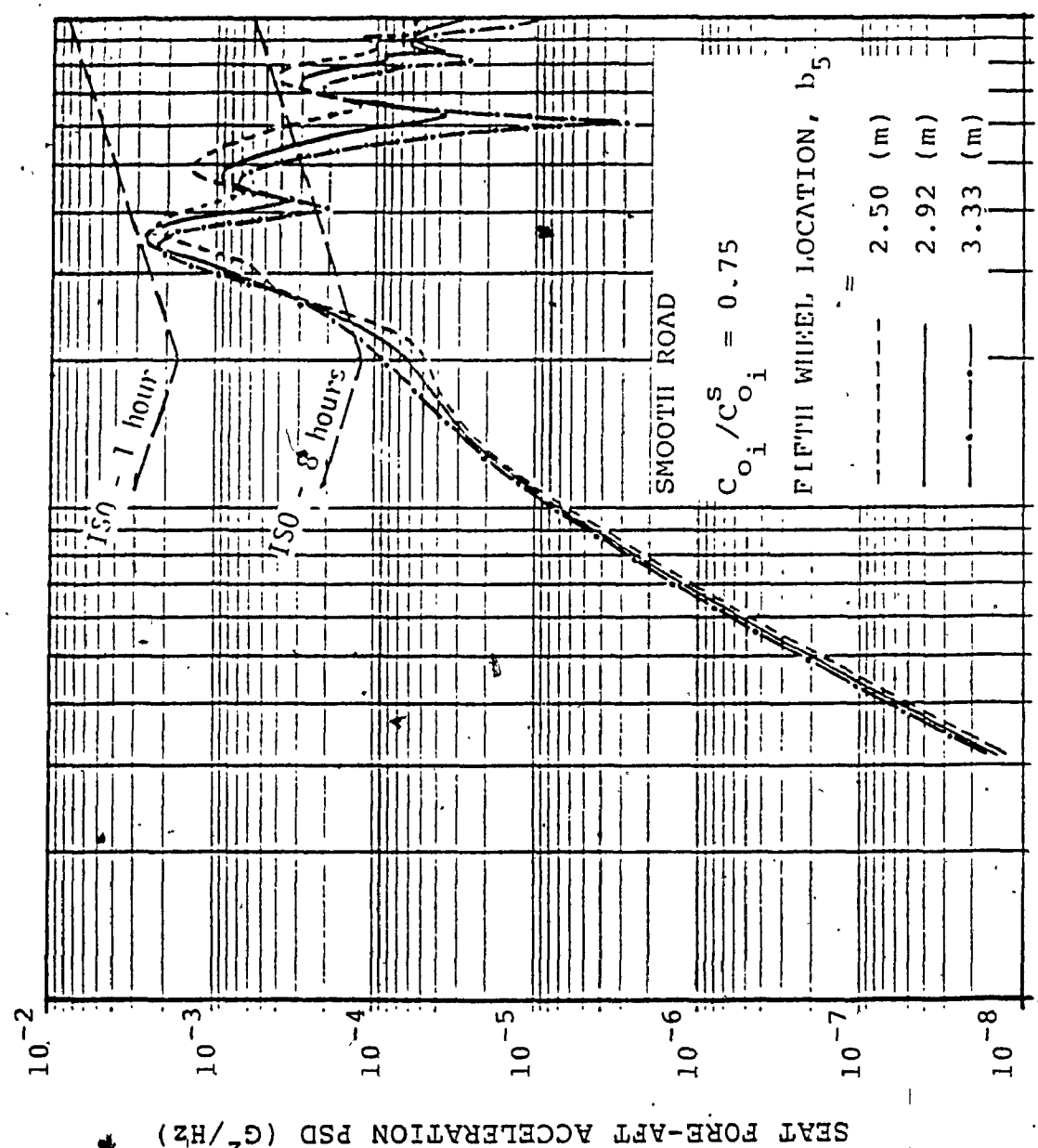

FIGURE 5.37: Influence of fifth-wheel location on seat fore-aft acceleration spectra - nonlinear, two-dimensional model

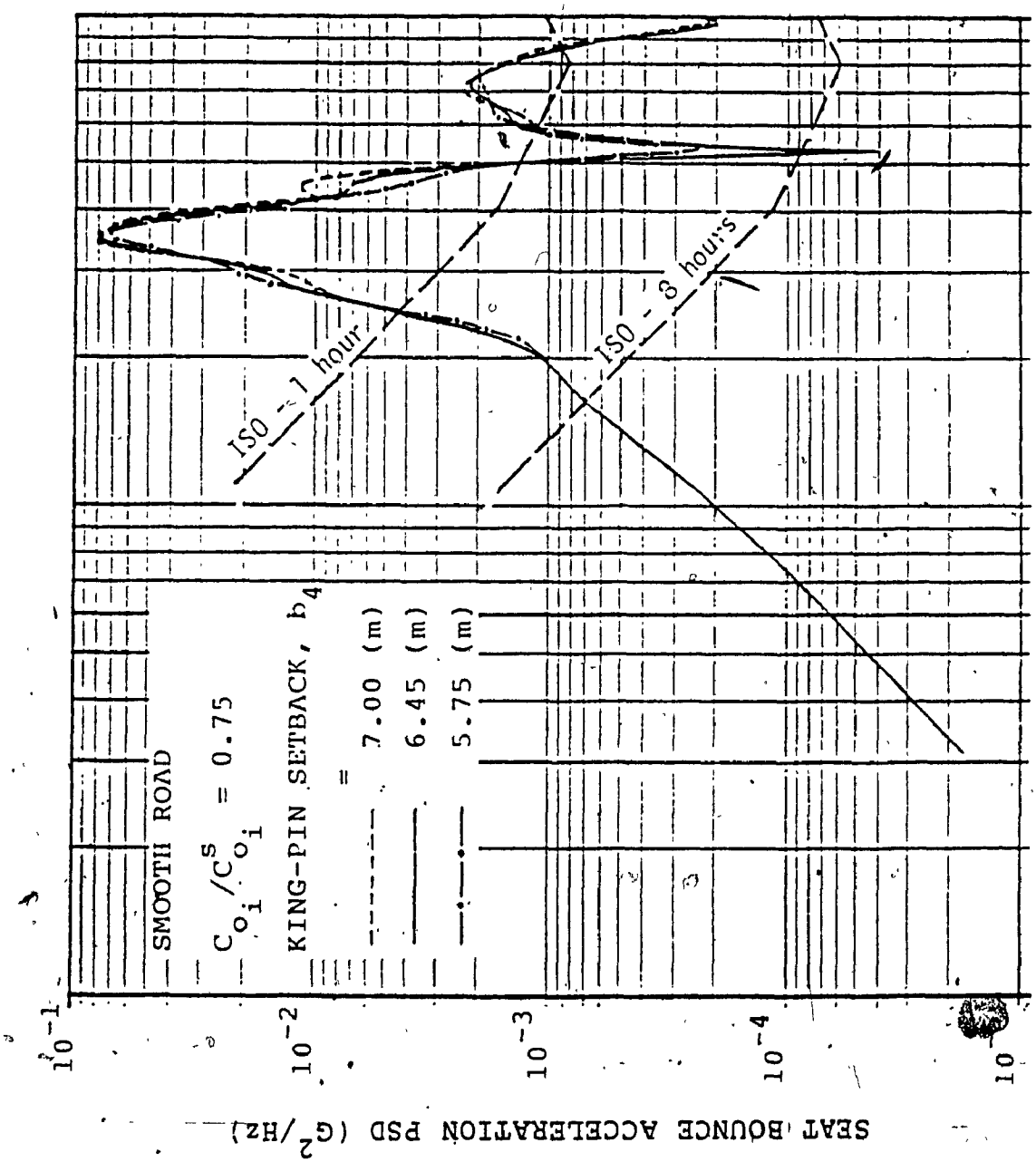

FIGURE 5.38: Influence of kingpin setback on seat bounce acceleration spectra - nonlinear, two-dimensional model

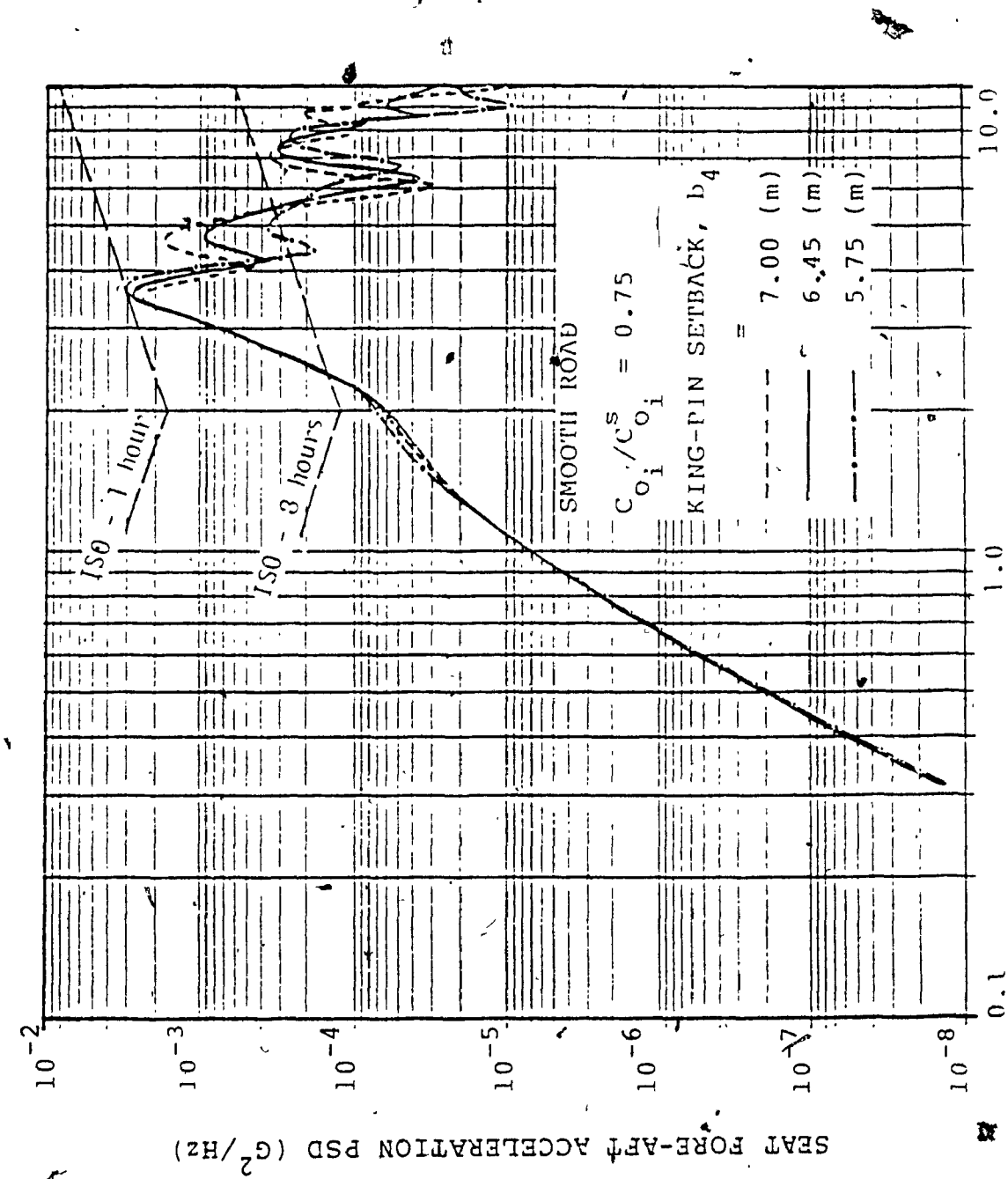

FIGURE 5.39: Influence of kingpin setback on seat fore-aft acceleration spectra - nonlinear, two-dimensional model

and fore-aft ride levels are reduced around dominant peak, but are increased considerably in frequency range 4-5 Hz.

5.6.2.7 INFLUENCE OF DRIVER LOCATION

As driver sits forward and well above the tractor c.g., he is subjected to vertical and fore-aft motion resulting from the bouncing and pitching modes of vibrations. The influence of variations in the horizontal and vertical locations of the driver on bounce and fore-aft acceleration spectra are demonstrated in Figures 5.40 and 5.41, respectively. The bounce vibration levels increase as driver location is moved further ahead of tractor c.g., as shown in Figure 5.40. An increase in the vertical distance above the tractor c.g. causes a definite increase in the fore-aft vibration levels in the entire frequency range of interest (Fig. 5.41).

5.6.2.8 INFLUENCE OF LOAD PATTERN

The load pattern associated with vehicle cargo affect the vehicle ride considerably e.g. the ride comfort of a loaded vehicle is significantly different than that of an unloaded vehicle. Load placed in the front portion of semitrailer yield different ride than if placed in the middle or back of the trailer. The load pattern basically determines the horizontal and vertical location of cargo c.g. from fifth-wheel, and fifth-wheel load.

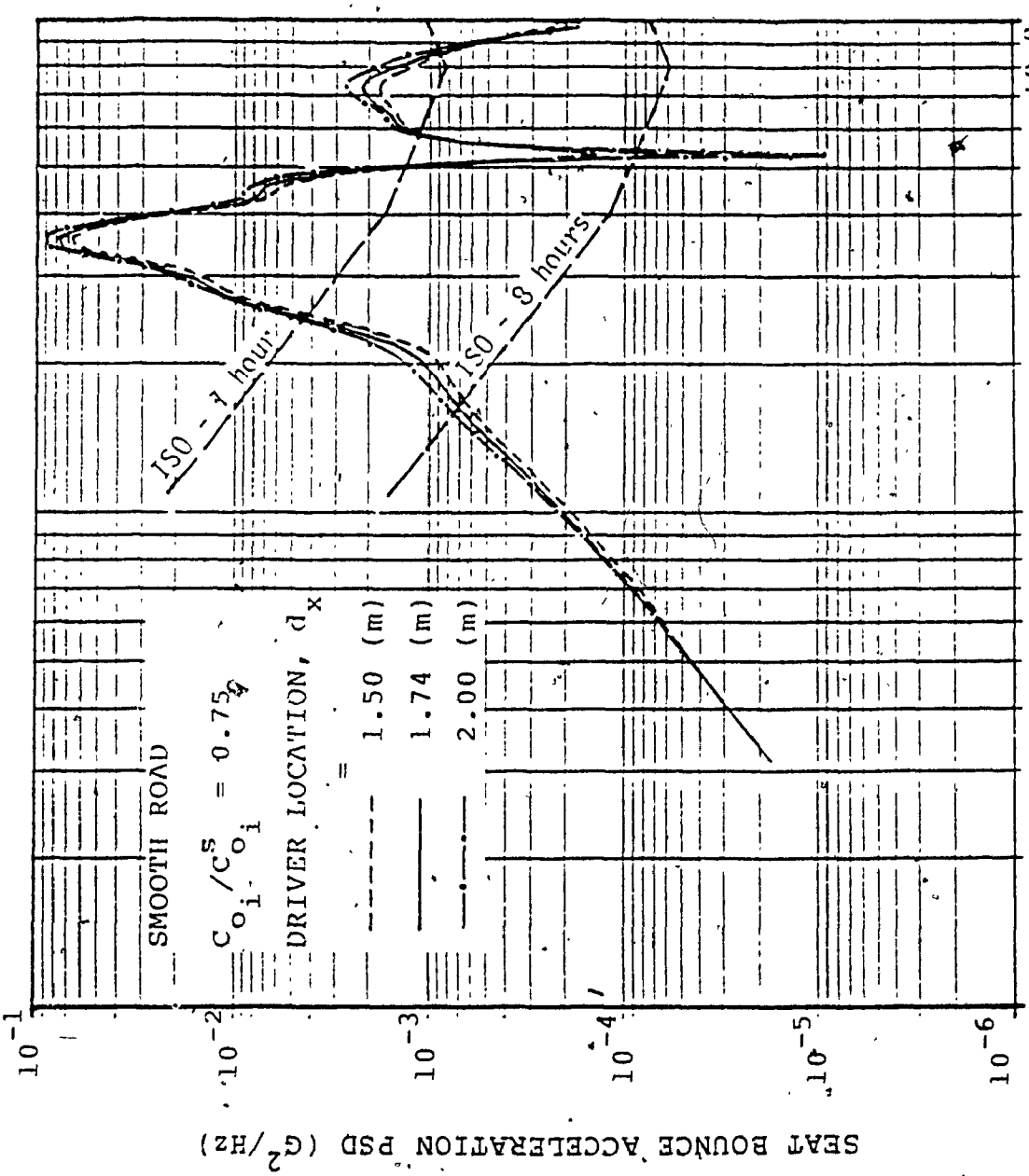

FIGURE 5.40: Influence of driver's location on seat bounce acceleration spectra - nonlinear, two-dimensional model

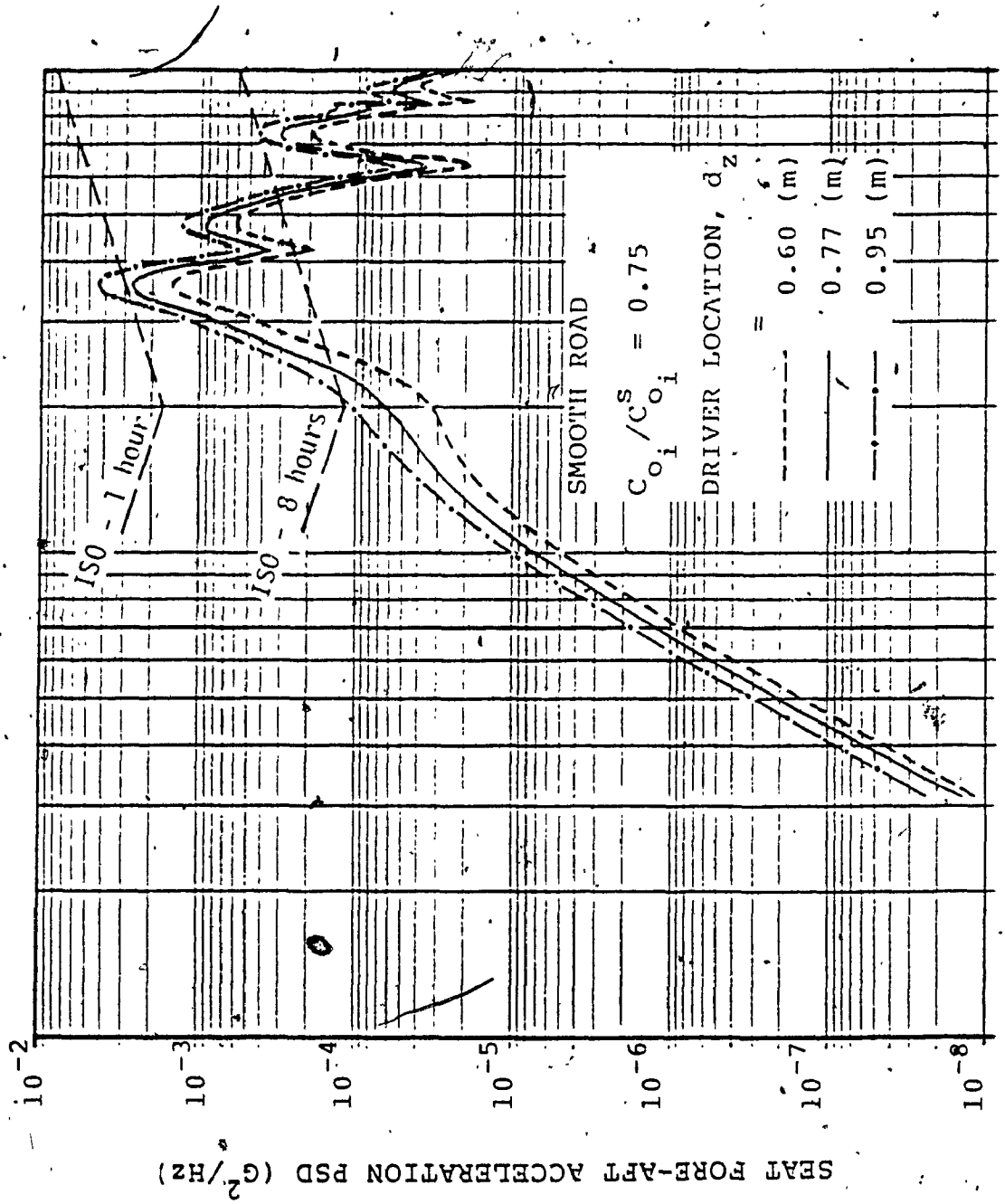

FIGURE 5.41: Influence of driver's location on seat fore-aft acceleration spectra - nonlinear, two-dimensional model

Figures 5.42 and 5.43 show the influence of the variation of load pattern in vertical direction on seat bounce and fore-aft acceleration spectra. For unloaded vehicle, the resonant peaks of bounce as well as fore-aft acceleration at driver's location are suppressed. But the comfort of unloaded vehicle is considerably worsened in frequency range 5-8 Hz, specifically the fore-aft ride levels exceed 1-hr ISO guide.

Influence of the location of load along the semitrailer bed on ride vibration levels is investigated. A cargo load of one third of the baseline value is considered to be placed in the front, middle, and rear of the trailer, independently. The resonant peaks of bounce and fore-aft acceleration spectra at driver's position are suppressed for a vehicle carrying a load in its rear. But there is considerable increase in ride levels in frequency range 5-8 Hz, as shown in Figures 5.44 and 5.45.

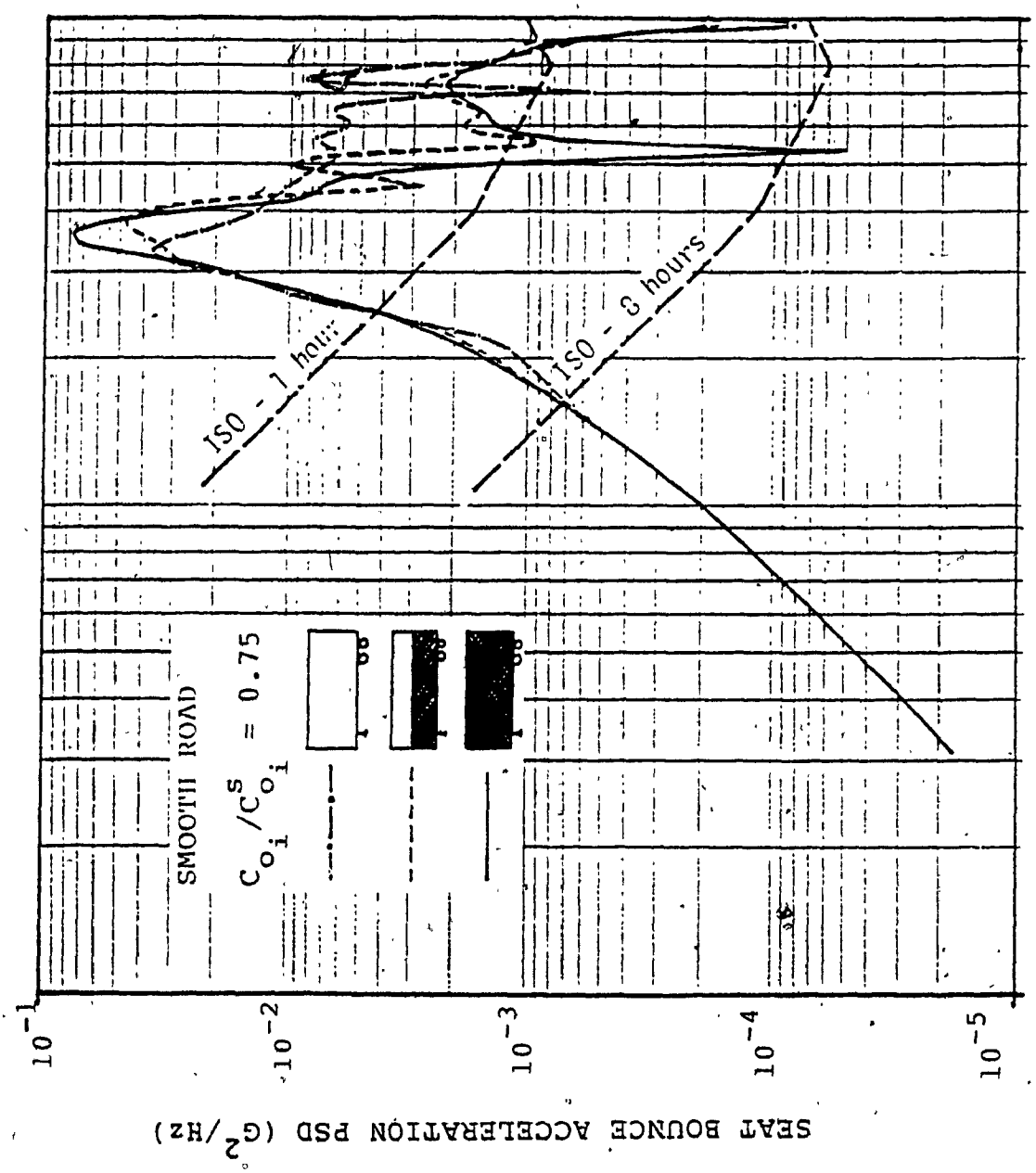

FIGURE 5.42: Influence of load pattern in vertical direction on seat bounce acceleration spectra - nonlinear, two-dimensional model

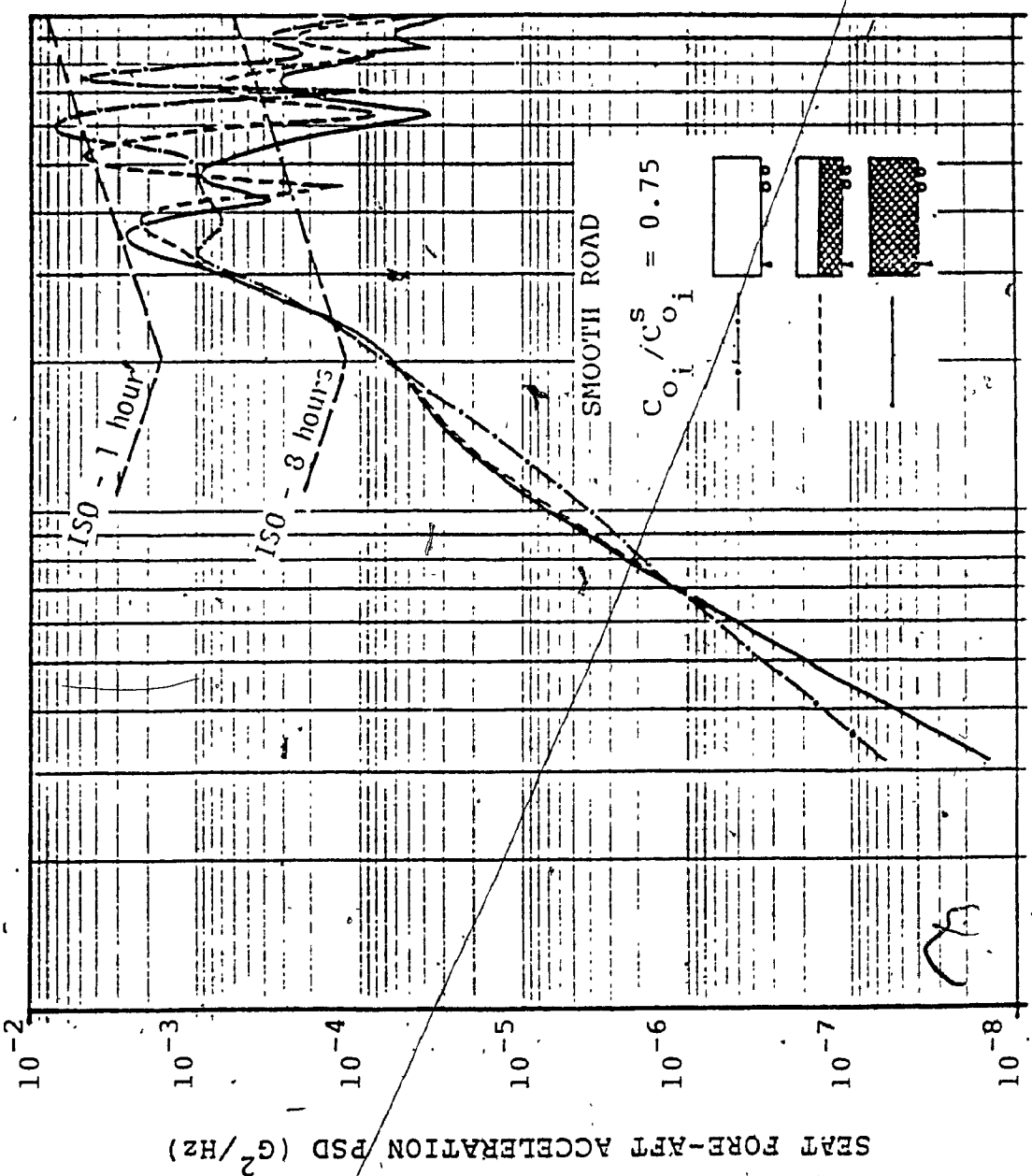

FIGURE 5.43: Influence of load pattern in vertical direction on seat fore-aft acceleration spectra - nonlinear, two-dimensional

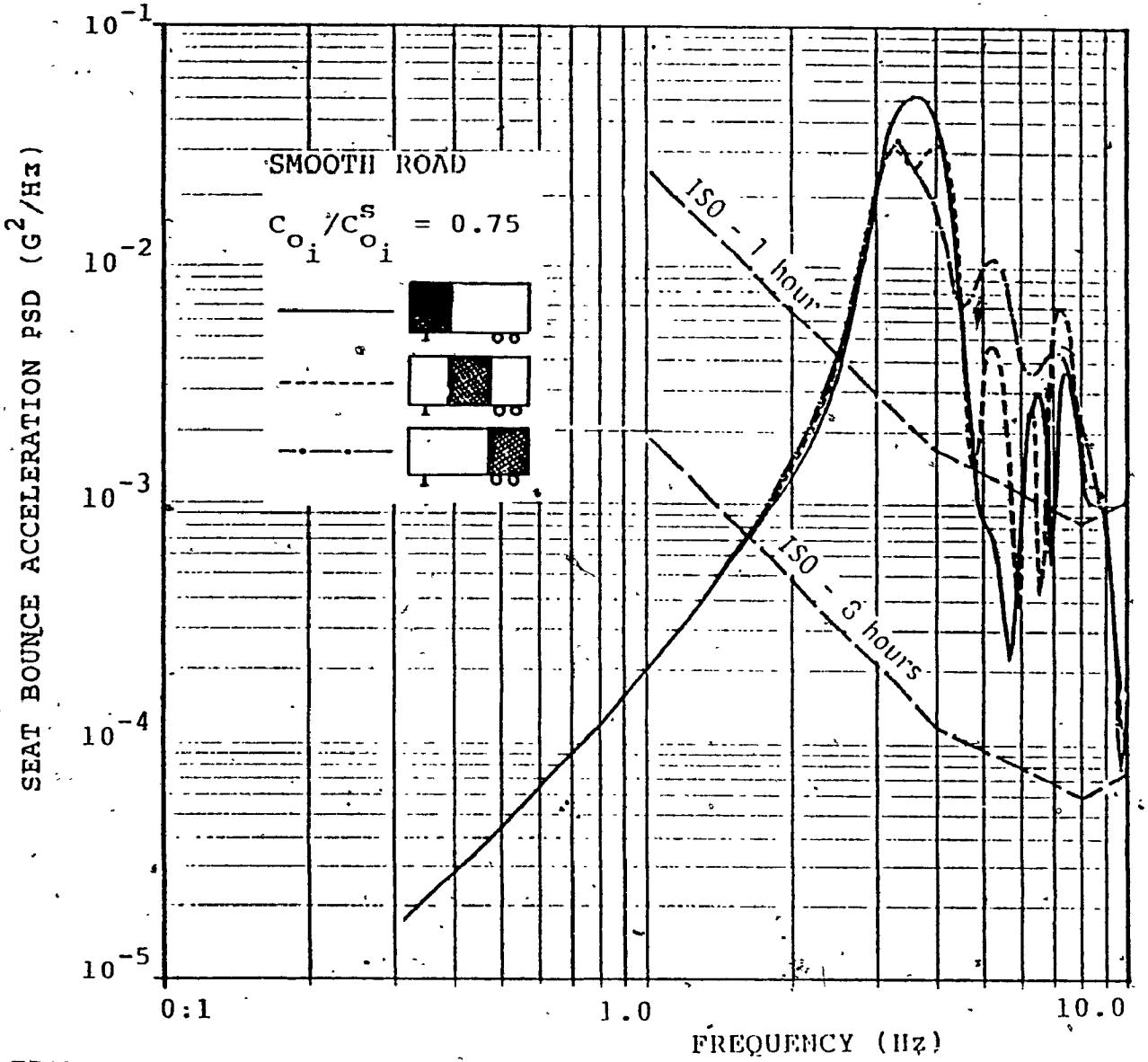

FIGURE 5.44: Influence of load pattern in horizontal direction on seat bounce acceleration spectra - nonlinear, two-dimensional model

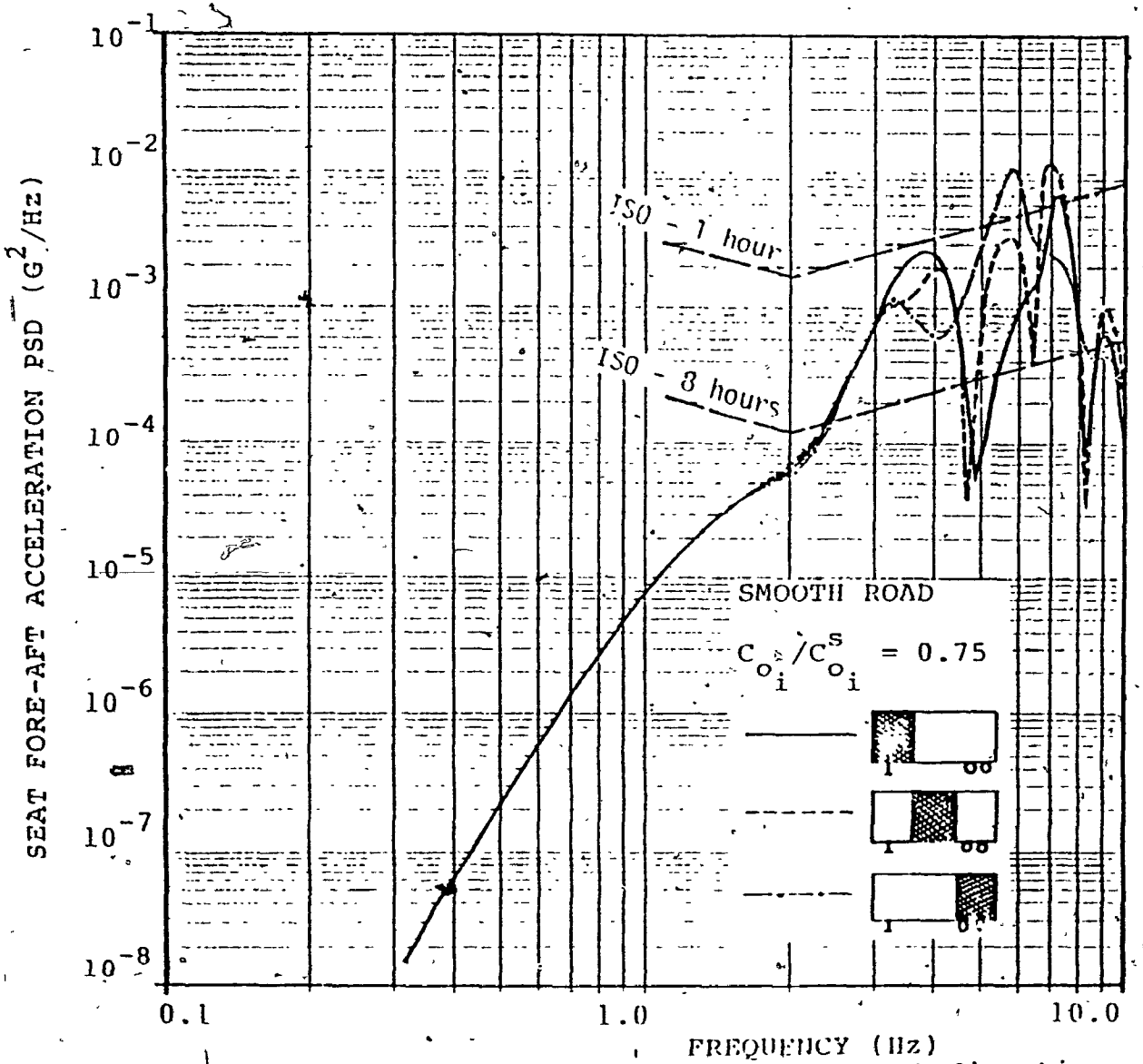

FIGURE 5.45: Influence of load pattern in horizontal direction on seat fore-aft acceleration spectra - nonlinear, two-dimensional

5.7 SUMMARY

The dynamic response of the articulated vehicle subjected to random road irregularities is investigated in-depth by means of nonlinear analysis. The influence of the frictional forces generated in the multi-leaf springs on the ride dynamics are discussed and investigated. A method based on local equivalent approach is adapted and further developed to give a technique applicable to study the stationary response of nonlinear articulated vehicle model. This technique is based on replacing the nonlinear damping mechanism by an array of local constants. The critical lock-up behaviour due to Coulomb friction is taken into consideration such that the nonlinear behaviour of the system can be effectively simulated by the equivalent linear system. The next chapter presents the conclusions from the present investigation and recommendations for future work.

CHAPTER 6

CONCLUSIONS AND RECOMMENDATIONS FOR FUTURE WORK

6.1 GENERAL

In this thesis, the ride dynamics of a complex articulated vehicle have been studied using linear as well as nonlinear mathematical models subjected to road inputs represented as stationary Gaussian random excitations. The analytical techniques employed to solve the linear and nonlinear mathematical models of baseline vehicle provide an attractive and convenient solution that yields a great deal of insight into the vehicle behaviour. These analytical techniques will assist in the interpretation of experimental test results on vehicle ride quality.

The linear analysis of the articulated vehicle, in general, is useful in studying the modal parameters of the vehicle, such as, system eigenvalues and eigenvectors, and the general effects on the ride quality due to generic changes in various vehicle parameters. In situation, where a more complete understanding of the qualitative and quantitative behaviour of an articulated vehicle is required, it is often necessary to include nonlinear effects resulting from primary suspension system.

A local equivalent linearization technique based on the dissipation of energy is adopted to represent the nonlinear

suspension models by their linear equivalent. The critical lock-up behaviour due to Coulomb friction is inspected such that the nonlinear behaviour of the system can be effectively simulated by the equivalent linear system. A parametric study of nonlinear vehicle model is carried out to establish the influence of various parameters on the articulated vehicle dynamic behaviour. The ride performance of the vehicle model is assessed with reference to ISO specified criteria for ride comfort.

6.2 CONCLUSIONS

There are two types of conclusions which can be drawn from this study. The first set of conclusions are from the modelling aspect, and the in-depth study of the local equivalent linearization technique. The second set of conclusions are drawn from the parametric study of the baseline vehicle.

Based on the studies, the following specific conclusions are drawn :

- Three-dimensional mathematical model with seat and cab suspensions represents the ride behaviour of vehicle more realistically. However, adequate information on the vehicle ride quality can be obtained from a simple, two-dimensional model.
- The comparison of transmissibility characteristics

obtained from local equivalent linearization technique and numerical integration shows that the local equivalent linearization technique can duplicate the response behaviour of nonlinear system quite precisely.

- Unlike statistical linearization technique, the local equivalent linearization technique represents the nonlinear damping mechanism by a local constant corresponding to a discrete frequency. In addition, the lock-up due to critical effects of Coulomb friction can be effectively simulated by the local equivalent approach.

From the parametric investigation, following conclusions are drawn :

- Presence of large Coulomb friction in the suspensions deteriorates the ride comfort in reference to ISO criteria. An increase in Coulomb friction stiffens the suspensions. Consequently, the tires become the main suspension medium and more energy is transmitted to the sprung masses. This results in inadequate damped vibrations with resonance at frequencies less tolerable by human beings. However, small value of Coulomb friction could provide an excellent compromise between resonant vibration control and high frequency vibration isolation.

- A softer suspension with decreased suspension force contributes to improved ride quality at the driver's position.
- Vehicle ride behaviour is considerably influenced by the road profile. Rough road surface deteriorates the vehicle ride quality in all directions.
- An increase in vehicle speed deteriorates the ride quality in all directions.
- Increased front axle load deteriorates the bounce ride at the driver's seat. Fifth wheel located at the tandem center yields the best bounce ride at the driver's position. The fore-aft ride is also affected adversely by the increased front axle load.
- Fifth wheel load as determined by the kingpin setback value affects the vehicle ride quality considerably. Increased fifth wheel load deteriorates the vehicle ride quality.
- High location of the driver produces large acceleration levels in both the vertical and longitudinal directions.
- An unloaded vehicle has a poor ride quality as compared to a fully loaded vehicle.
- A load placed in the rear of the semitrailer yields a poor ride quality in comparison to the same load being placed in the front.

6.3 RECOMMENDATIONS FOR FUTURE WORK

Mathematical models and computer simulation provide the theoretical ride performance analysis results, but the experimental verification in controlled laboratory conditions is necessary for the validation of the results.

Seat and cab dynamics should be included in the nonlinear model of the articulated vehicle model for a better simulation of the ride performance. Efforts are also needed to integrate this analysis with other design considerations such as location of cab mounts, cab c.g. height, seat location within cab, etc..

An optimization technique could be integrated in this technique to evaluate the optimal value of vehicle parameters for which the optimum ride quality could be achieved.

Study should be undertaken to integrate advanced suspension concepts such as active, semi-active, and interlinked hydropneumatic suspensions.

REFERENCES

[1] Allan, A.B., ElMadany, M.M., and Dokainish, M.A. , " Articulated Vehicle Models ", SAE Paper No. 801420, 1980.

[2] Anon, " Guide for the Evaluation of Human Exposure to Whole-Body Vibrations ", International Standard ISO 2631-1974 (E), International Organization for Standardization, New York, U.S.A..

[3] Anon., " NORPAK User's Manual ", Computer Research for Interactive Graphics Laboratory, Concordia University, Montreal, Canada, 1986.

[4] Anon, " Vehicle Weight and Dimension Study : Computer Simulation of Heavy Vehicle Dynamic Behaviour ", Interim Technical Report, Road and Transport Association of Canada, No. 3, June, 1985.

[5] Ariaratnam, S.T., " Random Response of Non-Linear Suspensions ", Journal of Mechanical Engineering Science, 1960, Vol. 2, No. 3, pp. 195-201.

[6] Bandstra, J.P., " Comparison of Equivalent Viscous Damping and Nonlinear Damping in Discrete and Continuous Vibrating Systems ", Journal of Vibration, Acoustics, Stress and Reliability in Design, Trans. of ASME, July 1983, Vol. 105, pp. 382-392.

[7] Beer, Ferdinand P., and Johnston, E. Russell Jr., " Mechanics for Engineers - Statics and Dynamics ",

McGraw-Hill Inc., New York, 1976.

[8] Bendat, J.S., and Piersol, A.G. , " Random Data : Analysis and Measurement Procedures ", Wiley-Interscience, 1971, Toronto, Ontario, Canada.

[9] Bhat, R.B., Sankar, S., and Rakheja, S., Ride Vibration Levels at the Driver Seat Interface ", Interim Report, Department of Mechanical Engineering, Concordia University, Montreal, Quebec, 1985.

[10] Bogdanoff, J.L., Cote, L.J., and Kojin, F., " Introduction to a Statistical Theory of Land Locomotion - II Ground Roughness ", Journal of Terra-Mechanics, 1965, vol. 2, no. 3, pp. 17-27.

[11] Bootan, R.C., " Nonlinear Control Systems with Random Inputs ", Trans. IRE Circuit Theory, 1954, CT-1, pp. 9-18.

[12] Caughey, T.K., " Derivation and Application of the Fokker-Planck Equation to Discrete Nonlinear Dynamical System Subjected to White Random Excitation ", Journal of the Acoustical Society of America, 1963, Vol. 35, No. 11, pp. 1683-1692.

[13] Caughey, T.K., " Equivalent Linearization Techniques ", Journal of the Acoustical Society of America, 1963, Vol. 35, No. 11, pp. 1706-1711.

[14] Crandall, S.H., " Perturbation Techniques for Random Vibration of Nonlinear Systems ", The

Journal of the Acoustical Society of America, 1963, Vol. 35, No. 11, pp. 1700-1705.

[15] Dailey, G., Caywood, W.C., and O'Connor, J.C., " A General Purpose Computer Program for the Dynamic Simulation of Vehicle-Guideway Interactions ", AIAA Journal, 1973; Vol. 3, No. 3, pp. 278-288.

[16] Dodds, C.J., " The Laboratory Simulation of Vehicle Service Stress ", Journal of Engineering for Industry, ASME transactions, vol. 96, no. 2, pp. 391-398.

[17] Dodds, C.J., and Robson, J.D., " The Description of Road Surface Roughness ", Journal of Sound and Vibration, 1973, vol. 31, no. 2, pp. 175-184.

[18] Donati, F., Genesio, R., Laurentini, A., Mauro, V., Menga, G., and Milanese, M., " Dynasim 3: A Computer Program for Simulation of Vehicle Riding Motions ", VSD, 1974, 3, pp. 141-161.

[19] Ellis, J.R., " The ride and handling of semitrailer articulated vehicle ", Automobile Engineering, vol. 26, 1966, pp. 523-529.

[20] ElMadany, M.M., " Random Response of Articulated Road Vehicles ", Ph.D. Thesis, McMaster University, Hamilton, Canada.

[21] ElMadany, M.M., and Dokainish, M.A.," An Assessment of Ride Quality of Heavy-Duty Trucks ", SAE Paper No. 801418, 1980.

[22] ElMadany, M.M., and Dokainish, M.A., " Optimum Design of Tractor-Semitrailer Suspension Systems ", SAE Paper No. 801419, 1980.

[23] ElMadany, M.M., and Dokainish, M.A., " Articulated Vehicle Dynamics Analyses using Equivalent Linearization Technique ", SAE Paper No. 801421, 1980.

[24] Ervin, R.D., and Guy, Y., " The Influence of Weight and Dimensions on the Stability and Control of Heavy Duty Trucks in Canada ", The University of Michigan Transportation Research Institute, Michigan, U.S.A., Report No. UMTRI-86-35/I, July 1986.

[25] Hullender, P.A. , " Generation of a Random Time Series with a Specific Spectral Density Function ", Proceedings of Joint Automatic Control Conference, Denver, Colo, Published by AICHE, New York, 1979, pp. 532-535.

[26] Iwan, W.D., and I-Min Yang, " Application of Statistical Linearization Techniques of Non-Linear Multi-Degree-of-Freedom Systems ", Journal of Applied Mechanics, Trans. of ASME, June 1972, pp. 545-550.

[27] Kamash, K.M.A., and Robson, J.D. , " Implication of Isotrophy in Random Surfaces ", Journal of Sound and Vibration, 1977, vol. 54, no. 1, pp. 131-145.

[28] Kamash, K.M.A., and Robson, J.D., " The Application of Isotrophy in Road Surface Modelling ", Journal of Sound and Vibration, 1978, vol. 57, no. 1, pp. 89-100.

[29] Krylov, N., and Bogoliubov, N., " Introduction a la Mechanique Nonlineaire: Les Methodes Approachies et Asymptotiques ", Uke. Ukad Nauk. Inst. Mech. Chaire Phys. Math. Ann., 1937.

[30] Levy, S., and Wilkinson, J.P.D. , " Generation of Artificial Time Histories Rich in all Frequencies from given Response Spectra ", Joint Automatic Control Conference of the American Automatic Control Council, Paper No. k1/7.

[31] Lins, W.F., " Vehicle Vibration Analyses using Frequency Domain Techniques ", Journal of Engineering for Industry, Trans. of ASME, November 1969, pp. 1075-1080.

[32] Macaulay, M.A., " Measurement of Road Surfaces ", Advances in Automobile Engineering, Cranfield International Symposium, series 4, 1963, pp. 93-112.

[33] Metawalli, S.M., and Mayne, R.W. , " Random to Deterministic Transform ", Journal of Sound and Vibration, 1981, vol. 79, no. 2, pp. 197-204.

[34] Metcalf, W.W., " The Ride Behaviour of a Multi-Element Vehicle Traversing Cross-Country Terrain ",

Cornell Aeronautical Laboratory, Cornell University, Buffalo, New York, 1961.

[35] Noon, W.D., " The application of an analog computer to the study of a tractor-trailer suspension system , General Motors Engineering Journal, 1960, April-May-June, pp.27-31.

[36] Potts, G.R., and Walker, H.S., " Nonlinear Truck Ride Analysis ", Journal of Engineering for Industry, Trans. ASME, May 1974, pp. 597-602.

[37] Rakheja, S. , " Computer Aided Dynamic Analysis and Optimal Design of Suspension for Off-Road Tractors, Ph.D Thesis,1983, Concordia University, Montreal, Quebec, Canada.

[38] Rakheja, S., Van Vliet, M., and Sankar, S., " A Discrete Harmonic Linearization Technique for Simulating Non-Linear Mechanical Systems ", Journal of Sound and Vibration, 1985, Vol. 100, No. 4, pp. 511-526.

[39] Rakheja, S., and Sankar, S., " Local Equivalent Constant Representation of Nonlinear Damping Mechanisms ", Engineering Computations, International, Journal of Computer-Aided Engineering, 1985, Vol. 3, No. 1, pp. 11-17.

[40] Rakheja, S., Sankar, S., and Bhat, R.B., " Ride Vibration Levels at Driver-Seat Interface - Development of Ride Dynamic Model of an Articulated

Vehicle ", Final Report prepared for Transport Canada Research and Development Centre, Concave Research Centre, Department of Mechanical Engineering, Concordia University, Montreal, Quebec, June, 1987.

[41] Rakheja, S., Sankar, S., and Dhir, A., " Analytical Prediction of the Dynamic Response of an Articulated Vehicle with Nonlinear Damping ", accepted for publication in International Journal of Vehicle Dynamics.

[42] Roberts, J.B., " Response of Nonlinear Mechanical Systems to Random Excitations. Part 2: Equivalent Linearization and Other Methods ", Shock and Vibration Digest, May 1981, Vol. 13, No. 5, pp. 15-29.

[43] Roberts, J.B., " Techniques for Nonlinear Random Vibration Problems ", Shock and Vibration Digest, Sept. 1984, Vol. 16, No. 9, pp. 3-14.

[44] Roberts, J.B., " Stationary Response of Oscillators with Non-Linear Damping to Random Excitation ", Journal of Sound and Vibration, 1977, Vol. 55, No.1, pp. 145-156.

[45] Robson, J.D., and Dodds, C.J., " Stochastic Road Inputs and Vehicle Response ", Vehicle System Dynamics, 1975/1976, vol. 5, pp. 1-13.

[46] Robson, J.D. , " Road Surface Description and

Vehicle Response ", International Journal of Vehicle Design, 1979, vol. 1, no. 1, pp. 25-35.

[47] Ruzicka, Jerome F., and Derby, Thomas F.," Vibration Isolation with Nonlinear Damping ", Journal of Engineering for Industry, Trans. of ASME, May 1971, pp. 627-635.

[48] Scanlon, R.H., " Linear Damping Models and Casuality in Vibration ", Journal of Sound and Vibration, 1970, Vol. 12, No. 4, pp. 499-509.

[49] Sharan, A.M., Sankar, S., Sankar, T.S., " A New Approach for the Calculation of Response Spectral Density of a Linear Stationary Random Multi-degree-of-Freedom-System ", Journal of Sound and Vibration, 1982, Vol. 83, No. 4, pp. 513-519.

[50] Smith, C.C., " On Using the ISO Standard to Evaluate the Ride Quality of Broad-band Vibration Spectra in Transportation Vehicles ", Journal of Dynamic Systems, Measurement and Control, Trans. of ASME, December 1976, pp. 440-443.

[51] Stearns, B.K., " Response Animation of Finite Element Models ", General Electric Company, Burlington, Vermont, U.S.A..

[52] Subbiah, R., Bhat, R.B., and Sankar, T.S., " Response of Rotors Subjected to Random Support Excitations ", Paper No. 85-DET-25, ASME Design Engineering Technical Conference, Cincinnati, Ohio,

Sept. 10-13, 1985.

[53] Thompson, W.T.," Vibration Theory and Applications, Prentice Hall Inc., New Jersey, U.S.A., 1981.

[54] Tsai, Nien-Chien, " Spectrum Compatible Motions for Design Purposes ", Journal of Engineering Mechanics, Proc. ASCE, April, 1972.

[55] Van Deusen, B.D., " Truck suspension system optimization ", Journal of Terramechanics, 1973, vol. 9, no. 2, pp. 83-100.

[56] Walls, J.H., et.al. , " Some Measurements and Power Spectra of Runaway Roughness ", NACA, T.N. 3305.

[57] Walter, W.D., Gossard, D., and Fensel, P. , " Truck ride - a mathematical and empirical study ", SAE Paper No. 690099, January 13-17, 1969.

[58] Winkler, C.B.," Measurements of Inertial Properties and Suspension Parameters of Heavy Highway Vehicles ", SAE Paper No. 730182, 1973.

APPENDIX I

CONSTRAINT EQUATIONS AND MATRICES DESCRIBING EQUATIONS OF MOTION OF LINEAR, TWO-DIMENSIONAL VEHICLE MODEL

Constraint Equations:

The articulation between the tractor and semitrailer sprung masses provides two equations of kinematic constraints:

$$x_s = x_t + a_1\theta_t - a_2\theta_s \tag{I.1}$$

and

$$z_s = z_t + b_5\theta_t + b_4\theta_s \tag{I.2}$$

One dynamical equation revealed an ignorable coordinate which provided the integrated equation,

$$x_t = -\left(\frac{M_5}{M_4 + M_5}\right)(a_1\theta_t - a_2\theta_s) \tag{I.3}$$

where $M_4 = m_t + m_1 + m_2$

$M_5 = m_s + m_3$

Upon substituting (I.3) in (I.1), we obtain,

$$x_s = \left(\frac{M_4}{M_4 + M_5}\right) a_1\theta_t - \left(\frac{M_5}{M_4 + M_5}\right) a_2\theta_s \tag{I.4}$$

The longitudinal and bounce motion at the driver's location can be expressed by following kinematic constraints,

$$x_o = x_t - \theta_t d_z \tag{I.5}$$

and

$$z_o = z_t - \theta_t d_x \tag{I.6}$$

Upon substituting (I.3) in (I.5), we obtain,

$$\ddot{x}_o = a_2 \left(\frac{M_4}{M_4 + M_5} \right) \theta_s - \left(a_1 \left(\frac{M_4}{M_4 + M_5} \right) + d_z \right) \theta_t \qquad (I.7)$$

Equations of Motion:

$$[M] = \begin{bmatrix} m_t + m_s & b_5 m_s & b_4 m_s & & & \\ & I_{tp} + b_5^2 m_s + a_1^2 M_m & b_4 b_5 m_s - a_1 a_2 M_m & & & \\ & & (I_{sp} + b_4^2 m_s + a_2^2 M_m) & & & \\ & \text{(Symmetric)} & & m_1 & & \\ & & & & m_2 & \\ & & & & & m_3 \end{bmatrix}_{(6x6)} \qquad (I.8)$$

$$[C] = \begin{bmatrix} c_1 + c_2 + c_2 & -b_1 c_1 + b_2 c_2 + b_5 c_3 & L_s c_3 & -c_1 & -c_2 & -c_3 \\ & b_1^2 c_1 + b_2^2 c_2 + b_5^2 c_3 & b_5 L_s c_3 & b_1 c_1 & -b_2 c_2 & -b_5 c_3 \\ & & L_s^2 c_3 & 0 & 0 & -L_s c_3 \\ & \text{(Symmetric)} & & c_t + c_1 & & \\ & & & & 4c_t + c_2 & \\ & & & & & 4c_t + c_3 \end{bmatrix}_{(6x6)} \qquad (I.9)$$

$$[K] = \begin{bmatrix} k_1+k_2+k_3 & -b_1k_1+b_2k_2+b_5k_3 & L_sk_3 & -k_1 & -k_2 & -k_3 \\ & b_1^2k_1+b_2^2k_2+b_5^2k_5 & b_5L_sk_3 & b_1k_1 & -b_2k_2 & -b_5k_3 \\ & & L_s^2c_3 & 0 & 0 & -L_sc_3 \\ & & & k_t+k_1 & & \\ & & & & 4k_t+k_2 & \\ & & & & & 4k_t+k_3 \end{bmatrix}_{(6\times6)} \quad (I.10)$$

(Symmetric)

where $M_m = \dfrac{m_t M_5^2 + m_s M_4^2}{(M_4 + M_5)^2}$

and $L_s = b_3 + b_4$

$$[C_F] = \left[\begin{array}{ccc|ccc} & & & & & \\ & -0- & & & -0- & \\ & & & & & \\ \hline & & & c_t & 0 & 0 \\ & -0- & & 0 & 4c_t & 0 \\ & & & 0 & 0 & 4c_t \end{array}\right]_{(6\times6)} \begin{matrix} \\ \\ \\ 3 \\ \\ \\ \end{matrix} \quad (I.11)$$

$$[K_1] = \begin{bmatrix} & -0- & \vdots & -0- & \\ & & \vdots & & \\ \cdots & \cdots & \vdots & \cdots & \cdots \\ & & \vdots & k_t \quad 0 \quad 0 & \\ & -0- & \vdots & 0 \quad 4k_t \quad 0 & \\ & & \vdots & 0 \quad 0 \quad 4k_t & \end{bmatrix}_{(6\times6)}^{3} \qquad (I.12)$$

$$[\Gamma_1] = \frac{S(\omega)}{v} \begin{bmatrix} & -0- & \vdots & -0- & \\ & & \vdots & & \\ \cdots & \cdots & \vdots & \cdots & \cdots \\ & & \vdots & 1 \quad e^{-i\mu_{12}} \quad e^{-i\mu_{13}} & \\ & -0- & \vdots & e^{i\mu_{12}} \quad 1 \quad e^{-i\mu_{23}} & \\ & & \vdots & e^{i\mu_{13}} \quad e^{i\mu_{23}} \quad 1 & \end{bmatrix}_{(6\times6)}^{3} \qquad (I.13)$$

APPENDIX II

CONSTRAINT EQUATIONS AND MATRICES DESCRIBING EQUATIONS OF MOTION OF LINEAR, THREE DIMENSIONAL VEHICLE MODEL

Constraint Equations:

The articulation between tractor and semitrailer sprung masses provides three equations of kinematic constraints:

$$x_s = x_t - a_1\theta_t - a_2\theta_s \tag{II.1}$$

$$y_s = y_t + a_1\phi_t + a_2\phi_s \tag{II.2}$$

and

$$z_s = z_t + b_5\theta_t + b_4\theta_s \tag{II.3}$$

The longitudinal and lateral motions at the cab and driver's seat can be expressed by following kinematic constraints:

$$x_c = x_t - a_3\theta_t \tag{II.4}$$

$$x_o = x_t + (a_c - a_o)\theta_c - a_3\theta_t \tag{II.5}$$

and

$$y_c = y_t + a_3\theta_t \tag{II.6}$$

$$y_o = y_t - (a_c - a_o)\phi_c + a_3\theta_t \tag{II.7}$$

One dynamical equation reveals an ignorable coordinate which yields the intergrated equation:

$$x_t = \frac{-E_1\theta_c + E_2\theta_t + E_3\theta_s}{M_G} \tag{I.8}$$

where M_G = Gross Vehicle Mass

$$= m_o + m_c + m_t + m_s + m_1 + m_2 + m_3$$

$$E_1 = (a_c - a_o)m_o$$

$$E_2 = a_3 S_M + a_1 M_5$$

$$E_3 = a_2 M_5$$

where

S_M = Secondary Mass
$= m_o + m_c$

M_5 = Total mass of semitrailer unit
$= m_s + m_3$

Upon substituting (II.8) in equations (II.1),(II.4), and (II.5), we get,

$$x_o = \frac{-E_4\theta_c + E_5\theta_t + E_3\theta_s}{M_G} \qquad (II.9)$$

$$x_c = \frac{-E_1\theta_c + E_5\theta_t + E_3\theta_s}{M_G} \qquad (II.10)$$

and

$$x_s = \frac{-E_1\theta_c + E_6\theta_t + E_7\theta_s}{M_G} \qquad (II.11)$$

where

$$E_4 = (a_c - a_o)(M_G - m_o)$$

$$E_5 = a_1 M_5 - a_3(M_G - S_M)$$

$$E_6 = a_3 S_M - a_1(M_G - M_5)$$

$$E_7 = -a_2(M_G - M_5)$$

The lateral motion at the tractor c.g. is expressed in terms of tractor front and rear unsprung masses lateral motion, given by,

$$y_t = \frac{b_2 y_1 + b_1 y_2}{L_t} \qquad (II.12)$$

where, L_t = Tractor wheel base

$= b_1 + b_2$

Upon substituting (II.12) in equations (II.2), (II.6) and (II.7), we get,

$$y_o = \frac{b_2 y_1 + b_1 y_2 - F_1 \phi_c + F_2 \phi_t}{L_t} \qquad (II.13)$$

$$y_c = \frac{b_2 y_1 + b_1 y_2 + F_2 \phi_t}{L_t} \qquad (II.14)$$

and

$$y_s = \frac{b_2 y_1 + b_1 y_2 + F_3 \phi_t + F_4 \phi_s}{L_t} \qquad (II.15)$$

where

$$F_1 = (a_c - a_o) L_t$$

$$F_2 = a_3 L_t$$

$$F_3 = a_1 L_t$$

$$F_4 = a_2 L_t$$

Equations of Motion:

Mass, damping and stiffness matrices of three-dimensional vehicle model are symmetric, and are described as follows:

Elements of Mass Matrix, [M]:

$$M(1,1) = m_o$$

$$M(2,2) = m_c$$

$$M(3,3) = (E_4^2 m_o + E_1^2(m_c+m_t+m_s))/M_G^2 + I_{cp} + I_{op}$$

$$M(3,6) = (E_4 E_5 m_o - E_1 E_6 m_c - E_1 E_2 m_t - E_1 E_7 m_s)/M_G^2$$

$$M(3,8) = (E_3 E_4 m_o - E_1 E_3(m_c+m_t) - E_1 E_8 m_s)/M_G^2$$

$$M(4,4) = (r_1/L_t)^2 m_o + I_{or} + I_{cr}$$

$$M(4,7) = -(r_1 F_2/L_t^2) m_o$$

$$M(4,12) = -(F_1 b_2/L_t^2) m_o$$

$$M(4,17) = -(F_1 b_1/L_t^2) m_o$$

$$M(5,5) = m_t + m_s$$

$$M(5,6) = b_5 m_s$$

$$M(5,8) = b_4 m_s$$

$$M(6,6) = (E_5^2 m_o + E_6^2 m_c + E_2^2 m_t + E_7^2 m_s)/M_G^2 + I_{tp} + b_5^2 m_s$$

$$M(6,8) = (E_3(E_5 m_o + E_6 m_c + E_2 m_t) + E_7 E_8 m_s)M_G^2 + b_4 b_5 m_s$$

$$M(7,7) = (F_2^2 S_M + F_3^2 m_s)/L_t^2 + I_{tr}$$

$$M(7,9) = F_3 r_4 m_s / L_t^2$$

$$M(7,12) = (b_2/L_t^2)(F_2 S_M + F_3 m_s)$$

$$M(7,17) = (b_1/L_t^2)(F_2 S_M + F_3 m_s)$$

$$M(8,8) = (E_3^2(S_M+m_t) + E_7^2 m_s)/M_G^2 + b_4^2 m_s + I_{sp} + I_{spr}$$

$$M(9,9) = (F_4/L_t)^2 m_s + I_{sr} + I_{srp}$$

$$M(9,12) = (b_2 F_4/L_t^2) m_s$$

$$M(9,17) = (b_1 F_4/L_t^2) m_s$$

$$M(10,10) = m_1/2$$

$$M(11,11) = m_1/2$$

$$M(12,12) = m_1 + (b_2/L_t)^2 (S_M + m_t + m_s)$$

$$M(12,17) = (b_1 b_2/L_t^2)(S_M + m_t + m_s)$$

$$M(13,13) = m_2/2$$

$$M(14,14) = m_2/2$$

$$M(15,15) = l_2^2 m_2/2 + I_2$$

$$M(16,16) = l_2^2 m_2/2 + I_2$$

$$M(17,17) = m_2 + (b_1/L_t)^2 (S_M + m_t + m_s)$$

$$M(18,18) = m_3/2$$

$$M(19,19) = m_3/2$$

$$M(20,20) = l_3^2 m_3/2 + I_3$$

$$M(21,21) = l_3^2 m_3/2 + I_3$$

$$M(22,22) = m_3$$

Elements of Viscous Damping Matrix, [C]:

$$C(1,1) = c_o$$

$$C(1,2) = -c_o$$

$C(1,3) = r_o c_o$

$C(1,4) = -p_o c_o$

$C(2,2) = c_f + c_r + c_o$

$C(2,3) = -r_1 c_f + r_2 c_r - r_o c_o$

$C(2,4) = p_o c_o$

$C(2,5) = -c_f - c_r$

$C(2,6) = r_3 c_f - r_4 c_r$

$C(3,3) = r_1^2 c_f + r_2^2 c_r + r_o^2 c_o$

$C(3,4) = -r_o p_o c_o$

$C(3,5) = r_1 c_f - r_2 c_r$

$C(3,6) = r_1 r_3 c_f - r_2 r_4 c_r$

$C(4,4) = p_1^2 c_f + p_2^2 c_r + p_o^2 c_o$

$C(4,7) = -p_1^2 c_f - p_2^2 c_r$

$C(5,5) = c_f + c_r + c_1 + c_2 + c_3$

$C(5,6) = -r_3 c_f + r_4 c_r - b_1 c_1 + b_2 c_2 + b_5 c_3$

$C(5,8) = L_s c_3$

$C(5,10) = -c_1/2$

$C(5,11) = -c_1/2$

$C(5,13) = -c_2/2$

$C(5,14) = -c_2/2$

$$C(5,18) = -c_3/2$$

$$C(5,19) = -c_3/2$$

$$C(6,6) = r_3^2 c_f + r_4^2 c_r + b_1^2 c_1 + b_2^2 c_2 + b_5^2 c_3$$

$$C(6,8) = b_5 L_s c_3$$

$$C(6,10) = b_1 c_1/2$$

$$C(6,11) = b_1 c_1/2$$

$$C(6,13) = -b_2 c_2/2$$

$$C(6,14) = -b_2 c_2/2$$

$$C(6,18) = -b_5 c_3/2$$

$$C(6,19) = -b_5 c_3/2$$

$$C(7,7) = p_1^2 c_f + p_2^2 c_r + l_{s_1}^2 c_1 + l_{s_2}^2 c_2$$

$$C(7,10) = -(l_{s_1}^2 / l_{t_1}) c_1/2$$

$$C(7,11) = (l_{s_1}^2 / l_{t_1}) c_1/2$$

$$C(7,13) = -(l_{s_2}^2 / l_{t_2}) c_2/2$$

$$C(7,14) = (l_{s_2}^2 / l_{t_2}) c_2/2$$

$$C(8,8) = L_s^2 c_3$$

$$C(8,18) = -L_s c_3/2$$

$$C(8,19) = -L_s c_3/2$$

$$C(9,9) = l_{s_3}^2 c_3 + c_A$$

$$C(9,18) = -l_{s_3} c_3/2$$

$$C(9,19) = (l_{s_3}^2/l_{t_3})c_3/2$$

$$C(10,10) = (1 + (l_{s_1}/l_{t_1})^2)c_1/4 + c_t/2$$

$$C(10,11) = -(1 + (l_{s_1}/l_{t_1})^2)c_1/4$$

$$C(11,11) = (1 + (l_{s_1}/l_{t_1})^2)c_1/4 + c_t/2$$

$$C(12,12) = c_{tl}$$

$$C(13,13) = (1 + (l_{s_2}/l_{t_2})^2)c_2/4 + 2c_t$$

$$C(13,14) = -(1 + (l_{s_2}/l_{t_2})^2)c_2/4$$

$$C(14,14) = (1 + (l_{s_2}/l_{t_2})^2)c_2/4 + 2c_t$$

$$C(15,15) = 2l_2^2 c_t$$

$$C(16,16) = 2l_2^2 c_t$$

$$C(17,17) = 4c_{tl}$$

$$C(18,18) = (1+(l_{s_3}/l_{t_3})^2)c_3/4 + 2c_t$$

$$C(18,19) = -(1+(l_{s_3}/l_{t_3})^2)c_3/4$$

$$C(19,19) = (1+(l_{s_3}/l_{t_3})^2)c_3/4 + 2c_t$$

$$C(20,20) = 2l_3^2 c_t$$

$$C(21,21) = 2l_3^2 c_t$$

$$C(22,22) = 4c_{t1}^2$$

Elements of Stiffness Matrix, [K]:

$$K(1,1) = k_o$$

$$K(1,2) = -k_o$$

$$K(1,3) = r_o k_o$$

$$K(1,4) = -p_o k_o$$

$$K(2,2) = k_f + k_r + k_o$$

$$K(2,3) = -r_1 k_f + r_2 k_r - r_o k_o$$

$$K(2,4) = p_o k_o$$

$$K(2,5) = -k_f - k_r$$

$$K(2,6) = r_3 k_f - r_4 k_r$$

$$K(3,3) = r_1^2 k_f + r_2^2 k_r + r_o^2 k_o$$

$$K(3,4) = -r_o p_o k_o$$

$$K(3,5) = r_1 k_f - r_2 k_r$$

$$K(3,6) = r_1 r_3 k_f - r_2 r_4 k_r$$

$$K(4,4) = p_1^2 k_f + p_2^2 k_r + p_o^2 k_o$$

$$K(4,7) = -p_1^2 k_f - p_2^2 k_r$$

$$K(5,5) = k_f + k_r + k_1 + k_2 + k_3$$

$$K(5,6) = -r_3 k_f + r_4 k_r - b_1 k_1 + b_2 k_2 + b_5 k_3$$

$$K(5,8) = L_s k_3$$

$K(5,10) = -k_1/2$

$K(5,11) = -k_1/2$

$K(5,13) = -k_2/2$

$K(5,14) = -k_2/2$

$K(5,18) = -k_3/2$

$K(5,19) = -k_3/2$

$K(6,6) = r_3^2 k_f + r_4^2 k_r + b_1^2 k_1 + b_2^2 k_2 + b_5^2 k_3$

$K(6,8) = b_5 L_s k_3$

$K(6,10) = b_1 k_1/2$

$K(6,11) = b_1 k_1/2$

$K(6,13) = -b_2 k_2/2$

$K(6,14) = -b_2 k_2/2$

$K(6,18) = -b_5 k_3/2$

$K(6,19) = -b_5 k_3/2$

$K(7,7) = p_1^2 k_f + p_2^2 k_r + l_{s_1}^2 k_1 + l_{s_2}^2 k_2$

$K(7,10) = -(l_{s_1}^2/l_{t_1})k_1/2$

$K(7,11) = (l_{s_1}^2/l_{t_1})k_1/2$

$K(7,13) = -(l_{s_2}^2/l_{t_2})k_2/2$

$K(7,14) = (l_{s_2}^2/l_{t_2})k_2/2$

$$K(8,8) = L_s^2 k_3$$

$$K(8,18) = -L_s k_3/2$$

$$K(8,19) = -L_s k_3/2$$

$$K(9,9) = l_{s_3}^2 k_3 + k_A$$

$$K(9,18) = -l_{s_3} k_3/2$$

$$K(9,19) = (l_{s_3}^2/l_{t_3})k_3/2$$

$$K(10,10) = (1 + (l_{s_1}/l_{t_1})^2)k_1/4 + k_t/2$$

$$K(10,11) = -(1 + (l_{s_1}/l_{t_1})^2)k_1/4$$

$$K(11,11) = (1 + (l_{s_1}/l_{t_1})^2)k_1/4 + k_t/2$$

$$K(12,12) = k_{t1}$$

$$K(13,13) = (1 + (l_{s_2}/l_{t_2})^2)k_2/4 + 2k_t$$

$$K(13,14) = -(1 + (l_{s_2}/l_{t_2})^2)k_2/4$$

$$K(14,14) = (1 + (l_{s_2}/l_{t_2})^2)k_2/4 + 2k_t$$

$$K(15,15) = 2l_2^2 k_t$$

$$K(16,16) = 2l_2^2 k_t$$

$$K(17,17) = 4k_{t1}$$

$$K(18,18) = (1+(l_{s_3}/l_{t_3})^2)k_3/4 + 2k_t$$

$$K(18,19) = -(1+(l_{s_3}/l_{t_3})^2)k_3/4$$

$$K(19,19) = (1+(l_{s_3}/l_{t_3})^2)k_3/4 + 2k_t$$

$$K(20,20) = 2l_3^2k_t$$

$$K(21,21) = 2l_3^2k_t$$

$$K(22,22) = 4k_{tl}$$

$$[C_l] = \begin{bmatrix} & & & & & & & & & & \\ & & & & & & & & & & \\ & & & & & & & & & & \\ & & & & & & & & & & \\ & & & & & & & & & & \\ & & & & & & & & & & \\ & & & & & & & & & & \\ & & & & & & & & & & \\ & & & & & & & & & & \\ & & & & & & & & & & \\ & & & & & & & & & & \end{bmatrix}$$

(22x22)

$$[K_F] = \left[\begin{array}{c|c|c} & 9 & \\ \hline & & \\ \hline & & 9 \end{array}\right]$$

$$\begin{array}{cccccccccccc}
 & & & & & & & & & & & \\
 & & & & & & & & & & & \\
 & & & & & & & & & & & \\
 & & & & & & & & & & & \\
 & & & & & & & & & & & \\
 & & & & & & & & & & & \\
 & & & & & & & & & & & \\
 & & & & & & & & & & & \\
 & & & & & & & & & & & \\
 & & & & & & & & & & & \\
 & & & & & & & & & & & \\
 & & & & & & & & & & & \\
 & & & & & & & & & & & \\
 & & & & & & & & & & & \\
 & & & & & & & & & & & \\
 & & & & & & & & & & & \\
 & & & & & & & & & & & \\
 & & & & & & & & & & & \\
 & & & & & & & & & & & \\
 & & & & & & & & & & & \\
 & & & & & & & & & & & \\
 & & & & & & & & & & &
\end{array}$$

(22X22)

$$\left[S_i\right] = \frac{S(n)}{v}$$

1	0	0	$e^{-i\mu_{12}}$	0	$e^{-i\mu_{13}}$	0	0	$e^{-i\mu_{14}}$	0	$e^{-i\mu_{15}}$	0	0
0	1	0	0	$e^{-i\mu_{12}}$	0	$e^{-i\mu_{13}}$	0	0	$e^{-i\mu_{14}}$	0	$e^{-i\mu_{15}}$	0
0	0	0	0	0	0	0	0	0	0	0	0	0
$e^{i\mu_{12}}$	0	0	1	0	$e^{-i\mu_{23}}$	0	0	$e^{-i\mu_{24}}$	0	$e^{-i\mu_{25}}$	0	0
0	$e^{i\mu_{12}}$	0	0	1	0	$e^{-i\mu_{23}}$	0	0	$e^{-i\mu_{24}}$	0	$e^{-i\mu_{25}}$	0
$e^{i\mu_{13}}$	0	0	$e^{i\mu_{23}}$	0	1	0	0	$e^{-i\mu_{34}}$	0	$e^{-i\mu_{35}}$	0	0
0	$e^{i\mu_{13}}$	0	0	$e^{i\mu_{23}}$	0	1	0	0	$e^{-i\mu_{34}}$	0	$e^{-i\mu_{35}}$	0
0	0	0	0	0	0	0	0	0	0	0	0	0
$e^{i\mu_{14}}$	0	0	$e^{i\mu_{24}}$	0	$e^{i\mu_{34}}$	0	0	1	0	$e^{-i\mu_{45}}$	0	0
0	$e^{i\mu_{14}}$	0	0	$e^{i\mu_{24}}$	0	$e^{i\mu_{34}}$	0	0	1	0	$e^{-i\mu_{45}}$	0
$e^{i\mu_{15}}$	0	0	$e^{i\mu_{25}}$	0	$e^{i\mu_{35}}$	0	0	$e^{i\mu_{45}}$	0	1	0	0
0	$e^{i\mu_{15}}$	0	0	$e^{i\mu_{25}}$	0	$e^{i\mu_{35}}$	0	0	$e^{i\mu_{45}}$	0	1	0
0	0	0	0	0	0	0	0	0	0	0	0	0

22×22